Fall 2016

Bayesian inference for dynamic pose estimation using directional statistics

Jacob E. Darling

BAYESIAN INFERENCE FOR DYNAMIC POSE ESTIMATION USING DIRECTIONAL

STATISTICS

by

JACOB E. DARLING

A DISSERTATION

Presented to the Graduate Faculty of the

MISSOURI UNIVERSITY OF SCIENCE AND TECHNOLOGY

In Partial Fulfillment of the Requirements for the Degree

DOCTOR OF PHILOSOPHY

in

AEROSPACE ENGINEERING

2016

Approved by:

Kyle J. DeMars, Co-advisor
Henry J. Pernicka, Co-advisor
S.N. Balakrishnan
Serhat Hosder
T. Alan Lovell
Renato Zanetti

ABSTRACT

The dynamic pose of an object, where the object can represent a spacecraft, aircraft, or mobile robot, among other possibilities, is defined to be the position, velocity, attitude, and angular velocity of the object. A new method to perform dynamic pose estimation is developed that leverages directional statistics and operates under the Bayesian estimation framework, as opposed to the minimum mean square error (MMSE) framework that conventional methods employ. No small attitude uncertainty assumption is necessary using this method, and, therefore, a more accurate estimate of the state can be obtained when the attitude uncertainty is large.

Two new state densities, termed the Gauss-Bingham and Bingham-Gauss mixture (BGM) densities, are developed that probabilistically represent a state vector comprised of an attitude quaternion and other Euclidean states on their natural manifold, the unit hypercylinder. When the Euclidean states consist of position, velocity, and angular velocity, the state vector represents the dynamic pose. An uncertainty propagation scheme is developed for a Gauss-Bingham-distributed state vector, and two demonstrations of this uncertainty propagation scheme are presented that show its applicability to quantify the uncertainty in dynamic pose, especially when the attitude uncertainty becomes large.

The BGM filter is developed, which is an approximate Bayesian filter in which the true temporal and measurement evolution of the BGM density, as quantified by the Chapman-Kolmogorov equation and Bayes' rule, are approximated by a BGM density. The parameters of the approximating BGM density are found via integral approximation on a component-wise basis, which is shown to be the Kullback-Leibler divergence optimal parameters of each component. The BGM filter is then applied to three simulations in order to compare its performance to a multiplicative Kalman filter and demonstrate its efficacy in estimating dynamic pose. The BGM filter is shown to be more statistically consistent than the multiplicative Kalman filter when the attitude uncertainty is large.

ACKNOWLEDGMENTS

TABLE OF CONTENTS

LIST OF ILLUSTRATIONS

LIST OF TABLES

1. INTRODUCTION

1.1. MOTIVATION AND PREVIOUS WORK

As a motivating example, consider the planar translation and rotation of a body, which are quantified by Cartesian position coordinates and heading angle, respectively. The position of the body is typically assumed Gaussian-distributed since it is not bounded to a given interval; however, the heading angle cannot be assumed Gaussian-distributed since it is required to be in the interval $[-\pi, \pi)$, and the support of the Gaussian density is infinite. A circular density, such as the wrapped normal density or von Mises density, which are defined on the interval $[-\pi, \pi)$, can be used to probabilistically quantify the heading angle. The position and heading angle of the body are correlated in general, but they are properly quantified by two different densities; they must, therefore, be considered under a common state density in order to properly represent their correlation.

Estimation approaches have been developed when the state consists of *only* a von Mises- or wrapped normal-distributed circular variable [1, 2]. These approaches quantify the temporal and measurement evolution of the von Mises or wrapped normal density; however, they do not extend to a state with *both* a circular variable and other Euclidean (additive and unbounded) variables. Mardia and Sutton first proposed a density to quantify a circular and Euclidean variable in which the state density is constructed as the product of a von Mises density and a Gaussian density conditioned on the von Mises-distributed random variable [3]. The Gauss von Mises density is constructed in a similar manner to quantify a state with both a circular variable and other Euclidean variables as the product of a multivariate Gaussian density and a von Mises density conditioned on the multivariate Gaussian-distributed random variable [4].

A single circular variable can be used to quantify the heading angle, or one-dimensional attitude, of a body. While the aforementioned methods operate on a single circular variable, a more general problem is given by the case when the three-dimensional attitude and other Euclidean states (such as position, velocity, angular velocity, etc.) of a body are quantified by an attitude quaternion and Cartesian coordinates, respectively. The attitude quaternion exists on the unit hypersphere and is antipodally symmetric; that is, opposing quaternions represent the same attitude. The attitude quaternion is a globally nonsingular attitude representation, and thus, it is a popular choice to represent the three-dimensional attitude of a body [5, 6, 7]. The wrapped normal and von Mises densities, which can be used to quantify the heading angle of a vehicle, cannot be used to quantify the attitude quaternion since they are not antipodally symmetric densities.

The Bingham density, which is developed in References [8] and [9], is constructed as a zero-mean Gaussian density that is conditioned to lie on the unit sphere. As such, it is an antipodally symmetric distribution for a unit vector of arbitrary dimension. Since the quaternion representation of attitude is constrained to be unit-norm, it also lies on the unit sphere. In addition, as mentioned previously, antipodal quaternions represent the same physical attitude, which implies that, in a probabilistic context, they must be equiprobable. As such, given the properties of the Bingham density, the Bingham density can be a proper probabilistic representation of the attitude quaternion. Estimation approaches have been developed for a state that consists only of an attitude quaternion [10, 11, 12]. In particular, Reference [12] leverages an unscented transform to propagate the uncertainty of a Bingham-distributed attitude quaternion when the system dynamics are nonlinear; however, Reference [12] assumes that the quaternion state is measured and is corrupted by Bingham-distributed noise. This assumption does not allow for nonlinear measurements of the attitude state to be considered. Furthermore, the approaches pursued in References [10, 11, 12] do not quantify the correlation between the Bingham-distributed attitude quaternion and other Euclidean variables.

A state density that is similar to the Bingham density has been proposed to quantify the dual quaternion representing the pose (position and attitude) of a body [13]; however, this density does not extend to arbitrarily high dimensions to include the velocity, angular velocity, and other Euclidean states since it is constructed using a dual quaternion. The partially wrapped normal density has recently been proposed, which wraps m coordinates of an n-dimensional Gaussian density in order to quantify the correlation between m angular and $n-m$ Euclidean states [14]. This density applies to arbitrarily high m and n, so it can potentially be used to represent the uncertainty of a rotation sequence representing the three-dimensional attitude and other Euclidean states of a body. Because the temporal evolution of a rotation sequence is potentially singular [5, 6, 7], the temporal evolution of this uncertainty representation will be potentially singular as well.

Typically, the multiplicative extended Kalman filter (MEKF) [5] is used to estimate a state vector that consists of an attitude quaternion and other Euclidean states. The MEKF operates under the linear minimum mean square error (MMSE) framework, in which a small attitude uncertainty assumption is used to project the error in the attitude quaternion into a three-parameter local tangent space that is constructed about the current estimated attitude quaternion. This small attitude uncertainty assumption incurs little error when enough measurement information is available such that the attitude uncertainty assumption remains small; however, if the attitude uncertainty is large, this assumption can potentially incur error and degrade the state estimate. Furthermore, the MEKF quantifies only the estimated state, which is given by the attitude quaternion, and its error covariance, which is quantified in the three-parameter tangent space. The MEKF does *not* quantify the

probability density function (pdf) of the state vector, which is an artifact of its operation under the linear MMSE framework.

1.2. CONTRIBUTIONS

This dissertation proposes an approximate Bayesian filter to estimate a state vector that consists of an attitude quaternion and other Euclidean states. Since this filter operates under the Bayesian framework, it quantifies the pdf of the state vector and not just its estimate and error covariance, like the MEKF. In order to develop this filter, two new state densities, termed the Bingham-Gauss and Gauss-Bingham densities, are developed. These densities probabilistically quantify a state vector consisting of an attitude quaternion and other states that exist in Euclidean space. When these other states consist of the body's position, velocity, and angular velocity, the dynamic pose of the body is probabilistically quantified. These densities are constructed by conditioning a Gaussian density on the Bingham-distributed random variable, and conditioning a Bingham density on the Gaussian-distributed random variable, respectively. Furthermore, the Bingham-Gauss density is extended to develop the Bingham-Gauss mixture density, which is used to probabilistically quantify non-Bingham-Gauss-distributed state vectors. The approximation of a Bingham-Gauss density by a Bingham-Gauss mixture (BGM) density is developed, which includes the development of an approximation method of both a uniform and non-uniform Bingham density by an Bingham mixture (BM) density.

Additionally, a minimum divergence filtering framework is developed, which approximates each step in the Bayesian recursion by an assumed density. The parameters of the assumed density are found by minimizing an information divergence measure of the true state density, as defined by the Chapman-Kolmogorov equation and Bayes' rule, with respect to the assumed density. An analytic result for this minimization is proved for general exponential family pdfs, which includes the well-known Gaussian density and the Bingham-Gauss density. The minimum divergence filtering framework is specialized to a Gaussian mixture (GM) state density to develop the Gaussian mixture minimum divergence filter (GMMDF), and the GMMDF is then compared and contrasted to other GM Kalman filters. This allows for the minimum divergence filtering framework to be analyzed in a more typical application before it is extended to estimate the dynamic pose of a body using an assumed Bingham-Gauss mixture density.

Finally, an approximate Bayesian filter, termed the BGM filter, that estimates a state vector consisting of an attitude quaternion and other states that exist in Euclidean space is developed. Since the estimation scheme operates under the approximate Bayesian minimum divergence filtering framework (as opposed to the linear MMSE framework), no small attitude uncertainty assumption is necessary to project the attitude uncertainty into the three-parameter tangent space, as is inherent

to the MEKF. Because of this, the BGM filter lends itself to applications in which the attitude uncertainty is large, in which case the small attitude uncertainty assumption inherent to the MEKF is violated.

1.3. ORGANIZATION

The remainder of this dissertation is organized as follows:

- Section 2 first provides an overview of one- and three-dimensional attitude, including the various attitude representations used throughout the dissertation. The concept of orientation is presented, which is a higher-dimensional extension to attitude.

- Section 3 provides an overview of the pdfs used throughout the dissertation, including the established Gaussian, GM, and Bingham densities. The BM, Gauss-Bingham, Bingham-Gauss, and BGM densities are then developed.

- Section 4 provides an overview of Kalman filtering, including the Kalman filter (KF), extended Kalman filter (EKF), unscented Kalman filter (UKF), and quadrature Kalman filter (QKF). The MEKF is then presented, which is the most common filter used to estimate the attitude quaternion and other Euclidean states of a body. Quadrature variations of the MEKF, including the multiplicative unscented Kalman filter (MUKF) and multiplicative quadrature Kalman filter (MQKF) are presented.

- Section 5 provides an overview of Bayesian filtering, including the Bayesian Kalman filter, Gaussian mixture Kalman filter (GMKF), Gaussian mixture extended Kalman filter (GMEKF), Gaussian mixture unscented Kalman filter (GMUKF), and Gaussian mixture quadrature Kalman filter (GMQKF). The minimum divergence filtering framework is developed and is used to develop the GMMDF.

- Section 6 provides the development of an unscented uncertainty propagation scheme using the Gauss-Bingham density. Two examples of this uncertainty propagation are shown in order to illustrate the efficacy of this method of uncertainty propagation.

- Section 7 provides the development of the BGM filter, which is derived using the minimum divergence filtering framework developed in Section 5.

- Section 8 presents three simulations to evaluate the BGM filter:

  - First, a Monte Carlo analysis is performed on a single component BGM filter and a multiplicative Kalman filter applied to estimate the one-dimensional attitude quaternion

and angular velocity of a body with an initially equiprobable attitude quaternion, given measurements of the heading angle of the body.

– Next, two instantiations of the BGM filter, the first operating on a single component BGM density and the second operating on a multiple component BGM density, are applied to estimate the planar dynamic pose of an inspector spacecraft performing proximity operations about a chief spacecraft, given nonlinear measurements of the range and bearing between the spacecraft.

– Finally, the BGM filter is applied to estimate the three-dimensional dynamic pose of a spacecraft in low-Earth orbit, given measurements of the spacecraft's position and the Earth's magnetic field.

• Section 9 draws conclusions regarding the material presented in Sections 2-8.

2. ATTITUDE AND ORIENTATION

The attitude of a body is fundamentally quantified by the rotation from a reference coordinate frame to a body-fixed coordinate frame of interest and exists in either one or three dimensions. To illustrate the idea of attitude in one dimension, consider a robot translating in a plane. The attitude of the robot contains only one degree of freedom, which is typically quantified by its heading angle, the angle of rotation about the axis perpendicular to the plane in which it travels. Attitude in one dimension is, in fact, a subset of attitude in three dimensions, in which case the axis of rotation relating the reference coordinate frame to the body-fixed coordinate frame is known and fixed. The angle of rotation about this axis fully defines the attitude in one dimension. Attitude in three dimensions requires that both the axis and the angle of rotation about this axis be quantified in order to fully define the attitude. In three dimensions, attitude has three degrees of freedom, which is apparent because the axis of rotation contains two degrees of freedom and the angle of rotation about this axis contains the third degree of freedom. In order to easily denote attitude in one and three dimensions, "attitude" is used to denote attitude in three dimensions, and "one-dimensional attitude" is used to denote attitude in one dimension hereafter.

The concept of attitude can be extended to arbitrarily high dimension, in which case the concept of *orientation* is born. In higher dimensions, multiple rotations are necessary to specify an an orientation, in general. In fact, in r-dimensional space, $\lfloor \frac{r}{2} \rfloor$ higher-dimensional rotations are necessary to construct an orientation, where $\lfloor \frac{r}{2} \rfloor$ represents the floor of $\frac{r}{2}$, which rounds $\frac{r}{2}$ towards negative infinity. In three-dimensional space, $\lfloor \frac{3}{2} \rfloor = 1$ rotation is necessary to specify an orientation, and the concept of rotation and orientation are the same. This is stated by Euler's theorem, which says that any rotation in three dimensions can be accomplished by a single rotation about a stationary (fixed) axis. When $r > 3$, the concepts of rotation and orientation are no longer the same, and multiple rotations are necessary to specify an orientation, in general.

In this chapter, first, attitude is defined in terms of the attitude matrix, which fundamentally defines the attitude of a body as the direction cosine matrix (DCM) relating the body-fixed and reference coordinate frames. Because the attitude matrix can be difficult to quantify directly, alternate attitude representations, including the axis-angle, rotation vector, and attitude quaternion are also presented. Each attitude representation is also specialized to its equivalent one-dimensional attitude representation. The explicit relationships between the attitude quaternion and the other attitude parameterizations are also presented, because the attitude quaternion is commonly used to quantify attitude due to its global nonsingularity and single constraint (as compared to the attitude matrix, which is nonsingular, but possesses six constraints). Next, the kinematic relationship between the attitude quaternion and the angular velocity of the body is presented. An overview of

attitude dynamics is presented next, which govern the temporal evolution of the angular velocity of the vehicle given the inertia tensor of the body and the external moments acting on the body. Finally, the concept of orientation is introduced, which is a higher-dimensional extension to attitude. Furthermore, a method using left- and right-isoclonic rotations to construct the orientation matrix in four dimensions from a minimum set of parameters is presented.

2.1. ATTITUDE

Many different parameterizations can be used to represent attitude [5, 6, 7]. These different attitude representations have either three, four, or nine parameters; however, attitude possesses only three degrees of freedom. Because of this, four- and nine-parameter representations have one and six constraints, respectively. Three- and four-parameter representations satisfy certain properties, regardless of the specific representation chosen. All three-parameter attitude representations provide a one-to-one representation of attitude; however, they are singular. Three-parameter attitude parameterizations can either be singular in representing an attitude or in propagation. The former of these singularities occurs when a parameterization becomes infinite in order to represent a certain rotation. The latter occurs when the temporal derivative of the representation becomes infinite for certain values of the parameterization. Four-parameter attitude representations are globally nonsingular, but are constrained because attitude contains only three degrees of freedom. Four-parameter attitude representations provide a two-to-one representation of attitude; that is, two different sets of parameters quantify the same attitude. Because of the unique advantages and disadvantages of three- and four-parameter attitude representations, a four-parameter representation is typically used to globally quantify attitude and a three-parameter representation is used to locally quantify attitude errors in order to avoid their singularities.

2.1.1. Attitude Matrix. The attitude of a body is fundamentally quantified by the attitude matrix, $\boldsymbol{A}$, which is a nine-parameter attitude representation. In order to formally define the attitude matrix, first, the DCM, denoted in general by $\boldsymbol{T}$, must be defined. The DCM that transforms the expression of an arbitrary, physical vector in the I coordinate frame to its expression in the B coordinate frame, which is denoted by $\boldsymbol{T}_I^B$, is defined according to

$$\boldsymbol{x}^B = \boldsymbol{T}_I^B \boldsymbol{x}^I , \tag{2.1}$$

where $\boldsymbol{x}^I$ and $\boldsymbol{x}^B$ denote the arbitrary, physical vector $\boldsymbol{x} \in \mathbb{R}^3$ expressed in the I and B frames, respectively. $\mathbb{R}^r$ is used to denoted Euclidean space in r dimensions; thus, $\mathbb{R}^3$ represents 3-dimensional

Euclidean space. The vector $\boldsymbol{x}$ expressed in the I frame, $\boldsymbol{x}^I$, is formally defined as

$$\boldsymbol{x}^I \triangleq \begin{bmatrix} x \\ y \\ z \end{bmatrix} = x\boldsymbol{u}_x^I + y\boldsymbol{u}_y^I + z\boldsymbol{u}_z^I\,, \tag{2.2}$$

where $\boldsymbol{u}_x^I$, $\boldsymbol{u}_y^I$, and $\boldsymbol{u}_z^I$ are the vectors defining the basis of the I coordinate frame, and $\boldsymbol{x}^B$ is defined similarly. If $\boldsymbol{u}_x^I$, $\boldsymbol{u}_y^I$, and $\boldsymbol{u}_z^I$ are defined such that

$$\boldsymbol{u}_x^I \times \boldsymbol{u}_y^I = \boldsymbol{u}_z^I \tag{2.3a}$$

$$\boldsymbol{u}_x^I \cdot \boldsymbol{u}_y^I = \boldsymbol{u}_x^I \cdot \boldsymbol{u}_z^I = \boldsymbol{u}_y^I \cdot \boldsymbol{u}_z^I = 0 \tag{2.3b}$$

$$||\boldsymbol{u}_x^I|| = ||\boldsymbol{u}_y^I|| = ||\boldsymbol{u}_z^I|| = 1\,, \tag{2.3c}$$

then the coordinate frame is said to be a right-handed, orthonormal (orthogonal and normal) coordinate frame. The right-handed property is defined by Eq. (2.3a), the orthogonal property is defined by Eq. (2.3b), and the normal property is defined by Eq. (2.3c). All coordinate frames are assumed right-handed and orthonormal in this work, unless otherwise stated.

Through the definition of the DCM in Eq. (2.1), it can be shown that coordinate transformations can be applied sequentially according to

$$\boldsymbol{x}^B = \boldsymbol{T}_C^B \boldsymbol{x}^C = \boldsymbol{T}_C^B \underbrace{\boldsymbol{T}_I^C \boldsymbol{x}^I}_{\boldsymbol{x}^C}\,, \tag{2.4}$$

where the C coordinate frame is an arbitrary, intermediate coordinate frame. Equating Eqs. (2.1) and (2.4) shows the property of DCMs to compose coordinate transformations by multiplying the matrices according to

$$\boldsymbol{T}_I^B = \boldsymbol{T}_C^B \boldsymbol{T}_I^C\,. \tag{2.5}$$

DCMs exist in the special orthogonal group of dimension three, which is denoted by SO(3). The special orthogonal group of arbitrary dimension r is defined by

$$\mathrm{SO}(r) \triangleq \{\boldsymbol{T} \in \mathbb{R}^{r \times r} : \boldsymbol{T}^T \boldsymbol{T} = \boldsymbol{I} = \boldsymbol{T}\boldsymbol{T}^T, \det\{\boldsymbol{T}\} = 1\},$$

where $\det\{\boldsymbol{T}\}$ represents the determinant of $\boldsymbol{T}$ and the "T" superscript is used to represent the matrix transpose operator and not a coordinate frame. Because $\boldsymbol{T} \in \mathrm{SO}(3)$, it is a matrix of row- and column-dimension three, but is subject to the constraints $\boldsymbol{T}^T \boldsymbol{T} = \boldsymbol{I} = \boldsymbol{T}\boldsymbol{T}^T$ and $\det\{\boldsymbol{T}\} = 1$. DCMs possess nine parameters, but only three degrees of freedom, which implies that they have six

constraints. The constraint imposed on the DCM of $\boldsymbol{T}^T\boldsymbol{T} = \boldsymbol{I}$ is now post-multiplied by $\boldsymbol{T}^{-1}$ and simplified to show an important property of the DCM, which is given by

$$\boldsymbol{T}^T = \boldsymbol{T}^{-1}, \tag{2.6}$$

where the "-1" superscript is used to represent the matrix inverse operator and not a coordinate frame.

In order to show another important property of DCMs, Eq. (2.1) is solved for $\boldsymbol{x}^I$ to yield

$$\boldsymbol{x}^I = \left[\boldsymbol{T}_I^B\right]^{-1}\boldsymbol{x}^B,$$

and the property of DCMs given in Eq. (2.6) is exploited to yield

$$\boldsymbol{x}^I = \left[\boldsymbol{T}_I^B\right]^T\boldsymbol{x}^B. \tag{2.7}$$

Through the definition of the DCM given in Eq. (2.1), Eq. (2.7) can also be expressed as

$$\boldsymbol{x}^I = \boldsymbol{T}_B^I\boldsymbol{x}^B. \tag{2.8}$$

Equations (2.7) and (2.8) are now combined, which shows that transposed DCMs represent opposite coordinate transformations according to

$$\boldsymbol{T}_B^I = \left[\boldsymbol{T}_I^B\right]^T. \tag{2.9}$$

Now that the DCM and some of its important properties have been defined, the attitude matrix is defined as

$$\boldsymbol{A} \triangleq \boldsymbol{T}_I^B, \tag{2.10}$$

which shows that the attitude matrix is defined as the DCM quantifying the coordinate transformation from the I to the B coordinate frame. Typically, the I frame is taken to be an inertially-fixed frame and the B frame is taken to be a body-fixed frame, but it is not required for the I frame to be inertially fixed in order for the attitude matrix to be valid. Because the attitude matrix is defined as a DCM, it follows that the attitude matrix possesses equivalent properties to a DCM. This means that the attitude matrix possesses nine parameters, but only three degrees of freedom, which implies that they have six constraints. In practice, these constraints make it difficult to quantify the attitude matrix directly. Typically the attitude matrix is parameterized by a three- or four-parameter attitude representation in order to overcome this difficulty.

The properties of DCMs can be used to quantify the error between an estimated attitude and the true attitude of a body. This error is defined as the DCM relating the estimated body frame, $\hat{B}$, and the true body frame, B, which is given by $\boldsymbol{T}_{\hat{B}}^{B}$. This DCM defines the attitude matrix representation of the attitude error, denoted by $\delta\boldsymbol{A}$, and is given by

$$\delta\boldsymbol{A} \triangleq \boldsymbol{T}_{\hat{B}}^{B} = \boldsymbol{T}_{I}^{B}\boldsymbol{T}_{\hat{B}}^{I} = \boldsymbol{T}_{I}^{B}[\boldsymbol{T}_{I}^{\hat{B}}]^{T} = \boldsymbol{A}\hat{\boldsymbol{A}}^{T}\,, \tag{2.11}$$

where $\hat{\boldsymbol{A}}$ is the estimated attitude matrix. As the attitude error approaches zero, the estimated attitude matrix, $\hat{\boldsymbol{A}}$, approaches the true attitude matrix, $\boldsymbol{A}$, and the attitude matrix representation of the attitude error, $\delta\boldsymbol{A}$, approaches the identity matrix. This is an intuitive result because, as the estimated body frame and the true body frame approach each other, the rotation between the frames approaches identity.

When quantifying one-dimensional attitude, the axis of rotation is known and fixed, and is typically taken to be $\boldsymbol{u}_{z}^{I} \triangleq \boldsymbol{u}_{z}^{B} \triangleq [0\ \ 0\ \ 1]^{T}$. This stems from the fact that the translational motion is typically taken to be in the plane defined by $\boldsymbol{u}_{x}^{I}$ and $\boldsymbol{u}_{y}^{I}$, and, equivalently, $\boldsymbol{u}_{x}^{B}$ and $\boldsymbol{u}_{y}^{B}$. In order to simplify the attitude matrix to quantify this one-dimensional attitude, first note that the attitude matrix, as defined by Eqs. (2.1) and (2.10), can be expressed in scalar components according to

$$\begin{bmatrix} x^{B} \\ y^{B} \\ z^{B} \end{bmatrix} = \begin{bmatrix} A_{11} & A_{12} & A_{13} \\ A_{21} & A_{22} & A_{23} \\ A_{31} & A_{32} & A_{33} \end{bmatrix} \begin{bmatrix} x^{I} \\ y^{I} \\ z^{I} \end{bmatrix}.$$

Because the axis of rotation is defined as $\boldsymbol{u}_{z}^{I} \triangleq \boldsymbol{u}_{z}^{B}$, it follows that the z-component of both x^{I} and x^{B} must be equal for arbitrary $\boldsymbol{x}$, which implies that five of the parameters of the attitude matrix become constant and the attitude matrix must be equal to

$$\boldsymbol{A} = \begin{bmatrix} A_{11} & A_{12} & 0 \\ A_{21} & A_{22} & 0 \\ 0 & 0 & 1 \end{bmatrix}. \tag{2.12}$$

Because the z-component of both x^{I} and x^{B} must be equal due to the definition of the axis of rotation, the z-component of x^{I} and x^{B} is typically not quantified when considering one-dimensional attitude. This allows the third row and column to be neglected in Eq. (2.12), which gives the final form of the attitude matrix quantifying one-dimensional attitude as

$$\boldsymbol{A} = \begin{bmatrix} A_{11} & A_{12} \\ A_{21} & A_{22} \end{bmatrix}.$$

An abuse of notation is committed when using $\boldsymbol{A}$ to quantify both the attitude matrix and the one-dimensional attitude matrix; however, which attitude matrix is meant by $\boldsymbol{A}$ will be clear in context. For one-dimensional attitude, $\boldsymbol{A}$ is a DCM with both row and column dimension two, and, thus, $\boldsymbol{A} \in \mathrm{SO}\,(2)$. In this case, the attitude matrix contains four parameters, and only one degree of freedom (or, equivalently, three constraints).

2.1.2. Axis-Angle. An intuitive four-parameter representation of a rotation in three dimensions is the *axis-angle* representation. Euler's theorem states that any rotation in three dimensions can be accomplished by a single rotation about a stationary (fixed) axis. The axis of this rotation is known as the *Euler* axis and is denoted by the unit vector $\boldsymbol{e}$. Let the corresponding rotation angle about the Euler axis be $\theta \in [-\pi, \pi)$. The axis-angle representation of this rotation is then given by the parameter set $\{\boldsymbol{e},\, \theta\}$.

The Euler axis is invariant under a rotation about itself, i.e. $\boldsymbol{e}^B = \boldsymbol{e}^I$. Because of this, the frame in which the Euler axis is expressed is omitted in order to simplify notation according to $\boldsymbol{e}^B = \boldsymbol{e}^I \triangleq \boldsymbol{e}$. This rotational invariance allows the Euler axis corresponding to the rotation to be found from the attitude matrix according to the relationship

$$\boldsymbol{A}\boldsymbol{e} = \boldsymbol{e}\,, \tag{2.13}$$

which defines the Euler axis according to the eigenvector/eigenvalue decomposition of the attitude matrix. The eigenvalues, λ_i, and eigenvectors, $\boldsymbol{v}_i$, of the attitude matrix are defined according to

$$\boldsymbol{A}\boldsymbol{v}_i = \lambda_i \boldsymbol{v}_i, \quad \text{for} \quad i = 1, 2, 3\,. \tag{2.14}$$

Comparing Eq. (2.13) and Eq. (2.14) shows that the Euler axis is defined as the eigenvector of the attitude matrix corresponding to the unity eigenvalue; the other two eigenvalues are a complex conjugate pair [5, 15, 16]. These properties of the eigenvalues stem from the fact that the attitude matrix exists in the special orthogonal group of dimension three.

In order to find the attitude matrix corresponding to the axis-angle attitude parameterization, the arbitrary vector $\boldsymbol{x} \in \mathbb{R}^3$ is first decomposed into components that are parallel and perpendicular to $\boldsymbol{e}$ according to [5]

$$\boldsymbol{x} = \boldsymbol{x}_{\parallel} + \boldsymbol{x}_{\perp}\,, \tag{2.15}$$

where $\boldsymbol{x}_{\parallel}$ and $\boldsymbol{x}_{\perp}$ represent the parallel and perpendicular components, respectively, and are expressed as

$$\boldsymbol{x}_{\parallel} \triangleq (\boldsymbol{e} \cdot \boldsymbol{x})\boldsymbol{e} = \left(\boldsymbol{e}\boldsymbol{e}^T\right)\boldsymbol{x} \tag{2.16a}$$

$$x_\perp \triangleq x - (e \cdot x)e = \left(I - ee^T\right) x\,. \tag{2.16b}$$

Equation (2.15) is now expressed in the I frame, and the resulting expression is then transformed to the B frame by pre-multiplying both sides of the expression by the attitude matrix, which yields

$$Ax^I = A(x_\parallel^I + x_\perp^I)\,.$$

The portion of x that is parallel to the Euler axis, $x_\parallel$, is invariant to rotation about the Euler axis; therefore,

$$Ax^I = x_\parallel^I + Ax_\perp^I\,. \tag{2.17}$$

It is now necessary to quantify $Ax_\perp^I$, which represents the rotation of $x_\perp^I$ about e through the angle θ, which are the Euler axis and angle of rotation, respectively, corresponding to A. This rotation is performed by decomposing $Ax_\perp^I$ into the sum of two vectors: The vector in the $x_\perp^I$ direction that remains after the rotation, and the vector produced perpendicular to e and $x_\perp^I$ after the rotation. This decomposition of $Ax_\perp^I$ into these vectors allows it to be expressed directly in terms of the Euler axis and rotation angle according to

$$Ax_\perp^I = \cos(\theta)x_\perp^I - \sin\theta \left(e \times x^I\right)\,. \tag{2.18}$$

The first term in the right-hand-side of Eq. (2.18) represents the vector component of $Ax_\perp^I$ in the $x_\perp^I$ direction, while the second term represents the vector component of component of $Ax_\perp^I$ perpendicular to e and $x_\perp^I$ (that is, the direction defined by $e \times x^I$). If a rotation of either $-180°$ or $0°$ is performed, the second term vanishes. Similarly, if a rotation of either $-90°$ or $90°$ is performed, the first term vanishes. These results are consistent with what is expected of rotations of these magnitudes about the Euler axis and provide a verification that the decomposition of $Ax_\perp^I$ into these components is correct. Equation (2.18) is now substituted into Eq. (2.17), and the definitions of $x_\parallel$ and $x_\perp$ from Eqs. (2.16) are then substituted into the resulting expression to yield

$$Ax^I = \left(ee^T\right) x^I + \cos(\theta) \left(I - ee^T\right) x^I - \sin\theta \left(e \times x^I\right)\,. \tag{2.19}$$

Equation (2.19) defines the relationship between the attitude matrix and the axis-angle attitude parameterization; however, it is not yet in a useful form since is still depends on x^I.

In order to manipulate Eq. (2.19) into a useful form, the skew-symmetric cross product matrix is first defined. This matrix is defined for $\boldsymbol{e} \triangleq [e_x \ e_y \ e_z]^T$ as

$$[\boldsymbol{e}\times] \triangleq \begin{bmatrix} 0 & -e_z & e_y \\ e_z & 0 & -e_x \\ -e_y & e_x & 0 \end{bmatrix}, \tag{2.20}$$

such that $[\boldsymbol{e}\times]\boldsymbol{x} = \boldsymbol{e} \times \boldsymbol{x}$ for arbitrary $\boldsymbol{x} \in \mathbb{R}^3$. The skew-symmetric cross product matrix possesses the following properties for the arbitrary unit vector $\boldsymbol{u}$ [5]:

$$[\boldsymbol{u}\times]^2 = \boldsymbol{u}\boldsymbol{u}^T - \boldsymbol{I} \tag{2.21a}$$

$$[\boldsymbol{u}\times]^3 = -[\boldsymbol{u}\times] \tag{2.21b}$$

$$\text{tr}\,[\boldsymbol{u}\times] = 0 \tag{2.21c}$$

$$\text{tr}\,[\boldsymbol{u}\times]^2 = -2 \tag{2.21d}$$

$$a^n[\boldsymbol{u}\times]^n = [a\boldsymbol{u}\times]^n, \tag{2.21e}$$

where $[\boldsymbol{u}\times]^2 \triangleq [\boldsymbol{u}\times][\boldsymbol{u}\times]$, "tr" represents the trace operator, a is an arbitrary constant, and n is a positive integer.

Noting the definition of the skew-symmetric cross product matrix given in Eq. (2.20), as well as the property given in Eq. (2.21a), the relationship between the attitude matrix and the axis-angle attitude parameterization, given in Eq. (2.19), can now be expressed as

$$\boldsymbol{A}\boldsymbol{x}^I = \left(\boldsymbol{I} - \sin\theta[\boldsymbol{e}\times] + (1 - \cos\theta)\,[\boldsymbol{e}\times]^2\right)\boldsymbol{x}^I, \tag{2.22}$$

Because Eq. (2.22) must be valid for arbitrary $\boldsymbol{x}^I$, the attitude matrix is given in terms of the Euler axis and rotation angle about the Euler axis by

$$\boldsymbol{A} = \boldsymbol{I} - \sin\theta[\boldsymbol{e}\times] + (1 - \cos\theta)\,[\boldsymbol{e}\times]^2, \tag{2.23}$$

which defines the attitude matrix solely in terms of the Euler axis and rotation angle.

In order to find the Euler axis and rotation angle given the attitude matrix, the Euler axis is first found according to the eigenvector/eigenvalue decomposition defined by Eq. (2.13). The angle of rotation is then found by taking the trace of Eq. (2.23), which yields

$$\text{tr}\,\boldsymbol{A} = 3 + 2\,(1 - \cos\theta)\,, \tag{2.24}$$

where the properties of the skew-symmetric cross product matrix given in Eqs. (2.21c) and (2.21d) are exploited to arrive at this result. Equation (2.24) is then solved for θ to yield the rotation angle

about the Euler axis in terms of the attitude matrix as

$$\theta = \cos^{-1}\left(\frac{\operatorname{tr}\boldsymbol{A} - 1}{2}\right).$$

(2.25)

The solution to the eigenvalue problem posed by Eq. (2.13) and Eq. (2.25) define the Euler axis and rotation angle, respectively, solely in terms of the attitude matrix.

Reference [17] gives the axis-angle parameterization for sequential rotations about non-parallel Euler axes. Opposite rotations are given by changing the sign of *either* the Euler axis *or* the rotation angle, i.e., $\{\boldsymbol{e}, \theta\}$ and $\{-\boldsymbol{e}, \theta\}$ represent opposite rotations, as do $\{\boldsymbol{e}, \theta\}$ and $\{\boldsymbol{e}, -\theta\}$. If the sign of *both* the Euler axis *and* the rotation angle are changed, the rotation is unaffected, which can be observed by substituting $\{-\boldsymbol{e}, -\theta\}$ for $\{\boldsymbol{e}, \theta\}$ into Eq. (2.23). This shows the two-to-one nature of the axis-angle parameterization of attitude; two sets of the Euler axis and rotation angle parameters correspond to the same attitude matrix. Another important property of the axis-angle parameterization is apparent when $\theta = \pm\pi$. In this case $\{\boldsymbol{e}, \pm\pi\}$ and $\{-\boldsymbol{e}, \pm\pi\}$ represent equivalent rotations.

When quantifying one-dimensional attitude, the axis of rotation (which is the definition of the Euler axis) is known and fixed, and is typically taken to be $\boldsymbol{e} = \boldsymbol{u}_z^I \triangleq \boldsymbol{u}_z^B \triangleq [0 \ \ 0 \ \ 1]^T$. Therefore, Eq. (2.23) is specialized to one-dimensional attitude according to

$$\boldsymbol{A} = \boldsymbol{I} - \sin\theta \left[\begin{bmatrix} 0 \\ 0 \\ 1 \end{bmatrix}\times\right] + (1 - \cos\theta)\left[\begin{bmatrix} 0 \\ 0 \\ 1 \end{bmatrix}\times\right]^2,$$

which is simplified to yield

$$\boldsymbol{A} = \begin{bmatrix} \cos\theta & \sin\theta & 0 \\ -\sin\theta & \cos\theta & 0 \\ 0 & 0 & 1 \end{bmatrix}.$$

(2.26)

This result is further simplified by neglecting the third row and column of Eq. (2.26), similarly to Eq. (2.12), to yield

$$\boldsymbol{A} = \begin{bmatrix} \cos\theta & \sin\theta \\ -\sin\theta & \cos\theta \end{bmatrix},$$

(2.27)

which defines the attitude matrix representing one-dimensional attitude in terms of the rotation angle about the known axis of rotation. This shows that the attitude matrix quantifying one-dimensional attitude possesses a single degree-of-freedom, given by θ, which is expected because the attitude

matrix quantifying one-dimensional attitude motion exists in the special orthogonal group of dimension two.

      2.1.3. Rotation Vector. A three-parameter representation of the attitude matrix is born as the product of the Euler axis and the rotation angle about the Euler axis as

$$\boldsymbol{\theta} = \theta \boldsymbol{e} \,. \tag{2.28}$$

This attitude parameterization is known as the *rotation vector*. In order to find the attitude matrix in terms of the rotation vector, the $\sin \theta$ and $1 - \cos \theta$ terms in Eq. (2.23) are first replaced with their Taylor series expansions to yield [5]

$$\boldsymbol{A} = \boldsymbol{I} - \sum_{i=0}^{\infty} \frac{(-1)^i \, \theta^{2i+1}}{(2i+1)!} [\boldsymbol{e}\times] - \sum_{i=1}^{\infty} \frac{(-1)^i \, \theta^{2i}}{(2i)!} [\boldsymbol{e}\times]^2 \,. \tag{2.29}$$

Exploiting the property of the skew-symmetric cross product matrix given in Eq. (2.21b), Eq. (2.29) can be expressed as

$$\boldsymbol{A} = \boldsymbol{I} + \sum_{i=0}^{\infty} \frac{[-\theta\boldsymbol{e}\times]^{2i+1}}{(2i+1)!} + \sum_{i=1}^{\infty} \frac{[-\theta\boldsymbol{e}\times]^{2i}}{(2i)!} \,. \tag{2.30}$$

It is now apparent from Eq. (2.28) that the rotation vector is present in Eq. (2.30), which is now expressed explicitly using the rotation vector as

$$\boldsymbol{A} = \boldsymbol{I} + \sum_{i=0}^{\infty} \frac{[-\boldsymbol{\theta}\times]^{2i+1}}{(2i+1)!} + \sum_{i=1}^{\infty} \frac{[-\boldsymbol{\theta}\times]^{2i}}{(2i)!} \,.$$

The summations are now manipulated such that this can be simplified to yield

$$\boldsymbol{A} = \sum_{i=0}^{\infty} \frac{[-\boldsymbol{\theta}\times]^i}{i!} \triangleq \exp\left\{-[\boldsymbol{\theta}\times]\right\}, \tag{2.31}$$

where $\exp\left\{-[\boldsymbol{\theta}\times]\right\}$ represents the matrix exponential of $-[\boldsymbol{\theta}\times]$. Equation (2.31) defines the attitude matrix solely in terms of the rotation vector.

      In order to find the rotation vector in terms of the attitude matrix, the Euler axis and rotation angle are first found according to the solution to the eigenvalue problem posed by Eq. (2.13) and Eq. (2.25), respectively. Equation (2.28) is then used to find the rotation vector. In order to find the Euler axis and angle of rotation in terms of the rotation vector, first, the Euler axis is found, which is observed from Eq. (2.28) to be the unit vector representing the direction of the rotation vector,

and is given by

$$e = \frac{\theta}{||\theta||} \,.$$

(2.32)

Equation (2.32) shows that the Euler axis is undefined if $||\theta|| = 0$. This is not an issue, however, because this corresponds to a rotation angle of zero and $A = I$ in this case. Equation (2.28) shows that the rotation angle is defined according to

$$\theta = ||\theta|| \,.$$

(2.33)

Equations (2.32) and (2.33) define the Euler axis and rotation angle solely in terms of the rotation vector.

It is intuitive from Eq. (2.32) that θ and $-\theta$ represent opposite rotations since the Euler axis is negated. Because the rotation vector is a three-parameter representation of attitude, it possesses a singularity either in representing a certain attitude, or in its temporal evolution. The singularity of the rotation vector occurs when propagating the rotation vector. The norm of the rotation vector is constrained to be no greater than π because $\theta \in [-\pi, \pi)$. During propagation, if the magnitude of the rotation vector is equal to π and has a positive temporal derivative, then the rotation vector must instantaneously change sign because $\{e, \pm\pi\}$ and $\{-e, \pm\pi\}$ represent equivalent rotations. This discontinuity makes the rotation vector a poor choice to globally represent the attitude of a rigid body; however, it does not encounter this singularity when quantifying small rotations, making it a good choice to quantify small attitude errors.

When quantifying one-dimensional attitude, the axis of rotation (which is the definition of the Euler axis) is known and stationary, and is typically taken to be $e \triangleq [0 \ \ 0 \ \ 1]^T$. Because the rotation vector is the product of the Euler axis and rotation angle, it is an intuitive result that the norm of the rotation vector defines the angle of rotation about the known and fixed Euler axis. Because the norm of the rotation vector is defined as the rotation angle, as is shown in Eq. (2.33), it follows that the attitude matrix quantifying one-dimensional attitude for the axis-angle and rotation vector attitude parameterizations are identical, and is given by Eq. (2.27), where θ is defined by the norm of the rotation vector according to Eq. (2.33).

2.1.4. Attitude Quaternion. In 1840, Olinde Rodrigues introduced a four-parameter representation of a rotation in three dimensions, known as the *Euler-Rodrigues symmetric parameters*, *quaternion of rotation*, or simply *quaternion*. In 1843, Sir William Hamilton introduced the quaternion, which was developed as a new algebra and not as an attitude representation. Arthur Cayley connected the work of Rodrigues and Hamilton. Hamilton defined the quaternion as a hypercomplex

extension of a complex number according to

$$\bar{q} = q_4 + iq_1 + jq_2 + kq_3 \,, \tag{2.34}$$

where $i^2 = j^2 = k^2 = -1$, $ij = -ji = k$, $jk = -kj = i$, and $ki = -ik = j$, which shows that the attitude quaternion is given in terms of the basis $\{1, i, j, k\}$. When using the quaternion to represent rotations in three dimensions, it is more convenient to consider the attitude quaternion as a four-component unit "vector" according to

$$\bar{q} = \begin{bmatrix} \boldsymbol{q} \\ q \end{bmatrix} \in \mathbb{S}^3 \,,$$

where $\boldsymbol{q} \triangleq [q_1 \ q_2 \ q_3]^T$ and $q \triangleq q_4$ are the vector and scalar parts of the quaternion, respectively. $\mathbb{S}^s$ is used to represent the s-dimensional unit-hypersphere, which is defined by $\mathbb{S}^s \triangleq \{ \boldsymbol{z} \in \mathbb{R}^{s+1 \times s+1} : \boldsymbol{z}^T \boldsymbol{z} = 1 \}$; thus, $\mathbb{S}^3$ represents the 3-dimensional unit hypersphere. The existence of the attitude quaternion on the unit hypersphere stems from the fact that the quaternion is constrained to unit-length. In order to illustrate $\mathbb{S}^3$, first consider $\mathbb{S}^1$ and $\mathbb{S}^2$, which represent the unit-circle and unit-sphere, respectively. $\mathbb{S}^3$ extends the concept of the unit-sphere one dimension higher and, therefore, cannot easily be visualized.

Two important quaternion operations are multiplication and inversion, which are given for unit quaternions by [5]

$$\bar{q} \otimes \bar{p} = \begin{bmatrix} p\boldsymbol{q} + q\boldsymbol{p} - \boldsymbol{q} \times \boldsymbol{p} \\ qp - \boldsymbol{q} \cdot \boldsymbol{p} \end{bmatrix} = \begin{bmatrix} q\boldsymbol{I} - [\boldsymbol{q}\times] & \boldsymbol{q} \\ -\boldsymbol{q}^T & q \end{bmatrix} \boldsymbol{p}$$

and

$$\bar{q}^{-1} = \begin{bmatrix} -\boldsymbol{q} \\ q \end{bmatrix} \,,$$

respectively. Quaternion multiplication is not commutative, i.e. $\bar{q} \otimes \bar{p} \neq \bar{p} \otimes \bar{q}$ in general.

The attitude quaternion is arguably the most widely used attitude representation because it is globally nonsingular, and quaternion multiplication and inversion are used to represent sequential and opposite coordinate transformations, respectively. Sequential and opposite coordinate transformations, which are represented in terms of DCMs in Eqs. (2.5) and (2.9), are represented using their equivalent quaternion representations according to

$$\bar{q}_I^B = \bar{q}_C^B \otimes \bar{q}_I^C \,,$$

and

$$\bar{q}_B^I = \left[\bar{q}_I^B\right]^{-1},$$

respectively, where $\bar{q}_I^B$ is the attitude quaternion representing the coordinate transformation from the I to the B frame, and similarly for $\bar{q}_C^B$ and $\bar{q}_I^C$. The identity quaternion, which corresponds to the identity attitude matrix, is defined as

$$\bar{p} \triangleq \begin{bmatrix} \mathbf{0} \\ 1 \end{bmatrix}$$

and is the quaternion representing zero rotation, such that

$$\bar{q} = \bar{q} \otimes \bar{p} = \bar{p} \otimes \bar{q}$$
$$\bar{p} = \bar{q} \otimes \bar{q}^{-1} = \bar{q}^{-1} \otimes \bar{q}.$$

Using these relationships, the attitude error defined in Eq. (2.11) can be equivalently expressed using the quaternion representations of the corresponding attitude matrices according to

$$\delta\bar{q} = \bar{q} \otimes \hat{\bar{q}}^{-1},$$

where $\delta\bar{q}$ is the quaternion representation of δA and $\hat{\bar{q}}$ is the estimated attitude quaternion, which corresponds to $\hat{A}$. As the attitude estimation error approaches zero, the estimated attitude quaternion, $\hat{\bar{q}}$, approaches the true attitude quaternion, $\bar{q}$, and the quaternion representation of the attitude error, $\delta\bar{q}$, approaches the identity quaternion, $\bar{p}$.

In order to find the attitude matrix in terms of the attitude quaternion, it is first necessary to express the attitude quaternion in terms of its corresponding axis-angle attitude representation, which is given by

$$\bar{q} = \begin{bmatrix} q \\ q \end{bmatrix} = \begin{bmatrix} \sin\frac{\theta}{2}e \\ \cos\frac{\theta}{2} \end{bmatrix}. \tag{2.35}$$

The unit-norm constraint imposed on the attitude quaternion is evident in Eq. (2.35) due to trigonometric identities. It is also apparent in Eq. (2.35) that the attitude quaternion is a two-to-one attitude parameterization. Recall that the axis-angle pairs given by $\{e, \theta\}$ and $\{-e, -\theta\}$ represent equivalent rotations equivalent rotations given by the rotation vector θ. By substituting these axis angle pairs and their corresponding rotation vector into Eq. (2.35) and noting the even and odd symmetry of cosine and sine, respectively, it is apparent that $\bar{q}$ and $-\bar{q}$ quantify equivalent coordinate transformations.

The attitude matrix is now found in terms of the attitude quaternion by substituting the trigonometric identities

$$\sin \theta = 2 \sin \frac{\theta}{2} \cos \frac{\theta}{2}$$

$$1 - \cos \theta = 2 \sin^2 \frac{\theta}{2}$$

into Eq. (2.23), which yields [5]

$$\boldsymbol{A} = \boldsymbol{I} - 2 \sin \frac{\theta}{2} \cos \frac{\theta}{2} [\boldsymbol{e} \times] + 2 \sin^2 \frac{\theta}{2} [\boldsymbol{e} \times]^2 . \tag{2.36}$$

Noting the properties of the skew-symmetric cross product matrix given in Eq. (2.21e), Eq. (2.36) is now expressed as

$$\boldsymbol{A} = \boldsymbol{I} - 2 \cos \frac{\theta}{2} \left[\sin \frac{\theta}{2} \boldsymbol{e} \times \right] + 2 \left[\sin \frac{\theta}{2} \boldsymbol{e} \times \right]^2 . \tag{2.37}$$

Substituting the definition of the vector and scalar parts of the attitude quaternion in terms of the Euler axis and rotation angle, given in Eq. (2.35), into Eq. (2.37) yields

$$\boldsymbol{A} = \boldsymbol{I} - 2 q [\boldsymbol{q} \times] + 2 [\boldsymbol{q} \times]^2 , \tag{2.38}$$

which defines the attitude matrix solely in terms of the attitude quaternion.

The attitude quaternion can be found in terms of the attitude matrix by normalizing any one of the following four vectors [5, 6, 18]:

$$\begin{bmatrix} 1 + 2A_{11} - \operatorname{tr} \boldsymbol{A} \\ A_{12} + A_{21} \\ A_{13} + A_{31} \\ A_{23} - A_{32} \end{bmatrix} = 4 q_1 \bar{\boldsymbol{q}} \tag{2.39a}$$

$$\begin{bmatrix} A_{21} + A_{12} \\ 1 + 2A_{22} - \operatorname{tr} \boldsymbol{A} \\ A_{23} + A_{32} \\ A_{31} - A_{13} \end{bmatrix} = 4 q_2 \bar{\boldsymbol{q}} \tag{2.39b}$$

$$\begin{bmatrix} A_{31} + A_{13} \\ A_{32} + A_{23} \\ 1 + 2A_{33} - \operatorname{tr} \boldsymbol{A} \\ A_{12} - A_{21} \end{bmatrix} = 4 q_3 \bar{\boldsymbol{q}} \tag{2.39c}$$

$$\begin{bmatrix} A_{23} - A_{32} \\ A_{31} - A_{13} \\ A_{12} - A_{21} \\ 1 + \text{tr}\,\boldsymbol{A} \end{bmatrix} = 4q\bar{\boldsymbol{q}}\,. \tag{2.39d}$$

The vector with the largest norm should be used to find the attitude quaternion from the attitude matrix in order to minimize the numerical error. In order to find the vector with the largest norm without having to compute all four norms, first, the largest of A_{11}, A_{22}, A_{33}, and $\text{tr}\,\boldsymbol{A}$ is found. Next, Eq. (2.39a), (2.39b), (2.39c), or (2.39d) is used depending on whether A_{11}, A_{22}, A_{33}, or $\text{tr}\,\boldsymbol{A}$ is the largest, respectively.

In order to find the Euler axis and rotation angle in terms of the attitude quaternion, the system of equations relating the vector and scalar parts of the quaternion to the Euler axis and rotation angle, defined by Eq. (2.35), is solved for the Euler axis and rotation angle. This defines the Euler axis and rotation angle in terms of the attitude quaternion as

$$\boldsymbol{e} = \csc\frac{\theta}{2}\,\boldsymbol{q}$$

and

$$\theta = 2\arccos q\,,$$

respectively. After finding the Euler axis and angle of rotation in terms of the attitude quaternion, Eq. (2.28) is used to find the rotation vector in terms of the attitude quaternion according to

$$\boldsymbol{\theta} = \frac{2\arccos q}{(1-q^2)^{\frac{1}{2}}}\boldsymbol{q}\,. \tag{2.40}$$

In order to find the attitude quaternion in terms of the rotation vector, Eqs. (2.13) and (2.25) are substituted into Eq. (2.35) to yield

$$\bar{\boldsymbol{q}} = \begin{bmatrix} \sin\frac{\|\boldsymbol{\theta}\|}{2}\frac{\boldsymbol{\theta}}{\|\boldsymbol{\theta}\|} \\ \cos\frac{\|\boldsymbol{\theta}\|}{2} \end{bmatrix}\,.$$

The relationships presented in this subsection between the attitude quaternion and the attitude matrix, Euler axis and rotation angle, and rotation vector are exploited when necessary in later sections.

When quantifying one-dimensional attitude, the Euler axis is known and stationary, and is typically taken to be $\boldsymbol{e} \triangleq [0\ 0\ 1]^T$. Therefore, for one-dimensional attitude, Eq. (2.35) is specialized

to one-dimensional attitude according to

$$\bar{q} = \begin{bmatrix} 0 \\ 0 \\ \sin\frac{\theta}{2} \\ \cos\frac{\theta}{2} \end{bmatrix} \triangleq \begin{bmatrix} 0 \\ 0 \\ q_z \\ q \end{bmatrix} \in \mathbb{S}^1 . \tag{2.41}$$

Equation (2.41) is typically simplified because the first two zeros are constant in order to yield the attitude quaternion quantifying one-dimensional attitude as

$$\bar{q} = \begin{bmatrix} \sin\frac{\theta}{2} \\ \cos\frac{\theta}{2} \end{bmatrix} \triangleq \begin{bmatrix} q_z \\ q \end{bmatrix} \in \mathbb{S}^1 . \tag{2.42}$$

In order to find the attitude matrix quantifying one-dimensional attitude, Eq. (2.41) is substituted into Eq. (2.38) to yield

$$A = \begin{bmatrix} 1 - 2q_z^2 & 2qq_z & 0 \\ -2qq_z & 1 - 2q_z^2 & 0 \\ 0 & 0 & 1 \end{bmatrix} . \tag{2.43}$$

This result is further simplified by neglecting the third row and column of Eq. (2.43), similarly to Eq. (2.12), to yield

$$A = \begin{bmatrix} 1 - 2q_z^2 & 2qq_z \\ -2qq_z & 1 - 2q_z^2 \end{bmatrix} .$$

2.2. QUATERNION KINEMATICS

The temporal evolution of the attitude quaternion representing the rotation from the I frame to the B frame is given by [5, 7]

$$\dot{\bar{q}}_I^B = \frac{1}{2}\bar{\omega}_{B/I}^B \otimes \bar{q}_I^B , \tag{2.44}$$

where $\bar{\omega}_{B/I}^B$ is the angular velocity vector of the B frame with respect to the I frame expressed in the B frame, expressed as a pure quaternion. A pure quaternion is a quaternion with the scalar component equal to zero and is constructed from the angular velocity vector according to

$$\bar{\omega}_{B/I}^B = \begin{bmatrix} \omega_{B/I}^B \\ 0 \end{bmatrix} .$$

The angular velocity is defined as the instantaneous time rate of change of the rotation vector representing the rotation from the I frame to the B frame, expressed in the B frame, which is denoted by $[\boldsymbol{\theta}_I^B]^B$. Therefore, the angular velocity is defined by

$$\boldsymbol{\omega}_{B/I}^B(t) = \lim_{\Delta t \to 0} \frac{[\boldsymbol{\theta}_I^B]^B(t + \Delta t) - [\boldsymbol{\theta}_I^B]^B(t)}{\Delta t}, \qquad (2.45)$$

where the explicit dependence on time is denoted for clarity. In general, rotation vectors cannot be added or subtracted in order to quantify sequential rotations; however, because the limit as Δt approaches zero is taken in Eq. (2.45), $[\boldsymbol{\theta}_I^B]^B(t + \Delta t)$ approaches $[\boldsymbol{\theta}_I^B]^B(t)$, and, therefore, the subtraction is valid in the limit sense.

Equation (2.44) represents the kinematic relationship between the attitude quaternion and the angular velocity of a body, which defines the temporal evolution of the attitude quaternion. No restrictions on the I and B frames are made in order for this kinematic relationship to be valid. This is the rotational equivalent of the kinematic relationship between translational position and velocity, which defines the temporal evolution of the translational position.

2.3. ATTITUDE DYNAMICS

The temporal evolution of the angular velocity defined in Eq. (2.45) is given by [5, 7]

$$\boldsymbol{J}^B \dot{\boldsymbol{\omega}}_{B/I}^B = \boldsymbol{\tau}^B - \boldsymbol{\omega}_{B/I}^B \times \boldsymbol{J}^B \boldsymbol{\omega}_{B/I}^B, \qquad (2.46)$$

where $\boldsymbol{J}^B$ is the inertia tensor of the rigid body about the center of mass and $\boldsymbol{\tau}^B$ is the external torque acting on the rigid body relative to the center of mass, both expressed in the B frame. In deriving Eq. (2.46), it is assumed that the I frame is an inertial frame. This assumption can be relaxed to yield a similar expression to Eq. (2.46) if I is not an inertial frame. In the remainder of this work, the I frame is restricted to be an inertial frame.

Equation (2.46) represents the dynamic relationship relating the temporal evolution of the angular velocity to the inertia tensor of the rigid body and the net external torque acting on the rigid body. This relationship is analogous to the dynamic relationship relating the temporal evolution of the translational velocity to the mass and net external force acting on the rigid body.

2.4. ORIENTATION

Euler's theorem, which states that an arbitrary rotation in three dimensions can be accomplished by a single rotation about a fixed axis, is now generalized to spaces of arbitrary dimension,

in which case the concept of orientation (instead of rotation) is born [15, 16]. In three dimensions, the concept of rotation and orientation are one-in-the-same; however, in dimensions greater than three, the concepts of rotation and orientation diverge. Euler's theorem extended to r-dimensional space states that $\lfloor \frac{r}{2} \rfloor$ rotations are necessary to construct an orientation, in general. In order to differentiate the concepts of rotation and orientation, $\boldsymbol{R}$ and $\boldsymbol{M}$ are used to represent rotation and orientation matrices, respectively.

Before defining the orientation matrix, it is first necessary to extend the idea of a vector expressed in a right-handed, orthonormal coordinate frame in three dimensions, defined by Eqs. (2.2) and (2.3), to spaces of arbitrary dimension. In r dimensions, the r-vector $\boldsymbol{x}$ expressed in terms of the I basis, denoted by $\boldsymbol{x}^I$, is given by

$$\boldsymbol{x}^I \triangleq \begin{bmatrix} x_1 \\ x_2 \\ \vdots \\ x_r \end{bmatrix} = x_1 \boldsymbol{u}_1^I + x_2 \boldsymbol{u}_2^I + \ldots + x_r \boldsymbol{u}_r^I \,,$$

where the I basis is denoted by $\{\boldsymbol{u}_{1:r}^I\}$ and is defined as

$$\{\boldsymbol{u}_{1:r}^I\} \triangleq \{\boldsymbol{u}_1^I, \boldsymbol{u}_2^I, \ldots, \boldsymbol{u}_r^I\} \,.$$

The I basis is assumed right-handed and orthonormal, which means it possesses the following properties:

$$\det \{[\boldsymbol{u}_1^I | \boldsymbol{u}_2^I | \ldots | \boldsymbol{u}_r^I]\} = 1$$

$$\boldsymbol{u}_i^I \cdot \boldsymbol{u}_j^I = \begin{cases} 1 \,, & \text{if } i = j \\ 0 \,, & \text{if } i \neq j \end{cases} \quad \forall \ i, j = 1, 2, \ldots, r \,,$$

where $[\boldsymbol{u}_1^I | \boldsymbol{u}_2^I | \ldots | \boldsymbol{u}_r^I]$ represents the concatenation of the vectors $\boldsymbol{u}_1^I$, $\boldsymbol{u}_2^I$, and $\boldsymbol{u}_r^I$ to form a square matrix of dimension r. The r-vector $\boldsymbol{x}$ expressed in terms of the B basis, $\boldsymbol{x}^B$ is defined in a similar manner. If $r = 3$, the definition of a right-handed, orthonormal basis simplifies to the definition of a right-handed, orthonormal coordinate frame given in Eqs. (2.2) and (2.3), as expected.

Now that the concept of a basis has been defined for arbitrary dimension, the orientation matrix relating the I and B bases is defined according to

$$\boldsymbol{x}^B = \boldsymbol{M}_I^B \boldsymbol{x}^I \,, \tag{2.47}$$

where $\boldsymbol{x}^B$ and $\boldsymbol{x}^I$ denote the vector $\boldsymbol{x} \in \mathbb{R}^r$ expressed in the B and I bases, respectively. Orientation matrices exist in the special orthogonal group of dimension r, i.e., $\boldsymbol{M}_I^B \in \mathrm{SO}(r)$. Because of this, the inverse of the orientation matrix is given by its transpose according to

$$\boldsymbol{M}^{-1} = \boldsymbol{M}^T .$$

Furthermore, through the definition of the orientation matrix given in Eq. (2.47), it can be shown that sequential orientations can be applied according to

$$\boldsymbol{x}^B = \boldsymbol{M}_C^B \boldsymbol{x}^C = \boldsymbol{M}_C^B \underbrace{\boldsymbol{M}_I^C \boldsymbol{x}^I}_{\boldsymbol{x}^C} , \tag{2.48}$$

where the C basis is an arbitrary, intermediate basis. Equating Eqs. (2.47) and (2.48) shows the property of orientation matrices to compose orientations by multiplying the matrices according to

$$\boldsymbol{M}_I^B = \boldsymbol{M}_C^B \boldsymbol{M}_I^C .$$

The properties of orientations are equivalent to the properties of the DCM in three dimensions, which stems from the fact that a DCM in three dimensions is itself, an orientation matrix, because only one rotation is necessary to quantify an orientation in three dimensions.

Euler's theorem is extended to r-dimensional space [15], in which case a minimum of $\lfloor \frac{r}{2} \rfloor$ rotations in orthogonal planes is necessary to describe an arbitrary orientation. In this case, the orientation matrix is defined by the product of $\lfloor \frac{r}{2} \rfloor$ orthogonal rotations according to

$$\boldsymbol{M} = \prod_{i=1}^{\lfloor \frac{r}{2} \rfloor} \boldsymbol{R}(\boldsymbol{P}_i, \phi_i) , \tag{2.49}$$

where $\boldsymbol{R}(\boldsymbol{P}, \phi)$ represents the rotation matrix defined by the rotation of magnitude ϕ performed in the plane defined by $\boldsymbol{P}$. In order to define the plane of rotation, the matrix $\boldsymbol{P}$ is constructed according to

$$\boldsymbol{P} = [\boldsymbol{p}_1 | \boldsymbol{p}_2] ,$$

where $\boldsymbol{p}_1$ and $\boldsymbol{p}_2$ are orthogonal unit r-vectors that lie in the plane of rotation, $\boldsymbol{p}_1$ defines zero rotation, and $\boldsymbol{p}_2$ defines the direction of the rotation. The rotation matrix is now given in terms of the plane of rotation and the magnitude of the rotation in this plane according to

$$\boldsymbol{R}(\boldsymbol{P}, \phi) = \boldsymbol{I} + (\cos \phi - 1) \boldsymbol{P} \boldsymbol{P}^T + \boldsymbol{P} \boldsymbol{J}_2 \boldsymbol{P}^T \sin \phi ,$$

where $\boldsymbol{J}_2$ is the 2×2 symplectic matrix defined by

$$\boldsymbol{J}_2 = \begin{bmatrix} 0 & -1 \\ 1 & 0 \end{bmatrix}.$$

Equation (2.49) defines the orientation matrix in terms of its elementary orthogonal planes of rotation and the magnitudes of the rotations in these planes. Because the planes of rotation are restricted to be orthogonal for the validity of Eq. (2.49), the order in which the elementary rotations used to construct the orientation matrix is arbitrary.

In practice, parameterizing these planes of rotation and their corresponding angles of rotation in each plane in order to construct the orientation matrix can be difficult due to the constraints imposed on these parameters. A minimum of $r(r-1)/2$ parameters are necessary to specify an orientation in r-dimensional space [16]; however, $\lfloor \frac{r}{2} \rfloor (2r+1)$ parameters are required to specify the planes of rotation and their corresponding angles of rotation directly. For example, in four- and five-dimensional space, six and ten parameters are the minimum number of parameters necessary to specify an orientation, respectively, but 18 and 33 parameters are necessary to specify the planes of rotation and their corresponding angles of rotation, respectively. This implies that 12 and 23 constraints must be satisfied for four- and five-dimensional space in order to correctly parameterize the planes of rotation and their corresponding angles of rotation.

In this work, it is only necessary to construct an orientation matrix in four-dimensional space. In order to construct the orientation matrix without directly specifying the two planes of rotation and their corresponding angles of rotation, the orientation matrix is specified in terms of its elemental left- and right-isoclonic rotations [19]. In order to define the left- and right-isoclonic rotations, first note that a basis can be found such that an arbitrary rotation matrix in four dimensions can be expressed in that basis according to [20]

$$\boldsymbol{R} = \begin{bmatrix} \cos \alpha_1 & -\sin \alpha_1 & 0 & 0 \\ \sin \alpha_1 & \cos \alpha_1 & 0 & 0 \\ 0 & 0 & \cos \alpha_2 & -\sin \alpha_2 \\ 0 & 0 & \sin \alpha_2 & \cos \alpha_2 \end{bmatrix}. \tag{2.50}$$

If $\alpha_1 = \pm \alpha_2$, then this rotation matrix defines an *isoclonic* rotation. Furthermore, if $\alpha_1 = \alpha_2$, the rotation is defined as a *right-isoclonic* rotation, and if $\alpha_1 = -\alpha_2$, the rotation is defined as a *left-isoclonic* rotation. The rotation matrices representing these left- and right-isoclonic rotations

can be expressed as

$$
\boldsymbol{R}_L = \begin{bmatrix} \ell_0 & -\ell_3 & \ell_2 & -\ell_1 \\ \ell_3 & \ell_0 & -\ell_1 & -\ell_2 \\ -\ell_2 & \ell_1 & \ell_0 & -\ell_3 \\ \ell_1 & \ell_2 & \ell_3 & \ell_0 \end{bmatrix}
\tag{2.51}
$$

and

$$
\boldsymbol{R}_R = \begin{bmatrix} r_0 & -r_3 & r_2 & r_1 \\ r_3 & r_0 & -r_1 & r_2 \\ -r_2 & r_1 & r_0 & r_3 \\ -r_1 & -r_2 & -r_3 & r_0 \end{bmatrix},
\tag{2.52}
$$

respectively, where $\ell_0^2 + \ell_1^2 + \ell_2^2 + \ell_3^2 = 1$ and $r_0^2 + r_1^2 + r_2^2 + r_3^2 = 1$. The zeros present in the elements of Eq. (2.50) are not present in Eqs. (2.51) and (2.52), even though they all represent isoclonic rotations. This is because Eqs. (2.51) and (2.52) are expressed in an arbitrary basis, and not in the basis that results in the zero elements observed in Eq. (2.50). In order for a rotation to be isoclonic, it is only necessary that a basis *exists* such that the matrix representing the rotation can be expressed in this basis in the form in Eq. (2.50); it is not required that the rotation has to be expressed in this basis.

It is now noted that $\boldsymbol{R}_L$ and $\boldsymbol{R}_R$ can be expressed in terms of the bases $\{\boldsymbol{I}, \boldsymbol{A}_1, \boldsymbol{A}_2, \boldsymbol{A}_3\}$ and $\{\boldsymbol{I}, \boldsymbol{B}_1, \boldsymbol{B}_2, \boldsymbol{B}_3\}$, respectively, according to

$$
\boldsymbol{R}_L = \ell_0 \boldsymbol{I} + \ell_1 \boldsymbol{A}_1 + \ell_2 \boldsymbol{A}_2 + \ell_3 \boldsymbol{A}_3
$$
$$
\boldsymbol{R}_R = r_0 \boldsymbol{I} + r_1 \boldsymbol{B}_1 + r_2 \boldsymbol{B}_2 + r_3 \boldsymbol{B}_3,
$$

where

$$
\boldsymbol{A}_1 = \begin{bmatrix} 0 & 0 & 0 & -1 \\ 0 & 0 & -1 & 0 \\ 0 & 1 & 0 & 0 \\ 1 & 0 & 0 & 0 \end{bmatrix} \quad
\boldsymbol{A}_2 = \begin{bmatrix} 0 & 0 & 1 & 0 \\ 0 & 0 & 0 & -1 \\ -1 & 0 & 0 & 0 \\ 0 & 1 & 0 & 0 \end{bmatrix} \quad
\boldsymbol{A}_3 = \begin{bmatrix} 0 & -1 & 0 & 0 \\ 1 & 0 & 0 & 0 \\ 0 & 0 & 0 & -1 \\ 0 & 0 & 1 & 0 \end{bmatrix}
$$

$$
\boldsymbol{B}_1 = \begin{bmatrix} 0 & 0 & 0 & 1 \\ 0 & 0 & -1 & 0 \\ 0 & 1 & 0 & 0 \\ -1 & 0 & 0 & 0 \end{bmatrix} \quad
\boldsymbol{B}_2 = \begin{bmatrix} 0 & 0 & 1 & 0 \\ 0 & 0 & 0 & 1 \\ -1 & 0 & 0 & 0 \\ 0 & -1 & 0 & 0 \end{bmatrix} \quad
\boldsymbol{B}_3 = \begin{bmatrix} 0 & -1 & 0 & 0 \\ 1 & 0 & 0 & 0 \\ 0 & 0 & 0 & 1 \\ 0 & 0 & -1 & 0 \end{bmatrix}.
$$

These bases satisfy the properties that

$$A_1^2 = A_2^2 = A_3^2 = -I$$
$$A_1 A_2 = -A_2 A_1 = A_3$$
$$A_2 A_3 = -A_3 A_2 = A_1$$
$$A_3 A_1 = -A_1 A_3 = A_2$$

and

$$B_1^2 = B_2^2 = B_3^2 = -I$$
$$B_1 B_2 = -B_2 B_1 = B_3$$
$$B_2 B_3 = -B_3 B_2 = B_1$$
$$B_3 B_1 = -B_1 B_3 = B_2,$$

which are observed to be the same properties that the basis for the attitude quaternion, given in Eq. (2.34), satisfy. Because of this, the rotation matrices representing left- and right-isoclonic rotations can be equivalently specified in terms of the attitude quaternion according to

$$R_L = \begin{bmatrix} q & -q_z & q_y & -q_x \\ q_z & q & -q_x & -q_y \\ -q_y & q_x & q & -q_z \\ q_x & q_y & q_z & q \end{bmatrix} \tag{2.53}$$

and

$$R_R = \begin{bmatrix} q & -q_z & q_y & q_x \\ q_z & q & -q_x & q_y \\ -q_y & q_x & q & q_z \\ -q_x & -q_y & -q_z & q \end{bmatrix}. \tag{2.54}$$

It is important to note that the quaternion parameterizations of the left- and right-isoclonic rotations satisfy the $\ell_0^2 + \ell_1^2 + \ell_2^2 + \ell_3^2 = 1$ and $r_0^2 + r_1^2 + r_2^2 + r_3^2 = 1$ constraints. The orientation matrix is then constructed from the left- and right-isoclonic rotation matrices according to

$$M = R_L R_R = R_R R_L. \tag{2.55}$$

If two attitude quaternions are specified, one to define each of the left- and right-isoclonic rotations, eight parameters are necessary to specify the orientation matrix; thus, two constraints must be satisfied, which is apparent because the attitude quaternion is constrained to be unit-norm. In order to parameterize the orientation matrix by a minimum parameter set, each of the attitude quaternions is first parameterized by a rotation vector. In this case, the orientation matrix is parameterized by six parameters in total, i.e, three parameters for each of the two rotation vectors.

3. PROBABILITY DENSITY FUNCTIONS

The pdf of a continuous random variable contains all of the statistical information about the random variable. In order to define the pdf for a continuous random variable, it is first necessary to define its probability distribution function (or cumulative density function to some) according to

$$F(x) = \Pr\left(\mathrm{x} < x\right),$$

where x is a realization of the random variable x. The probability distribution function of x is nondecreasing and exists on the interval $[0, 1]$. Furthermore, the probability distribution function satisfies $F(-\infty) = 0$ and $F(\infty) = 1$. The pdf of x is then defined in terms of the probability distribution function according to

$$p(x) = \frac{\mathrm{d}F(x)}{\mathrm{d}x}.$$

From the definition of the derivative, the pdf can be expressed as

$$p(x) = \lim_{\mathrm{d}x \to 0} \frac{F(x + \mathrm{d}x) - F(x)}{\mathrm{d}x} = \lim_{\mathrm{d}x \to 0} \frac{\Pr\left(x < \mathrm{x} < x + \mathrm{d}x\right)}{\mathrm{d}x}, \tag{3.1}$$

and thus, it is apparent that the probability *density* function quantifies the density of the probability that x takes place in the infinitesimally small region surrounding x.

The inverse relationship between the probability distribution function and the pdf is given according to

$$F(x) = \int_{-\infty}^{x} p(u) \, \mathrm{d}u,$$

and therefore

$$F(\infty) = \int_{-\infty}^{\infty} p(u) \, \mathrm{d}u = 1,$$

which shows that the pdf must integrate to unity over the support of x, that is, all regions such that $p(x) \neq 0$. This is an important property of pdfs, and stems from the fact that the probability of any x happening in the support of x must be unity, which is an intuitive result because x is a realization of x.

Now, consider the joint probability distribution function of two random variables, defined as

$$F(x, y) = \Pr(\mathrm{x} < x, \mathrm{y} < y),$$

where y is a realization of the random variable y. The joint pdf is then given by

$$p(x, y) = \frac{\delta^2 F(x, y)}{\delta x \delta y}. \tag{3.2}$$

The *marginal* probability distribution function of x is given by

$$F_x(x) = F(x, \infty),$$

which yields the marginal pdf of x to be given by

$$p_x(x) = \int_{-\infty}^{\infty} p(x, y) \, \mathrm{d}y \, ;$$

that is, the pdf of x if y is "integrated out." If the probability distribution function of x and y is equal to the product of the marginal pdfs of x and y, that is

$$F(x, y) = F_x(x) F_y(y), \tag{3.3}$$

then x and y are said to be *independent*. If x and y are independent, the probability that $\mathrm{x} < x$ does not depend on the probability that $\mathrm{y} < y$. Substituting Eq. (3.3) into Eq. (3.2) and simplifying yields

$$p(x, y) = \frac{\delta^2 F_x(x) F_y(y)}{\delta x \delta y} = \frac{\delta F_x(x)}{\delta x} \frac{\delta F_y(y)}{\delta y} = p_x(x) p_y(y),$$

which shows that, if x and y are independent, then the joint pdf of x and y is equivalent to the product of the marginal pdfs of x and y. This is another important property of pdfs, and will be exploited in certain applications.

The probability distribution and density functions can be extended to vector quantities. Consider the random vector $\boldsymbol{x} = \begin{bmatrix} x_1 & x_2 & \cdots & x_r \end{bmatrix}^T$, and a realization of this vector, $\mathrm{x} = \begin{bmatrix} \mathrm{x}_1 & \mathrm{x}_2 & \cdots & \mathrm{x}_r \end{bmatrix}^T$. The probability distribution function of $\boldsymbol{x}$ is simply the joint probability distribution function of $x_1, x_2, \ldots, x_r$; that is,

$$F(\boldsymbol{x}) = \Pr(\mathrm{x}_1 < x_1, \mathrm{x}_2 < x_2, \cdots, \mathrm{x}_r < x_r).$$

The pdf of x is then found according to

$$p(\boldsymbol{x}) = \frac{\delta^r F(\boldsymbol{x})}{\delta x_1 \delta x_2 \cdots \delta x_r}.$$

Using the definition of the partial derivatives (in a similar fashion to Eq. (3.1)), it can be shown that the pdf of x quantifies the density of the probability that $\mathbf{x}$ takes place in the infinitesimally small region surrounding x.

In this chapter, first the Gaussian and GM densities, which are established and well-studied pdfs, are introduced. These densities probabilistically quantify a vector that exists in Euclidean (additive and unbounded) space. Next, the Bingham density, as well as its efficacy to probabilistically quantify the attitude quaternion on its natural manifold, the unit-hypersphere, is presented. The BM density is then developed, including methods to approximate a nonuniform Bingham density on the unit circle and a uniform Bingham density on the unit-hypersphere with a BM density. Next, the Gauss-Bingham and Bingham-Gauss densities are developed, which probabilistically quantify the joint density of a vector in Euclidean space and the attitude quaternion. Finally, the BGM density is developed, including a method to approximate a Bingham-Gauss density with a BGM density. Note that the remainder of this chapter uses $\mathbf{x}$ or $\mathbf{z}$ to denote a vector that exists in Euclidean space, $\bar{\boldsymbol{q}}$ or $\bar{\boldsymbol{p}}$ to denote a unit-vector (that is equivalent to the attitude quaternion under certain conditions), and $\boldsymbol{x} = [\bar{\boldsymbol{q}}^T \ \mathbf{x}^T]^T$ or $\boldsymbol{z} = [\bar{\boldsymbol{p}}^T \ \mathbf{z}^T]^T$ to denote the concatenation of a unit-vector and a vector in Euclidean space; these quantities are not to be confused with the notation used in the introductory material of this chapter introducing the properties of the pdf.

3.1. GAUSSIAN DENSITY

The well-known Gaussian density is given for a random vector $\mathbf{x} \in \mathbb{R}^r$ by

$$p_g(\mathbf{x}; \boldsymbol{m}, \boldsymbol{P}) = \det\left\{2\pi\boldsymbol{P}\right\}^{-\frac{1}{2}} \exp\left\{-\tfrac{1}{2}(\mathbf{x} - \boldsymbol{m})^T \boldsymbol{P}^{-1}(\mathbf{x} - \boldsymbol{m})\right\}, \tag{3.4}$$

where $\boldsymbol{m} \in \mathbb{R}^r$ is the mean and $\boldsymbol{P} = \boldsymbol{P}^T > \mathbf{0} \in \mathbb{R}^{r \times r}$ is the covariance of the Gaussian density. The Gaussian density is a two-parameter density in the exponential family and is parameterized directly by its first moment (mean), and its second central moment (covariance). The mean and covariance of the Gaussian density are formally defined as

$$\boldsymbol{m} = \mathrm{E}_{p_g}\{\mathbf{x}\}$$
$$\boldsymbol{P} = \mathrm{E}_{p_g}\left\{(\mathbf{x} - \boldsymbol{m})(\mathbf{x} - \boldsymbol{m})^T\right\},$$

where the expected value is defined for the arbitrary, (potentially) nonlinear function $\boldsymbol{g}(\mathbf{x})$ with respect to the arbitrary pdf $p(\mathbf{x})$ as

$$\mathrm{E}_p\{\boldsymbol{g}(\mathbf{x})\} = \int_{\boldsymbol{\Omega}} \boldsymbol{g}(\mathbf{x}) p(\mathbf{x}) \mathrm{d}\mathbf{x}, \tag{3.5}$$

and $\boldsymbol{\Omega}$ is the support of $p(\mathbf{x})$, which is defined by all regions of $\mathbf{x}$ such that $(\mathbf{x}) \neq 0$. The support of the Gaussian density is $\mathbb{R}^r$; thus, it is not restricted to a given interval and can only be used to rigorously quantify states that are not restricted to a given interval (unbounded).

The standard normal density, which is denoted as the canonical Gaussian density for consistent nomenclature with the canonical form of other densities, is introduced by substituting the transformation

$$\mathbf{x} = \boldsymbol{S}\mathbf{z} + \boldsymbol{m} \tag{3.6}$$

into Eq. (3.4), which yields the canonical Gaussian density as

$$\tilde{p}_g(\mathbf{z}) \triangleq p_g(\mathbf{z}; \boldsymbol{0}, \boldsymbol{I}) = (2\pi)^{-\frac{r}{2}} \exp\left\{-\tfrac{1}{2}\mathbf{z}^T\mathbf{z}\right\},$$

where the tilde notation is used to denote the canonical form of the density. In Eq. (3.6), $\boldsymbol{S}$ is defined as the Cholesky factor of $\boldsymbol{P}$ according to

$$\boldsymbol{S}\boldsymbol{S}^T \triangleq \boldsymbol{P}.$$

Through the change of variables defined in Eq. (3.6), the canonical Gaussian density becomes zero-mean and possesses identity covariance; thus, the elements of the canonical Gaussian variable, $\mathbf{z}$, are independent. Certain operations can be performed for the canonical Gaussian density, and the results of these operations can then be transformed according to the change of variables defined by Eq. (3.6) to represent the Gaussian density of interest. In some cases, this allows these operations to be performed off-line and saved for the standard normal density, and the saved result can be transformed to the Gaussian density of interest when needed to reduce computational expense.

3.2. GAUSSIAN MIXTURE DENSITY

The GM density is defined by [21]

$$p_{gm}(\mathbf{x}) = \sum_{\ell=1}^{L} w^{(\ell)} p_g\left(\mathbf{x}; \boldsymbol{m}^{(\ell)}, \boldsymbol{P}^{(\ell)}\right), \tag{3.7}$$

where $w^{(\ell)}$ is the weight of the ℓth component, $\boldsymbol{m}^{(\ell)}$ and $\boldsymbol{P}^{(\ell)}$ are the mean and covariance defining the ℓth component, respectively, and L is the number of components in the GM. The weights of the mixture are constrained such that

$$w^{(\ell)} > 0 \quad \forall \quad \ell = 1, 2, \ldots, L \qquad \text{and} \qquad \sum_{\ell=1}^{L} w^{(\ell)} = 1,$$

which ensures that the GM is a valid pdf.

The GM density can be used to approximate arbitrary pdfs in Euclidean space. In fact, if the pdf to approximate is "defined and continuous at all but a finite number of locations," the GM approximation of this pdf converges uniformly as the number of components in the mixture increase [21]. This result implies that a GM density can be used to approximate many pdfs of practical concern.

In this work, the approximation of a Gaussian density by a GM density is considered. This approximation is considered in References [22, 23], among others. While the Gaussian density can be equivalently expressed as a single-component GM density, it is advantageous in certain applications to approximate the Gaussian density by a GM density with more than one component. By approximating the Gaussian density in this way, the covariance of each component of the approximating GM density is smaller than the Gaussian density, in general. In order to find the GM approximation of a Gaussian density, first, the GM approximation of the canonical density is found. The parameters of the GM approximation of the canonical Gaussian density are then transformed according to the change of variables defined in Eq. (3.6) in order to approximate the Gaussian density of interest. Let the GM density approximating the canonical Gaussian density be defined by

$$p_{gm}(\mathbf{z}) = \sum_{\ell=1}^{L} \tilde{w}^{(\ell)} \, p_g\left(\mathbf{z}; \tilde{\boldsymbol{m}}^{(\ell)}, \widetilde{\boldsymbol{P}}^{(\ell)}\right), \tag{3.8}$$

where the tilde notation indicates that these parameters correspond to the GM approximating the *canonical* Gaussian density. Ideally, $\tilde{w}^{(\ell)}$, $\tilde{\boldsymbol{m}}^{(\ell)}$, and $\widetilde{\boldsymbol{P}}^{(\ell)}$ for $\ell = 1, 2, \ldots, L$ would be found for a given L such that a given measure of the difference between the canonical Gaussian density and its approximating GM density is minimized. The L_2 distance between the canonical Gaussian density and its approximating GM density is used as this measure, and is given by

$$L_2[\tilde{p}_g || p_{gm}] = \int_{\mathbb{R}^r} \left[\tilde{p}_g(\boldsymbol{\zeta}) - p_{gm}(\boldsymbol{\zeta})\right]^2 \mathrm{d}\boldsymbol{\zeta}. \tag{3.9}$$

This L_2 distance can be manipulated into a closed form, as is shown in Appendix A.

In general, finding $\tilde{w}^{(\ell)}$, $\tilde{\boldsymbol{m}}^{(\ell)}$, and $\widetilde{\boldsymbol{P}}^{(\ell)}$ for $\ell = 1, 2, \ldots, L$ that minimize Eq. (3.9) without first making simplifications becomes intractable, especially as the number of components in the

mixture increases. In order to simplify this minimization problem, first, it is noted that the elements of the canonical Gaussian-distributed variable, $\mathbf{z}$, are independent and uncorrelated. This allows the canonical Gaussian density to be expressed as the product of the canonical Gaussian-distributed scalar elements of $\mathbf{z} \triangleq [z_1 \ z_2 \ \cdots \ z_r]^T$ according to

$$\tilde{p}_g(\mathbf{z}) = \prod_{i=1}^{r} \tilde{p}_g(z_i) \,.$$

Because of this, the problem of approximating the multivariate canonical Gaussian density with a GM density in r dimensions reduces to the approximation of r scalar canonical Gaussian densities by a scalar GM density. This allows Eq. (3.8) to be expressed as

$$p_{gm}(\mathbf{z}) = \prod_{i=1}^{r} p_{gm}(z_i) \,, \tag{3.10}$$

where

$$p_{gm}(z_i) = \sum_{\ell_i=1}^{L_i} \tilde{w}_i^{(\ell_i)} \, p_g\left(z_i; \tilde{m}_i^{(\ell_i)}, \widetilde{P}_i^{(\ell_i)}\right) \tag{3.11}$$

is the GM approximating the ith scalar element of the canonical Gaussian-distributed vector $\mathbf{z}$. Ideally, the parameters defining the scalar GM density would be found such that the L_2 distance to the scalar canonical Gaussian density is minimized; however, in practice, further simplifications about these parameters need to be made in order to make this minimization feasible.

In order to reduce the number of parameters necessary to find via minimization, first, the means of the GM density are assumed to be equally spaced away from zero, with the mean of the central component placed at zero. This gives the mean of each component explicitly as a function of the spacing between the means, Δm_i, as

$$\tilde{m}_i^{(\ell_i)} \triangleq \left[\ell_i - \frac{L_i + 1}{2}\right] \Delta m_i \,, \tag{3.12a}$$

for $\ell_i = 1, 2, \ldots, L_i$. Spacing the means of the components in this manner restricts L_i to be odd. Next, a power law [23] is assumed for the $\widetilde{P}_i^{(\ell_i)}$ according to

$$\widetilde{P}_i^{(\ell_i)} = L_i^{-\frac{3}{4}} \,, \tag{3.13}$$

for $\ell_i = 1, 2, \ldots, L_i$. This power law showed the best performance in [23]; however, the mean of each component is specified differently in this work, so no claim that the $(-3/4)$ power law performs best can be made. This power law was chosen heuristically and shows good performance in this application. Using this power law, the covariance of each component is explicitly defined by the number of components of the GM. Finally, the weights of the components are assumed symmetric about zero (which stems from the symmetry in the mean and covariance of the components) according to

$$\tilde{w}_i^{(\ell_i)} = \tilde{w}_i^{(L_i - \ell_i + 1)} , \tag{3.14}$$

for $\ell_i = 1, 2, \ldots, (L_i - 1)/2$. By parameterizing the weights in this manner, only $(L_i - 1)/2$ weights are unique due to the fact that the weights must sum to unity.

Under these assumptions, only $\tilde{w}_i^{(\ell_i)}$ for $\ell_i = 1, 2, \ldots, (L_i - 1)/2$ and Δm_i (a total of $(L_i + 1)/2$ parameters) need to be found in order to find $\tilde{w}_i^{(\ell_i)}$, $\tilde{m}_i^{(\ell_i)}$, and $\widetilde{P}_i^{(\ell_i)}$ for $\ell_i = 1, 2, \ldots, L_i$, which fully define the scalar GM density. These parameters are found such that the L_2 distance between the scalar GM density and the scalar canonical Gaussian density is minimized. Constrained numerical minimization is employed to find these parameters, which ensures that the weights and spacing between the components are positive. After this minimization is performed, the parameters of the scalar GM, which is given in Eq. (3.11), that minimize the L_2 distance to the scalar canonical Gaussian density are known. Two example GM densities approximating the standard normal density are presented in Figure (3.1). It is observed that, as the number of components in the mixture increases, the GM density becomes a better approximation of the Gaussian density, as expected.

(a) $L_i = 3$ (b) $L_i = 11$
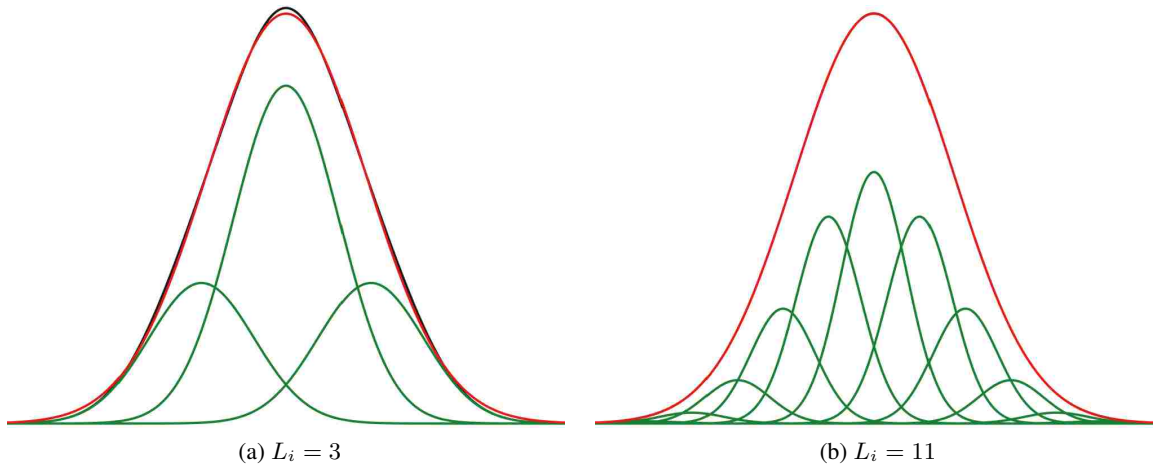
Figure 3.1. GM approximations of the standard normal density. The Gaussian density is red, the GM is black, and the components are green.

Now that the GM approximation of a scalar canonical Gaussian density has been constructed, the GM approximation of the multivariate canonical Gaussian density can be constructed. This is accomplished by substituting the scalar GM approximation of the ith component of $\mathbf{z}$, given by Eq. (3.11), into Eq. (3.10), which yields

$$p_{gm}(\mathbf{z}) = \prod_{i=1}^{r} \sum_{\ell_i=1}^{L_i} \tilde{w}_i^{(\ell_i)} \, p_g\left(z_i; \tilde{m}_i^{(\ell_i)}, \widetilde{P}_i^{(\ell_i)}\right). \tag{3.15}$$

Equation (3.15) can be manipulated into vector-matrix form to yield the parameters of the GM density approximating the multivariate canonical Gaussian density, given in Eq. (3.8), to yield

$$\tilde{w}^{(\ell)} = \prod_{j=1}^{r} \tilde{w}_j^{(\ell_j)} \tag{3.16a}$$

$$\tilde{\boldsymbol{m}}^{(\ell)} = \begin{bmatrix} \tilde{m}_1^{(\ell_1)} \\ \tilde{m}_2^{(\ell_2)} \\ \vdots \\ \tilde{m}_r^{(\ell_r)} \end{bmatrix} \tag{3.16b}$$

$$\widetilde{\boldsymbol{P}}^{(\ell)} = \begin{bmatrix} \widetilde{P}_1^{(\ell_1)} & & & \\ & \widetilde{P}_2^{(\ell_2)} & & \\ & & \ddots & \\ & & & \widetilde{P}_r^{(\ell_r)} \end{bmatrix}, \tag{3.16c}$$

where $\ell = 1, 2, \ldots, L$, the number of components in the resulting multivariate GM density is $L = L_1 L_2 \cdots L_r$, and each ℓ corresponds to a unique permutation of ℓ_1, ℓ_2, ..., ℓ_r. The number of components in the GM density approximating the canonical Gaussian density is given by the product of the number of components of the scalar GM density approximating each entry of $\mathbf{z}$. Special care must be taken when selecting the number of components chosen to approximate each component of $\mathbf{z}$, because the number of components in the resulting multivariate mixture suffers from the *curse of dimensionality*; that is, the number of components in the resulting mixture increase exponentially with r. This can easily result in an infeasible number of components for large r.

The parameters of the GM density approximating a Gaussian density, defined by $\boldsymbol{m}$ and $\boldsymbol{P}$, are now found by transforming the parameters of the GM density approximating the canonical Gaussian density according to the transformation of variables given in Eq. (3.6). This yields the parameters of the GM density approximating the Gaussian density, defined by Eq. (3.7), according to

$$w^{(\ell)} = \tilde{w}^{(\ell)} \tag{3.17a}$$

$$\boldsymbol{m}^{(\ell)} = \boldsymbol{S}\tilde{\boldsymbol{m}}^{(\ell)} + \boldsymbol{m} \tag{3.17b}$$

$$\boldsymbol{P}^{(\ell)} = \boldsymbol{S}\widetilde{\boldsymbol{P}}^{(\ell)}\boldsymbol{S}^T \tag{3.17c}$$

for $\ell = 1, 2, \ldots, L$.

3.3. BINGHAM DENSITY

The Bingham density is an antipodally symmetric density on the unit-hypersphere that is defined as a zero-mean Gaussian density conditioned on the unit-hypersphere. In this context, "conditioned" means that the Gaussian density is evaluated on the unit-hypersphere and is subsequently renormalized such that it is a valid pdf. Because antipodal attitude quaternions ($\bar{\boldsymbol{q}}$ and $-\bar{\boldsymbol{q}}$) represent the same attitude, the Bingham density can quantify the uncertainty in the quaternion representation of attitude without ambiguity between $\bar{\boldsymbol{q}}$ and $-\bar{\boldsymbol{q}}$. The Bingham density is defined for a random unit-vector $\bar{\boldsymbol{q}} \in \mathbb{S}^s$ and is given by [8, 9]

$$p_b(\bar{\boldsymbol{q}}; \boldsymbol{M}, \boldsymbol{Z}) = \frac{1}{F(\boldsymbol{Z})} \exp\left\{\bar{\boldsymbol{q}}^T \boldsymbol{M} \boldsymbol{Z} \boldsymbol{M}^T \bar{\boldsymbol{q}}\right\}, \tag{3.18}$$

where $\boldsymbol{M} \in \mathrm{SO}(s+1)$ is the orientation matrix describing the orientation of the density on the unit-hypersphere, $\boldsymbol{Z}$ is a diagonal square matrix of dimension $s+1$ of concentration parameters with nondecreasing diagonal elements $Z_1 \leq \cdots \leq Z_s \leq Z_{s+1} \triangleq 0$, and $F(\boldsymbol{Z})$ is the normalization constant that ensures that $p_b(\bar{\boldsymbol{q}}; \boldsymbol{M}, \boldsymbol{Z})$ is a valid pdf. The Bingham density possesses the property that $p_b(\bar{\boldsymbol{q}}; \boldsymbol{M}, \boldsymbol{Z}) = p_b(\bar{\boldsymbol{q}}; \boldsymbol{M}, \boldsymbol{Z} + c\boldsymbol{I})$ for all $c \in \mathbb{R}$; thus, Z_{s+1} is defined to be zero with an appropriate choice of c for a given Bingham density without any change to the characteristics of the density. An abuse of notation is used for $\bar{\boldsymbol{q}}$ because it is used to represent both a generic antipodally symmetric unit-vector of arbitrary dimension s as well as the attitude quaternion; when $\bar{\boldsymbol{q}} \in \mathbb{S}^1$ or $\bar{\boldsymbol{q}} \in \mathbb{S}^3$, $\bar{\boldsymbol{q}}$ is a valid attitude quaternion representing the one- and three-dimensional attitude of a body, respectively. Whether $\bar{\boldsymbol{q}}$ represents a generic antipodally symmetric unit-vector or the attitude quaternion is clear in the surrounding context.

The parameters of $\boldsymbol{Z}$ control how tightly clustered the Bingham density is around its mean direction, while the orientation matrix, $\boldsymbol{M}$, specifies the mean direction itself. The normalization constant of the Bingham density is given by the hypergeometric function of a matrix argument according to

$$F(\boldsymbol{Z}) = \int_{\mathbb{S}^s} \exp\left\{\bar{\boldsymbol{q}}^T \boldsymbol{Z} \bar{\boldsymbol{q}}\right\} \mathrm{d}\mathbb{S}^s = |\mathbb{S}^s|\, {}_1F_1\left(\frac{1}{2}; \frac{s+1}{2}; \boldsymbol{Z}\right), \tag{3.19}$$

where $|\mathbb{S}^s|$ represents the area of the unit-hypersphere of dimension s and $_.F._.(\cdot;\cdot;\cdot)$ represents the hypergeometric function of a matrix argument. The normalization constant is independent of the orientation matrix, which is intuitive since the orientation matrix simply changes the orientation of the density on the unit-hypersphere. Many methods exist for calculating the normalization constant, including series expansions [24], saddle point approximations [25, 26], the holonomic gradient method [27], and interpolation of precomputed tabulated values [28]. In this work, the normalizing constant is interpolated from precomputed tabulated values. In order to generate the tabulated values of the normalizing constant, the normalizing constant is approximated over a discrete grid of Z_1, $Z_2, \ldots, Z_s$ for $s = 1$, 2, and 3 using Gauss-Legendre quadrature in spherical coordinates to approximate the integral in Eq. (3.19). This approximation is detailed in Appendix B.

Parallels between the parameters of the well-known and well-understood Gaussian density and the parameters of the Bingham density can be drawn in order to better understand the Bingham density. The Bingham density is a directional density; that is, it probabilistically quantifies the direction of a unit-vector in $\mathbb{S}^s$. The orientation matrix, M, is similar to the mean of the Gaussian density, m, in that it specifies the mean *direction* of the Bingham density, while m specifies the mean *location* of the Gaussian density. The matrix of concentration parameters of the Bingham density, Z, is similar to the covariance matrix of the Gaussian density, P, in that it specifies how tightly clustered the Bingham density is about its mean direction. Making the elements of Z more negative leads to a more tightly clustered density about the mean direction for the Bingham density similarly to how decreasing P towards 0 leads to a more tightly clustered density about the mean for the Gaussian density. It is important to note that Z is not the covariance of the Bingham density; however, they are directly related.

Representing the uncertainty of an attitude quaternion using the Bingham density has three key advantages as compared to other methods of attitude uncertainty representation:

- The Bingham density is antipodally symmetric; thus, antipodal quaternions $\bar{q}$ and $-\bar{q}$ (which represent the same physical attitude) are equiprobable,

- the Bingham density quantifies the uncertainty of the attitude quaternion $\bar{q}$ on its natural manifold ($\mathbb{S}^1$ or $\mathbb{S}^3$, for one- and three-dimensional attitude, respectively) instead of projecting the attitude uncertainty into a local tangent space, which can potentially incur approximation errors, and

- the Bingham density possesses a simple representation of a uniformly distributed attitude quaternion on this manifold, which occurs when the Z matrix is null.

In order to visualize how the Bingham density represents the distribution of an attitude quaternion in $\mathbb{S}^3$, the Bingham density is illustrated in $\mathbb{S}^1$ and $\mathbb{S}^2$, where straightforward visualizations exist. The Bingham density is first shown for one-dimensional attitude uncertainty representation, where the axis of rotation is defined to be the z-axis. In this case, the one-dimensional attitude quaternion is given by Eq. (2.42). Figure (3.2) shows the Bingham-distributed one-dimensional attitude quaternion for the identity orientation matrix and different values of Z_1. Observation of Figure (3.2) shows that the Bingham density is antipodally symmetric; that is, $\bar{q}$ and $-\bar{q}$ are equiprobable. Further observation highlights that as Z_1 becomes more negative, the uncertainty in the attitude quaternion decreases. Similarly, as Z_1 approaches zero, the uncertainty in the attitude quaternion increases until $Z_1 = 0$, in which case the attitude quaternion is uniformly-distributed.

Figure (3.3) shows the Bingham density in $\mathbb{S}^1$ for a fixed matrix of concentration parameters, $\mathbf{Z}$, and varying values of the orientation matrix, $\mathbf{M}$. In this dimension, the orientation matrix is parameterized by a single parameter, according to Eq. (2.27). In this case, ϕ is used in place of θ in Eq. (2.27) to yield the orientation matrix of the Bingham density in terms of ϕ according to

$$\mathbf{M} = \begin{bmatrix} \cos\phi & \sin\phi \\ -\sin\phi & \cos\phi \end{bmatrix}. \tag{3.20}$$

The angle ϕ is used to parameterize the orientation matrix of the Bingham density instead of θ in order to emphasize that ϕ defines the mean direction of the attitude quaternion, and is not the heading angle of the vehicle, in general. Observation of Figure (3.3) shows that ϕ specifies the rotation of the mean direction of the quaternion away from the direction of the identity quaternion ($\bar{p} = \begin{bmatrix} 0 & 1 \end{bmatrix}^T$), as expected from the definition of the orientation matrix. Observation of Figures. (3.3a) and (3.3d) shows that the Bingham density is identical for orientation matrices defined by $\phi = 0$ and $\phi = 180°$ and results in identical Bingham densities, which makes intuitive sense because $\pm\mathbf{M}$ (which are defined by $\phi = 0$ and $\phi = 180°$), result in the same exponential argument in Eq. (3.18).

No valid attitude quaternion exists on $\mathbb{S}^2$; however, the Bingham density for the unit-vector $\bar{q} = \begin{bmatrix} q_1 & q_2 & q_3 \end{bmatrix}^T \in \mathbb{S}^2$ is illustrated in Figure (3.4) for the orientation matrix

$$\mathbf{M} = \begin{bmatrix} \frac{\sqrt{2}}{2} & \frac{\sqrt{2}}{2} & 0 \\ 0 & 0 & 1 \\ \frac{\sqrt{2}}{2} & -\frac{\sqrt{2}}{2} & 0 \end{bmatrix}$$

and varying values of Z_1 and Z_2 to demonstrate how the $\mathbf{Z}$ matrix affects the Bingham density in this dimension. When $Z_1 = Z_2 = 0$, all $\bar{q}$ are equiprobable. When $Z_2 = 0$, the $\bar{q}$ along a great circle defined by the orientation matrix $\mathbf{M}$ are equiprobable, as observed in Figures. (3.4a) and (3.4c). In this case, the Z_1 parameter dictates how tightly clustered the pdf of $\bar{q}$ is along the

(a) $Z_1 = -100$

(b) $Z_1 = -50$

(c) $Z_1 = -25$

(d) $Z_1 = -10$

(e) $Z_1 = -2$

(f) $Z_1 = 0$
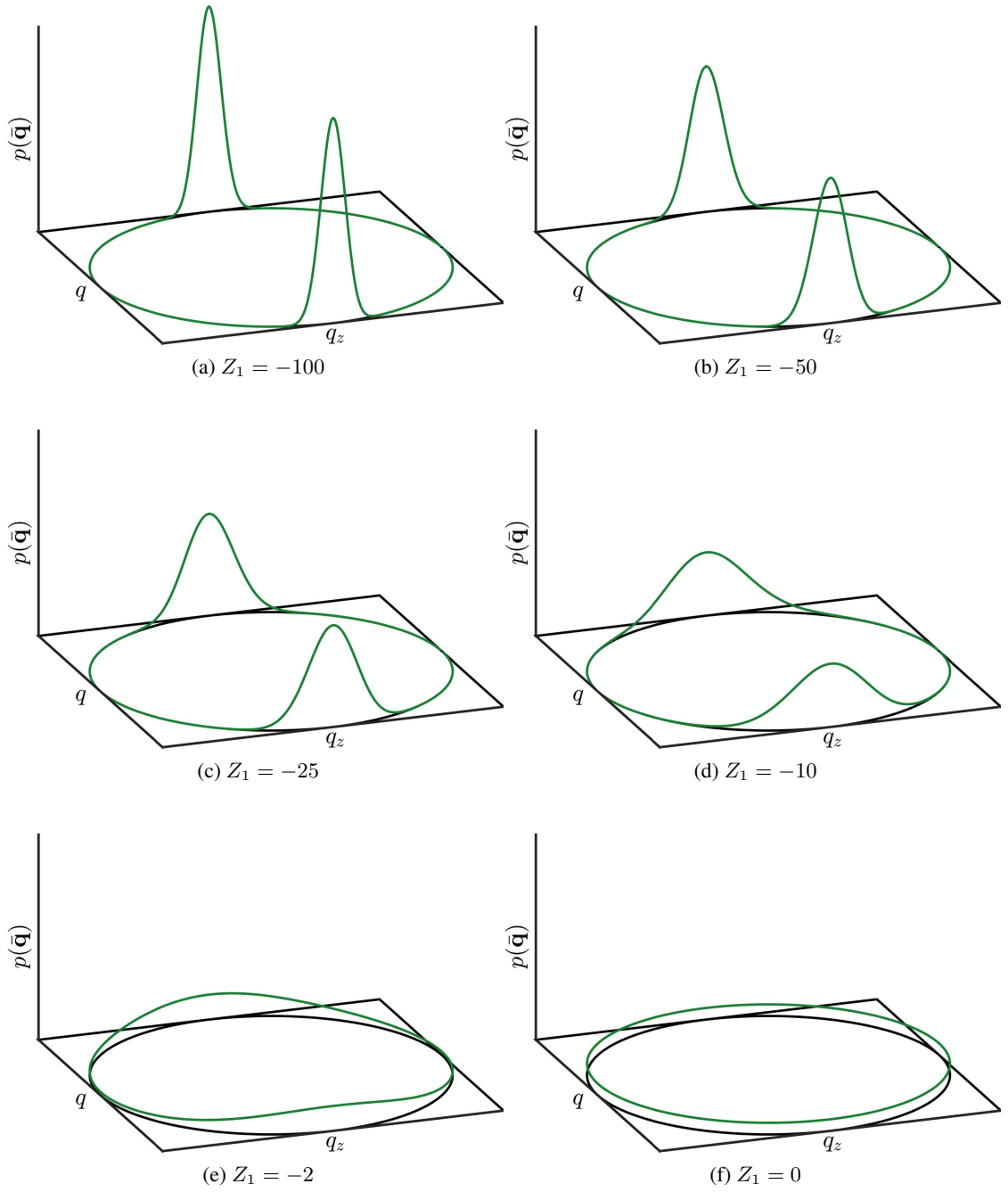
Figure 3.2. Bingham densities on $\mathbb{S}^1$ for $\boldsymbol{M} = \boldsymbol{I}$ and varying values of Z_1.

(a) $\phi = 0$

(b) $\phi = 10°$

(c) $\phi = 30°$

(d) $\phi = 60°$

(e) $\phi = 90°$

(f) $\phi = 180°$
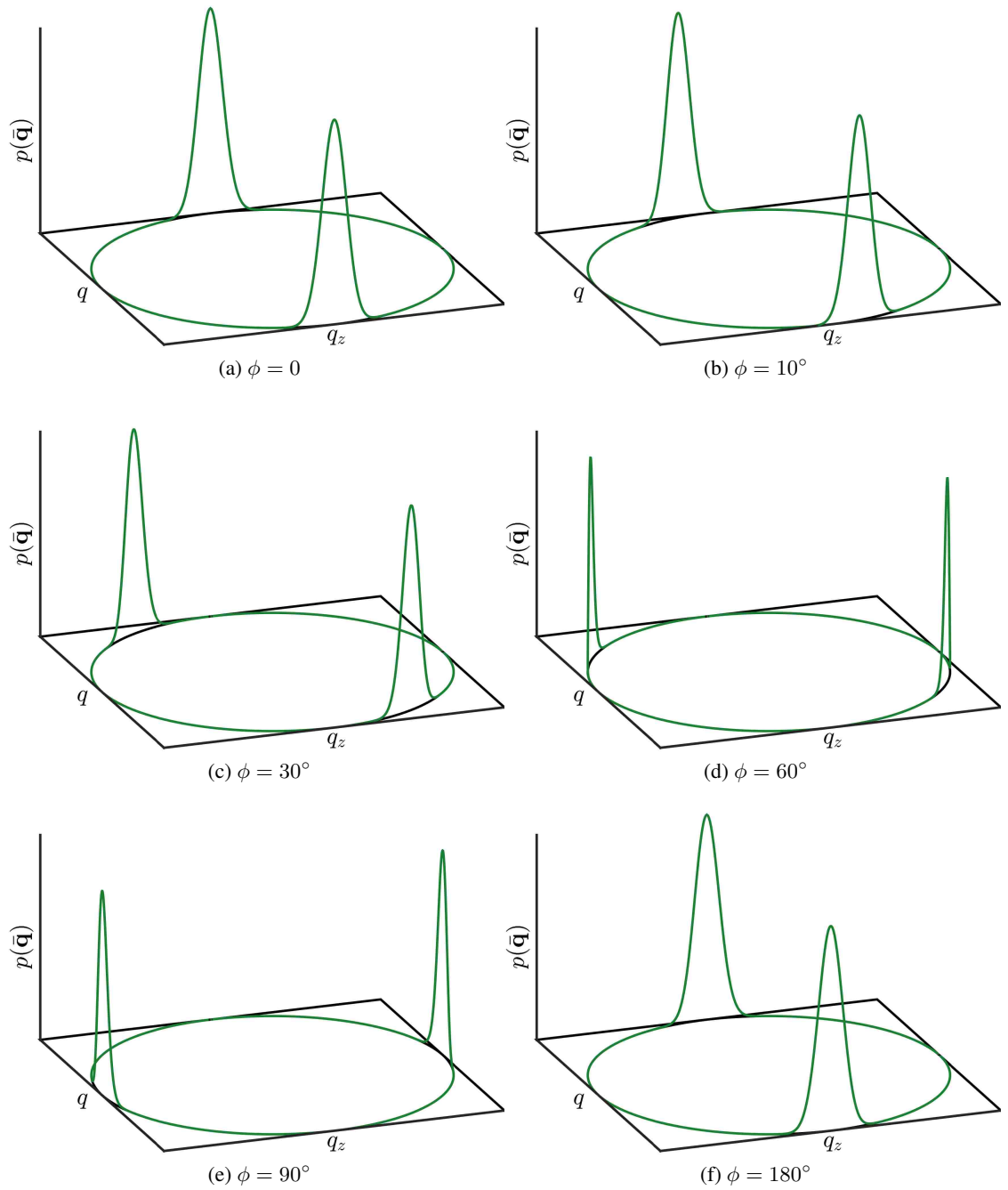
Figure 3.3. Bingham densities on $\mathbb{S}^1$ for $Z_1 = -100$ and varying values of M.

great circle. When Z_2 decreases from zero, the pdf of $\bar{q}$ decreases in the direction defined by the orientation matrix $\boldsymbol{M}$, as observed in Figures. (3.4b) and (3.4d).

No straightforward visualization of the Bingham density exists in $\mathbb{S}^3$. Similar trends, however, are present as the entries of $\boldsymbol{Z}$ change for the Bingham densities in $\mathbb{S}^3$ as they do for the Bingham density in $\mathbb{S}^1$ and $\mathbb{S}^2$. A uniformly distributed attitude quaternion is given by the null $\boldsymbol{Z}$ matrix, and as Z_1, Z_2, and Z_3 decrease, the uncertainty in the attitude quaternion decreases. If any of the Z_1, Z_2, and Z_3 are equal to zero, then the attitude quaternion becomes equiprobable around a higher-dimensional circle or sphere, similarly to Figures. (3.4a) and (3.4c) for the Bingham density in $\mathbb{S}^2$.

The canonical Bingham density is introduced by substituting the transformation

$$\bar{q} = M\bar{p} \tag{3.21}$$

into Eq. (3.18), which yields the canonical Bingham density as

$$\tilde{p}_b(\bar{p}; \boldsymbol{Z}) = p_b(\bar{p}; \boldsymbol{I}, \boldsymbol{Z}) = F^{-1}(\boldsymbol{Z}) \exp\left\{\bar{p}^T \boldsymbol{Z} \bar{p}\right\},$$

where the tilde notation is used to denote the canonical form of the density. The canonical Bingham density still depends on the matrix of concentration parameters, $\boldsymbol{Z}$; however, the elements of $\bar{p}$ are uncorrelated (but not independent because $\bar{p}$ is constrained to be unit-norm), which can be exploited for certain operations. Similar to the canonical Gaussian density, certain operations can be performed for the canonical Bingham density, and the results of these operations can then be transformed according to the change of variables defined by Eq. (3.21) to represent the Bingham density of interest. When using the canonical Bingham density, typically these operations cannot be performed off line and saved for the canonical Bingham density, because the canonical Bingham density still depends on the matrix of concentration parameters, $\boldsymbol{Z}$.

While the canonical Bingham density is only defined on $\mathbb{S}^s$, it is still possible to express its mean and covariance in $\mathbb{R}^{s+1}$. Due to the antipodal symmetry of the canonical Bingham density, its mean in $\mathbb{R}^{s+1}$ is

$$\mathrm{E}_{\tilde{p}_b}\{\bar{p}\} = \boldsymbol{0},$$

(a) $Z_1 = -100, Z_2 = 0$

(b) $Z_1 = -100, Z_2 = -10$

(c) $Z_1 = -25, Z_2 = 0$

(d) $Z_1 = -25, Z_2 = -10$
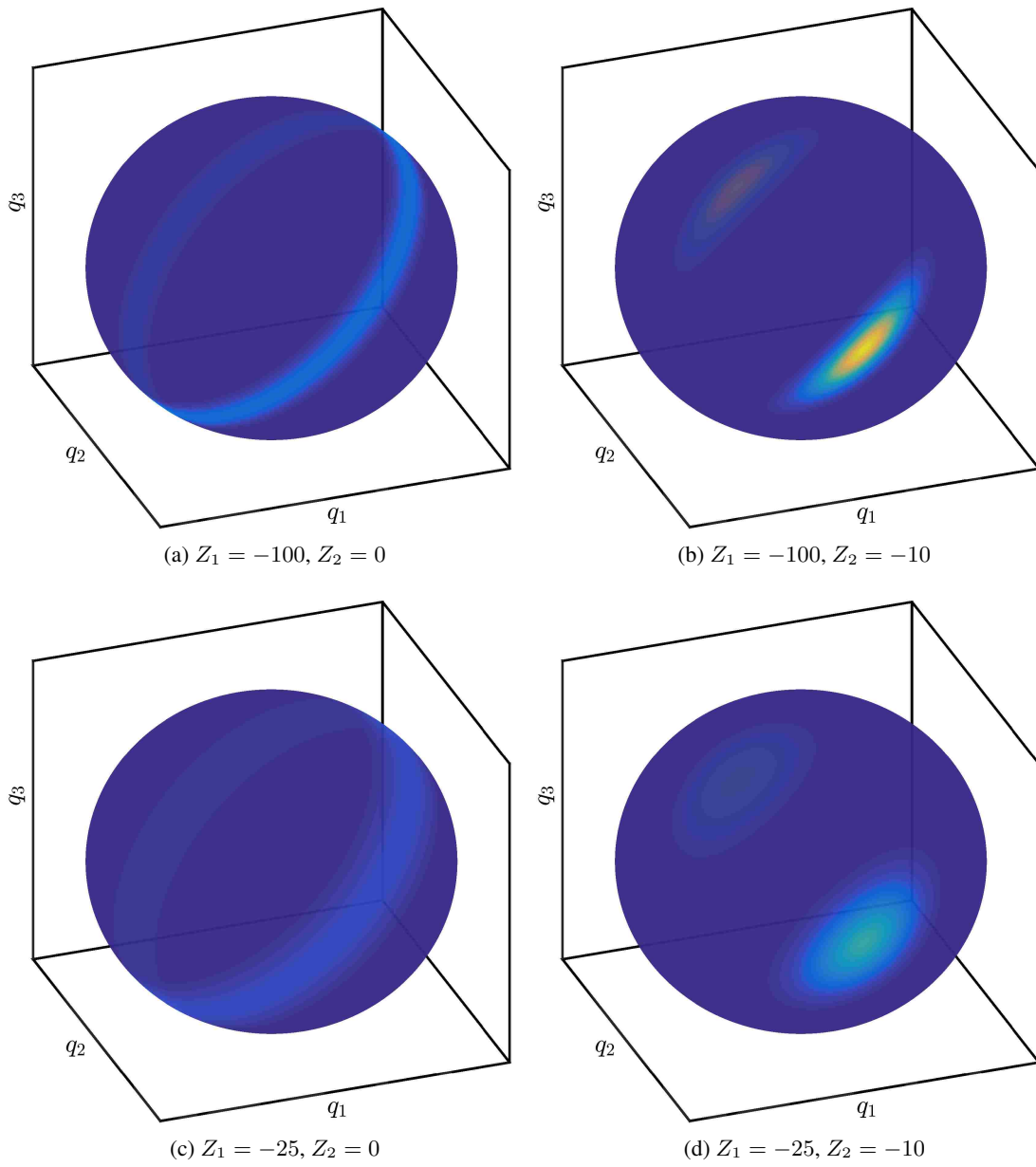
Figure 3.4. Bingham densities on $\mathbb{S}^2$ for varying values of Z_1 and Z_2.

where the expected value is defined by Eq. (3.5). Because the elements of $\bar{p}$ are uncorrelated, the covariance of the canonical Bingham density in $\mathbb{R}^{s+1}$ is given by Eq. (2.9) from Reference [8] as

$$
\boldsymbol{P}_p \triangleq \mathrm{E}_{\tilde{p}_b}\{\bar{\boldsymbol{p}}\bar{\boldsymbol{p}}^T\} = \begin{bmatrix} f_1 & & & \\ & f_2 & & \\ & & \ddots & \\ & & & f_{s+1} \end{bmatrix} , \tag{3.22}
$$

where the off-diagonal elements of the matrix in Eq. (3.22) are equal to zero. The f_i terms are defined in terms of the normalizing constant and its partial derivatives with respect to Z_i according to

$$
f_i \triangleq F^{-1}(\boldsymbol{Z})\frac{\partial F(\boldsymbol{Z})}{\partial Z_i} . \tag{3.23}
$$

The f_i terms satisfy several important properties, given by

$$
\sum_{i=1}^{s+1} f_i = 1 \tag{3.24a}
$$

$$
f_i > 0 , \quad i = 1, 2, \ldots, s+1 \tag{3.24b}
$$

$$
\lim_{Z_i \to -\infty} f_i = 0^+ , \quad i = 1, 2, \ldots, s \tag{3.24c}
$$

$$
\lim_{Z_1, Z_2, \ldots, Z_s \to -\infty} f_{s+1} = 1^- . \tag{3.24d}
$$

These properties can be interpreted from the fact that the f_1, f_2, ..., f_{s+1} represent the diagonal elements of the covariance matrix of the canonical Bingham density according to Eq. (3.22). The canonical Bingham density exists on the unit-hypersphere and is antipodally symmetric, i.e., it probabilistically quantifies an antipodally symmetric vector that is constrained to be unit-norm. Because of this, the trace of its covariance matrix is constrained to be unity, which is given by Eq. (3.24a). Furthermore, the diagonal elements of the covariance matrix must be positive, which is given by Eq. (3.24b). Finally, the properties of the f_1, f_2, ..., f_{s+1} given in Eqs. (3.24c) and (3.24d) stem from the facts that Z_1, Z_2, ..., Z_s are less than or equal to zero, $Z_{s+1} \triangleq 0$, and the unity trace constraint on the covariance matrix.

In this work, the partial derivatives of the normalizing constant, as defined by Eq. (3.23), are interpolated from precomputed tabulated values. In order to generate these tabulated values, the partial derivatives of Eq. (3.19) with respect to each of Z_1, Z_2, ..., Z_s are first found, and are then numerically evaluated using Gauss-Legendre quadrature in spherical coordinates to approximate the

remaining integral. This approximation is detailed in Appendix B, along with the approximation of the normalizing constant itself.

The covariance of the canonical Bingham density, $\boldsymbol{P}_p$, uniquely defines the canonical Bingham density. If $\boldsymbol{P}_p$ is known, then the matrix of concentration parameters, $\boldsymbol{Z}$, defining the canonical Bingham density that possesses this covariance can be found. In order to find the elements of $\boldsymbol{Z}$, given by $Z_1, Z_2, \ldots, Z_s$, reverse interpolation of the tabulated values of $f_1, f_2, \ldots, f_s$ (which are the unique parameters of $\boldsymbol{P}_p$) over the grid of $Z_1, Z_2, \ldots, Z_s$ is used. Because of this, either the covariance of the canonical Bingham density, or the matrix of concentration parameters is sufficient to specify a unique canonical Bingham density.

Like the canonical Bingham density, the mean of the Bingham density is given in $\mathbb{R}^{s+1}$ as

$$\mathrm{E}_{p_b}\{\bar{\boldsymbol{q}}\} = \boldsymbol{0}$$

due to antipodal symmetry. The covariance of the Bingham density in $\mathbb{R}^{s+1}$ is defined by $\mathrm{E}_{p_b}\{\bar{\boldsymbol{q}}\bar{\boldsymbol{q}}^T\}$. In order to calculate this expected value, its argument is first pre- and post-multiplied by $\boldsymbol{M}\boldsymbol{M}^T = \boldsymbol{I}$, such that the covariance can be expressed as

$$\boldsymbol{P}_q \triangleq \mathrm{E}_{p_b}\{\bar{\boldsymbol{q}}\bar{\boldsymbol{q}}^T\} = \mathrm{E}_{p_b}\{\boldsymbol{M}\boldsymbol{M}^T\bar{\boldsymbol{q}}\bar{\boldsymbol{q}}^T\boldsymbol{M}\boldsymbol{M}^T\}. \tag{3.25}$$

Introducing the transformation of variables defined in Eq. (3.21) and noting that $\boldsymbol{M}$ is deterministic, Eq. (3.25) can be expressed as

$$\boldsymbol{P}_q = \boldsymbol{M}\mathrm{E}_{\tilde{p}_b}\{\bar{\boldsymbol{p}}\bar{\boldsymbol{p}}^T\}\boldsymbol{M}^T. \tag{3.26}$$

$\mathrm{E}_{\tilde{p}_b}\{\bar{\boldsymbol{p}}\bar{\boldsymbol{p}}^T\}$ is simply the covariance of the canonical Bingham density, which is defined by Eq. (3.22). Substituting Eq. (3.22) into Eq. (3.26) yields the covariance of the Bingham density in $\mathbb{R}^{s+1}$ as

$$\boldsymbol{P}_q = \boldsymbol{M}\boldsymbol{P}_p\boldsymbol{M}^T, \tag{3.27}$$

which is seen to be a similarity transformation of the covariance of the canonical Bingham density according to the orientation matrix of the Bingham density.

The covariance of the Bingham density, $\boldsymbol{P}_q$, uniquely defines the Bingham density. If $\boldsymbol{P}_q$ is known, then the orientation matrix, $\boldsymbol{M}$, and the matrix of concentration parameters, $\boldsymbol{Z}$, defining the Bingham density that possess this covariance can be found. In order to find $\boldsymbol{M}$ and the elements of $\boldsymbol{Z}$, given by $Z_1, Z_2, \ldots, Z_s$, first an eigen-decomposition is performed on $\boldsymbol{P}_q$ to find $\boldsymbol{M}$ and the diagonal matrix $\boldsymbol{P}_p$ according to Eq. (3.27). Reverse interpolation of the tabulated values of $f_1, f_2, \ldots, f_s$ (which are the unique parameters of $\boldsymbol{P}_p$) over the grid of $Z_1, Z_2, \ldots, Z_s$ is then used to find $Z_1, Z_2, \ldots, Z_s$. Because of this, either the covariance of the Bingham density or the orientation

matrix and matrix of concentration parameters is sufficient to specify a unique Bingham density. Special care must be taken when taking the eigen-decomposition of $\boldsymbol{P}_q$ in order to ensure that the properties of $\boldsymbol{M} \in \mathrm{SO}(s+1)$ and the diagonal matrix $\boldsymbol{P}_p$ (which are given by Eqs. (3.24)) are met.

3.4. BINGHAM MIXTURE DENSITY

The BM density is defined by

$$
p_{bm}(\bar{\boldsymbol{q}}) = \sum_{\ell=1}^{L} w^{(\ell)} \, p_b\Big(\bar{\boldsymbol{q}}; \boldsymbol{M}^{(\ell)}, \boldsymbol{Z}^{(\ell)}\Big) \,,
\tag{3.28}
$$

where $w^{(\ell)}$ is the weight of the ℓth component, $\boldsymbol{M}^{(\ell)}$ and $\boldsymbol{Z}^{(\ell)}$ are the orientation matrix and matrix of concentration parameters defining the ℓth component, respectively, and L is the number of components in the BM density. The weights of the mixture are constrained such that

$$
w^{(\ell)} > 0 \quad \ell = 1, 2, \ldots, L \qquad \text{and} \qquad \sum_{\ell=1}^{L} w^{(\ell)} = 1 \,,
$$

which ensures that the BM is a valid pdf.

The BM density can be used to approximate pdfs on the unit-hypersphere, similarly to how the GM density can be used to approximate pdfs in Euclidean space. In this work, the approximation of the Bingham density by a BM density is considered. While the Bingham density can be equivalently expressed as a single-component BM density, it is advantageous in certain applications to approximate the Bingham density by a BM density with more than one component. By approximating the Bingham density in this way, the uncertainty of each component of the approximating BM density is smaller than that of the Bingham density it approximates, in general. The parameters of the approximating BM density are found differently depending on whether the Bingham density to approximate is a uniform density or not (i.e, whether $\boldsymbol{Z}$ is null or not). A method to find the parameters of the BM density that approximate a nonuniform Bingham density on $\mathbb{S}^1$ is presented first. Next, a method to find the parameters of the BM density that approximates a uniform Bingham density for arbitrary dimension s is presented.

3.4.1. Approximation of the Nonuniform Bingham Density on $\mathbb{S}^1$. The approximation of a nonuniform Bingham density by a BM density on $\mathbb{S}^1$ is now considered. The parameters of the BM approximation of the nonuniform canonical Bingham density are first found, and then, these parameters are transformed according to the change of variables defined in Eq. (3.21) in order to yield the parameters of the BM density that approximates the Bingham density of interest. Let the

BM density approximating the canonical Bingham density be defined by

$$p_{bm}(\bar{\boldsymbol{p}}) = \sum_{\ell=1}^{L} \tilde{w}^{(\ell)} \, p_b\left(\bar{\boldsymbol{p}}; \widetilde{\boldsymbol{M}}^{(\ell)}, \widetilde{\boldsymbol{Z}}^{(\ell)}\right), \tag{3.29}$$

where the tilde notation indicates that these parameters correspond to the BM density that approximates the *canonical* Bingham density. Ideally, $\tilde{w}^{(\ell)}$, $\widetilde{\boldsymbol{M}}^{(\ell)}$, and $\widetilde{\boldsymbol{Z}}^{(\ell)}$ would be found for a given L such that a given measure of the difference between the canonical Bingham density and its approximating BM density is minimized. The L_2 distance between the canonical Bingham density and its approximating BM density is used as this measure and is given by

$$L_2[\tilde{p}_b || p_{bm}] = \int_{\mathbb{S}^s} \left[\tilde{p}_b(\boldsymbol{\zeta}) - p_{bm}(\boldsymbol{\zeta})\right]^2 \mathrm{d}\boldsymbol{\zeta}. \tag{3.30}$$

This L_2 distance can be manipulated into a closed form, as is shown in Appendix C.

In general, finding the $\tilde{w}^{(\ell)}$, $\widetilde{\boldsymbol{M}}^{(\ell)}$, and $\widetilde{\boldsymbol{Z}}^{(\ell)}$ that minimize Eq. (3.30) without first making simplifications becomes intractable, especially as the number of components in the mixture increases. When constructing the GM density, the fact that the elements of the canonical Gaussian-distributed variable, $\mathbf{z}$, are uncorrelated is exploited in order to simplify the construction of a GM approximation of a multivariate Gaussian density in r dimensions into the construction of r scalar GM approximations of a scalar canonical Gaussian density. While the elements of the canonical Bingham state vector, $\bar{\boldsymbol{p}}$, are uncorrelated like the elements of $\mathbf{z}$, the resulting densities of the elements of $\bar{\boldsymbol{p}}$ are not Bingham. This is in contrast to the resulting densities of the elements of $\mathbf{z}$, which are canonical Gaussian; thus, a similar approach to constructing the GM for each component of $\mathbf{z}$ and combining the result cannot be followed for the construction of the BM approximating the Bingham density. This is why the approximation of a nonuniform Bingham density is only considered in $\mathbb{S}^1$, and not higher dimensions, in this work. In theory, a similar approach could be used to construct a BM density in higher dimensions; however, in practice, the minimization vector becomes intractably large and, thus, does not provide a useful framework to construct the BM mixture in these higher dimensions.

The parameters of the BM density approximating the canonical Bingham density in $\mathbb{S}^1$ are now sought. Similarly to finding the parameters of the GM density, ideally, the parameters defining this BM density would be found such that the L_2 distance to the canonical Bingham density is minimized; however, in practice, further simplifications about these parameters need to be made in order to make this minimization feasible. Before making these simplifications, first note that

Eq. (3.29) can be simplified to

$$p_{bm}(\bar{\boldsymbol{p}}) = \sum_{\ell=1}^{L} \tilde{w}^{(\ell)} \, p_b\left(\bar{\boldsymbol{p}}; \boldsymbol{M}(\tilde{\phi}^{(\ell)}), \widetilde{\boldsymbol{Z}}^{(\ell)}\right), \tag{3.31}$$

where $\boldsymbol{M}(\phi)$ represents the orientation matrix parameterized by the scalar parameter ϕ, according to Eq. (3.20), which quantifies the mean direction of each component in terms an angular displacement from the zero direction instead of the orientation matrix directly.

The mean directions of the BM density, $\tilde{\phi}^{(\ell)}$ for $\ell = 1, 2, \ldots, L$, are assumed to be equally spaced away from the zero direction, with the mean direction of the central component placed at zero. This gives the mean direction of each component of the BM explicitly as a function of the spacing between the means, $\Delta\phi$, as

$$\tilde{\phi}^{(\ell)} \triangleq \left[\ell - \frac{L+1}{2}\right]\Delta\phi, \tag{3.32}$$

for $\ell = 1, 2, \ldots, (L-1)/2$. Spacing the means of the components in this manner restricts L to be odd. Next, a power law similar to that used to define the covariance of each component of the GM desnity is used for the matrix of concentration parameters of each component of the BM density. This yields the matrix of concentration parameters for each component as

$$\widetilde{\boldsymbol{Z}}^{(\ell)} = L^{\frac{3}{4}}\boldsymbol{Z}, \tag{3.33}$$

for $\ell = 1, 2, \ldots, L$. This power law was chosen heuristically and shows good performance in this application. Using this power law, the matrix of concentration parameters of each component is explicitly defined by the number of components of the BM. Finally, the weights of the components are assumed symmetric about zero because of this symmetry in the mean direction and covariance of the components according to

$$\tilde{w}^{(\ell)} = \tilde{w}^{(L-\ell+1)}, \tag{3.34}$$

for $\ell = 1, 2, \ldots, (L-1)/2$, and, thus, only $(L-1)/2$ weights are unique due to the fact that the weights must sum to unity.

Under these assumptions, only $\tilde{w}^{(\ell)}$ for $\ell = 1, 2, \ldots, (L-1)/2$ and $\Delta\phi$ (a total of $(L+1)/2$ parameters) need to be found in order to find $\tilde{w}^{(\ell)}$, $\widetilde{\boldsymbol{M}}^{(\ell)}$, and $\widetilde{\boldsymbol{Z}}^{(\ell)}$ for $\ell = 1, 2, \ldots, L$, which fully define the BM density. These parameters are found such that the L_2 distance between the BM density and the canonical Bingham density is minimized. Constrained numerical minimization is employed to find these parameters, which ensures that the weights and spacing between the components are positive. Two example BM densities approximating the canonical Bingham density

in $\mathbb{S}^1$ are presented in Figure (3.5). It is observed that, as the number of components in the mixture increases, the BM density becomes a better approximation of the Bingham density, as expected.

(a) $L = 3$ (b) $L = 11$
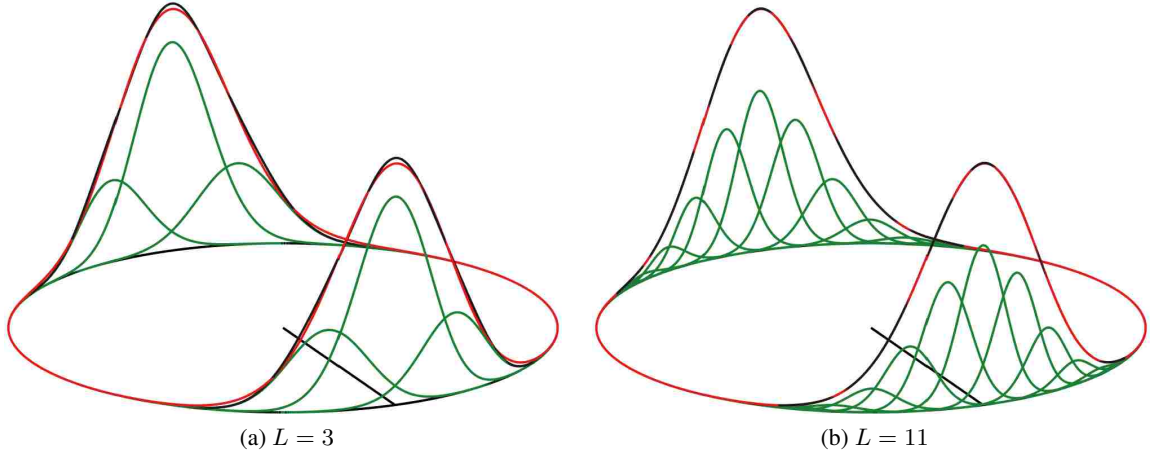
Figure 3.5. BM approximations of the Bingham density defined by $Z_1 = -10$. The Bingham density is red, the BM is black, and the components are green.

The parameters of the BM density approximating the Bingham density of interest, defined by M and Z, are now found by transforming the parameters of the BM density approximating the canonical Bingham density according to the transformation of variables given in Eq. (3.21). This yields the parameters of the BM density approximating the Bingham density of interest, defined by Eq. (3.28), according to

$$w^{(\ell)} = \tilde{w}^{(\ell)} \tag{3.35a}$$

$$\boldsymbol{M}^{(\ell)} = \boldsymbol{M}\tilde{\boldsymbol{M}}^{(\ell)} \tag{3.35b}$$

$$\boldsymbol{Z}^{(\ell)} = \widetilde{\boldsymbol{Z}}^{(\ell)} \tag{3.35c}$$

for $\ell = 1, 2, \ldots, L$.

3.4.2. Approximation of the Uniform Bingham Density on $\mathbb{S}^s$. Now the approximation of the uniform Bingham density, that is, a Bingham density with $\boldsymbol{Z} = \boldsymbol{0}$, by a BM density is considered on the unit-hypersphere of arbitrary dimension, $\mathbb{S}^s$. Before considering this approximation, first note that the unit-vector $\bar{\boldsymbol{q}} = [q_1 \ q_2 \ \cdots \ q_{s+1}]^T$ can be expressed in terms of spherical coordinates by [29]

$$q_1 = \sin \phi_1 \cos \phi_2 \tag{3.36a}$$

$$q_2 = \sin \phi_1 \sin \phi_2 \cos \phi_3 \tag{3.36b}$$

$$\vdots \tag{3.36c}$$

$$q_s = \sin\phi_1 \sin\phi_2 \cdots \sin\phi_{s-1} \cos\phi_s \tag{3.36d}$$

$$q_{s+1} = \cos\phi_1 \,, \tag{3.36e}$$

where ϕ_1, ϕ_2, ..., $\phi_{s-1} \in [0, \pi]$ and $\phi_s \in [0, 2\pi)$. The spherical coordinates ϕ_1, ϕ_2, ..., ϕ_s represent a minimum parameter set to quantify the unit-vector of arbitrary dimension, $\bar{q} \in \mathbb{S}^s$. For notational convenience, define the collection of spherical coordinates corresponding to $\bar{q}$ as

$$\boldsymbol{\phi} = \begin{bmatrix} \phi_1 & \phi_2 & \cdots & \phi_s \end{bmatrix}^T \,,$$

such that $\bar{q}(\boldsymbol{\phi})$ represents the unit-vector parameterized by spherical coordinates. The differential area of the hypersphere swept out by the unit-vector is given as a function of the spherical coordinates and their differential variations according to

$$\mathrm{d}A(\boldsymbol{\phi}) = \sin^{s-1}\phi_1 \sin^{s-2}\phi_2 \cdots \sin\phi_{s-1} \,\mathrm{d}\phi_1 \,\mathrm{d}\phi_2 \cdots \mathrm{d}\phi_s \,, \tag{3.37}$$

where "d" is used to denote a differential variation in the following quantity. This relationship is true in the limiting case as the variations in the spherical coordinates approach zero. In the general case, the linear relationship between the area swept out on the unit-hypersphere and the angle swept by each spherical coordinate is given by

$$\Delta A(\boldsymbol{\phi}) = \sin^{s-1}\phi_1 \sin^{s-2}\phi_2 \cdots \sin\phi_{s-1} \Delta\phi_1 \Delta\phi_2 \cdots \Delta\phi_s \,, \tag{3.38}$$

where Δ is used to denote a finite variation in the following quantity. The spherical coordinates defined in Eqs. (3.36), and the linear relationship between the area swept on the unit-hypersphere and the angles swept by the spherical coordinates defined in Eqs. (3.38), are used in order to parameterize the weights and mean directions of the components of the BM density that is used to approximate the uniform Bingham density.

Let the BM approximating the uniform Bingham density be defined by Eq. (3.28). The parameters $w^{(\ell)}$, $\boldsymbol{M}^{(\ell)}$, and $\boldsymbol{Z}^{(\ell)}$ for $\ell = 1, 2, \ldots, L$, which define the BM density, are now sought such that the BM density approximates the uniform Bingham density. Similarly to the GM and BM approximations in Sections 3.2 and 3.4.1, the L_2 distance between the canonical Bingham density and its approximating BM density, as given by Eq. (3.30), would be minimized to find the parameters of the BM density. If this L_2 distance is minimized without restricting $\boldsymbol{Z}^{(\ell)}$ for $\ell = 1, 2, \ldots, L$, each $\boldsymbol{Z}^{(\ell)}$ would be null, and the BM mixture would become degenerate (because each component of the mixture is identical). Because of this, the L_2 distance is not explicitly minimized to construct the BM density approximating the uniform Bingham density. First, the $w^{(\ell)}$

and $\boldsymbol{M}^{(\ell)}$ for $\ell = 1, 2, \ldots, L$ are specified using spherical coordinates and their differential area swept out on the unit hypercylinder. Then, the $\boldsymbol{Z}^{(\ell)} \neq \boldsymbol{0}$ for $\ell = 1, 2, \ldots, L$ are specified such that the L_2 distance is sufficiently small in the context of the given application.

Now, the mean directions of the BM components are specified by constructing a uniform grid over the spherical coordinates. Note that the mean direction of each component does not fully define the orientation matrix of the component; rather, it defines only the last column of the orientation matrix. This can be observed from Eq. (3.21). It is straightforward to see that the identity quaternion, $\bar{p}$, represents the mean direction of the canonical Bingham density; therefore, the last column of the orientation matrix, $\boldsymbol{M}$, represents the mean direction of $\bar{q}$ according to Eq. (3.21). In order to specify the mean directions of the components, a uniform grid for each spherical coordinate is constructed according to

$$\phi_i^{(\ell_i)} = \frac{\pi(2\ell_i - 1)}{2\bar{L}} \tag{3.39}$$

for $\ell_i = 1, 2, \ldots, \bar{L}$ and $i = 1, 2, \ldots, s$, where $\bar{L}$ is the number of points in the discrete grid of each ϕ_i and is chosen to be the same for each spherical coordinate (thus, the L_i notation is omitted in favor of the $\bar{L}$ notation). This choice stems from the fact that, if the angles swept out by each spherical coordinate between points on the grid, $\Delta\phi_1$, $\Delta\phi_2$, $\cdots$, $\Delta\phi_s$, are the same, the parameterization of the weights of the BM density is simplified. The uniform grids for each spherical coordinate are then combined to yield the grid of mean directions of the components of the BM, expressed as spherical coordinates, according to

$$\boldsymbol{\phi}^{(\ell)} = \begin{bmatrix} \phi_1^{(\ell_1)} & \phi_2^{(\ell_2)} & \cdots & \phi_s^{(\ell_s)} \end{bmatrix}^T, \tag{3.40}$$

where $\ell = 1, 2, \ldots, L$, $L = \bar{L}^s$ is the number of components in the BM density approximating the uniform Bingham density, and each ℓ corresponds to a unique permutation of ℓ_1, ℓ_2, $\ldots$, ℓ_s. Therefore, the mean direction of each component is expressed as unit-vector according to $\bar{q}(\boldsymbol{\phi}^{(\ell)})$ for $\ell = 1, 2, \ldots, L$. Figure (3.6) shows the grid of mean directions for $\bar{L} = 10$ on $\mathbb{S}^1$ and $\mathbb{S}^2$.

Note that the discrete grid for each spherical coordinate is constructed in the interval $[0, \pi]$, even though $\phi_s \in [0, 2\pi)$; this stems from the antipodal symmetry of each component of the BM. By restricting the grid for ϕ_s to lie in the interval $[0, \pi)$, the antipodal symmetry of each component then covers the other half of the unit-hypersphere, as can be observed in Figure (3.6). By discretizing the mean direction of each component over the spherical coordinates in this manner, it is observed that $L = \bar{L}^s$ components exist in the BM approximating the Bingham density on the unit-hypersphere. Special care must be taken when selecting $\bar{L}$, because the number of components in the resulting BM suffers from the curse of dimensionality, similarly to the construction of the multivariate GM density.
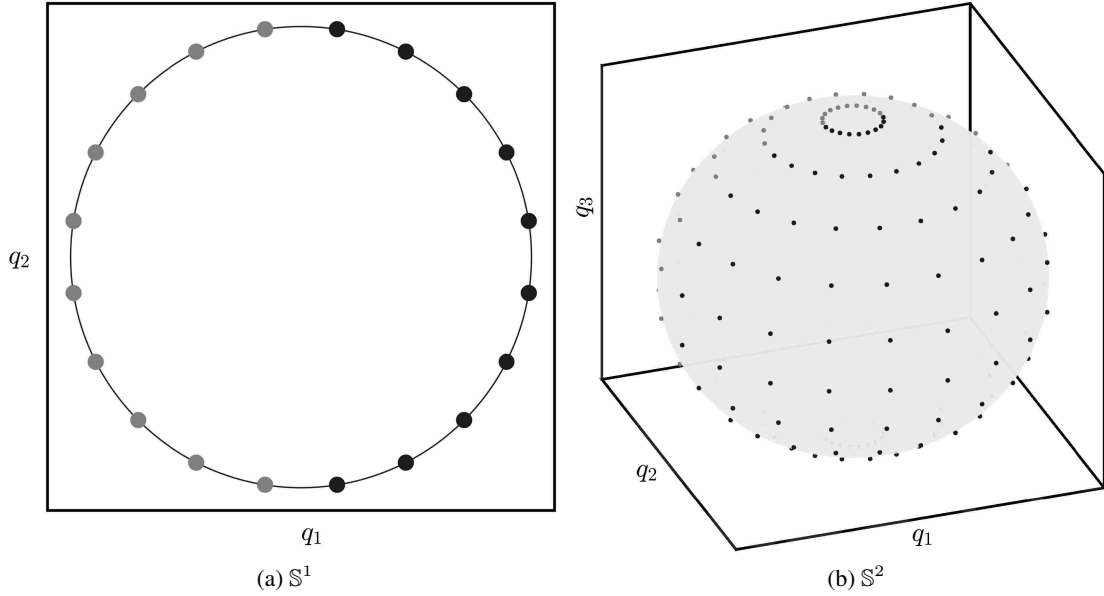
Figure 3.6. Grid of mean directions for $\bar{L} = 10$ on $\mathbb{S}^1$ and $\mathbb{S}^2$. The black markers denote the mean direction, and the gray markers denote the antipodal direction of each mean direction.

Now that the mean direction of each component, $\bar{q}(\phi^{(\ell)})$ for $\ell = 1, 2, \ldots, L$, has been defined, the orientation matrix of each component can be found. In order to find the orientation matrix for each component of the BM density given its mean direction, it is first necessary to restrict each component to be isotropic; that is, the concentration parameters of the each component are restricted to be identical ($Z_1 = Z_2 = \cdots = Z_s$). Under this restriction, each component of the BM is rotationally invariant about its mean direction, and the last column of the orientation matrix, which is given by the mean direction of the component, sufficiently specifies the orientation matrix of each component. The other columns of the orientation matrix are arbitrary as long as they are found such that the orientation matrix belongs to $\mathrm{SO}(s + 1)$. This gives the orientation matrix of each component of the mixture as

$$\boldsymbol{M}^{(\ell)} = \left[\boldsymbol{v}_1^{(\ell)} | \boldsymbol{v}_2^{(\ell)} | \cdots | \boldsymbol{v}_s^{(\ell)} | \bar{\boldsymbol{q}}(\phi^{(\ell)}) \right], \tag{3.41}$$

for $\ell = 1, 2, \ldots, L$, where $\boldsymbol{v}_1^{(\ell)}$, $\boldsymbol{v}_2^{(\ell)}$, $\ldots$, $\boldsymbol{v}_s^{(\ell)}$ are arbitrary under the restriction that $\boldsymbol{M}^{(\ell)} \in \mathrm{SO}(s + 1)$. This is performed by first defining the entries of the last column of the orientation matrix using $\bar{\boldsymbol{q}}(\phi^{(\ell)})$, and then using Eq. (2.27) when $s = 1$ or Eq. (2.52) when $s = 3$ to find the remaining entries of the orientation matrix. For the $s = 3$ case, the orientation matrix is defined by a single right-isoclonic rotation, which is sufficient to specify the orientation matrix because its

first three columns are arbitrary provided $\boldsymbol{M}^{(\ell)} \in \mathrm{SO}(s+1)$, which is satisfied by the rotation matrix defining the right-isoclonic rotation. When $s = 2$, the first two columns of $\boldsymbol{M}^{(\ell)}$ are found as orthonormal vectors to $\bar{\boldsymbol{q}}(\boldsymbol{\phi}^{(\ell)})$ and each other, and are ordered such that $\det\left\{\boldsymbol{M}^{(\ell)}\right\} = 1$.

While this grid is uniform and equally spaced in the spherical coordinates, the resulting mean directions are not equally spaced on the hypersphere for dimensions $s > 1$, as is observed in Figure (3.6b). In order to compensate for this, the weights of the components are chosen to be proportional to the linearized area according to Eq. (3.38) of the unit-hypersphere swept out by the spherical coordinates defining the mean direction of each component. By selecting the weights in this manner, the components that are spaced closer together possess lower weights. This weighting scheme will yield a perfectly uniform BM density (with nonuniform components) as the number of components in the mixture approaches infinity. This yields the weights of the mixture as

$$w^{(\ell)} = \frac{\bar{w}^{(\ell)}}{\sum_{i=1}^{L} \bar{w}^{(i)}} \, , \tag{3.42}$$

for $\ell = 1, 2, \ldots, L$, where

$$\bar{w}^{(\ell)} \propto \Delta A(\boldsymbol{\phi}^{(\ell)}) \tag{3.43}$$

$$\propto \sin^{s-1} \phi_1^{(\ell)} \sin^{s-2} \phi_2^{(\ell)} \cdots \sin \phi_{s-1}^{(\ell)} . \tag{3.44}$$

Because the grid is uniform in each spherical coordinate, $\Delta\phi_1, \Delta\phi_2, \cdots, \Delta\phi_s$ are constant in the evaluation of Eq. (3.43) and may be neglected in its calculation due to the proportionality and not equality. Analysis of Eqs. (3.42) and (3.43) shows that the weight of each component of the BM is approximately proportional to the area of the unit-hypersphere assigned to each grid point. This proportionality is approximate because the area assigned to each grid point is the calculated using the linear relationship between the area of the unit-hypersphere and grid size of each point in the discrete grid. Equation (3.42) ensures that the weights of the BM density sum to unity while maintaining their desired proportionality to the area on the unit-hypersphere. Parameterizing the weights in this manner accounts for the nonuniform grid of mean directions on the unit-hypersphere and will allow for the uncertainty of each component to approach zero in the limiting case as $\bar{L}$ goes to infinity.

So far, the weights and orientation matrices of the BM density have been specified; now, the matrix of concentration parameters must be specified. Recall that the matrix of concentration parameters for each component has been restricted to be isotropic; that is, $Z_1 = Z_2 = \cdots = Z_s$ in the matrix of concentration parameters. Furthermore, the BM is restricted such that each component possesses the same matrix of concentration parameters. Under these restrictions, the matrix of concentration parameters for all components can be parameterized by a single parameter,

ζ, according to

$$Z^{(\ell)} = \zeta \begin{bmatrix} I & 0 \\ 0^T & 0 \end{bmatrix}, \tag{3.45}$$

for $\ell = 1, 2, \ldots, L$, where $\zeta < 0$. If $\zeta = 0$, the BM density would be a perfect approximation of the uniform Bingham density; however, in this case, the mixture is degenerate, which is why ζ is restricted to be strictly negative. As ζ decreases, the error (in the L_2 sense) between the BM density and the uniform Bingham density increases, while the uncertainty of each component decreases. The parameter ζ should be chosen as small as possible, which yields the smallest uncertainty in each of the components, without incurring "significant error" between the BM approximation and the uniform Bingham density, where "significant" is problem dependent, and, thus, not further guidelines can be imposed.

Two example BM densities in $\mathbb{S}^1$ approximating the uniform Bingham density are presented in Figure (3.7). Both of these Bingham mixture densities approximate the uniform density well; however, as the number of components increases, the uncertainty in each component is decreases, which can be desirable for certain applications.

(a) $L = 11$ (b) $L = 51$
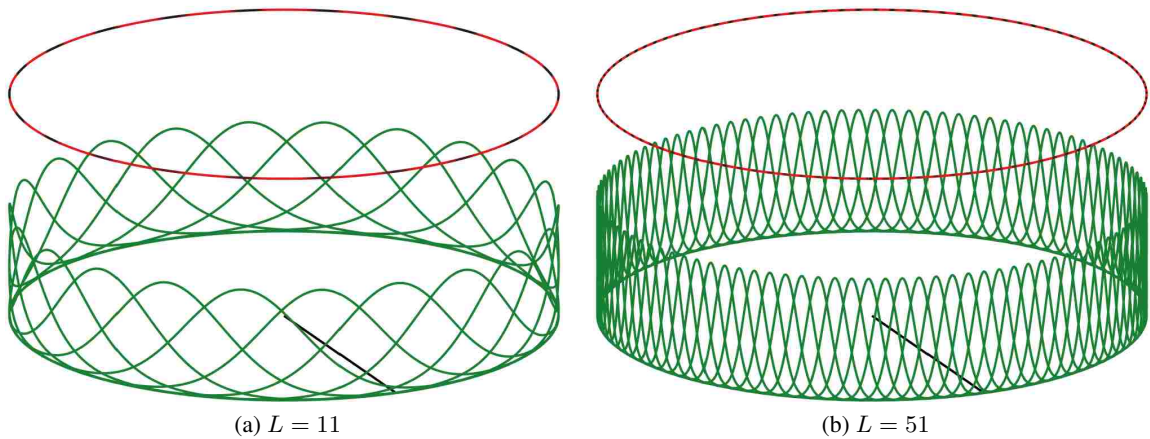
Figure 3.7. BM approximations of the uniform Bingham density. The Bingham density is red, the BM is black, and the components are green.

3.5. GAUSS-BINGHAM DENSITY

The Gauss-Bingham density probabilistically represents a state vector composed of a Gaussian-distributed vector, $\mathbf{x} \in \mathbb{R}^r$, and a Bingham-distributed unit-vector, $\bar{q} \in \mathbb{S}^s$, on its natural manifold

defined by $\mathbb{S}^s \times \mathbb{R}^r$. Before constructing the Gauss-Bingham density, first consider the motivating example of manipulating two jointly Gaussian-distributed random vectors given by $\boldsymbol{x}$ and $\boldsymbol{y}$ into the product of the density of $\boldsymbol{x}$ and the density of $\boldsymbol{y}$ conditioned on $\boldsymbol{x}$. The joint density of $[\boldsymbol{x}^T \ \boldsymbol{y}^T]^T$ is Gaussian and is given by

$$p(\boldsymbol{x}, \boldsymbol{y}) = p_g \left(\begin{bmatrix} \boldsymbol{x} \\ \boldsymbol{y} \end{bmatrix}; \begin{bmatrix} \boldsymbol{m}_x \\ \boldsymbol{m}_y \end{bmatrix}, \begin{bmatrix} \boldsymbol{P}_x & \boldsymbol{P}_{xy} \\ \boldsymbol{P}_{xy}^T & \boldsymbol{P}_y \end{bmatrix} \right) ,$$

where $\boldsymbol{m}$ and $\boldsymbol{P}$ represent the mean and covariance of their subscripted vector(s), respectively, and $\boldsymbol{P}_{xy}$ quantifies the correlations between $\boldsymbol{x}$ and $\boldsymbol{y}$. The density of $\boldsymbol{y}$ conditioned on $\boldsymbol{x}$ is Gaussian-distributed and is given by [30]

$$p_g(\boldsymbol{y}|\boldsymbol{x}; \boldsymbol{m}_{y|x}(\boldsymbol{x}), \boldsymbol{P}_{y|x}) = p_g(\boldsymbol{y}|\boldsymbol{x}; \boldsymbol{m}_y + \boldsymbol{P}_{xy}^T \boldsymbol{P}_x^{-1}(\boldsymbol{x} - \boldsymbol{m}_x), \boldsymbol{P}_y - \boldsymbol{P}_{xy}^T \boldsymbol{P}_x^{-1} \boldsymbol{P}_{xy}) ,$$

where $\boldsymbol{m}_{y|x}(\boldsymbol{x})$ and $\boldsymbol{P}_{y|x}$ are the mean and covariance, respectively, of $\boldsymbol{y}$ conditioned on $\boldsymbol{x}$. It is interesting to note the functional dependence of $\boldsymbol{m}_{y|x}$ on $\boldsymbol{x}$. From the definition of conditional probability, it follows that the joint density of $\boldsymbol{x}$ and $\boldsymbol{y}$ can be expressed as

$$p(\boldsymbol{x}, \boldsymbol{y}) = p_g(\boldsymbol{x}; \boldsymbol{m}_x, \boldsymbol{P}_x) \, p_g(\boldsymbol{y}|\boldsymbol{x}; \boldsymbol{m}_y + \boldsymbol{P}_{xy}^T \boldsymbol{P}_x^{-1}(\boldsymbol{x} - \boldsymbol{m}_x), \boldsymbol{P}_y - \boldsymbol{P}_{xy}^T \boldsymbol{P}_x^{-1} \boldsymbol{P}_{xy}) . \qquad (3.46)$$

The conditional mean and covariance of $p(\boldsymbol{y}|\boldsymbol{x})$ are not restricted to be

$$\boldsymbol{m}_{y|x}(\boldsymbol{x}) = \boldsymbol{m}_y + \boldsymbol{P}_{xy}^T \boldsymbol{P}_x^{-1}(\boldsymbol{x} - \boldsymbol{m}_x) \qquad (3.47a)$$

$$\boldsymbol{P}_{y|x} = \boldsymbol{P}_y - \boldsymbol{P}_{xy}^T \boldsymbol{P}_x^{-1} \boldsymbol{P}_{xy} \qquad (3.47b)$$

for the definition of conditional probability to be valid; however, Eqs. (3.47) must hold for the result to be Gaussian-distributed.

The left- and right-hand sides of Eq. (3.46) express the joint Gaussian density of $[\boldsymbol{x}^T \ \boldsymbol{y}^T]^T$ in two different forms. In the case where the vectors $\boldsymbol{x}$ and $\boldsymbol{y}$ are jointly Gaussian-distributed, as they are in this example, little (if anything) is gained by manipulating the left-hand side of Eq. (3.46) into the ride-hand side of Eq. (3.46); however, in the case when one or both of the jointly distributed vectors are not Gaussian-distributed, correlation between the vectors can be introduced in a similar fashion to Eq. (3.46) by utilizing the definition of conditional probability. This allows the density of two jointly distributed random vectors, $\boldsymbol{x}_1$ and $\boldsymbol{x}_2$, to be written as the product of the density of $\boldsymbol{x}_1$ and the density of $\boldsymbol{x}_2$ conditioned on $\boldsymbol{x}_1$; i.e.,

$$p(\boldsymbol{x}_1, \boldsymbol{x}_2) = p(\boldsymbol{x}_1) \, p(\boldsymbol{x}_2|\boldsymbol{x}_1) .$$

Using the definition of conditional probability, the Gauss-Bingham density is constructed as the product of a Gaussian density and a Bingham density conditioned on the Gaussian-distributed random variable as

$$p_{gb}(\boldsymbol{x}; \boldsymbol{m}, \boldsymbol{P}, \boldsymbol{M}(\mathbf{z}), \boldsymbol{Z}) \triangleq p_g(\mathbf{x}; \boldsymbol{m}, \boldsymbol{P}) \, p_b(\bar{\boldsymbol{q}}; \boldsymbol{M}(\mathbf{z}), \boldsymbol{Z}), \qquad (3.48)$$

where $\boldsymbol{x}$ represents the state vector comprised of the antipodally symmetric unit-vector, $\bar{\boldsymbol{q}} \in \mathbb{S}^s$, and a vector of other Euclidean states, $\mathbf{x} \in \mathbb{R}^r$, according to

$$\boldsymbol{x} = \begin{bmatrix} \bar{\boldsymbol{q}} \\ \mathbf{x} \end{bmatrix} \in \mathbb{S}^s \times \mathbb{R}^r, \qquad (3.49)$$

and $\mathbf{x}$ and $\mathbf{z}$ are related according to Eq. (3.6). $\mathbb{S}^s \times \mathbb{R}^r$ represents the unit hypercylinder of dimension s and r, which is the intersection of the unit-hypersphere of dimension s, $\mathbb{S}^s$, and Euclidean space of dimension r, $\mathbb{R}^r$. If $s = 1$ and $r = 1$, the unit hypercylinder is defined by $\mathbb{S}^1 \times \mathbb{R}^1$, which reduces to a unit cylinder, as expected. The conditional orientation matrix, $\boldsymbol{M}(\mathbf{z})$, quantifies the correlation between the Gaussian-distributed random variable $\mathbf{x}$ and the conditional Bingham-distributed random variable $\bar{\boldsymbol{q}}$.

The Gauss-Bingham density, as defined by Eq. (3.48), is constructed as the product of the Gaussian-distributed $\mathbf{x}$, and the conditional Bingham-distributed $\bar{\boldsymbol{q}}$, in which the orientation matrix of the conditional Bingham density is functionally dependent on the Gaussian-distributed variable, $\mathbf{x}$. The conditional Bingham density is conditioned on the Gaussian-distributed random variable $\mathbf{x}$ through the orientation matrix $\boldsymbol{M}(\mathbf{z})$, using the transformation of variables that defines the canonical Gaussian density, which is given by Eqs. (3.6). Because of this, the conditional orientation matrix of the Gauss-Bingham density can be equivalently parameterized by

$$\boldsymbol{M}(\mathbf{z}) = \boldsymbol{M}(\mathbf{x}; \boldsymbol{m}, \boldsymbol{P}),$$

such that the Gauss-Bingham density in Eq. (3.48) can be equivalently expressed as

$$p_{gb}(\boldsymbol{x}; \boldsymbol{m}, \boldsymbol{P}, \boldsymbol{M}(\mathbf{x}; \boldsymbol{m}, \boldsymbol{P}), \boldsymbol{Z}) \triangleq p_g(\mathbf{x}; \boldsymbol{m}, \boldsymbol{P}) \, p_b(\bar{\boldsymbol{q}}; \boldsymbol{M}(\mathbf{x}; \boldsymbol{m}, \boldsymbol{P}), \boldsymbol{Z}), \qquad (3.50)$$

The orientation matrix is expressed using $\mathbf{z}$ instead of $\mathbf{x}$ for better numerical stability because $\mathbf{z}$ is nondimensional. The functional dependence of the orientation matrix on $\mathbf{z}$ is discussed in Section 3.5.1.

The Gauss-Bingham density possesses the following favorable properties for probabilistically quantifying the attitude quaternion (when $s = 1$ or $s = 3$) and other Euclidean states:

   – The Gauss-Bingham density is antipodally symmetric in the attitude quaternion; thus, antipodal quaternions $\bar{q}$ and $-\bar{q}$ (which represent the same physical attitude) are equiprobable,

   – the Gauss-Bingham density quantifies the uncertainty of Euclidean states and the attitude quaternion on their natural manifold $\mathbb{S}^s \times \mathbb{R}^r$, and

   – the Gauss-Bingham density possesses a simple representation of an equiprobable attitude quaternion for a given angular velocity when the $\boldsymbol{Z}$ matrix is null.

In order to illustrate these properties, consider an application of the Gauss-Bingham density to quantify the uncertainty of the one-dimensional attitude quaternion and angular velocity of a body undergoing rotation about the z-axis. In this case, the state vector is defined as

$$\boldsymbol{x} = \begin{bmatrix} \bar{q} \\ \omega \end{bmatrix} \in \mathbb{S}^1 \times \mathbb{R}^1 \,, \tag{3.51}$$

where $\omega \in \mathbb{R}^1$ is the angular velocity of the body about the z-axis and $\bar{q} \in \mathbb{S}^1$ is the one-dimensional attitude quaternion of the body, which is defined by Eq. (2.42). No correlation structure for the orientation matrix, $\boldsymbol{M}(\mathbf{z})$, has yet been defined. Before formally defining this correlation structure, first consider two types of correlation, which are introduced into a set of parameters used to specify $\boldsymbol{M}(\mathbf{z})$: linear and quadratic. Figures (3.8a) and (3.8b) show examples of the Gauss-Bingham density (with $Z_1 \neq 0$) for the linear and quadratic correlation structures, respectively. The marginalized attitude quaternion for the linear and quadratic correlation structures are shown in Figures. (3.8c) and (3.8d), respectively. It can be observed in these figures that the probability of the antipodal attitude quaternions is equal for any given angular velocity, which is a desirable property as these quaternions represent the same physical attitude.

When $\boldsymbol{Z} = \boldsymbol{0}$, the marginalized attitude quaternion is equiprobable regardless of the correlation structure used. This is illustrated in Figures. (3.9a) and (3.9b), which show the Gauss-Bingham density in $\mathbb{S}^1 \times \mathbb{R}^1$ and the marginal density of the attitude quaternion when $Z_1 = 0$. This property of the Gauss-Bingham density is advantageous for representing the attitude quaternion as equiprobable when no prior attitude information is available.

3.5.1. Correlation Structure. In order to define the correlation structure for the orientation matrix $\boldsymbol{M}(\mathbf{z})$, it is important to note that $\boldsymbol{M}(\mathbf{z}) \in \mathrm{SO}(s+1) \ \forall \ \mathbf{z} \in \mathbb{R}^r$. In order to ensure that this condition is met, the correlation structure is introduced into a minimum set of parameters necessary to specify the orientation matrix, denoted by $\phi(\mathbf{z})$, such that the orientation matrix is given by $\boldsymbol{M}(\phi(\mathbf{z}))$. A minimum parameter set, which is comprised of $s(s+1)/2 \triangleq n_\phi$ parameters, is necessary to define the orientation matrix; therefore $\phi(\mathbf{z}) \in \mathbb{R}^{s(s+1)/2}$ [15, 16]. The method for constructing the orientation matrix from the set of minimum parameters depends on s and the

(a) Linear correlation

(b) Quadratic correlation

(c) Marginalized quaternion

(d) Marginalized quaternion
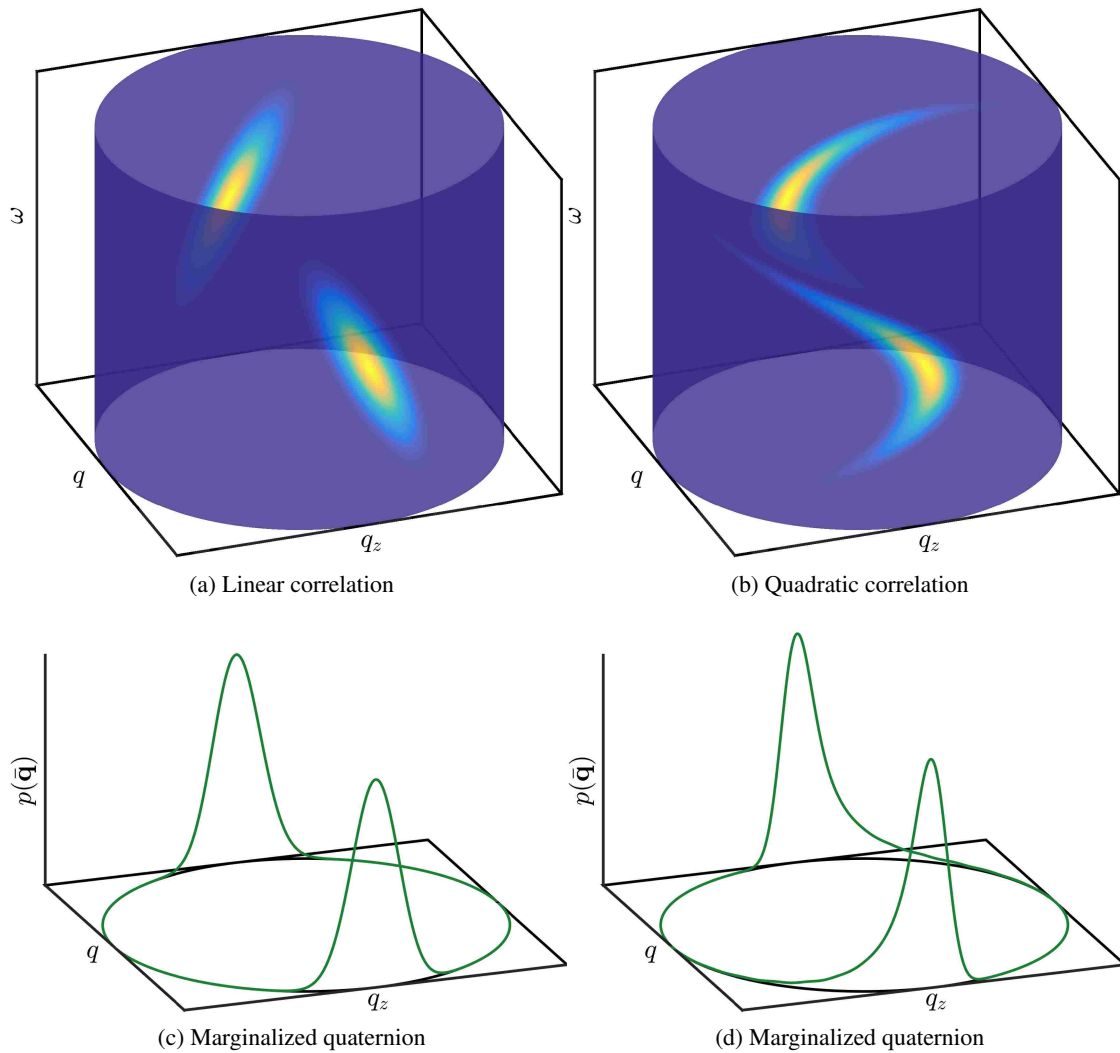
Figure 3.8. Gauss-Bingham densities on $\mathbb{S}^1 \times \mathbb{R}^1$ for a linear and quadratic correlation structure.

parameter set chosen. Methods for constructing the orientation matrix for dimensions $s = 1, 2$, and 3 are now presented.

3.5.1.1. Correlation Structure for s = 1. First, consider the Gauss-Bingham density specialized to $s = 1$. Only one parameter is necessary to specify the orientation matrix in this dimension because $n_\phi = 1$. This parameter is chosen to be the rotation about the known axis of rotation, which is given by $\theta(\mathbf{z})$, such that $\phi(\mathbf{z}) = \theta(\mathbf{z})$. The orientation matrix is then defined by a

(a) Gauss-Bingham density

(b) Marginalized quaternion density
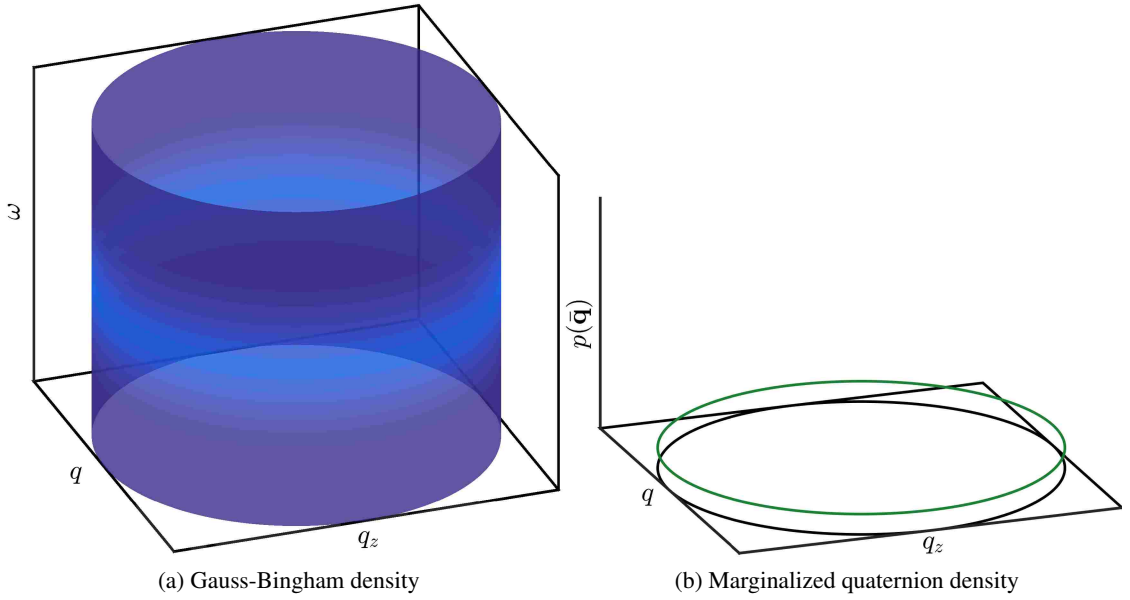
Figure 3.9. Gauss-Bingham density on $\mathbb{S}^1 \times \mathbb{R}^1$ for $Z_1 = 0$.

specialization of Eq. (2.27) according to

$$
\boldsymbol{M}(\boldsymbol{\phi}(\mathbf{z})) = \boldsymbol{M}(\theta(\mathbf{z})) = \begin{bmatrix} \cos \theta(\mathbf{z}) & \sin \theta(\mathbf{z}) \\ -\sin \theta(\mathbf{z}) & \cos \theta(\mathbf{z}) \end{bmatrix}.
$$

This orientation matrix is constructed identically to the one-dimensional attitude matrix defined by the heading angle of the body; however, it is important to realize that $\theta(\mathbf{z})$ defines the mean direction of the quaternion, which in turn defines the heading angle of the body. This orientation matrix is *not* defined by the heading angle directly. The angle of rotation, $\theta(\mathbf{z})$, is defined on the interval $[-\pi, \pi)$ for all $\mathbf{z}$. Because

$$
\boldsymbol{M}(\theta(\mathbf{z})) = \boldsymbol{M}(\theta(\mathbf{z}) + 2\pi k) \quad \text{for all} \quad k \in \mathbb{Z},
$$

where $\mathbb{Z}$ is the set of integers, $\theta(\mathbf{z})$ can be bounded to the interval $[-\pi, \pi)$ for all $\mathbf{z}$ by adding the appropriate multiple of 2π.

3.5.1.2. Correlation Structure for s = 2. Now, consider the Gauss-Bingham density specialized to $s = 2$. Three parameters are necessary to specify the orientation matrix in this dimension. These parameters are chosen to be the rotation vector, such that $\boldsymbol{\phi}(\mathbf{z}) = \boldsymbol{\theta}(\mathbf{z})$. The orientation

matrix is then given by the specialization of Eq. (2.31) according to

$$M(\phi(\mathbf{z})) = M(\boldsymbol{\theta}(\mathbf{z})) = \exp\left\{-[\boldsymbol{\theta}(\mathbf{z})\times]\right\}.$$

Similarly to the correlation structure for $s = 1$, $\boldsymbol{\theta}(\mathbf{z})$ represents the mean direction of the conditional Bingham-distributed unit-vector in $s = 2$ like $\theta(\mathbf{z})$ does for $s = 1$. Instead of using the matrix exponential operator to find the orientation matrix in this dimension, first, the equivalent axis-angle parameterization of the rotation vector, $\boldsymbol{\theta}(\mathbf{z})$, can be found according to Eqs. (2.32) and (2.33). The orientation matrix can then be found by substituting the equivalent axis-angle parameterization into Eq. (2.23) to yield

$$M(\phi(\mathbf{z})) = M(\boldsymbol{\theta}(\mathbf{z})) = \boldsymbol{I} - \sin\|\boldsymbol{\theta}(\mathbf{z})\| \left[\frac{\boldsymbol{\theta}(\mathbf{z})}{\|\boldsymbol{\theta}(\mathbf{z})\|}\times\right] + (1 - \cos\|\boldsymbol{\theta}(\mathbf{z})\|) \left[\frac{\boldsymbol{\theta}(\mathbf{z})}{\|\boldsymbol{\theta}(\mathbf{z})\|}\times\right]^2.$$

If $\|\boldsymbol{\theta}(\mathbf{z})\| = 0$, it follows that $M(\mathbf{z}) = \boldsymbol{I}$, because the angle of rotation is zero. The norm of the rotation vector, $\|\boldsymbol{\theta}(\mathbf{z})\|$, is defined on the interval $[-\pi, \pi)$ for all $\mathbf{z}$. Because

$$M(\boldsymbol{\theta}(\mathbf{z})) = M\left(\boldsymbol{\theta}(\mathbf{z}) + 2\pi k\frac{\boldsymbol{\theta}(\mathbf{z})}{\|\boldsymbol{\theta}(\mathbf{z})\|}\right) \quad \text{for all} \quad k \in \mathbb{Z},$$

$\|\boldsymbol{\theta}(\mathbf{z})\|$ can be bounded to the interval $[-\pi, \pi)$ for all $\mathbf{z}$ by adding the appropriate multiple of $2\pi\boldsymbol{\theta}(\mathbf{z})/\|\boldsymbol{\theta}(\mathbf{z})\|$.

3.5.1.3. Correlation Structure for s = 3. Finally, consider the Gauss-Bingham density specialized to $s = 3$. Six parameters are necessary to specify the orientation matrix in this dimension. These parameters are chosen to be two rotation vectors representing a left- and right-isoclonic rotation, as detailed in Section 2.4. Let these rotation vectors be denoted by $\boldsymbol{\theta}_L(\mathbf{z})$ and $\boldsymbol{\theta}_R(\mathbf{z})$, respectively, such that $\phi(\mathbf{z})$ is given by the concatenation of these vectors according to

$$\phi(\mathbf{z}) = \begin{bmatrix} \boldsymbol{\theta}_L(\mathbf{z}) \\ \boldsymbol{\theta}_R(\mathbf{z}) \end{bmatrix}.$$

Given these two rotation vectors representing the left- and right-isoclonic rotations, the method presented in Section 2.4 is used to construct the orientation matrix for $s = 3$, which yields the orientation matrix as

$$M(\phi(\mathbf{z})) = M\left(\begin{bmatrix} \boldsymbol{\theta}_L(\mathbf{z}) \\ \boldsymbol{\theta}_R(\mathbf{z}) \end{bmatrix}\right) = \boldsymbol{R}_L(\bar{\boldsymbol{q}}_L(\boldsymbol{\theta}_L(\mathbf{z})))\boldsymbol{R}_R(\bar{\boldsymbol{q}}_R(\boldsymbol{\theta}_R(\mathbf{z}))),$$

where the functional dependence of $\bar{\boldsymbol{q}}_L$ on $\boldsymbol{\theta}_L(\mathbf{z})$, and subsequently $\boldsymbol{R}_L$ on $\bar{\boldsymbol{q}}_L(\boldsymbol{\theta}_L(\mathbf{z}))$, is shown explicitly for clarity, and similarly for the right-isoclonic rotation.

The norm of each of these rotation vectors, $||\boldsymbol{\theta}_L(\mathbf{z})||$ and $||\boldsymbol{\theta}_R(\mathbf{z})||$, is defined on the interval $[-\pi,\ \pi)$ for all $\mathbf{z}$. Because

$$M\left(\begin{bmatrix}\boldsymbol{\theta}_L(\mathbf{z})\\\boldsymbol{\theta}_R(\mathbf{z})\end{bmatrix}\right) = M\left(\begin{bmatrix}\boldsymbol{\theta}_L(\mathbf{z}) + 2\pi k_L\frac{\boldsymbol{\theta}_L(\mathbf{z})}{||\boldsymbol{\theta}_L(\mathbf{z})||}\\\boldsymbol{\theta}_R(\mathbf{z}) + 2\pi k_R\frac{\boldsymbol{\theta}_R(\mathbf{z})}{||\boldsymbol{\theta}_R(\mathbf{z})||}\end{bmatrix}\right)$$

for all $k_L, k_R \in \mathbb{Z}$, $||\boldsymbol{\theta}_L(\mathbf{z})||$ and $||\boldsymbol{\theta}_R(\mathbf{z})||$ can be bounded to the interval $[-\pi,\ \pi)$ for all $\mathbf{z}$ by adding the appropriate multiple of $2\pi\boldsymbol{\theta}_L(\mathbf{z})/||\boldsymbol{\theta}_L(\mathbf{z})||$ and $2\pi\boldsymbol{\theta}_R(\mathbf{z})/||\boldsymbol{\theta}_R(\mathbf{z})||$ to $\boldsymbol{\theta}_L(\mathbf{z})$ and $\boldsymbol{\theta}_R(\mathbf{z})$, respectively.

Now that the functional dependence of the orientation matrix, $M(\boldsymbol{\phi}(\mathbf{z}))$, on the minimal set of parameters, $\boldsymbol{\phi}(\mathbf{z})$, has been defined for $s = 1, 2, 3$, the functional dependence of $\boldsymbol{\phi}(\mathbf{z})$ on $\mathbf{z}$ needs to be defined. Two choices for this functional dependence are considered: linear and quadratic. It is noted that the quadratic form of this functional dependence is not used after it is presented; however, it is a valid form of this functional dependence and is presented to show the flexibility of the Gauss-Bingham density.

First, consider the quadratic dependence of $\boldsymbol{\phi}(\mathbf{z})$ on $\mathbf{z}$, which is defined by

$$\boldsymbol{\phi}(\mathbf{z}) = \boldsymbol{\phi}_0 + \boldsymbol{\beta}\mathbf{z} + \begin{bmatrix}\mathbf{z}^T\boldsymbol{\Gamma}_1\mathbf{z} & \mathbf{z}^T\boldsymbol{\Gamma}_2\mathbf{z} & \cdots & \mathbf{z}^T\boldsymbol{\Gamma}_{n_\phi}\mathbf{z}\end{bmatrix}^T, \tag{3.52}$$

where $\boldsymbol{\phi}_0 \in \mathbb{R}^{n_\phi}$, $\boldsymbol{\beta} \in \mathbb{R}^{n_\phi \times r}$ and $\boldsymbol{\Gamma}_i \in \{\mathbb{R}^{r \times r} : \boldsymbol{\Gamma}_i = \boldsymbol{\Gamma}_i^T\}$, $i = 1, \ldots, n_\phi$ quantify the zeroth-, first-, and second-order correlation, respectively, of $\mathbf{z}$ on $\boldsymbol{\phi}(\mathbf{z})$. The choice of implementing $\mathbf{z}$ instead of $\mathbf{x}$ in the correlation structure results in nondimensional coefficients $\boldsymbol{\beta}$ and $\boldsymbol{\Gamma}_i$, which is preferred for numerical stability. Noting that the orientation matrix $M(\mathbf{z})$ is now explicitly defined by $\mathbf{z}$, $\boldsymbol{\phi}_0$, $\boldsymbol{\beta}$, $\boldsymbol{\Gamma}_1, \ldots, \boldsymbol{\Gamma}_{n_\phi}$ and that $\mathbf{z}$ is explicitly defined by $\mathbf{x}$, $\boldsymbol{m}$, and $\boldsymbol{P}$, the orientation matrix using the quadratic correlation structure is parameterized as

$$M(\mathbf{z}) = M(\mathbf{x}; \boldsymbol{m}, \boldsymbol{P}, \boldsymbol{\phi}_0, \boldsymbol{\beta}, \boldsymbol{\Gamma}_1, \ldots, \boldsymbol{\Gamma}_{n_\phi}),$$

and the Gauss-Bingham density is given by the specialization of Eq. (3.50) as

$$p_{gb}(\boldsymbol{x}; \boldsymbol{m}, \boldsymbol{P}, \boldsymbol{\phi}_0, \boldsymbol{\beta}, \boldsymbol{\Gamma}_1, \ldots, \boldsymbol{\Gamma}_{n_\phi}, \boldsymbol{Z}) =$$
$$p_g(\mathbf{x}; \boldsymbol{m}, \boldsymbol{P})\, p_b(\bar{q}; M(\mathbf{x}; \boldsymbol{m}, \boldsymbol{P}, \boldsymbol{\phi}_0, \boldsymbol{\beta}, \boldsymbol{\Gamma}_1, \ldots, \boldsymbol{\Gamma}_{n_\phi}), \boldsymbol{Z})\,.$$

The number of parameters necessary to quantify the quadratic correlation between $\mathbf{z}$ and $\boldsymbol{\phi}(\mathbf{z})$ is $\frac{1}{2}n_\phi(2+2r+r(r+1))$, which increases quadratically with r. For one-dimensional attitude ($\mathbb{R}^1 \times \mathbb{S}^1$), three-dimensional attitude ($\mathbb{S}^3 \times \mathbb{R}^3$), and dynamic pose ($\mathbb{S}^3 \times \mathbb{R}^9$) quantification, 3, 60, and 330 unique parameters are needed to quantify the quadratic relationship between $\boldsymbol{\phi}(\mathbf{z})$ and $\mathbf{z}$.

Now, consider the linear correlation structure for $\phi(\mathbf{z})$, which is given by a simplification of Eq. (3.52) as

$$\phi(\mathbf{z}) = \phi_0 + \boldsymbol{\beta}\mathbf{z}\,.$$

Using the linear correlation structure, the orientation matrix is parameterized as

$$\boldsymbol{M}(\mathbf{z}) = \boldsymbol{M}(\mathbf{x}; \boldsymbol{m}, \boldsymbol{P}, \phi_0, \boldsymbol{\beta})\,,$$

and the Gauss-Bingham density is given by the specialization of Eq. (3.50) as

$$p_{gb}(\boldsymbol{x}; \boldsymbol{m}, \boldsymbol{P}, \phi_0, \boldsymbol{\beta}, \boldsymbol{Z}) = p_g(\mathbf{x}; \boldsymbol{m}, \boldsymbol{P})\, p_b(\bar{q}; \boldsymbol{M}(\mathbf{x}; \boldsymbol{m}, \boldsymbol{P}, \phi_0, \boldsymbol{\beta}), \boldsymbol{Z})\,. \tag{3.53}$$

The number of parameters necessary to quantify the linear correlation between $\mathbf{z}$ and $\phi(\mathbf{z})$ is $n_\phi(1+r)$, which increases linearly with r. For one-dimensional attitude, three-dimensional attitude, and dynamic pose quantification, 2, 24, and 60 unique parameters are needed to quantify the linear relationship between $\phi(\mathbf{z})$ and $\mathbf{z}$. Because the number of parameters necessary to quantify the linear correlation between $\mathbf{z}$ and $\phi(\mathbf{z})$ increases linearly (as opposed to quadratically) with r, the linear correlation structure is used in the remainder of this work.

3.5.2. Canonical Gauss-Bingham Density. The canonical Gauss-Bingham density is introduced by substituting the transformations

$$\mathbf{x} = \boldsymbol{S}\mathbf{z} + \boldsymbol{m} \tag{3.54a}$$

$$\bar{q} = \boldsymbol{M}(\mathbf{z})\,\bar{\boldsymbol{p}} \tag{3.54b}$$

into Eq. (3.48), which yields the canonical Gauss-Bingham density as

$$\tilde{p}_{gb}(\boldsymbol{z}; \boldsymbol{Z}) = \tilde{p}_g(\mathbf{z})\, \tilde{p}_b(\bar{\boldsymbol{p}}; \boldsymbol{Z})\,, \tag{3.55}$$

where $\boldsymbol{z} = [\bar{\boldsymbol{p}}^T \ \mathbf{z}^T]^T$. The elements of $\boldsymbol{z}$ are uncorrelated and zero mean, such that the covariance of $\boldsymbol{z}$ is defined by the diagonal concatenation of $\boldsymbol{I}$ and $\boldsymbol{P}_p$ according to

$$\mathrm{E}_{\tilde{p}_{gb}}\{\boldsymbol{z}\boldsymbol{z}^T\} = \begin{bmatrix} \mathrm{E}_{\tilde{p}_b}\{\bar{\boldsymbol{p}}\bar{\boldsymbol{p}}^T\} & \boldsymbol{0} \\ \boldsymbol{0} & \mathrm{E}_{\tilde{p}_g}\{\mathbf{z}\mathbf{z}^T\} \end{bmatrix} = \begin{bmatrix} \boldsymbol{P}_p & \boldsymbol{0} \\ \boldsymbol{0} & \boldsymbol{I} \end{bmatrix}\,.$$

The canonical Gauss-Bingham density still depends on the matrix of concentration parameters, $\boldsymbol{Z}$; however, the elements of $\boldsymbol{z}$ are uncorrelated, which can be exploited to make certain operations easier to implement. Similar to the canonical Gaussian and Bingham densities, certain operations can be performed for the canonical Gauss-Bingham density, and the results of these operations can

then be transformed according to the change of variables defined by Eq. (3.54) to represent the Gauss-Bingham density of interest. When using the canonical Gauss-Bingham density, typically these operations cannot be performed off line and saved, because the canonical Gauss-Bingham density still depends on the matrix of concentration parameters, $\boldsymbol{Z}$.

The orientation matrix of the conditional Bingham density used to construct the Gauss-Bingham density, as given in Eq. (3.53), is parameterized by $\boldsymbol{m}$, $\boldsymbol{P}$, ϕ_0, and $\boldsymbol{\beta}$. Because the orientation matrix is nonlinearly related to these parameters, quantifying these parameters for certain applications can become numerically intensive and potentially intractable.

3.6. BINGHAM-GAUSS DENSITY

In order to overcome this apparent intractability, consider an alternate definition of the Gauss-Bingham density in which the order of the conditioning is reversed; that is, the Gaussian density is conditioned on the Bingham-distributed variable instead of conditioning the Bingham density on the Gaussian-distributed variable. This density is called the Bingham-Gauss density, as is performed in Eq. (3.48). The naive definition of the Bingham-Gauss density is given by

$$
\begin{aligned}
p_{bg}^*&(\boldsymbol{x}; \boldsymbol{m}_\mathrm{x}, \boldsymbol{P}_\mathrm{x}, \boldsymbol{P}_q, \boldsymbol{P}_{q\mathrm{x}}) \\
&= p_b(\bar{\boldsymbol{q}}; \boldsymbol{M}, \boldsymbol{Z})\, p_g(\mathbf{x}; \boldsymbol{m}_\mathrm{x} + \boldsymbol{P}_{q\mathrm{x}}^T \boldsymbol{P}_q^{-1} \bar{\boldsymbol{q}}, \boldsymbol{P}_\mathrm{x} - \boldsymbol{P}_{q\mathrm{x}}^T \boldsymbol{P}_q^{-1} \boldsymbol{P}_{q\mathrm{x}})\,,
\end{aligned}
\tag{3.56}
$$

where $\boldsymbol{M}$ and $\boldsymbol{Z}$ are the orientation matrix and matrix of concentration parameters defining the Bingham density of covariance $\boldsymbol{P}_q$ and the fact that the quaternion is zero-mean is exploited n the definition of the naive form of the Bingham-Gauss density. The definition of the naive version of the Bingham-Gauss density is motivated by the expression of the density of two jointly-Gaussian distributed random variables, as given by Eq. (3.46). The naive version of the Bingham-Gauss density is parameterized directly by the first moment of the Gaussian portion of the state vector, $\boldsymbol{m}_\mathrm{x}$, as well as the second central moment of the total state vector, which are defined by

$$
\boldsymbol{m}_\mathrm{x} = \mathrm{E}_{p_{bg}^*}\{\mathbf{x}\}
$$

$$
\begin{bmatrix} \boldsymbol{P}_q & \boldsymbol{P}_{q\mathrm{x}} \\ \boldsymbol{P}_{q\mathrm{x}}^T & \boldsymbol{P}_\mathrm{x} \end{bmatrix} \triangleq \mathrm{E}_{p_{bg}^*}\left\{ \begin{bmatrix} \bar{\boldsymbol{q}} \\ \mathbf{x} - \boldsymbol{m}_\mathrm{x} \end{bmatrix} \begin{bmatrix} \bar{\boldsymbol{q}} \\ \mathbf{x} - \boldsymbol{m}_\mathrm{x} \end{bmatrix}^T \right\}
$$

$$
= \begin{bmatrix} \mathrm{E}_{p_{bg}^*}\{\bar{\boldsymbol{q}}\bar{\boldsymbol{q}}^T\} & \mathrm{E}_{p_{bg}^*}\{\bar{\boldsymbol{q}}(\mathbf{x} - \boldsymbol{m}_\mathrm{x})^T\} \\ \mathrm{E}_{p_{bg}^*}\{(\mathbf{x} - \boldsymbol{m}_\mathrm{x})\bar{\boldsymbol{q}}^T\} & \mathrm{E}_{p_{bg}^*}\{(\mathbf{x} - \boldsymbol{m}_\mathrm{x})(\mathbf{x} - \boldsymbol{m}_\mathrm{x})^T\} \end{bmatrix}.
$$

Equation (3.56) is the *naive* definition of the Bingham-Gauss density because it is not antipodally symmetric in $\bar{\boldsymbol{q}}$, in general; that is, $\bar{\boldsymbol{q}}$ and $-\bar{\boldsymbol{q}}$, which quantify the same physical attitude, are not

equiprobable. This can be observed by evaluating Eq. (3.56) for $-\bar{q}$ instead of $\bar{q}$, which yields

$$p_{bg}^* \left(\begin{bmatrix} -\bar{q}^T & \mathbf{x}^T \end{bmatrix}^T ; \boldsymbol{m}_\mathrm{x}, \boldsymbol{P}_\mathrm{x}, \boldsymbol{P}_q, \boldsymbol{P}_{qx} \right) \tag{3.57}$$

$$= p_b(-\bar{q}; \boldsymbol{M}, \boldsymbol{Z}) \, p_g(\mathbf{x}; \boldsymbol{m}_\mathrm{x} + \boldsymbol{P}_{qx}^T \boldsymbol{P}_q^{-1}(-\bar{q}), \boldsymbol{P}_\mathrm{x} - \boldsymbol{P}_{qx}^T \boldsymbol{P}_q^{-1} \boldsymbol{P}_{qx})$$

$$= p_b(\bar{q}; \boldsymbol{M}, \boldsymbol{Z}) \, p_g(\mathbf{x}; \boldsymbol{m}_\mathrm{x} - \boldsymbol{P}_{qx}^T \boldsymbol{P}_q^{-1} \bar{q}, \boldsymbol{P}_\mathrm{x} - \boldsymbol{P}_{qx}^T \boldsymbol{P}_q^{-1} \boldsymbol{P}_{qx}) \,.$$

Comparison of Eqs. (3.56) and (3.57) shows that the naive version of the Bingham-Gauss density is only antipodally symmetric if $\boldsymbol{P}_{qx} = \boldsymbol{0}$; that is, the quaternion and Euclidean portions of the state vector are uncorrelated. This is an undesirable condition to enforce, because, in general, correlations are present between these portions of the state vector. Thus, the naive definition of the alternate form of the Gauss-Bingham density is not an appropriate density for a state vector consisting of a quaternion portion and other Euclidean quantities.

In order to define the Bingham-Gauss density as an appropriate density for the quaternion, its naive form is split between the two hemispheres of the unit-hypersphere and the correlation parameter, $\boldsymbol{P}_{qx}$, is negated on one of the halves to yield

$$p_{bg}(\boldsymbol{x}; \boldsymbol{m}_\mathrm{x}, \boldsymbol{P}_\mathrm{x}, \boldsymbol{P}_q, \boldsymbol{P}_{qx}) = \begin{cases} p_{bg}^* \left(\boldsymbol{x}; \boldsymbol{m}_\mathrm{x}, \boldsymbol{P}_\mathrm{x}, \boldsymbol{P}_q, \boldsymbol{P}_{qx} \right) & \bar{q} \in \mathbb{S}^{s+} \\ p_{bg}^* \left(\boldsymbol{x}; \boldsymbol{m}_\mathrm{x}, \boldsymbol{P}_\mathrm{x}, \boldsymbol{P}_q, -\boldsymbol{P}_{qx} \right) & \bar{q} \in \mathbb{S}^{s-} \end{cases} \tag{3.58}$$

where $\mathbb{S}^{s+}$ and $\mathbb{S}^{s-}$ represent opposing hemispheres of the unit-hypersphere. In order to appropriately split $\mathbb{S}^s$, the pole of each hemisphere is defined by the antipodal pair of most-likely quaternions. In order to determine which quaternion of the antipodal pair defines $\mathbb{S}^{s+}$ and which quaternion defines $\mathbb{S}^{s-}$, the last nonzero element of the quaternion is used; if the last nonzero element of the quaternion is positive, that quaternion defines $\mathbb{S}^{s+}$. Similarly, if the last nonzero element of the quaternion is negative, that quaternion defines $\mathbb{S}^{s-}$. Because the quaternion is constrained to be unit-norm, all of its entries cannot be zero; thus, this logic correctly splits the unit-hypersphere into two halves such that one of each pair of antipodal quaternions is contained in each $\mathbb{S}^{s+}$ and $\mathbb{S}^{s-}$ for any and all pairs of antipodal quaternions.

In order to analyze the splitting of the unit-hypersphere into $\mathbb{S}^{s+}$ and $\mathbb{S}^{s-}$, first consider the $\mathbb{S}^1$ case, which contains the one-dimensional attitude quaternion according to Eq. (2.42). The "positive" and "negative" hemispheres of $\mathbb{S}^1$ are shown in Figure (3.10), which are used to determine which of the antipodal pair of quaternions is used to define $\mathbb{S}^{1+}$ and which is used to define $\mathbb{S}^{1-}$. Observation of Figure (3.10) shows that, for any pair of antipodal quaternions in $\mathbb{S}^1$, one quaternion is included in the "positive" hemisphere, and the other quaternion is included in the "negative" hemisphere. The two halves of the hemisphere are shown in Figure (3.10), in which a closed endpoint of a line represents a point included in the line, and an open endpoint of a line represents a

point that is *not* included in the line. The quaternion of the antipodal pair that lies on the "positive" hemisphere is defined as the pole that subsequently defines $\mathbb{S}^{1+}$. The quaternion antipodal to the quaternion that lies on the "positive" hemisphere must lie on the "negative" hemisphere, and defines the pole that subsequently defines $\mathbb{S}^{1-}$.
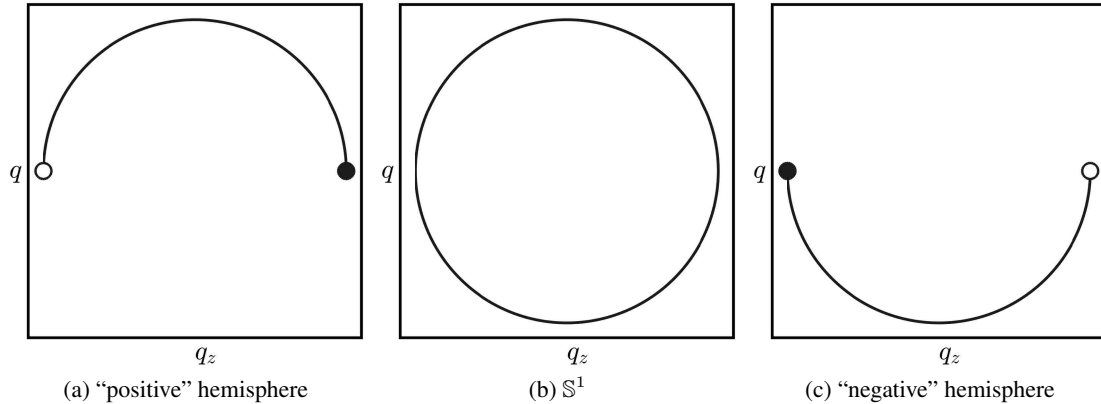
Figure 3.10. Hemispheres of $\mathbb{S}^1$ used to determine which of the antipodal quaternions defines $\mathbb{S}^{1+}$ and which defines $\mathbb{S}^{1-}$.

Now, consider the $\mathbb{S}^2$ case, which contains the arbitrary unit-vector $\bar{\boldsymbol{q}} = [q_1 \ q_2 \ q_3]^T$ and does not contain a valid attitude quaternion. The "positive" and "negative" hemispheres of $\mathbb{S}^1$ are shown in Figure (3.11), which are used to determine which of the antipodal pair of unit-vectors is used to define $\mathbb{S}^{2+}$ and which is used to define $\mathbb{S}^{2-}$. Similarly to the observation of Figure (3.10) for the $\mathbb{S}^1$ case, observation of Figure (3.11) shows that, for any pair of antipodal unit-vectors in $\mathbb{S}^s$, one unit-vector is included in the "positive" hemisphere, and the other quaternion is included in the "negative" hemisphere. The two halves of the hemisphere are shown in Figure (3.11), in which a closed endpoint of a line represents a point included in the line, and an open endpoint of a line represents a point that is *not* included in the line. Furthermore, a line drawn on the edge of a surface represents an edge of the surface included in the surface; the edge of a surface with no line represents an edge that is not included in the surface. The unit-vector of the antipodal pair that lies on the "positive" hemisphere is defined as the pole that subsequently defines $\mathbb{S}^{2+}$. The unit-vector antipodal to the unit-vector that lies on the "positive" hemisphere must lie on the "negative" hemisphere, and defines the pole that subsequently defines $\mathbb{S}^{2-}$. The same logic is applied to split $\mathbb{S}^3$, which contains the attitude quaternion, into $\mathbb{S}^{3+}$ and $\mathbb{S}^{3-}$; however, it is not possible to visualize the splitting in this dimension.

Because the Bingham-Gauss density is constructed by splitting its naive form across $\mathbb{S}^{s+}$ and $\mathbb{S}^{s-}$, it is discontinuous across the boundary joining these two hemispheres; however, if the density is numerically zero on both sides of this boundary, the density is effectively continuous. To
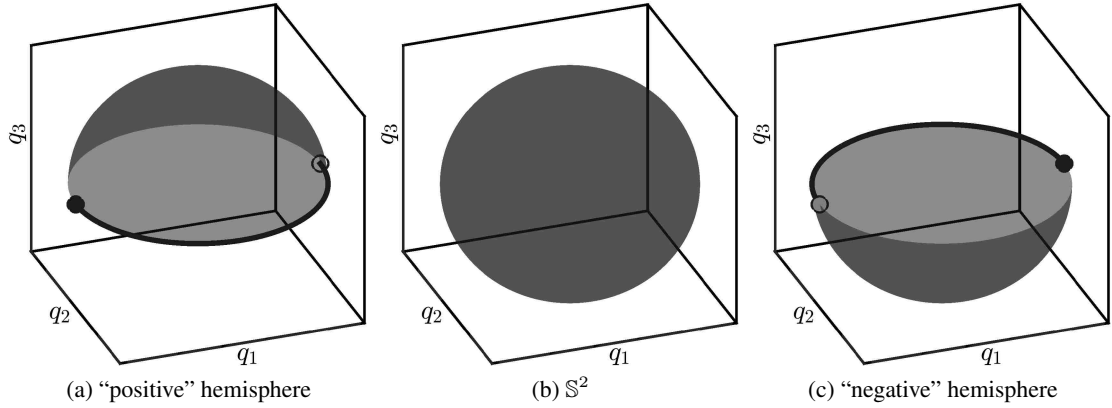
Figure 3.11. Hemispheres of $\mathbb{S}^2$ used to determine which of the antipodal unit-vectors defines $\mathbb{S}^{2+}$ and which defines $\mathbb{S}^{2-}$.

illustrate this, consider the Bingham-Gauss density in $\mathbb{S}^1 \times \mathbb{R}^1$, which can be used to quantify the uncertainty in the one-dimensional attitude quaternion and angular velocity about the z-axis as given by Eq. (3.51). Two example Bingham-Gauss densities are shown in Figure (3.12). Observation of Figure (3.12a) shows that, if the Bingham-Gauss density is not effectively zero at the boundary between the hemispheres, the discontinuity between the hemispheres is apparent and potentially problematic. Alternatively, the observation of Figure (3.12b) shows that, if the Bingham-Gauss density is numerically zero at the boundary between the hemispheres, the Bingham-Gauss density is effectively continuous. This motivates the need for a Bingham-Gauss mixture to represent an arbitrary state density, because a Bingham-Gauss mixture can be constructed such that each of its components is small enough that it has numerically zero probability along the boundary splitting $\mathbb{S}^{s+}$ and $\mathbb{S}^{s-}$ corresponding to each component.

The canonical Bingham-Gauss density is introduced by substituting the transformations

$$\bar{q} = M\bar{p} \tag{3.59a}$$

$$\mathbf{x} = \sqrt{P_{\mathrm{x}} + P_{q\mathrm{x}}^T P_q^{-1} P_{q\mathrm{x}}} \, \mathbf{z} + P_{q\mathrm{x}}^T P_q^{-1} M\bar{p} + m_{\mathrm{x}} \quad \bar{q} \in \mathbb{S}^{s+} \tag{3.59b}$$

$$\mathbf{x} = \sqrt{P_{\mathrm{x}} + P_{q\mathrm{x}}^T P_q^{-1} P_{q\mathrm{x}}} \, \mathbf{z} - P_{q\mathrm{x}}^T P_q^{-1} M\bar{p} + m_{\mathrm{x}} \quad \bar{q} \in \mathbb{S}^{s-} \, , \tag{3.59c}$$

where $\sqrt{A}\sqrt{A}^T \triangleq A$ into Eq. (3.58), which yields the canonical Bingham-Gauss density as

$$\tilde{p}_{bg}(\boldsymbol{z}; \boldsymbol{P}_p) = \begin{cases} \tilde{p}_b(\bar{\boldsymbol{p}}; \boldsymbol{Z}) \, \tilde{p}_g(\mathbf{z}) & \bar{q} \in \mathbb{S}^{s+} \\ \tilde{p}_b(\bar{\boldsymbol{p}}; \boldsymbol{Z}) \, \tilde{p}_g(\mathbf{z}) & \bar{q} \in \mathbb{S}^{s-} \end{cases} \tag{3.60}$$

(a) nonzero boundary probability   (b) effectively zero boundary probability
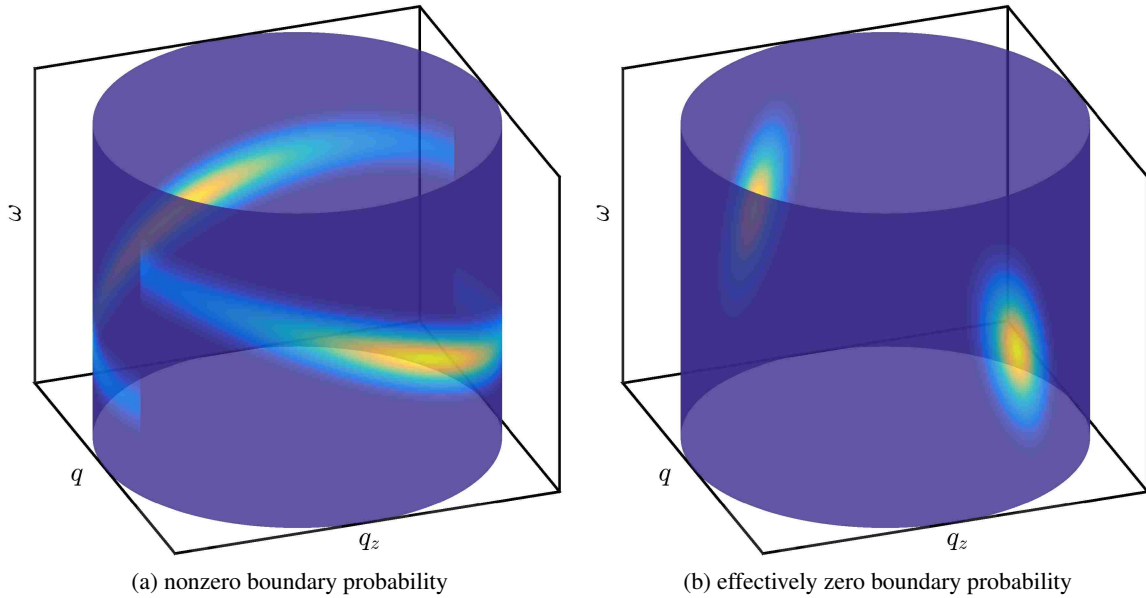
Figure 3.12. Bingham-Gauss densities on $\mathbb{S}^1 \times \mathbb{R}^1$.

where $\boldsymbol{Z}$ is the matrix of concentration parameters defining the canonical Bingham density with covariance $\boldsymbol{P}_p$. This transformation defines the poles of the hemispheres $\mathbb{S}^{s+}$ and $\mathbb{S}^{s-}$ as the positive and negative identity quaternions, since the canonical Bingham-Gauss density has mean direction defined by the identity quaternion. Equation (3.60) can be simplified to yield

$$\tilde{p}_{bg}(\boldsymbol{z}; \boldsymbol{P}_p) = \tilde{p}_b(\bar{\boldsymbol{p}}; \boldsymbol{Z}) \, \tilde{p}_g(\mathbf{z}) \tag{3.61}$$

The elements of $\boldsymbol{z}$ are uncorrelated and zero mean, such that the covariance of $\boldsymbol{z}$ is defined by the diagonal concatenation of $\boldsymbol{P}_p$ and $\boldsymbol{I}$ according to

$$\mathrm{E}_{\tilde{p}_{gb}}\{\boldsymbol{z}\boldsymbol{z}^T\} = \begin{bmatrix} \boldsymbol{P}_p & \boldsymbol{0} \\ \boldsymbol{0} & \boldsymbol{I} \end{bmatrix}.$$

The canonical Bingham-Gauss density still depends on the matrix of concentration parameters, $\boldsymbol{Z}$ (because $\boldsymbol{Z}$ defines the covariance of the canonical Bingham density, $\boldsymbol{P}_p$); however, certain operations can be performed for the canonical Gauss-Bingham density, and the results of these operations can then be transformed according to the change of variables defined by Eq. (3.54) to represent a

Gauss-Bingham density. When using the canonical Gauss-Bingham density, typically these operations cannot be performed off line and saved, because the canonical Gauss-Bingham density still depends on the matrix of concentration parameters, $\boldsymbol{Z}$.

Comparison of Eqs. (3.55) and (3.61) show that the canonical forms of the Gauss-Bingham and Bingham-Gauss densities are identical, which is expected since the Bingham and Gaussian portions of both densities are uncorrelated. This is a convenient result because techniques can be developed for the identical canonical Gauss-Bingham and canonical Bingham-Gauss densities, and the results can then be transformed according to the change of variables in either Eqs. (3.54) or Eqs. (3.59) in order to yield the desired Gauss-Bingham or Bingham-Gauss density of interest.

3.7. BINGHAM-GAUSS MIXTURE DENSITY

The BGM density is defined as

$$
p_{bgm}(\boldsymbol{x}) = \sum_{\ell=1}^{L} w^{(\ell)} \, p_{bg}\big(\boldsymbol{x}; \boldsymbol{m}_{\mathrm{x}}^{(\ell)}, \boldsymbol{P}_{\mathrm{x}}^{(\ell)}, \boldsymbol{P}_{q}^{(\ell)}, \boldsymbol{P}_{q\mathrm{x}}^{(\ell)}\big) \,, \tag{3.62}
$$

where $w^{(\ell)}$ is the weight of the ℓth component, $\boldsymbol{m}_{\mathrm{x}}^{(\ell)}$, $\boldsymbol{P}_{\mathrm{x}}^{(\ell)}$, $\boldsymbol{P}_{q}^{(\ell)}$, and $\boldsymbol{P}_{q\mathrm{x}}^{(\ell)}$ are the parameters defining the ℓth component, and L is the number of components in the mixture. The weights of the mixture are constrained such that

$$
w^{(\ell)} > 0 \quad \ell = 1, 2, \ldots, L \qquad \text{and} \qquad \sum_{\ell=1}^{L} w^{(\ell)} = 1 \,,
$$

which ensures that the BGM is a valid pdf. The explicit dependence on the parameters of the BGM density is not included in $p_{bgm}(\boldsymbol{x})$ in order to avoid cumbersome notation.

The problem of approximating a Bingham-Gauss density by a BGM density is now considered. In order to find the parameters of the BGM density that approximate a Bingham-Gauss density, first, the Bingham-Gauss density approximating the canonical form of the desired Bingham-Gauss density is found. The parameters of this BGM density approximating the canonical Bingham-Gauss density are then transformed according to the change of variables defined in Eqs. (3.59) to yield the parameters of the BGM density that approximate the Bingham-Gauss density of interest.

Because $\bar{\boldsymbol{p}}$ and $\mathbf{z}$, the random variables associated with the Bingham and Gaussian portions of the Bingham-Gauss density, respectively, are uncorrelated, the BM and GM densities approximating the canonical Bingham and Gaussian densities, respectively, can be constructed independently using the methods presented in Sections 3.2 and 3.4. Let the BGM approximating the canonical

Bingham-Gauss density be given by

$$p_{bgm}(\boldsymbol{z}) = \sum_{\ell=1}^{L} \tilde{w}^{(\ell)}\, p_{bg}\left(\boldsymbol{z}; \tilde{\boldsymbol{m}}_{\mathrm{x}}^{(\ell)}, \tilde{\boldsymbol{P}}_{\mathrm{x}}^{(\ell)}, \tilde{\boldsymbol{P}}_{q}^{(\ell)}, \tilde{\boldsymbol{P}}_{q\mathrm{x}}^{(\ell)}\right), \tag{3.63}$$

where the tilde notation indicates that these parameters correspond to the BGM density that approximates the *canonical* Bingham-Gauss density. Because $\bar{\boldsymbol{p}}$ and $\mathbf{z}$ are uncorrelated, Eq. (3.63) can be expressed as the product of the BM and GM densities approximating the canonical Bingham and canonical Gaussian densities, respectively, according to

$$p_{bgm}(\boldsymbol{z}) = \sum_{\ell_b=1}^{L_b} \tilde{w}_b^{(\ell_b)}\, p_b\left(\bar{\boldsymbol{p}}; \widetilde{\boldsymbol{M}}^{(\ell_b)}, \widetilde{\boldsymbol{Z}}^{(\ell_b)}\right) \sum_{\ell_g=1}^{L_g} \tilde{w}_g^{(\ell_g)}\, p_g\left(\mathbf{z}; \tilde{\boldsymbol{m}}^{(\ell_g)}, \widetilde{\boldsymbol{P}}^{(\ell_g)}\right), \tag{3.64}$$

where the weights, indices, and number of components of the BM and GM densities are subscripted with a "b" and "g," respectively, to differentiate them from each other. Manipulating Eq. (3.64) into a single summation of the form given in Eq. (3.63) and comparing the two yields the parameters of the BGM density that approximate the canonical Bingham-Gauss density in terms of the parameters of its elemental GM and BM densities according to

$$L = L_b L_g$$
$$\tilde{w}^{(\ell)} = \tilde{w}_g^{(\ell_g)} \tilde{w}_b^{(\ell_b)},$$
$$\tilde{\boldsymbol{m}}_{\mathrm{x}}^{(\ell)} = \tilde{\boldsymbol{m}}^{(\ell_g)}$$
$$\widetilde{\boldsymbol{P}}_{\mathrm{x}}^{(\ell)} = \widetilde{\boldsymbol{P}}^{(\ell_g)},$$
$$\widetilde{\boldsymbol{P}}_{q}^{(\ell)} = \widetilde{\boldsymbol{P}}_{q,b}^{(\ell_b)}$$
$$\widetilde{\boldsymbol{P}}_{q\mathrm{x}}^{(\ell)} = \boldsymbol{0},$$

for $\ell = 1, 2, \ldots, L$ and each ℓ corresponds to a unique pair of ℓ_b and ℓ_g. These parameters define the BGM density approximating the canonical Bingham-Gauss density defined by $\boldsymbol{P}_p$, and are transformed to define the BGM mixture density approximating the BGM density of interest defined by $p_{bg}(\boldsymbol{x}; \boldsymbol{m}_{\mathrm{x}}, \boldsymbol{P}_{\mathrm{x}}, \boldsymbol{P}_q, \boldsymbol{P}_{q\mathrm{x}})$ according to the change of variables in Eqs. (3.59), which yields

$$w^{(\ell)} = \tilde{w}^{(\ell)}$$
$$\boldsymbol{m}_{\mathrm{x}}^{(\ell)} = \sqrt{\boldsymbol{P}_{\mathrm{x}} - \boldsymbol{P}_{q\mathrm{x}}^{T} \boldsymbol{P}_{q}^{-1} \boldsymbol{P}_{q\mathrm{x}}}\, \tilde{\boldsymbol{m}}_{\mathrm{x}}^{(\ell)} + \boldsymbol{m}_{\mathrm{x}}$$
$$\begin{bmatrix} \boldsymbol{P}_{q}^{(\ell)} & \boldsymbol{P}_{q\mathrm{x}}^{(\ell)} \\ \boldsymbol{P}_{q\mathrm{x}}^{(\ell)T} & \boldsymbol{P}_{\mathrm{x}}^{(\ell)} \end{bmatrix} = \boldsymbol{A} \begin{bmatrix} \widetilde{\boldsymbol{P}}_{q}^{(\ell)} & \widetilde{\boldsymbol{P}}_{q\mathrm{x}}^{(\ell)} \\ \widetilde{\boldsymbol{P}}_{q\mathrm{x}}^{(\ell)T} & \widetilde{\boldsymbol{P}}_{\mathrm{x}}^{(\ell)} \end{bmatrix} \boldsymbol{A}^{T},$$

where $\ell = 1, 2, \ldots, L$, and $\boldsymbol{A}$ is defined as

$$\boldsymbol{A} \triangleq \begin{bmatrix} \boldsymbol{M} & \boldsymbol{0} \\ \boldsymbol{P}_{qx}^T \boldsymbol{P}_q^{-1} \boldsymbol{M} & \sqrt{\boldsymbol{P}_x - \boldsymbol{P}_{qx}^T \boldsymbol{P}_q^{-1} \boldsymbol{P}_{qx}} \end{bmatrix}.$$

The parameters $w^{(\ell)}$, $\boldsymbol{m}_x^{(\ell)}$, $\boldsymbol{P}_q^{(\ell)}$, $\boldsymbol{P}_{qx}^{(\ell)}$, and $\boldsymbol{P}_x^{(\ell)}$ for $\ell = 1, 2, \ldots, L$ now define the BGM density approximating the Bingham-Gauss density of interest.

4. KALMAN FILTERING

Under the MMSE filtering framework, commonly referred to as the Kalman filtering framework, the mean and error covariance of the state vector are used to probabilistically quantify the state vector. The pdf of the state is not explicitly quantified because only its mean and error covariance (first moment and second central moment) are quantified. The mean of the state vector serves as the estimated state, and the error covariance of the state vector serves to quantify the uncertainty in the state estimate. Two types of Kalman filtering are considered in this work: "additive" Kalman filtering (referred to hereafter as simply "Kalman filtering") and multiplicative Kalman filtering. Kalman filtering [31, 32] operates on state and measurement vectors that exist in Euclidean (additive and unbounded) space where a linear combination of the state and measurement vectors provides a meaningful result. Multiplicative Kalman filtering [5, 33] is an augmentation to Kalman filtering that operates on a state vector containing an attitude quaternion and other Euclidean states, in which case the state vector does not exist in Euclidean space because the attitude quaternion exists on the unit hypersphere, $\mathbb{S}^1$ or $\mathbb{S}^3$.

To illustrate why Kalman filtering requires that the state and measurement vectors exist in Euclidean space, consider the case when the state and measurement vectors are defined as attitude quaternions. First, quaternions are antipodally symmetric, meaning that $\bar{q}$ and $-\bar{q}$ represent the same attitude and are equiprobable; thus, the mean of the attitude quaternion is $\mathbf{0} \notin \mathbb{S}^1$ or $\mathbb{S}^3$. The mean and covariance of the attitude quaternion are therefore not a useful probabilistic representation of the attitude quaternion under the Kalman framework because they describe characteristics of the quaternion in $\mathbb{R}^2$ or $\mathbb{R}^4$ that are not meaningful on $\mathbb{S}^1$ or $\mathbb{S}^3$. Second, the measurement update would assume that the posterior quaternion mean is a linear function of the measured quaternion, which is invalid because the unit norm constraint implies that quaternions are not additive in general, i.e. $\bar{q}_1 + \bar{q}_2 \notin \mathbb{S}^3$. Because of these properties of the attitude quaternion, the Kalman filtering approach must be augmented when the state and/or measurement contains an attitude quaternion. One such augmentation is the multiplicative extended Kalman filter, which is addressed in this work. Other augmentations include the norm-constrained extended Kalman filter [34] and the q-method extended Kalman filter [35].

A numerical issue also presents itself when a Kalman filter is used to operate on a constrained state or measurement vector (such as the attitude quaternion). The state and measurement covariance matrices become ill-conditioned due to the quadratic norm constraint on the state vector as the attitude uncertainty approaches zero [5]. If the constraint on the state vector were linear, the covariance matrix would be singular. When the attitude uncertainty becomes small, the quadratic

constraint is well approximated by a linear constraint; thus, the covariance matrix becomes ill-conditioned. This numerical issue can be masked by process and measurement noise; however, the amount of process and measurement noise necessary to mask these numerical issues may not represent the true underlying noise processes of the dynamic system and measurement model and can lead to poor performance of the filter.

Both Kalman filtering and multiplicative Kalman filtering quantify the temporal and measurement evolution of the mean and error covariance of the state vector according to a dynamical system and measurement model. In the most general case, these models can be expressed as a nonlinear function of the state and noise according to

$$\boldsymbol{x}_k = \boldsymbol{f}(\boldsymbol{x}_{k-1}, \boldsymbol{w}_{k-1}) \tag{4.1a}$$

$$\boldsymbol{z}_k = \boldsymbol{h}(\boldsymbol{x}_k, \boldsymbol{v}_k), \tag{4.1b}$$

where f is the nonlinear function representing the dynamical system, h is the nonlinear function representing the measurement model, $\boldsymbol{x}$ is the state, $\boldsymbol{z}$ is the measurement, $\boldsymbol{w}$ and $\boldsymbol{v}$ are zero-mean white-noise sequences, and the k and $k-1$ subscripts refer to the subscripted variable at times t_k and t_{k-1}, respectively. The process and measurement noises are assumed zero-mean for convenience and clarity of the following sections and resulting algorithms; however, it is straightforward to relax this assumption through the introduction of a bias into $\boldsymbol{f}$ or $\boldsymbol{h}$, if desired. The process and measurement noise sequences have covariances defined by

$$\mathrm{E}\left\{\boldsymbol{w}_j \boldsymbol{w}_k^T\right\} = \boldsymbol{Q}_k \delta_{jk}$$

$$\mathrm{E}\left\{\boldsymbol{v}_j \boldsymbol{v}_k^T\right\} = \boldsymbol{R}_k \delta_{jk},$$

where δ_{jk} represents the Kronecker delta which is defined by

$$\delta_{jk} = \begin{cases} 1 & \text{if } j = k \\ 0 & \text{if } j \neq k \end{cases}$$

and the process and measurement noise are independent of each other and the initial state. It is important to note that no assumption about the pdfs of the process noise and measurement noise have been made, only that they are zero-mean white-noise sequences with the given covariances. Equations (4.1) can be expressed in an equivalent form according to

$$\boldsymbol{x}_k = \tilde{\boldsymbol{f}}(\tilde{\boldsymbol{x}}_{k-1}) \tag{4.2a}$$

$$\boldsymbol{z}_k = \bar{\boldsymbol{h}}(\bar{\boldsymbol{x}}_k), \tag{4.2b}$$

where $\tilde{f}$ is the nonlinear function representing the dynamical system, $\bar{h}$ is the nonlinear function representing the measurement model, $\tilde{\boldsymbol{x}}_{k-1} \triangleq [\boldsymbol{x}_{k-1}^T \ \ \boldsymbol{w}_{k-1}^T]^T$ is the state vector augmented with the process noise and $\bar{\boldsymbol{x}}_k \triangleq [\boldsymbol{x}_k^T \ \ \boldsymbol{v}_k^T]^T$ is the state vector augmented with measurement noise. The representations of the dynamical system and measurement model given in Eqs. (4.1) and (4.2) are equivalent; however, the forms given in Eqs. (4.2) are generally more convenient when using certain implementations of the Kalman filter.

If the process and measurement noise are additive, the discrete-time dynamics and measurement model given in Eqs. (4.1) can be expressed as

$$\boldsymbol{x}_k = \boldsymbol{f}(\boldsymbol{x}_{k-1}) + \boldsymbol{w}_{k-1} \tag{4.3a}$$

$$\boldsymbol{z}_k = \boldsymbol{h}(\boldsymbol{x}_k) + \boldsymbol{v}_k \,, \tag{4.3b}$$

An abuse of notation is used for $\boldsymbol{f}$ and $\boldsymbol{h}$ between Eqs. (4.1) and Eqs. (4.3); the meaning of which $\boldsymbol{f}$ or $\boldsymbol{h}$ is meant is clear depending on whether each has one or two arguments. If desired, the process noise and measurement noise can be premultiplied by shape matrices, typically denoted by $\boldsymbol{M}_{k-1}$ and $\boldsymbol{L}_k$, in order to map the process noise and measurement noise into the dynamical system and measurement model, respectively. These shape matrices are omitted in this work for simplicity; however, it is straightforward to include them in the following algorithms. Furthermore, if the discrete-time system dynamics and measurement model are linear, Eqs. (4.3) can be expressed according to

$$\boldsymbol{x}_k = \boldsymbol{F}_{k-1}\boldsymbol{x}_{k-1} + \boldsymbol{w}_{k-1} \tag{4.4a}$$

$$\boldsymbol{z}_k = \boldsymbol{H}_k\boldsymbol{x}_k + \boldsymbol{v}_k \,, \tag{4.4b}$$

where $\boldsymbol{F}_{k-1}$ and $\boldsymbol{H}_k$ are the matrices defining the dynamical system and the measurement model, respectively. The additivity of the process and measurement noise, as well as the linearity of the discrete-time system dynamics and measurement are exploited, when possible, in order to simplify subsequent filtering algorithms.

4.1. KALMAN FILTERING

Consider the case when the state and measurement vectors exist in Euclidean space; that is, the state and measurement vectors are additive and unbounded. To denote that state and measurement vectors exist in Euclidean space, they are denoted by $\mathbf{x}$ and $\mathbf{z}$, respectively. In this case, the mean and error covariance of the state are defined as

$$\boldsymbol{m} = \mathrm{E}\left\{\mathbf{x}\right\} \tag{4.5a}$$

$$\boldsymbol{P} = \mathrm{E}\left\{\delta\mathbf{x}\delta\mathbf{x}^T\right\}, \tag{4.5b}$$

respectively, where $\delta\mathbf{x}$ is the additive state error and is defined by

$$\delta\mathbf{x} \triangleq \mathbf{x} - \boldsymbol{m}. \tag{4.6}$$

To simplify the notation of the Kalman filter equations, the $p(\mathbf{x})$ subscript is omitted from the expected value operator, as defined in Eq. (3.5), when it is used in the context of the Kalman filter since $p(\mathbf{x})$ is not quantified. Under the Kalman filtering paradigm, the evolution of the mean and covariance of the state vector is quantified. This evolution is quantified either exactly or approximately, depending on the type of dynamical system and measurement model used, as well as the type of Kalman filter used. Before the different types of Kalman filters are presented, first, the general Kalman filtering equations, which are the linear MMSE estimator, are presented in terms of the expected value operator. The different types of Kalman filters are then obtained by calculating or approximating these expected values differently.

The predictor of the Kalman framework uses Eqs. (4.5) and the dynamic system model to calculate the prior mean and covariance at t_k, which are given for the most general expression of the dynamic system, as defined by Eq. (4.2a), according to

$$
\begin{aligned}
\boldsymbol{m}_k^- &= \mathrm{E}\left\{\mathbf{x}_k\right\} \\
&= \mathrm{E}\left\{\tilde{\boldsymbol{f}}(\tilde{\mathbf{x}}_{k-1})\right\} \\
\boldsymbol{P}_k^- &= \mathrm{E}\left\{\delta\mathbf{x}_k^- \delta\mathbf{x}_k^{-T}\right\} \\
&= \mathrm{E}\left\{(\mathbf{x}_k - \boldsymbol{m}_k^-)(\mathbf{x}_k - \boldsymbol{m}_k^-)^T\right\} \\
&= \mathrm{E}\left\{(\tilde{\boldsymbol{f}}(\tilde{\mathbf{x}}_{k-1}) - \boldsymbol{m}_k^-)(\tilde{\boldsymbol{f}}(\tilde{\mathbf{x}}_{k-1}) - \boldsymbol{m}_k^-)^T\right\},
\end{aligned}
$$

(4.7a)

(4.7b)

where $\delta\mathbf{x}_k^- \triangleq \mathbf{x}_k - \boldsymbol{m}_k^-$ is the "prior" state error. The superscript "$-$" is used to represent the "prior" of the superscripted quantity; that is, the value prior to incorporating any measurement information at t_k. Ideally, the expected values in Eqs. (4.7) are calculated exactly; however, this is only possible when the dynamic system can be expressed according to Eq. (4.4a), in which case the predictor of the KF is obtained and the temporal evolution of the mean and error covariance of the state are quantified without approximation. In general, these expected values must be approximated, in which case the approximate temporal evolution of the mean and error covariance of the state are obtained.

The corrector of the Kalman framework assumes that the posterior mean is a linear function of the measurement according to [36]

$$\boldsymbol{m}_k^+ = \boldsymbol{a}_k + \boldsymbol{K}_k\mathbf{z}_k, \tag{4.8}$$

where $\boldsymbol{a}_k$ and $\boldsymbol{K}_k$ are to be determined. The superscript "+" represents the posterior of the superscripted quantity; that is, the value after incorporating measurement information at t_k. The parameters of the linear function of the measurement, $\boldsymbol{a}_k$ and $\boldsymbol{K}_k$, are found by minimizing the mean square error of the posterior state density while enforcing an unbiased estimator. The mean square error of the posterior state density is given by

$$J = \mathrm{E}\left\{\delta \mathbf{x}_k^{+T} \delta \mathbf{x}_k^+\right\} = \mathrm{tr}\,\mathrm{E}\left\{\delta \mathbf{x}_k^+ \delta \mathbf{x}_k^{+T}\right\} = \mathrm{tr}\,\boldsymbol{P}_k^+\,, \tag{4.9}$$

where $\delta \mathbf{x}_k^+ \triangleq \mathbf{x}_k - \boldsymbol{m}_k^+$ and $\boldsymbol{P}_k^+$ are the posterior estimation error and error covariance, respectively. Minimizing Eq. (4.9) and forcing an unbiased estimator (that is, forcing $\mathrm{E}\left\{\delta \mathbf{x}_k^+\right\} = \mathbf{0}$) yields the linear MMSE corrector, which is given by

$$\boldsymbol{m}_k^+ = \boldsymbol{m}_k^- + \boldsymbol{K}_k(\mathbf{z}_k - \hat{\mathbf{z}}_k) \tag{4.10a}$$

$$\boldsymbol{P}_k^+ = \boldsymbol{P}_k^- - \boldsymbol{K}_k \boldsymbol{P}_{zz} \boldsymbol{K}_k^T\,, \tag{4.10b}$$

where $\boldsymbol{K}_k$ is the Kalman gain, which is given by

$$\boldsymbol{K}_k = \boldsymbol{P}_{xz} \boldsymbol{P}_{zz}^{-1}\,, \tag{4.11}$$

and the expected measurement, innovation (or residual) covariance, and state-measurement cross-covariance are given by

$$\begin{aligned}
\hat{\mathbf{z}}_k &= \mathrm{E}\left\{\mathbf{z}_k\right\} \\
&= \mathrm{E}\left\{\bar{\boldsymbol{h}}(\bar{\mathbf{x}}_k)\right\} \tag{4.12a} \\
\boldsymbol{P}_{zz} &= \mathrm{E}\left\{(\mathbf{z}_k - \hat{\mathbf{z}}_k)(\mathbf{z}_k - \hat{\mathbf{z}}_k)^T\right\} \\
&= \mathrm{E}\left\{(\bar{\boldsymbol{h}}(\bar{\mathbf{x}}_k) - \hat{\mathbf{z}}_k)(\bar{\boldsymbol{h}}(\bar{\mathbf{x}}_k) - \hat{\mathbf{z}}_k)^T\right\} \tag{4.12b} \\
\boldsymbol{P}_{xz} &= \mathrm{E}\left\{(\mathbf{x}_k - \boldsymbol{m}_k^-)(\mathbf{z}_k - \hat{\mathbf{z}}_k)^T\right\} \\
&= \mathrm{E}\left\{(\mathbf{x}_k - \boldsymbol{m}_k^-)(\bar{\boldsymbol{h}}(\bar{\mathbf{x}}_k) - \hat{\mathbf{z}}_k)^T\right\}\,, \tag{4.12c}
\end{aligned}$$

respectively. This corrector is known as the *linear* MMSE estimator since it is derived by assuming that the posterior mean is a linear function of the measurement, not because any linearization has been performed to arrive at Eqs. (4.10). Ideally, the expected values in Eqs. (4.12) are calculated exactly; however, this is only possible when the measurement model can be expressed according to Eq. (4.4b), in which case the corrector of the KF is obtained and the measurement evolution of the mean and error covariance of the state are quantified without approximation. In general, these expected values must be approximated, in which case the approximate measurement evolution of the mean and error covariance of the state are obtained.

4.1.1. The Kalman Filter. The Kalman filter [30, 31, 32] is applicable only to linear dynamic systems and measurement models with additive process and measurement noise, where the process and measurement noise are independent of each other and the initial state, as given in Eqs. (4.4). In this case, the predictor of the Kalman framework, as defined by Eqs. (4.7), simplifies to

$$m_k^- = F_{k-1}m_{k-1}^+ \tag{4.13a}$$

$$P_k^- = F_{k-1}P_{k-1}^+F_{k-1}^T + Q_{k-1}, \tag{4.13b}$$

and the expected values necessary to implement the corrector of the Kalman framework, as given by Eqs. (4.12), simplify to

$$\hat{z}_k = H_k m_k^- \tag{4.14a}$$

$$P_{zz} = H_k P_k^- H_k^T + R_k \tag{4.14b}$$

$$P_{xz} = P_k^- H_k^T. \tag{4.14c}$$

If the dynamical system and measurement model are linear with additive process and measurement noise, the Kalman filter is the exact implementation of the linear MMSE estimator without any approximation. Many dynamical systems and measurement models are nonlinear and/or possess non-additive process or measurement noise. In these cases, it is necessary to make approximations to obtain the expected values in Eqs. (4.7) and (4.12).

4.1.2. The Extended Kalman Filter. The EKF [30] uses linearization of the system dynamics and measurement model about the posterior mean at t_{k-1} and the prior mean at t_k, respectively, to approximate the expected values in Eqs. (4.7) and (4.12). First consider the case when the dynamical system and measurement model are nonlinear with additive process and measurement noise, as given by Eqs. (4.3). In this case, the predictor of the Kalman framework, as defined by Eqs. (4.7), simplifies to give the predictor of the EKF according to

$$m_k^- = f(m_{k-1}^+) \tag{4.15a}$$

$$P_k^- = F(m_{k-1}^+)P_{k-1}^+F^T(m_{k-1}^+) + Q_{k-1}, \tag{4.15b}$$

where $F(m_{k-1}^+)$ is the Jacobian matrix of the dynamical system model, which is given by

$$F(m_{k-1}^+) \triangleq \left.\frac{\partial f(\mathbf{x})}{\partial \mathbf{x}}\right|_{\mathbf{x}=m_{k-1}^+}.$$

The expected values necessary to implement the corrector of the Kalman framework, as given by Eqs. (4.12), simplify to give the corrector of the EKF according to

$$\hat{\mathbf{z}}_k = \boldsymbol{h}(\boldsymbol{m}_k^-)$$
$$\boldsymbol{P}_{zz} = \boldsymbol{H}(\boldsymbol{m}_k^-)\boldsymbol{P}_k^-\boldsymbol{H}^T(\boldsymbol{m}_k^-) + \boldsymbol{R}_k$$
$$\boldsymbol{P}_{xz} = \boldsymbol{P}_k^-\boldsymbol{H}^T(\boldsymbol{m}_k^-)\,,$$

where $\boldsymbol{H}(\boldsymbol{m}_k^-)$ is the Jacobian matrix of the measurement model, which is given by

$$\boldsymbol{H}_k \triangleq \left.\frac{\partial \boldsymbol{h}(\mathbf{x})}{\partial \mathbf{x}}\right|_{\mathbf{x}=\boldsymbol{m}_k^-}.$$

Now, consider the most general case when the dynamical system and measurement model are nonlinear with non-additive process and measurement noise, as given by Eqs. (4.1) or Eqs. (4.2). In this case, the predictor of the Kalman framework, as defined by Eqs. (4.7), simplifies to give the predictor of the EKF according to

$$\boldsymbol{m}_k^- = \boldsymbol{f}(\boldsymbol{m}_{k-1}^+, \mathbf{0})$$
$$\boldsymbol{P}_k^- = \boldsymbol{F}(\boldsymbol{m}_{k-1}^+)\boldsymbol{P}_{k-1}^+\boldsymbol{F}^T(\boldsymbol{m}_{k-1}^+) + \boldsymbol{M}(\boldsymbol{m}_{k-1}^+)\boldsymbol{Q}_{k-1}\boldsymbol{M}^T(\boldsymbol{m}_{k-1}^+)\,,$$

where the $\boldsymbol{F}(\boldsymbol{m}_{k-1}^+)$ and $\boldsymbol{M}(\boldsymbol{m}_{k-1}^+)$ matrices are given by

$$\boldsymbol{F}_{k-1}(\boldsymbol{m}_{k-1}^+) \triangleq \left.\frac{\partial \boldsymbol{f}(\mathbf{x},\boldsymbol{w})}{\partial \mathbf{x}}\right|_{\mathbf{x}=\boldsymbol{m}_{k-1}^+,\boldsymbol{w}=\mathbf{0}} \tag{4.17a}$$

$$\boldsymbol{M}_{k-1}(\boldsymbol{m}_{k-1}^+) \triangleq \left.\frac{\partial \boldsymbol{f}(\mathbf{x},\boldsymbol{w})}{\partial \boldsymbol{w}}\right|_{\mathbf{x}=\boldsymbol{m}_{k-1}^+,\boldsymbol{w}=\mathbf{0}}, \tag{4.17b}$$

and are evaluated at $\boldsymbol{w} = \mathbf{0}$ because the process noise is zero-mean. The expected values necessary to implement the corrector of the Kalman framework, as given by Eqs. (4.12), simplify to give the corrector of the EKF according to

$$\hat{\mathbf{z}}_k = \boldsymbol{h}(\boldsymbol{m}_k^-, \mathbf{0})$$
$$\boldsymbol{P}_{zz} = \boldsymbol{H}(\boldsymbol{m}_k^-)\boldsymbol{P}_k^-\boldsymbol{H}^T(\boldsymbol{m}_k^-) + \boldsymbol{L}(\boldsymbol{m}_k^-)\boldsymbol{R}_k\boldsymbol{L}^T(\boldsymbol{m}_k^-)$$
$$\boldsymbol{P}_{xz} = \boldsymbol{P}_k^-\boldsymbol{H}^T(\boldsymbol{m}_k^-)\,,$$

where the $H(m_k^-)$ and $L(m_k^-)$ matrices are given by

$$H(m_k^-) \triangleq \frac{\partial h(\mathbf{x}, v)}{\partial \mathbf{x}}\bigg|_{\mathbf{x}=m_k^-, v=0}$$

$$L(m_k^-) \triangleq \frac{\partial h(\mathbf{x}, v)}{\partial v}\bigg|_{\mathbf{x}=m_k^-, v=0},$$

and are evaluated at $v = 0$ because the measurement noise is zero-mean.

At the surface, the EKF appears to simply be a linearization of the nonlinear functions f and h about the mean of the state vector, process noise, and measurement noise in order to implement the Kalman filter equations; however, this linearization has an important ramification. When the dynamical system and measurement model are linear with additive process and measurement noise, the Kalman filter is the exact linear MMSE estimator. In this case, the evolution of the state error covariance is deterministic and it is not coupled with the evolution of the mean, which is stochastic because it depends on the stochastic measurements. When the dynamical system and/or measurement model are nonlinear, the EKF uses linearization about the current mean to implement the Kalman filter equations. Because of this, the evolution of the state error covariance becomes stochastic because its evolution now depends on the evolution of the mean, which is stochastic. This can cause convergence issues in the EKF, especially if the filter is initialized poorly, because the evolution of the state error covariance incurs more error when there is more error in the current mean. Even though the EKF possesses this property, it is still very effective when implemented properly and has been the most popular means for navigation since its conception in the early 1960s [37].

4.1.3. Quadrature-Based Kalman Filters. Quadrature methods [38, 39, 40, 41] can be used to approximate the expected values in Eqs. (4.7) and (4.12) instead of the linearized system dynamics and measurement model used by the EKF. First, consider the case when the dynamical system and measurement model are nonlinear with additive process and measurement noise, as given by Eqs. (4.3). In this case, the predictor of the Kalman framework, as defined by Eqs. (4.7), simplifies to give the predictor of a quadrature-based Kalman filter according to

$$m_k^- = \sum_i w_{k-1}^{(i)} f(\mathcal{X}_{k-1}^{(i)}) \tag{4.18a}$$

$$P_k^- = \sum_i w_{k-1}^{(i)} \left[f(\mathcal{X}_{k-1}^{(i)}) - m_k^- \right] \left[f(\mathcal{X}_{k-1}^{(i)}) - m_k^- \right]^T + Q_{k-1}, \tag{4.18b}$$

where $w_{k-1}^{(i)}$ and $\mathcal{X}_{k-1}^{(i)}$ represent the quadrature weights and points used in the predictor of the quadrature-based Kalman filter. How these weights and points are selected defines the type of quadrature-based Kalman filter and is addressed later in this section. Note that it was assumed that the same weights and points are used for each of the quadrature approximations given in Eqs. (4.18),

respectively; however, this is not required in general, and is the case for some versions of the unscented transform, including the scaled unscented transform [42].

The expected values necessary to implement the corrector of the Kalman framework, as given by Eqs. (4.12), simplify to define the corrector of a quadrature-based Kalman filter according to

$$\hat{\mathbf{z}}_k = \sum_i w_k^{(i)} \boldsymbol{h}\big(\boldsymbol{\mathcal{X}}_k^{(i)}\big) \tag{4.19a}$$

$$\boldsymbol{P}_{zz} = \sum_i w_k^{(i)} \Big[\boldsymbol{h}\big(\boldsymbol{\mathcal{X}}_k^{(i)}\big) - \hat{\mathbf{z}}_k\Big]\Big[\boldsymbol{h}\big(\boldsymbol{\mathcal{X}}_k^{(i)}\big) - \hat{\mathbf{z}}_k\Big]^T + \boldsymbol{R}_k \tag{4.19b}$$

$$\boldsymbol{P}_{xz} = \sum_i w_k^{(i)} \Big[\boldsymbol{\mathcal{X}}_k^{(i)} - \boldsymbol{m}_k^-\Big]\Big[\boldsymbol{h}\big(\boldsymbol{\mathcal{X}}_k^{(i)}\big) - \hat{\mathbf{z}}_k\Big]^T, \tag{4.19c}$$

where $w_k^{(i)}$ and $\boldsymbol{\mathcal{X}}_k^{(i)}$ represent the quadrature weights and points used in the corrector of the quadrature-based Kalman filter. Similarly to the predictor, the selection of these weights and points defines the type of quadrature-based Kalman filter. Furthermore, it was assumed that the same method is used to generate the weights and points for each of the quadrature approximations given in Eqs. (4.19), respectively; however, this is not required in general, and different quadrature schemes can be used for each of these equations.

Now, consider the most general case when the dynamical system and measurement model are nonlinear with non-additive process and measurement noise, as given by Eqs. (4.1) or Eqs. (4.2). In this case, the predictor of the Kalman framework, as defined by Eqs. (4.7), simplifies to give the predictor of a quadrature-based Kalman filter according to

$$\boldsymbol{m}_k^- = \sum_i \tilde{w}_{k-1}^{(i)} \tilde{\boldsymbol{f}}\big(\widetilde{\boldsymbol{\mathcal{X}}}_{k-1}^{(i)}\big) \tag{4.20a}$$

$$\boldsymbol{P}_k^- = \sum_i \tilde{w}_{k-1}^{(i)} \Big[\tilde{\boldsymbol{f}}\big(\widetilde{\boldsymbol{\mathcal{X}}}_{k-1}^{(i)}\big) - \boldsymbol{m}_k^-\Big]\Big[\tilde{\boldsymbol{f}}\big(\widetilde{\boldsymbol{\mathcal{X}}}_{k-1}^{(i)}\big) - \boldsymbol{m}_k^-\Big]^T, \tag{4.20b}$$

where $\tilde{w}_{k-1}^{(i)}$ and $\widetilde{\boldsymbol{\mathcal{X}}}_{k-1}^{(i)}$ represent the quadrature weights and points used in the predictor of the quadrature-based Kalman filter.

The expected values necessary to implement the corrector of the Kalman framework, as given by Eqs. (4.12), simplify to give the corrector of a quadrature-based Kalman filter according to

$$\hat{\mathbf{z}}_k = \sum_i \bar{w}_k^{(i)} \bar{\boldsymbol{h}}\big(\bar{\boldsymbol{\mathcal{X}}}_k^{(i)}\big) \tag{4.21a}$$

$$\boldsymbol{P}_{zz} = \sum_i \bar{w}_k^{(i)} \left[\bar{\boldsymbol{h}}\big(\bar{\boldsymbol{\mathcal{X}}}_k^{(i)}\big) - \hat{\mathbf{z}}_k\right]\left[\bar{\boldsymbol{h}}\big(\bar{\boldsymbol{\mathcal{X}}}_k^{(i)}\big) - \hat{\mathbf{z}}_k\right]^T \tag{4.21b}$$

$$\boldsymbol{P}_{xz} = \sum_i \bar{w}_k^{(i)} \left[\bar{\boldsymbol{\mathcal{X}}}_{\mathrm{x},k}^{(i)} - \boldsymbol{m}_k^-\right]\left[\bar{\boldsymbol{h}}\big(\bar{\boldsymbol{\mathcal{X}}}_k^{(i)}\big) - \hat{\mathbf{z}}_k\right]^T, \tag{4.21c}$$

where $\bar{w}_k^{(i)}$ and $\bar{\boldsymbol{\mathcal{X}}}_k^{(i)}$ represent the quadrature weights and points used in the corrector, and $\bar{\boldsymbol{\mathcal{X}}}_{\mathrm{x},k}^{(i)}$ represents the portion of the ith quadrature point corresponding to the original state vector; that is, the state vector before it is augmented with the measurement noise. Similarly to Eqs. (4.18) and (4.19), the weights and points used in each of Eqs. (4.20) and (4.21), respectively, define the type of quadrature-based Kalman filter used, and different weights and points can be used in each of the quadrature approximations, if desired.

The quadrature scheme chosen, which defines the weights and points used in the quadrature approximations, is a trade between the accuracy of the quadrature approximation and its computational burden. The UKF leverages the unscented transform, which approximates the first and second moments of the state density by a set of discrete weights and points. The unscented transform is an efficient quadrature scheme requiring no fewer than $n+1$ weights and points depending on the specific type of unscented transform used [43, 44, 45], where n is the dimension of the (augmented) state vector of interest, given by $\mathbf{x}$, $\tilde{\mathbf{x}}$, or $\bar{\mathbf{x}}$. Because the dimension of the augmented state vectors, $\tilde{\mathbf{x}}$ or $\bar{\mathbf{x}}$, is larger than the dimension of the original state vector, $\mathbf{x}$, more points are required when using the unscented transform for Eqs. (4.20) and (4.21) as compared to Eqs. (4.18) and (4.19); this is why the additivity of the process and measurement noise is exploited, when possible, to save computational expense in the quadrature approximation.

The QKF is an assumed density filter in which the state density is assumed Gaussian and defined by the current mean and covariance. Gauss-Hermite quadrature is then used to generate the quadrature weights and points for Eqs. (4.18) and (4.19). Gauss-Hermite quadrature is exact for polynomials of degree $2q-1$, where q is the number of points used in the quadrature rule. In general, arbitrarily high accuracy in calculating the expected values can be guaranteed by choosing q to be arbitrarily large. Gauss-Hermite quadrature requires q^n points due to the required Kronecker product between the dimensions and thus suffers from the *curse of dimensionality*; that is, the number of quadrature points grows exponentially with the state dimension, n. In order to use Gauss-Hermite quadrature for Eqs. (4.20) and (4.21), the process and measurement noise must be assumed jointly Gaussian-distributed with the original state vector, $\mathbf{x}$, such that the augmented state vectors, $\tilde{\mathbf{x}}$ and $\bar{\mathbf{x}}$, are Gaussian-distributed. Because Gauss-Hermite quadrature suffers from the curse of dimensionality, applying the QKF to systems with non-additive process and measurement noise can have a significant, and sometimes infeasible, computational burden since the dimension of the augmented state vectors can become quite large for practical systems. More efficient quadrature schemes, including sparse-grid methods [46] and the conjugate unscented transform [47, 48], can

be used in a similar framework as the QKF to decrease computational expense; however, all of these filters are still restricted by the linear measurement update used under the Kalman filter framework to perform the measurement update.

4.2. MULTIPLICATIVE KALMAN FILTERING

Now, consider the case when the state vector consists of an attitude quaternion and other Euclidean states. In this case, the state vector does not exist in Euclidean space due to the unit norm constraint present on the attitude quaternion, and additive Kalman filtering suffers from numerical issues due to this constraint. Let this state vector be defined by Eq. (3.49). Multiplicative Kalman filtering quantifies the state error in a local tangent space constructed about the estimated state vector, which is denoted by

$$\hat{\boldsymbol{x}} = \begin{bmatrix} \hat{\bar{\boldsymbol{q}}} \\ \boldsymbol{m}_{\mathrm{x}} \end{bmatrix} , \tag{4.22}$$

where $\hat{\bar{\boldsymbol{q}}}$ is the estimated quaternion and $\boldsymbol{m}_{\mathrm{x}}$ is the mean (and also the estimate) of the Euclidean portion of the state vector. The multiplicative state error is defined according to

$$\delta\boldsymbol{x} \triangleq \begin{bmatrix} \delta\boldsymbol{\theta} \\ \delta\mathbf{x} \end{bmatrix} , \tag{4.23}$$

where $\delta\mathbf{x} = \mathbf{x} - \boldsymbol{m}_{\mathrm{x}}$ is the additive error and $\delta\boldsymbol{\theta}$ is the multiplicative attitude error expressed using a minimum parameter representation in the local tangent space. This minimum parameter representation is linearly related to the quaternion representation of the multiplicative attitude error according to

$$\begin{bmatrix} \alpha\delta\boldsymbol{\theta} \\ 1 \end{bmatrix} = \delta\bar{\boldsymbol{q}} = \bar{\boldsymbol{q}} \otimes \hat{\bar{\boldsymbol{q}}}^{-1} , \tag{4.24}$$

where α is a constant relating the specific minimum parameter representation chosen and the attitude quaternion and $\bar{\boldsymbol{q}}$ represents the true quaternion. This constant is observed to be $\alpha = 1/2$ for the rotation vector from Eq. (2.35) after this equation is linearized about $\boldsymbol{\theta} = \mathbf{0}$. The linear relationship used to relate the minimum parameter error representation and the quaternion error representation requires the attitude error to be small, or else significant error can be incurred in this approximation.

A rigorous derivation of the multiplicative Kalman filter, as presented in Reference [49], uses an arbitrary reference quaternion, $\bar{\boldsymbol{q}}_{\mathrm{ref}}$, in order to initially define the quaternion error according

to

$$\delta\bar{q} = \bar{q} \otimes \bar{q}_{\mathrm{ref}}^{-1}\,,$$

and then enforces the condition that $\mathrm{E}\left\{\delta\boldsymbol{\theta}\right\} = \mathbf{0}$ to show that $\bar{q}_{\mathrm{ref}}$ must be $\hat{\bar{q}}$ in order for this condition to hold. Therefore, as long as $\hat{\bar{q}}$ is used as the reference quaternion, which is used to define the quaternion error, multiplicative Kalman filtering is unbiased and has error covariance defined as

$$\boldsymbol{P} = \mathrm{E}\left\{\delta\boldsymbol{x}\delta\boldsymbol{x}^{T}\right\}.$$ (4.25)

Multiplicative Kalman filtering quantifies the temporal and measurement evolution of the estimated state vector, as defined by Eq. (4.22), and its error covariance, as defined by Eq. (4.25). This evolution is quantified approximately, because attitude motion is nonlinear and, furthermore, the linearized relationship between the multiplicative quaternion error and the minimum parameter error representation is used. The predictor of the multiplicative Kalman filter cannot be expressed in terms of expected values like the predictor of the Kalman filter can according to Eqs. (4.7), because the error covariance is expressed in terms of a minimum parameter attitude representation and the discrete time evolution of the state vector is defined in terms of the attitude quaternion. The predictor of the multiplicative Kalman filter is derived differently depending on the specific type of multiplicative Kalman filter under consideration.

The corrector of the multiplicative Kalman filter leverages the standard Kalman corrector, as defined by Eqs. (4.10) and (4.12), to calculate the correction to the estimated state vector in the state error vector space. This correction is denoted by $\Delta\delta\boldsymbol{x}_k$, and is calculated along with the state error covariance update according to

$$\Delta\delta\boldsymbol{x}_k \triangleq \begin{bmatrix} \Delta\delta\boldsymbol{\theta}_k \\ \Delta\delta\mathbf{x}_k \end{bmatrix} = \boldsymbol{K}_k(\mathbf{z}_k - \hat{\mathbf{z}}_k)$$ (4.26a)

$$\boldsymbol{P}_k^+ = \boldsymbol{P}_k^- - \boldsymbol{K}_k\boldsymbol{P}_{zz}\boldsymbol{K}_k^T\,,$$ (4.26b)

where $\boldsymbol{K}_k$ is the Kalman gain which is given by Eq. (4.11), $\Delta\delta\boldsymbol{\theta}_k$ and $\Delta\delta\mathbf{x}_k$ are the updates to the attitude quaternion and Euclidean portions of the state vector, respectively, and the measurement is assumed to exist in Euclidean space, such that the measurement residual, $\mathbf{z}_k - \hat{\mathbf{z}}_k$, provides a meaningful result. The expected measurement, innovation (or residual) covariance, and state error-measurement cross-covariance are given by

$$\hat{\mathbf{z}}_k = \mathrm{E}\left\{\mathbf{z}_k\right\}$$ (4.27a)

$$P_{zz} = \mathrm{E}\left\{(\mathbf{z}_k - \hat{\mathbf{z}}_k)(\mathbf{z}_k - \hat{\mathbf{z}}_k)^T\right\} \tag{4.27b}$$

$$P_{xz} = \mathrm{E}\left\{\delta\boldsymbol{x}_k(\mathbf{z}_k - \hat{\mathbf{z}}_k)^T\right\}, \tag{4.27c}$$

respectively. Note that Eq. (4.12c), which is the state-measurement cross-covariance as calculated by the standard Kalman filter, is different from Eq. (4.27c), which is the state *error*-measurement cross-covariance as calculated by the multiplicative Kalman filter. This is is because the correction to the estimated state is calculated in the local error space for the multiplicative Kalman filter, and not in the global space as it is calculated for the standard Kalman filter. After this update is calculated in the error space, the estimated state vector is then updated according to

$$\hat{\bar{q}}_k^+ = \bar{q}(\Delta\delta\boldsymbol{\theta}_k) \otimes \hat{\bar{q}}_k^- \tag{4.28a}$$

$$\boldsymbol{m}_{\mathrm{x},k}^+ = \boldsymbol{m}_{\mathrm{x},k}^- + \Delta\delta\mathbf{x}_k, \tag{4.28b}$$

where $\bar{q}(\Delta\delta\boldsymbol{\theta}_k)$ is the quaternion representation of $\Delta\delta\boldsymbol{\theta}_k$ and is given to first-order according to

$$\bar{q}(\Delta\delta\boldsymbol{\theta}_k) = \begin{bmatrix} \alpha\Delta\delta\boldsymbol{\theta}_k \\ 1 \end{bmatrix}. \tag{4.29}$$

Because the linearized relationship is used to obtain $\bar{q}(\Delta\delta\boldsymbol{\theta}_k)$, it is necessary to renormalize the resulting quaternion estimate to ensure that it remains unit-norm. Similarly to the Kalman filter, the expected values in Eqs. (4.27) are calculated or approximated differently based on the type of multiplicative Kalman filter used.

The measurement is assumed to exist in Euclidean space in this work, such that the measurement residual, $\mathbf{z}_k - \hat{\mathbf{z}}_k$, provides a meaningful result. A "measurement" of the attitude quaternion, which is placed in quotation marks because the attitude quaternion is not a physical quantity, and, thus, cannot be measured, can also be processed, as is shown in Reference [50]. This quaternion "measurement" is obtained by processing other data, such as the direction to stars observed by a star camera, and is then treated as a measurement in the multiplicative Kalman filter.

4.2.1. The Multiplicative Extended Kalman Filter. Consider the most general, nonlinear discrete time dynamical system and measurement model, which is given by Eqs. (4.1) or equivalently Eqs. (4.2). In the spirit of the extended Kalman filter, the predictor of the MEKF propagates the estimated state vector in time according to the dynamical system evaluated at the current estimated state and the mean of the process noise according to

$$\hat{\boldsymbol{x}}_k^- = \boldsymbol{f}(\hat{\boldsymbol{x}}_{k-1}^+, \mathbf{0}). \tag{4.30}$$

In order to propagate the error covariance in time, first note that the dynamical system, as given in Eq. (4.1a), can be expressed as

$$\begin{bmatrix} \bar{q}_k \\ \mathsf{x}_k \end{bmatrix} = \begin{bmatrix} f_q(\boldsymbol{x}_{k-1}, \boldsymbol{w}_{k-1}) \\ f_{\mathsf{x}}(\boldsymbol{x}_{k-1}, \boldsymbol{w}_{k-1}) \end{bmatrix}, \tag{4.31}$$

such that the prior quaternion error and the additive error at t_k can be expressed as

$$\delta \bar{q}_k^- = \bar{q}_k \otimes \hat{\bar{q}}_k^{-1} = f_q(\boldsymbol{x}_{k-1}, \boldsymbol{w}_{k-1}) \otimes f_q(\hat{\boldsymbol{x}}_{k-1}^+, \boldsymbol{0})^{-1}$$
$$\delta \mathsf{x}_k^- = \mathsf{x}_k - \boldsymbol{m}_{\mathsf{x},k} = f_{\mathsf{x}}(\boldsymbol{x}_{k-1}, \boldsymbol{w}_{k-1}) - f_{\mathsf{x}}(\hat{\boldsymbol{x}}_{k-1}^+, \boldsymbol{0}).$$

These equations are then manipulated and linearized about the current state estimate, and Eq. (4.24) is used to project the quaternion error, $\delta \bar{q}_k^-$, into the minimum parameter representation error in the local tangent space, $\delta \boldsymbol{\theta}_k^-$. After these steps are performed, the approximate temporal evolution of the error vector can be expressed as

$$\delta \boldsymbol{x}_k^- = \boldsymbol{F}(\hat{\boldsymbol{x}}_{k-1}^+) \delta \boldsymbol{x}_{k-1}^+ + \boldsymbol{M}(\hat{\boldsymbol{x}}_{k-1}^+) \boldsymbol{w}_{k-1}.$$

Because this linearization process to find $\boldsymbol{F}(\hat{\boldsymbol{x}}_{k-1}^+)$ and $\boldsymbol{M}(\hat{\boldsymbol{x}}_{k-1}^+)$ depends on the specific dynamical system of interest, general expressions for them, as are given in Eqs. (4.17) for the extended Kalman filter, cannot be found. This process is detailed in References [50, 51, 52], among others. Noting the definition of the state error covariance in Eq. (4.25), its temporal evolution is obtained as

$$\boldsymbol{P}_k^- = \boldsymbol{F}(\hat{\boldsymbol{x}}_{k-1}^+) \boldsymbol{P}_{k-1}^+ \boldsymbol{F}^T(\hat{\boldsymbol{x}}_{k-1}^+) + \boldsymbol{M}(\hat{\boldsymbol{x}}_{k-1}^+) \boldsymbol{Q}_{k-1} \boldsymbol{M}^T(\hat{\boldsymbol{x}}_{k-1}^+). \tag{4.32}$$

In summary, the predictor of the MEKF is defined by Eqs. (4.30) and (4.32).

The expected values necessary to implement the corrector of the multiplicative Kalman filter, defined by Eqs. (4.27), are for the MEKF are obtained by linearization in the local error space about the current state estimate according to

$$\hat{\mathsf{z}}_k = \boldsymbol{h}(\hat{\boldsymbol{x}}_k^-, \boldsymbol{0})$$
$$\boldsymbol{P}_{zz} = \boldsymbol{H}(\hat{\boldsymbol{x}}_k^-) \boldsymbol{P}_k^- \boldsymbol{H}^T(\hat{\boldsymbol{x}}_k^-) + \boldsymbol{L}(\hat{\boldsymbol{x}}_k^-) \boldsymbol{R}_k \boldsymbol{L}^T(\hat{\boldsymbol{x}}_k^-)$$
$$\boldsymbol{P}_{xz} = \boldsymbol{P}_k^- \boldsymbol{H}^T(\hat{\boldsymbol{x}}_k^-),$$

where the $\boldsymbol{H}(\hat{\boldsymbol{x}}_k^-)$ and $\boldsymbol{L}(\hat{\boldsymbol{x}}_k^-)$ matrices are given by

$$\boldsymbol{H}(\hat{\boldsymbol{x}}_k^-) \triangleq \left. \frac{\partial \boldsymbol{h}(\boldsymbol{x}, \boldsymbol{v})}{\partial \delta \boldsymbol{x}} \right|_{\boldsymbol{x} = \hat{\boldsymbol{x}}_k^-, \boldsymbol{v} = \boldsymbol{0}} \tag{4.33a}$$

$$L(\hat{\boldsymbol{x}}_k^-) \triangleq \left. \frac{\partial \boldsymbol{h}(\boldsymbol{x}, \boldsymbol{v})}{\partial \boldsymbol{v}} \right|_{\boldsymbol{x}=\hat{\boldsymbol{x}}_k^-, \boldsymbol{v}=\boldsymbol{0}} . \tag{4.33b}$$

The partial derivative in Eq. (4.33a) is taken with respect to the state error, and is evaluated at the current estimated state. Both of the partial derivatives in Eqs. (4.33a) can be found according to the first-order Taylor series expansion of $\boldsymbol{h}(\boldsymbol{x}, \boldsymbol{v})$ about the estimated state, which is given by

$$\boldsymbol{h}(\boldsymbol{x}, \boldsymbol{v}) = \boldsymbol{h}(\hat{\boldsymbol{x}}_k^-, \boldsymbol{0}) + \boldsymbol{H}(\hat{\boldsymbol{x}}_k^-)\delta\boldsymbol{x} + \boldsymbol{L}(\hat{\boldsymbol{x}}_k^-)\boldsymbol{v}$$

and is rearranged to give

$$\boldsymbol{h}(\boldsymbol{x}, \boldsymbol{v}) - \boldsymbol{h}(\hat{\boldsymbol{x}}_k^-, \boldsymbol{0}) = \boldsymbol{H}(\hat{\boldsymbol{x}}_k^-)\delta\boldsymbol{x} + \boldsymbol{L}(\hat{\boldsymbol{x}}_k^-)\boldsymbol{v} .$$

This allows for the quantity $\boldsymbol{h}(\boldsymbol{x}, \boldsymbol{v}) - \boldsymbol{h}(\hat{\boldsymbol{x}}_k^-, \boldsymbol{0})$ to be expanded, linearized about the current state estimate, and manipulated while neglecting second-order and higher terms to find $\boldsymbol{H}(\hat{\boldsymbol{x}}_k^-)$ and $\boldsymbol{L}(\hat{\boldsymbol{x}}_k^-)$, as is performed in Reference [51]. The details of this process depend on the specific measurement quantified by the $\boldsymbol{h}$ function, and, thus, cannot be performed in general for an arbitrary $\boldsymbol{h}$.

4.2.2. Quadrature-Based Multiplicative Kalman Filters. Motivation from the quadrature-based Kalman filters can be used to develop quadrature-based multiplicative Kalman filters. The predictor of the quadrature-based Kalman filters uses a set of discrete weights and points generated around the estimated state and expected value of the process noise to approximate the estimated state and its uncertainty at t_{k-1}. These points are then transformed according to the dynamical system, and their mean and covariance are then found, which define the estimated state and its uncertainty at t_k. This process is given in Eq. (4.20), which are observed to be the mean and covariance of the transformed quadrature points. A similar process is now performed to develop the predictor of a quadrature-based multiplicative Kalman filter.

Consider the most general case when the dynamical system and measurement model are nonlinear with non-additive process and measurement noise, as given by Eqs. (4.1) or Eqs. (4.2). The predictor of a quadrature-based multiplicative Kalman filter uses a set of discrete weights and points, which are generated in the error space according to the desired quadrature rule to yield $\tilde{w}_{k-1}^{(i)}$ and $\delta\widetilde{\boldsymbol{\mathcal{X}}}_{k-1}^{(i)}$. Let the portions of these quadrature points corresponding to $\delta\boldsymbol{\theta}_{k-1}^+$ be denoted as $\delta\widetilde{\boldsymbol{\mathcal{X}}}_{\theta,k-1}^{(i)}$, and the portions of these quadrature points corresponding to $\delta\mathbf{x}_{k-1}^+$ be denoted by $\delta\widetilde{\boldsymbol{\mathcal{X}}}_{\mathrm{x},k-1}^{(i)}$. The quadrature points are then transformed from the local state error space into the global state space according to

$$\widetilde{\boldsymbol{\mathcal{X}}}_{q,k-1}^{(i)} = \boldsymbol{q}(\delta\widetilde{\boldsymbol{\mathcal{X}}}_{\theta,k-1}^{(i)}) \otimes \hat{\bar{\boldsymbol{q}}}_{k-1}^+ \tag{4.34}$$

$$\widetilde{\boldsymbol{\mathcal{X}}}_{\mathrm{x},k-1}^{(i)} = \hat{\mathbf{x}}_{k-1}^+ + \delta\widetilde{\boldsymbol{\mathcal{X}}}_{\mathrm{x},k-1}^{(i)} , \tag{4.35}$$

where $\widetilde{\boldsymbol{\mathcal{X}}}^{(i)}_{q,k-1}$ and $\widetilde{\boldsymbol{\mathcal{X}}}^{(i)}_{\mathrm{x},k-1}$ represent the portions of the quadrature point in the global state space corresponding to $\bar{q}$ and $\mathbf{x}$, respectively, such that

$$\widetilde{\boldsymbol{\mathcal{X}}}^{(i)}_{k-1} = \begin{bmatrix} \widetilde{\boldsymbol{\mathcal{X}}}^{(i)}_{q,k-1} \\ \widetilde{\boldsymbol{\mathcal{X}}}^{(i)}_{\mathrm{x},k-1} \end{bmatrix}, \tag{4.36}$$

and $\boldsymbol{q}(\delta\widetilde{\boldsymbol{\mathcal{X}}}^{(i)}_{\theta,k-1})$ is given by Eq. (4.29) (and thus $\widetilde{\boldsymbol{\mathcal{X}}}^{(i)}_{q,k-1}$ must be renormalized since the linearized relationship is used to define $\boldsymbol{q}(\delta\widetilde{\boldsymbol{\mathcal{X}}}^{(i)}_{\theta,k-1})$). The quadrature weights and points used by the predictor of the multiplicative Kalman filter are now defined by $\tilde{w}^{(i)}_{k-1}$ and $\widetilde{\boldsymbol{\mathcal{X}}}^{(i)}_{k-1}$. These points are now transformed according to the dynamical system to yield the transformed sigma points according to

$$\tilde{\boldsymbol{f}}(\widetilde{\boldsymbol{\mathcal{X}}}^{(i)}_{k-1}) \triangleq \begin{bmatrix} \tilde{\boldsymbol{f}}_q(\widetilde{\boldsymbol{\mathcal{X}}}^{(i)}_{k-1}) \\ \tilde{\boldsymbol{f}}_\mathrm{x}(\widetilde{\boldsymbol{\mathcal{X}}}^{(i)}_{k-1}) \end{bmatrix},$$

where $\tilde{\boldsymbol{f}}_q(\widetilde{\boldsymbol{\mathcal{X}}}^{(i)}_{k-1})$ and $\tilde{\boldsymbol{f}}_\mathrm{x}(\widetilde{\boldsymbol{\mathcal{X}}}^{(i)}_{k-1})$ are the portions of the transformed sigma points corresponding to $\bar{q}$ and $\mathbf{x}$, respectively. The estimated quaternion, defined as $\hat{\bar{\boldsymbol{q}}}^-_k$ is then obtained as the "average" quaternion [53], which is given by the eigenvector corresponding to the largest eigenvalue of the matrix

$$\boldsymbol{M} = \sum_i \tilde{w}^{(i)}_{k-1} \tilde{\boldsymbol{f}}_q(\widetilde{\boldsymbol{\mathcal{X}}}^{(i)}_{k-1}) \tilde{\boldsymbol{f}}^T_q(\widetilde{\boldsymbol{\mathcal{X}}}^{(i)}_{k-1}).$$

The mean of the Euclidean portion of the state vector is obtained as the mean of the $\tilde{\boldsymbol{f}}_\mathrm{x}(\widetilde{\boldsymbol{\mathcal{X}}}^{(i)}_{k-1})$, such that the prior estimated state at t_k is given by

$$\hat{\boldsymbol{x}}^-_k = \begin{bmatrix} \hat{\bar{\boldsymbol{q}}}^-_k \\ \boldsymbol{m}^-_{\mathrm{x},k} \end{bmatrix} = \begin{bmatrix} \mathrm{maxeigvec}\left(\sum_i \tilde{w}^{(i)}_{k-1} \tilde{\boldsymbol{f}}_q(\widetilde{\boldsymbol{\mathcal{X}}}^{(i)}_{k-1}) \tilde{\boldsymbol{f}}^T_q(\widetilde{\boldsymbol{\mathcal{X}}}^{(i)}_{k-1})\right) \\ \sum_i \tilde{w}^{(i)}_{k-1} \tilde{\boldsymbol{f}}_\mathrm{x}(\widetilde{\boldsymbol{\mathcal{X}}}^{(i)}_{k-1}) \end{bmatrix}, \tag{4.37}$$

where the "maxeigvec" operator denotes the eigenvector corresponding to the maximum eigenvalue of its input matrix.

In order to find the associated state error covariance, first, the quaternion representation of the deviation from the estimated quaternion is found for each quadrature point according to

$$\delta\bar{\boldsymbol{q}}^{(i)} = \tilde{\boldsymbol{f}}_q(\widetilde{\boldsymbol{\mathcal{X}}}^{(i)}_{k-1}) \otimes \hat{\bar{\boldsymbol{q}}}^{-1}_k,$$

which is then transformed to find the equivalent representation in the local error space, denoted by $\delta\boldsymbol{\theta}^{(i)}$, according to the linearized relationship given in Eq. (4.24). The error covariance is then found

according to

$$\boldsymbol{P}_k^- = \sum_i \tilde{w}_{k-1}^{(i)} \begin{bmatrix} \delta\boldsymbol{\theta}^{(i)} \\ \tilde{\boldsymbol{f}}_{\mathrm{x}}(\widetilde{\boldsymbol{\mathcal{X}}}_{k-1}^{(i)}) - \boldsymbol{m}_{\mathrm{x},k}^- \end{bmatrix} \begin{bmatrix} \delta\boldsymbol{\theta}^{(i)} \\ \tilde{\boldsymbol{f}}_{\mathrm{x}}(\widetilde{\boldsymbol{\mathcal{X}}}_{k-1}^{(i)}) - \boldsymbol{m}_{\mathrm{x},k}^- \end{bmatrix}^T . \tag{4.38}$$

In summary, the predictor of a quadrature-based Kalman filter is given by Eqs. (4.37) and (4.38).

The corrector of a quadrature-based multiplicative Kalman filter uses a set of discrete weights and points, which are generated in the error space according to the desired quadrature rule to approximate the expected values in Eqs. (4.27). Let these discrete weights and points expressed in the local error space be denoted by $\bar{w}_k^{(i)}$ and $\delta\bar{\boldsymbol{\mathcal{X}}}_k^{(i)}$. These quadrature points are transformed from the local state error space into the global state space the same way they were for the predictor, which is given by Eqs. (4.34) and (4.36). The quadrature weights and points expressed in the global state space are now defined by $\bar{w}_k^{(i)}$ and $\bar{\boldsymbol{\mathcal{X}}}_k^{(i)}$. The expected values in Eqs. (4.27) are then approximated according to

$$\hat{\mathbf{z}}_k = \sum_i \bar{w}_k^{(i)} \bar{\boldsymbol{h}}\big(\bar{\boldsymbol{\mathcal{X}}}_k^{(i)}\big) \tag{4.39a}$$

$$\boldsymbol{P}_{zz} = \sum_i \bar{w}_k^{(i)} \Big[\bar{\boldsymbol{h}}\big(\bar{\boldsymbol{\mathcal{X}}}_k^{(i)}\big) - \hat{\mathbf{z}}_k\Big]\Big[\bar{\boldsymbol{h}}\big(\bar{\boldsymbol{\mathcal{X}}}_k^{(i)}\big) - \hat{\mathbf{z}}_k\Big]^T \tag{4.39b}$$

$$\boldsymbol{P}_{xz} = \sum_i \bar{w}_k^{(i)} \delta\bar{\boldsymbol{\mathcal{X}}}_{x,k}^{(i)} \Big[\bar{\boldsymbol{h}}\big(\bar{\boldsymbol{\mathcal{X}}}_k^{(i)}\big) - \hat{\mathbf{z}}_k\Big]^T , \tag{4.39c}$$

where $\delta\bar{\boldsymbol{\mathcal{X}}}_{x,k}^{(i)}$ represents the portion of $\delta\bar{\boldsymbol{\mathcal{X}}}_k^{(i)}$ corresponding to the state error vector; that is, the state error vector before it is augmented with the measurement noise.

Similarly to the quadrature-based Kalman filters, the quadrature scheme chosen for the quadrature-based multiplicative Kalman filters is a trade between accuracy of the quadrature approximation and its computational burden. The MUKF leverages the unscented transform to generate the quadrature weights and points in the error space, in a similar manner to how the UKF leverages the unscented transformation. The MQKF assumes that the uncertainty in the error space is Gaussian-distributed such that Gauss-Hermite quadrature can be used to generate the quadrature weights and points in the error space, in a similar manner to the QKF. In general, better performance from the MQKF can be obtained by using more points in the quadrature rule at the expense of computational power required.

Because multiplicative Kalman filtering uses the small angle approximation given in Eq. (4.24) to quantify the attitude error in a local minimum parameter representation constructed about the estimated attitude quaternion, the performance of a multiplicative Kalman filter will suffer as the attitude uncertainty becomes large. This performance degradation is present, even if a "perfect"

quadrature rule is used that perfectly captures the uncertainty representation in the local state error space, since these quadrature points must be transformed to the global state space using the small angle assumption. Despite this property of multiplicative Kalman filtering, the MEKF is still extremely effective in navigation applications, especially in applications when the attitude sensors provide good enough information such that the attitude uncertainty remains small. In order to circumvent the small angle assumption inherent to multiplicative Kalman filtering, the uncertainty in the attitude quaternion can be quantified on the unit hypersphere directly using the Bingham or Bingham mixture density (if the state vector consists only of an attitude quaternion), or the Gauss-Bingham, Gauss-Bingham mixture, Bingham-Gauss, or Bingham-Gauss density (if the state vector consists of an attitude quaternion and other Euclidean states). The evolution of this uncertainty can the be quantified or approximated under the Bayesian framework in order to quantify its temporal and measurement evolution.

5. BAYESIAN FILTERING

Under the Bayesian framework, the full state density, instead of just its first and second moments as under the Kalman framework, is quantified. Assume that the state density is known at an initial time t_0 and is given by $p(\boldsymbol{x}_0)$. The predictor of the Bayesian filter propagates the posterior density from t_{k-1} to obtain the prior density at t_k when a measurement is available. If the dynamical system is a Markov process ($\boldsymbol{x}_k$ depends only on the previous state, $\boldsymbol{x}_{k-1}$), the temporal evolution of the state density is defined by the Chapman-Kolmogorov equation [30], which is given by

$$p(\boldsymbol{x}_k|\boldsymbol{z}_{1:k-1}) = \int p(\boldsymbol{x}_k|\boldsymbol{x}_{k-1})p(\boldsymbol{x}_{k-1}|\boldsymbol{z}_{1:k-1})\,\mathrm{d}\boldsymbol{x}_{k-1}\,, \tag{5.1}$$

where $p(\boldsymbol{x}_k|\boldsymbol{x}_{k-1})$ is the state transition density, which is obtained from the dynamical system model, $p(\boldsymbol{x}_{k-1}|\boldsymbol{z}_{1:k-1})$ is the posterior state density at t_{k-1}, $p(\boldsymbol{x}_k|\boldsymbol{z}_{1:k-1})$ is the prior state density at t_k, and $\boldsymbol{z}_{1:k-1}$ represents all measurement information up to and including t_{k-1}; that is, $\boldsymbol{z}_{1:k-1} = \{\boldsymbol{z}_1, \boldsymbol{z}_2, \ldots, \boldsymbol{z}_{k-1}\}$. The integration in Eq. (5.1) is performed over the domain of $\boldsymbol{x}_{k-1}$, which is not required to be Euclidean space; that is, the Chapman-Kolmogorov equation is valid for all state densities, not just those that probabilistically quantify a Euclidean random variable.

The corrector of the Bayesian filter updates the prior density when a measurement is received at t_k. Let the measurement at t_k be denoted by $\boldsymbol{z}_k$. The Bayesian corrector for a Markovian system is given by Bayes' rule [30], which is given by

$$p(\boldsymbol{x}_k|\boldsymbol{z}_{1:k}) = \frac{p(\boldsymbol{z}_k|\boldsymbol{x}_k)p(\boldsymbol{x}_k|\boldsymbol{z}_{1:k-1})}{\int p(\boldsymbol{z}_k|\boldsymbol{\xi})p(\boldsymbol{\xi}|\boldsymbol{z}_{1:k-1})\,\mathrm{d}\boldsymbol{\xi}}\,, \tag{5.2}$$

where $p(\boldsymbol{z}_k|\boldsymbol{x}_k, \boldsymbol{z}_{1:k-1})$ is the measurement likelihood, which is obtained from the measurement model and $p(\boldsymbol{x}_k|\boldsymbol{z}_{1:k-1})$ is the prior state density at t_{k-1}. Unlike the Kalman framework, the Bayesian framework does *not* enforce a linear update structure in the corrector; that is, it employs a nonlinear update. Similar to Eq. (5.1), the integration in Eq. (5.2) is performed over the domain of $\boldsymbol{x}_k$, which is not required to be Euclidean space. Because of this, the Bayes' rule, and thus the Bayesian recursion defined by Eqs. (5.1) and (5.2), is valid for all state densities, not just those that probabilistically quantify a Euclidean random variable.

Equations (5.1) and (5.2) provide the exact Bayesian filter. If the recursion defined by Eqs. (5.1) and (5.2) closes in a tractable manner, then the state density, and thus the complete probabilistic description of the state, is known for all time. This recursion closes for linear systems with additive noises, as defined by Eqs. (4.4), if the initial state and the process and measurement

noises are Gaussian-distributed and mutually independent. In this case, the Bayesian Kalman filter is obtained, in which the temporal and measurement evolution of the mean and covariance of the Gaussian-distributed state is identical to the Kalman filter. If the initial state is non-Gaussian-distributed, the process or measurement noise is non-Gaussian, or the dynamical system or measurement model is nonlinear or possesses non-additive noise, the recursion defined by Eqs. (5.1) and (5.2) does not generally close in a tractable manner, and approximations are typically made such that the recursion closes. These approximations result in an approximate Bayesian filter, in which the recursion is forced to close; however, the *approximate* temporal and measurement evolution of the state density is now quantified, which allows the recursion to close.

The Bayesian Kalman filter and GMKF are now presented, which exactly quantify the evolution of the Gaussian and GM densities under the Bayesian framework given a linear dynamical system and measurement model with additive, Gaussian-distributed process and measurement noise. Next, the GMEKF, GMUKF, and GMQKF are presented, which are extensions to the GMKF that approximately quantify the evolution of a GM density under the Bayesian framework, given a nonlinear dynamical system and measurement model with additive, Gaussian-distributed process and measurement noise. The concept of minimum divergence filtering is then presented and is subsequently used to derive the GMMDF. The GMMDF approximately quantifies the evolution of a GM density under the Bayesian framework by approximating each step in the Bayesian recursion by a GM density. The parameters of the GM density are found by minimizing the Kullback-Leibler (KL) divergence of the true density, defined by the Chapman-Kolmogorov equation and Bayes' rule, to the approximating GM density on a component-wise basis. The corrector of a single component GMMDF is then compared to the corrector of a single component GMEKF and GMQKF in order to compare and contrast the GMMDF to conventional GM filters.

5.1. BAYESIAN KALMAN FILTER

The Bayesian Kalman filter quantifies the temporal and measurement evolution of a Gaussian density when the dynamical system and measurement model are linear with additive, Gaussian-distributed noise. This dynamical system and measurement model are given by Eqs. (4.4), under the further restriction that $\boldsymbol{w}_{k-1}$ and $\boldsymbol{v}_k$ are Gaussian-distributed. Let the initial Gaussian density be defined by $p_g(\boldsymbol{x}_0; \boldsymbol{m}_0^+, \boldsymbol{P}_0^+)$. The temporal evolution is defined by Eq. (5.1) evaluated with the Gaussian state density and is given by

$$p(\boldsymbol{x}_k|\boldsymbol{z}_{1:k-1}) = \int p_g(\boldsymbol{x}_k; \boldsymbol{F}_{k-1}\boldsymbol{x}_{k-1}, \boldsymbol{Q}_{k-1}) p_g(\boldsymbol{x}_{k-1}; \boldsymbol{m}_{k-1}^+, \boldsymbol{P}_{k-1}^+) \, \mathrm{d}\boldsymbol{x}_{k-1} \,, \qquad (5.3)$$

where $p_g(\boldsymbol{x}_k; \boldsymbol{F}_{k-1}\boldsymbol{x}_{k-1}, \boldsymbol{Q}_{k-1})$ is the Gaussian transition density defined by the linear dynamical system with additive Gaussian-distributed noise. In order to solve the integral in Eq. (5.3), an important and well-known result in Bayesian filtering [54] is exploited, which is derived in Appendix D. Observation of Eq. (D.3) shows that the integral in Eq. (5.3) can be expressed as

$$
\begin{aligned}
p(\boldsymbol{x}_k|\boldsymbol{z}_{1:k-1}) &= p_g(\boldsymbol{x}_k; \boldsymbol{F}_{k-1}\boldsymbol{m}_{k-1}^+, \boldsymbol{F}_{k-1}\boldsymbol{P}_{k-1}^+\boldsymbol{F}_{k-1}^T + \boldsymbol{Q}_{k-1}) \\
&\triangleq p_g(\boldsymbol{x}_k; \boldsymbol{m}_k^-, \boldsymbol{P}_k^-),
\end{aligned}
\tag{5.4}
$$

which shows that $p(\boldsymbol{x}_k|\boldsymbol{z}_{1:k-1})$ is Gaussian. Therefore, it can be observed that the temporal evolution of the mean and covariance defining the Gaussian density are given by

$$
\boldsymbol{m}_k^- = \boldsymbol{F}_{k-1}\boldsymbol{m}_{k-1}^+
\tag{5.5a}
$$

$$
\boldsymbol{P}_k^- = \boldsymbol{F}_{k-1}\boldsymbol{P}_{k-1}^+\boldsymbol{F}_{k-1}^T + \boldsymbol{Q}_{k-1},
\tag{5.5b}
$$

which is algorithmically identical to the predictor of the Kalman filter given in Eqs. (4.13).

The corrector of the Bayesian Kalman filter, which incorporates the measurement data into the prior Gaussian density, is given by Eq. (5.2) evaluated with the Gaussian state density according to

$$
p(\boldsymbol{x}_k|\boldsymbol{z}_{1:k}) = \frac{p_g(\boldsymbol{z}_k; \boldsymbol{H}_k\boldsymbol{x}_k, \boldsymbol{R}_k)p_g(\boldsymbol{x}_k; \boldsymbol{m}_k^-, \boldsymbol{P}_k^-)}{\int p_g(\boldsymbol{z}_k; \boldsymbol{H}_k\boldsymbol{\xi}, \boldsymbol{R}_k)p_g(\boldsymbol{\xi}; \boldsymbol{m}_k^-, \boldsymbol{P}_k^-)\,\mathrm{d}\boldsymbol{\xi}},
\tag{5.6}
$$

where $p_g(\boldsymbol{z}_k; \boldsymbol{H}_k\boldsymbol{x}_k, \boldsymbol{R}_k)$ is the Gaussian measurement likelihood, which is defined by the linear measurement model with additive Gaussian-distributed noise. Equations (D.1) and (D.3) are now used to simplify the numerator and denominator of Eq. (5.6), respectively, which yields

$$
\begin{aligned}
p(\boldsymbol{x}_k|\boldsymbol{z}_{1:k}) &= \frac{p_g(\boldsymbol{z}_k; \boldsymbol{H}_k\boldsymbol{m}_k^-, \boldsymbol{H}_k\boldsymbol{P}_k^-\boldsymbol{H}_k^T + \boldsymbol{R}_k)p_g(\boldsymbol{x}_k; \boldsymbol{m}_k^+, \boldsymbol{P}_k^+)}{p_g(\boldsymbol{z}_k; \boldsymbol{H}_k\boldsymbol{m}_k^-, \boldsymbol{H}_k\boldsymbol{P}_k^-\boldsymbol{H}_k^T + \boldsymbol{R}_k)} \\
&= p_g(\boldsymbol{x}_k; \boldsymbol{m}_k^+, \boldsymbol{P}_k^+),
\end{aligned}
$$

where

$$
\boldsymbol{m}_k^+ = \boldsymbol{m}_k^- + \boldsymbol{K}_k(\boldsymbol{z}_k - \boldsymbol{H}_k\boldsymbol{m}_k^-)
\tag{5.7a}
$$

$$
\boldsymbol{P}_k^+ = \boldsymbol{P}_k^- - \boldsymbol{K}_k\boldsymbol{H}_k\boldsymbol{P}_k^-,
\tag{5.7b}
$$

and

$$
\boldsymbol{K}_k \triangleq \boldsymbol{P}_k^-\boldsymbol{H}_k^T(\boldsymbol{H}_k\boldsymbol{P}_k^-\boldsymbol{H}_k^T + \boldsymbol{R}_k)^{-1},
\tag{5.8}
$$

which shows that the posterior density is Gaussian with updated mean and covariance given by Eqs. (5.7). The corrector of the Bayesian Kalman filter is observed to be algorithmically identical to that of the Kalman filter, which is apparent if Eqs. (4.14) are substituted into Eqs. (4.10) and (4.11) and simplified, which yields the form of the Kalman gain and mean and covariance update given in Eqs. (5.7) and (5.8).

Observation of the Bayesian Kalman filter shows that, if a linear dynamical system and measurement model with additive, Gaussian-distributed process and measurement noise is considered, and the initial state is Gaussian-distributed, that the state remains Gaussian-distributed under the Bayesian recursion and the mean and covariance of the Gaussian density evolve identically to that of the Kalman filter. It is important to note, however, that the Kalman filter is derived under the linear MMSE framework, which quantifies only the first and second moment of the state density and does not require that the process and measurement noise be Gaussian-distributed. The Bayesian Kalman filter is derived under the Bayesian framework, which quantifies the evolution of the Gaussian state density and requires the process and measurement noise to be Gaussian-distributed.

5.2. GAUSSIAN MIXTURE KALMAN FILTER

The GMKF [21] quantifies the temporal and measurement evolution of a GM density when the dynamical system and measurement model are linear with additive, Gaussian-distributed noise. This dynamical system and measurement model are given by Eqs. (4.4), under the further restriction that $\boldsymbol{w}_{k-1}$ and $\boldsymbol{v}_k$ are Gaussian-distributed. Let the initial GM density be defined by

$$\sum_{\ell=1}^{L_0^+} w_0^{(\ell)+} p_g\left(\boldsymbol{x}_0; \boldsymbol{m}_0^{(\ell)+}, \boldsymbol{P}_0^{(\ell)+}\right).$$

The temporal evolution is defined by Eq. (5.1) evaluated using the GM state density and is given by

$$p(\boldsymbol{x}_k|\boldsymbol{z}_{1:k-1}) = \int p_g(\boldsymbol{x}_k; \boldsymbol{F}_{k-1}\boldsymbol{x}_{k-1}, \boldsymbol{Q}_{k-1}) \sum_{\ell=1}^{L_{k-1}^+} w_{k-1}^{(\ell)+} p_g\left(\boldsymbol{x}_{k-1}; \boldsymbol{m}_{k-1}^{(\ell)+}, \boldsymbol{P}_{k-1}^{(\ell)+}\right) \mathrm{d}\boldsymbol{x}_{k-1}. \quad (5.9)$$

Because integration and summation are both linear operators, their order can be reversed and Eq. (5.9) can be manipulated to yield

$$p(\boldsymbol{x}_k|\boldsymbol{z}_{1:k-1}) = \sum_{\ell=1}^{L_{k-1}^+} w_{k-1}^{(\ell)+} \int p_g(\boldsymbol{x}_k; \boldsymbol{F}_{k-1}\boldsymbol{x}_{k-1}, \boldsymbol{Q}_{k-1}) p_g\left(\boldsymbol{x}_{k-1}; \boldsymbol{m}_{k-1}^{(\ell)+}, \boldsymbol{P}_{k-1}^{(\ell)+}\right) \mathrm{d}\boldsymbol{x}_{k-1}. \quad (5.10)$$

Equation (D.3) is now used in order to express Eq. (5.10) according to

$$p(\boldsymbol{x}_k|\boldsymbol{z}_{1:k-1}) = \sum_{\ell=1}^{L_{k-1}^+} w_{k-1}^{(\ell)+} p_g(\boldsymbol{x}_k; \boldsymbol{F}_{k-1}\boldsymbol{m}_{k-1}^{(\ell)+}, \boldsymbol{F}_{k-1}\boldsymbol{P}_{k-1}^{(\ell)+}\boldsymbol{F}_{k-1}^T + \boldsymbol{Q}_{k-1}), \qquad (5.11)$$

which shows that $p(\boldsymbol{x}_k|\boldsymbol{z}_{1:k-1})$ is a GM density that is defined as

$$p(\boldsymbol{x}_k|\boldsymbol{z}_{1:k-1}) = \sum_{\ell=1}^{L_k^-} w_k^{(\ell)-} p_g\left(\boldsymbol{x}_k; \boldsymbol{m}_k^{(\ell)-}, \boldsymbol{P}_k^{(\ell)-}\right). \qquad (5.12)$$

Comparing Eqs. (5.11) and (5.12), it can be observed that the evolution of the number of components, weights, means, and covariances defining the GM density are given by

$$L_k^- = L_{k-1}^+ \qquad (5.13a)$$
$$w_k^{(\ell)-} = w_{k-1}^{(\ell)+} \qquad (5.13b)$$
$$\boldsymbol{m}_k^{(\ell)-} = \boldsymbol{F}_{k-1}\boldsymbol{m}_{k-1}^{(\ell)+} \qquad (5.13c)$$
$$\boldsymbol{P}_k^{(\ell)-} = \boldsymbol{F}_{k-1}\boldsymbol{P}_{k-1}^{(\ell)+}\boldsymbol{F}_{k-1}^T + \boldsymbol{Q}_{k-1}, \qquad (5.13d)$$

which defines the predictor of the GMKF.

The corrector of the GMKF is defined by Eq. (5.6) evaluated using the GM state density and is given by

$$p(\boldsymbol{x}_k|\boldsymbol{z}_{1:k}) = \frac{p_g(\boldsymbol{z}_k; \boldsymbol{H}_k\boldsymbol{x}_k, \boldsymbol{R}_k) \sum_{\ell=1}^{L_k^-} w_k^{(\ell)-} p_g\left(\boldsymbol{x}_k; \boldsymbol{m}_k^{(\ell)-}, \boldsymbol{P}_k^{(\ell)-}\right)}{\int p_g(\boldsymbol{z}_k; \boldsymbol{H}_k\boldsymbol{\xi}, \boldsymbol{R}_k) \sum_{\ell=1}^{L_k^-} w_k^{(\ell)-} p_g\left(\boldsymbol{\xi}; \boldsymbol{m}_k^{(\ell)-}, \boldsymbol{P}_k^{(\ell)-}\right) \mathrm{d}\boldsymbol{\xi}},$$

which can be manipulated to yield

$$p(\boldsymbol{x}_k|\boldsymbol{z}_{1:k}) = \frac{\sum_{\ell=1}^{L_k^-} w_k^{(\ell)-} p_g(\boldsymbol{z}_k; \boldsymbol{H}_k\boldsymbol{x}_k, \boldsymbol{R}_k) p_g\left(\boldsymbol{x}_k; \boldsymbol{m}_k^{(\ell)-}, \boldsymbol{P}_k^{(\ell)-}\right)}{\sum_{\ell=1}^{L_k^-} w_k^{(\ell)-} \int p_g(\boldsymbol{z}_k; \boldsymbol{H}_k\boldsymbol{\xi}, \boldsymbol{R}_k) p_g\left(\boldsymbol{\xi}; \boldsymbol{m}_k^{(\ell)-}, \boldsymbol{P}_k^{(\ell)-}\right) \mathrm{d}\boldsymbol{\xi}}, \qquad (5.14)$$

Equations (D.1) and (D.3) are now used to simplify the numerator and denominator of Eqs. (5.14), respectively, which yields

$$p(\boldsymbol{x}_k|\boldsymbol{z}_{1:k}) = \frac{\sum_{\ell=1}^{L_k^-} w_k^{(\ell)-} k_k^{(\ell)} p_g(\boldsymbol{x}_k; \boldsymbol{m}_k^{(\ell)+}, \boldsymbol{P}_k^{(\ell)+})}{\sum_{\ell=1}^{L_k^-} w_k^{(\ell)-} k_k^{(\ell)}}, \qquad (5.15)$$

where

$$k_k^{(\ell)} = p_g(\boldsymbol{z}_k; \boldsymbol{H}_k \boldsymbol{m}_k^{(\ell)-}, \boldsymbol{H}_k \boldsymbol{P}_k^{(\ell)-} \boldsymbol{H}_k^T + \boldsymbol{R}_k) \tag{5.16a}$$

$$\boldsymbol{m}_k^{(\ell)+} = \boldsymbol{m}_k^{(\ell)-} + \boldsymbol{K}_k^{(\ell)}(\boldsymbol{z}_k - \boldsymbol{H}_k \boldsymbol{m}_k^{(\ell)-}) \tag{5.16b}$$

$$\boldsymbol{P}_k^{(\ell)+} = \boldsymbol{P}_k^{(\ell)-} - \boldsymbol{K}_k^{(\ell)} \boldsymbol{H}_k \boldsymbol{P}_k^{(\ell)-} \tag{5.16c}$$

and

$$\boldsymbol{K}_k^{(\ell)} \triangleq \boldsymbol{P}_k^{(\ell)-} \boldsymbol{H}_k^T (\boldsymbol{H}_k \boldsymbol{P}_k^{(\ell)-} \boldsymbol{H}_k^T + \boldsymbol{R}_k)^{-1} \,.$$

Equation (5.15) can rearranged to be expressed as

$$p(\boldsymbol{x}_k|\boldsymbol{z}_{1:k}) = \sum_{\ell=1}^{L_k^-} \frac{w_k^{(\ell)-} k_k^{(\ell)}}{\sum_{j=1}^{L_k^-} w_k^{(j)-} k_k^{(j)}} p_g(\boldsymbol{x}_k; \boldsymbol{m}_k^{(\ell)+}, \boldsymbol{P}_k^{(\ell)+}) , \tag{5.17}$$

in which case it becomes apparent that the posterior density is a GM density, which is defined as

$$p(\boldsymbol{x}_k|\boldsymbol{z}_{1:k}) = \sum_{\ell=1}^{L_k^+} w_k^{(\ell)+} p_g\left(\boldsymbol{x}_k; \boldsymbol{m}_k^{(\ell)+}, \boldsymbol{P}_k^{(\ell)+}\right) . \tag{5.18}$$

Equations (5.17) and (5.18) are now compared to show that the corrector of the GMKF is given by Eqs. (5.16b), (5.16c), and

$$L_k^- = L_{k-1}^+$$

$$w_k^{(\ell)+} = \frac{w_k^{(\ell)-} k_k^{(\ell)}}{\sum_{j=1}^{L_k^-} w_k^{(j)-} k_k^{(j)}} \,.$$

The weight update shows that the weights of each component are updated according to the relative likelihood of the measurement from each component.

The GMKF shows that, if a linear dynamical system and measurement model with additive, Gaussian-distributed process and measurement noise is considered, and the initial state is GM-distributed, that the state remains GM-distributed under the Bayesian recursion and the mean and covariance of each component of the GM density evolve identically to that of the Kalman filter. Furthermore, it is observed that, if a single component GM is used, the GMKF reduces to the Bayesian Kalman filter. This is an expected result, since a single component GM density is simply a Gaussian density. The GMKF can be extended to applications in which the process and measurement noise are GM-distributed; however, this is not shown for clarity of the presented GMKF.

5.3. GAUSSIAN MIXTURE EXTENDED KALMAN FILTER

The GMEKF [55] in an extension to the GMKF that quantifies the approximate temporal and measurement evolution of a GM density when the dynamical system and measurement model are nonlinear with additive, Gaussian-distributed noise. This dynamical system and measurement model are given by Eqs. (4.3), under the further restriction that $\boldsymbol{w}_{k-1}$ and $\boldsymbol{v}_k$ are Gaussian-distributed. Reference [55] provides a complete derivation of the GMEKF; therefore, the explicit derivation of the GMEKF is omitted from this work.

Let the initial GM density be defined by

$$\sum_{\ell=1}^{L_0^+} w_0^{(\ell)+} p_g\left(\boldsymbol{x}_0; \boldsymbol{m}_0^{(\ell)+}, \boldsymbol{P}_0^{(\ell)+}\right).$$

The temporal evolution is defined by Eq. (5.1), and is given by

$$p(\boldsymbol{x}_k|\boldsymbol{z}_{1:k-1}) = \int p_g(\boldsymbol{x}_k; \boldsymbol{f}(\boldsymbol{x}_{k-1}), \boldsymbol{Q}_{k-1}) \sum_{\ell=1}^{L_{k-1}^+} w_{k-1}^{(\ell)+} p_g\left(\boldsymbol{x}_{k-1}; \boldsymbol{m}_{k-1}^{(\ell)+}, \boldsymbol{P}_{k-1}^{(\ell)+}\right) \mathrm{d}\boldsymbol{x}_{k-1}, \quad (5.19)$$

where $p_g(\boldsymbol{x}_k; \boldsymbol{f}(\boldsymbol{x}_{k-1}), \boldsymbol{Q}_{k-1})$ is the Gaussian transition density defined by a nonlinear dynamical system with additive, Gaussian-distributed noise. Because integration and summation are both linear operators, their order can be reversed and Eq. (5.19) can be manipulated to yield

$$p(\boldsymbol{x}_k|\boldsymbol{z}_{1:k-1}) = \sum_{\ell=1}^{L_{k-1}^+} w_{k-1}^{(\ell)+} \int p_g(\boldsymbol{x}_k; \boldsymbol{f}(\boldsymbol{x}_{k-1}), \boldsymbol{Q}_{k-1}) p_g\left(\boldsymbol{x}_{k-1}; \boldsymbol{m}_{k-1}^{(\ell)+}, \boldsymbol{P}_{k-1}^{(\ell)+}\right) \mathrm{d}\boldsymbol{x}_{k-1}. \quad (5.20)$$

The nonlinear function quantifying the dynamical system, $\boldsymbol{f}(\boldsymbol{x}_{k-1})$, is now linearized about the mean of each component, $\boldsymbol{m}_{k-1}^{(\ell)+}$, and the result is manipulated similarly to the predictor of the GMKF in order to derive the predictor of the GMEKF. This process shows that the density remains approximately a GM density in the predictor, with the evolution of its parameters defined by

$$L_k^- = L_{k-1}^+ \tag{5.21a}$$

$$w_k^{(\ell)-} = w_{k-1}^{(\ell)+} \tag{5.21b}$$

$$\boldsymbol{m}_k^{(\ell)-} = \boldsymbol{f}(\boldsymbol{m}_{k-1}^{(\ell)+}) \tag{5.21c}$$

$$\boldsymbol{P}_k^{(\ell)-} = \boldsymbol{F}(\boldsymbol{m}_{k-1}^{(\ell)+}) \boldsymbol{P}_{k-1}^{(\ell)+} \boldsymbol{F}(\boldsymbol{m}_{k-1}^{(\ell)+})^T + \boldsymbol{Q}_{k-1}, \tag{5.21d}$$

where $\boldsymbol{F}(\boldsymbol{m}_{k-1}^{(\ell)+})$ is the Jacobian matrix of the dynamical system and is given by

$$\boldsymbol{F}(\boldsymbol{m}_{k-1}^{(\ell)+}) \triangleq \frac{\partial \boldsymbol{f}(\boldsymbol{x})}{\partial \boldsymbol{x}}\bigg|_{\boldsymbol{x}=\boldsymbol{m}_{k-1}^{(\ell)+}}.$$

The corrector of the GMEKF is defined by Eq. (5.6) and given by

$$p(\boldsymbol{x}_k|\boldsymbol{z}_{1:k}) = \frac{p_g(\boldsymbol{z}_k; \boldsymbol{h}(\boldsymbol{x}_k), \boldsymbol{R}_k) \sum_{\ell=1}^{L_k^-} w_k^{(\ell)-} \, p_g\left(\boldsymbol{x}_k; \boldsymbol{m}_k^{(\ell)-}, \boldsymbol{P}_k^{(\ell)-}\right)}{\int p_g(\boldsymbol{z}_k; \boldsymbol{h}(\boldsymbol{\xi}), \boldsymbol{R}_k) \sum_{\ell=1}^{L_k^-} w_k^{(\ell)-} \, p_g\left(\boldsymbol{\xi}; \boldsymbol{m}_k^{(\ell)-}, \boldsymbol{P}_k^{(\ell)-}\right) \mathrm{d}\boldsymbol{\xi}}, \tag{5.22}$$

where $p_g(\boldsymbol{z}_k; \boldsymbol{h}(\boldsymbol{x}_k), \boldsymbol{R}_k)$ is the Gaussian measurement density defined by a nonlinear measurement model with additive, Gaussian-distributed noise. Equation (5.22) is manipulated to yield

$$p(\boldsymbol{x}_k|\boldsymbol{z}_{1:k}) = \frac{\sum_{\ell=1}^{L_k^-} w_k^{(\ell)-} p_g(\boldsymbol{z}_k; \boldsymbol{h}(\boldsymbol{x}_k), \boldsymbol{R}_k) p_g\left(\boldsymbol{x}_k; \boldsymbol{m}_k^{(\ell)-}, \boldsymbol{P}_k^{(\ell)-}\right)}{\sum_{\ell=1}^{L_k^-} w_k^{(\ell)-} \int p_g(\boldsymbol{z}_k; \boldsymbol{h}(\boldsymbol{\xi}), \boldsymbol{R}_k) p_g\left(\boldsymbol{\xi}; \boldsymbol{m}_k^{(\ell)-}, \boldsymbol{P}_k^{(\ell)-}\right) \mathrm{d}\boldsymbol{\xi}}. \tag{5.23}$$

The nonlinear measurement model, $\boldsymbol{h}(\boldsymbol{x}_k)$, is now linearized about the mean of each component, $\boldsymbol{m}_k^{(\ell)-}$, and the result is manipulated similarly to the corrector of the GMKF in order to derive the corrector of the GMEKF. This process shows that the density remains approximately a GM density in the corrector, with the measurement evolution of its parameters defined by

$$L_k^+ = L_{k-1}^- \tag{5.24a}$$

$$w_k^{(\ell)+} = \frac{w_k^{(\ell)-} k_k^{(\ell)}}{\sum_{j=1}^{L_k^-} w_k^{(j)-} k_k^{(j)}} \tag{5.24b}$$

$$\boldsymbol{m}_k^{(\ell)+} = \boldsymbol{m}_k^{(\ell)-} + \boldsymbol{K}_k^{(\ell)} \left[\boldsymbol{z}_k - \boldsymbol{h}\left(\boldsymbol{m}_k^{(\ell)-}\right)\right] \tag{5.24c}$$

$$\boldsymbol{P}_k^{(\ell)+} = \boldsymbol{P}_k^{(\ell)-} - \boldsymbol{K}_k^{(\ell)} \boldsymbol{H}\left(\boldsymbol{m}_k^{(\ell)-}\right) \boldsymbol{P}_k^{(\ell)-} \tag{5.24d}$$

where

$$k_k^{(\ell)} \triangleq p_g\left(\boldsymbol{z}_k; \boldsymbol{h}\left(\boldsymbol{m}_k^{(\ell)-}\right), \boldsymbol{H}\left(\boldsymbol{m}_k^{(\ell)-}\right) \boldsymbol{P}_k^{(\ell)-} \boldsymbol{H}\left(\boldsymbol{m}_k^{(\ell)-}\right)^T + \boldsymbol{R}_k\right) \tag{5.25a}$$

$$\boldsymbol{K}_k^{(\ell)} \triangleq \boldsymbol{P}_k^{(\ell)-} \boldsymbol{H}\left(\boldsymbol{m}_k^{(\ell)-}\right)^T \left[\boldsymbol{H}\left(\boldsymbol{m}_k^{(\ell)-}\right) \boldsymbol{P}_k^{(\ell)-} \boldsymbol{H}\left(\boldsymbol{m}_k^{(\ell)-}\right)^T + \boldsymbol{R}_k\right]^{-1}, \tag{5.25b}$$

and $\boldsymbol{H}\left(\boldsymbol{m}_k^{(\ell)-}\right)$ is the Jacobian matrix of the dynamical system and is given by

$$\boldsymbol{H}\left(\boldsymbol{m}_k^{(\ell)-}\right) \triangleq \frac{\partial \boldsymbol{h}(\boldsymbol{x})}{\partial \boldsymbol{x}}\bigg|_{\boldsymbol{x}=\boldsymbol{m}_k^{(\ell)-}}.$$

The linearization of $\boldsymbol{f}(\boldsymbol{x}_{k-1})$ and $\boldsymbol{h}(\boldsymbol{x}_k)$ about $\boldsymbol{m}_{k-1}^+$ and $\boldsymbol{m}_k^-$, respectively, in the GMEKF allows the Bayesian recursion to close; however, because of this linearization, the resulting GM density that is quantified is only an approximation to the true state density. As the state uncertainty in each component approaches zero, the error incurred by this linearization approaches zero and the exact evolution of the GM state density is captured. Because of this, if the uncertainty in each component of the the GM density is small, the error incurred by this linearization is small. This can be exploited by using a GM density approximation of another state density in the GMEKF. If the approximating GM has small uncertainty in each of its components, little error is incurred in quantifying the temporal and measurement evolution of the approximating GM [55]. Furthermore, an adaptive method to split Gaussian components can be implemented to monitor when the uncertainty in the components of the GM becomes too large and split the components into several smaller components [56].

5.4. QUADRATURE-BASED GAUSSIAN MIXTURE KALMAN FILTERS

The GMUKF and GMQKF are both quadrature-based GM Kalman filters. These filters are obtained by first noting that the GMEKF, as defined by Eqs. (5.21), (5.24), and (5.25), appears to be a "bank" of extended Kalman filters coupled with their corresponding weight updates. A quadrature-based GM Kalman filter replaces these extended Kalman filter equations with their equivalent quadrature-based forms, in an effort to reduce the error incurred by the linearization in the GMEKF. Therefore, the predictor of a quadrature-based GM Kalman filter is given by

$$
\begin{aligned}
L_k^- &= L_{k-1}^+ \\
w_k^{(\ell)-} &= w_{k-1}^{(\ell)+} \\
\boldsymbol{m}_k^{(\ell)-} &= \sum_i w_{k-1}^{(i,\ell)} \boldsymbol{f}(\boldsymbol{\mathcal{X}}_{k-1}^{(i,\ell)}) \\
\boldsymbol{P}_k^{(\ell)-} &= \sum_i w_{k-1}^{(i,\ell)} \Big[\boldsymbol{f}(\boldsymbol{\mathcal{X}}_{k-1}^{(i,\ell)}) - \boldsymbol{m}_k^{(\ell)-}\Big]\Big[\boldsymbol{f}(\boldsymbol{\mathcal{X}}_{k-1}^{(i,\ell)}) - \boldsymbol{m}_k^{(\ell)-}\Big]^T + \boldsymbol{Q}_{k-1} \ ,
\end{aligned}
$$

where $w_{k-1}^{(i,\ell)}$ and $\boldsymbol{\mathcal{X}}_{k-1}^{(i,\ell)}$ represent the quadrature weights and points corresponding to the ℓth component of the GM density used in the predictor of the quadrature-based GM Kalman filter.

The corrector of a quadrature-based GM Kalman filter is given by

$$
L_k^+ = L_{k-1}^- \tag{5.26}
$$

$$
w_k^{(\ell)+} = \frac{w_k^{(\ell)-} k_k^{(\ell)}}{\sum_{j=1}^{L_k^-} w_k^{(j)-} k_k^{(j)}} \tag{5.27}
$$

$$m_k^{(\ell)+} = m_k^{(\ell)-} + K_k^{(\ell)}(z_k - \hat{z}_k^{(\ell)}) \tag{5.28}$$

$$P_k^{(\ell)+} = P_k^{(\ell)-} - K_k^{(\ell)} P_{zz}^{(\ell)} K_k^{(\ell)T} , \tag{5.29}$$

where $K_k^{(\ell)}$ is the Kalman gain corresponding to the ℓth component of the GM density, which is defined by

$$K_k^{(\ell)} = P_{xz}^{(\ell)} P_{zz}^{(\ell)-1} ,$$

$k_k^{(\ell)}$ is the likelihood that the measurement originated from the ℓth component, which is given by

$$k_k^{(\ell)} = p_g(z_k; \hat{z}_k^{(\ell)}, P_{zz}^{(\ell)}) ,$$

and the expected measurement, innovation (or residual) covariance, and state-measurement cross-covariance corresponding to the ℓth component of the GM density are given by

$$\hat{z}_k^{(\ell)} = \sum_i w_k^{(i,\ell)} h(\mathcal{X}_k^{(i,\ell)})$$

$$P_{zz}^{(\ell)} = \sum_i w_k^{(i,\ell)} \left[h(\mathcal{X}_k^{(i,\ell)}) - \hat{z}_k^{(\ell)} \right] \left[h(\mathcal{X}_k^{(i,\ell)}) - \hat{z}_k^{(\ell)} \right]^T + R_k$$

$$P_{xz}^{(\ell)} = \sum_i w_k^{(i,\ell)} \left[\mathcal{X}_k^{(i,\ell)} - m_k^{(\ell)-} \right] \left[h(\mathcal{X}_k^{(i,\ell)}) - \hat{z}_k^{(\ell)} \right]^T ,$$

where $w_k^{(i,\ell)}$ and $\mathcal{X}_k^{(i,\ell)}$ represent the quadrature weights and points corresponding to the ℓth component of the GM density used in the corrector of the quadrature-based GM Kalman filter.

How the weights and points are selected for the predictor and corrector of a quadrature-based GM Kalman filter defines the specific type of quadrature-based GM Kalman filter used. If the unscented transform is used, the GMUKF is obtained. If Gauss-Hermite quadrature is used, the GMQKF is obtained. Different and more efficient quadrature schemes can be implemented, if desired; however, it is important to note that using quadrature methods for a GM Kalman filter has potentially limited benefit. In general, the GM can be split such that the uncertainty in each component is smaller, and, thus, the linearization in the GMEKF incurs less error. Because of this, it is typically computationally advantageous to split the GM density into a larger number of smaller components and use the GMEKF (or potentially the GMUKF) instead of using the GMQKF on the original GM density, especially in systems with high-dimensionality in which the Gauss-Hermite quadrature rule suffers from the curse of dimensionality.

5.5. MINIMUM DIVERGENCE FILTERING

Consider an approximate Bayesian filter in which the state density, which evolves according to Eqs. (5.1) and (5.2), is approximated by an assumed density at each step in the recursion. By approximating the true density by an assumed density, the recursion defining the Bayesian filter is now forced to close in a tractable manner. In order to find the parameters defining the assumed density, an information divergence measure between the assumed density and the state density is minimized.

An information divergence quantifies the directed distance between two state densities. An information divergence measure of the state density $p_2(\boldsymbol{x})$ with respect to the state density $p_1(\boldsymbol{x})$ is denoted by $D[p_1||p_2]$. $D[p_1||p_2]$ is always non-negative and is zero only when $p_1(\boldsymbol{x}) = p_2(\boldsymbol{x})$. An information divergence is a measure, but is not a metric, since $D[p_1||p_2] \neq D[p_2||p_1]$ in general. By minimizing an information divergence of an assumed density with respect to the true state density, the parameters that define the assumed density that best fits the true state density are found. It is important to note that the parameters of the *best fit* assumed density are defined according to the chosen information divergence measure. In this work, the KL divergence [57] is chosen as the divergence measure, which allows for an analytic minimization to be performed for exponential family pdfs.

5.5.1. Minimizing the Kullback-Leibler Divergence. Let $p(\boldsymbol{x})$ be a known state density and $q(\boldsymbol{x}; \boldsymbol{\theta})$ be the assumed state density, defined by the parameter set $\boldsymbol{\theta}$, that is chosen to approximate $p(\boldsymbol{x})$. The parameter set $\boldsymbol{\theta}$ is found by minimizing the KL divergence of $q(\boldsymbol{x}; \boldsymbol{\theta})$ with respect to $p(\boldsymbol{x})$, which is defined by

$$J = D_{KL}[p||q] = \int p(\boldsymbol{x}) \ln \frac{p(\boldsymbol{x})}{q(\boldsymbol{x}; \boldsymbol{\theta})} \, \mathrm{d}\boldsymbol{x} \,. \tag{5.30}$$

The KL divergence is chosen because an analytic condition that minimizes the KL divergence of an exponential family state density with respect to the true state density can be found, as will be shown. The integration in Eq. (A.2) is performed over the domain of $\boldsymbol{x}$, which is not required to be Euclidean space; therefore, the KL divergence is valid for all state densities, not just those that probabilistically quantify a Euclidean random variable, provided that the integral exists.

An exponential family density is any density that can be expressed in the form

$$p_e(\boldsymbol{x}; \boldsymbol{\theta}) = c(\boldsymbol{x}) \exp\left\{\boldsymbol{\phi}(\boldsymbol{\theta})^T \boldsymbol{u}(\boldsymbol{x}) + g(\boldsymbol{\phi}(\boldsymbol{\theta}))\right\}, \tag{5.31}$$

where $\boldsymbol{\theta}$ is the set of parameters defining the density, $c(\boldsymbol{x})$ and $g(\boldsymbol{\phi}(\boldsymbol{\theta}))$ are known functions, $\boldsymbol{\phi}(\boldsymbol{\theta})$ is the vector of natural parameters, and $\boldsymbol{u}(\boldsymbol{x})$ is the natural statistics vector. The natural statistics vector, $\boldsymbol{u}(\boldsymbol{x})$, contains enough information to fully characterize $\boldsymbol{x}$ in the exponential density of

interest, and $\phi(\theta)$ scales the entries of $u(x)$ according to the parameter set θ. For a given parameter set θ, $\phi(\theta)$ is constant, and thus it is sufficient to specify either θ or $\phi(\theta)$ in order to define the parameters of the general exponential density.

To illustrate the parameters of an exponential family density, consider the Gaussian density, as defined by Eq. (3.4), which can be expressed in the form of Eq. (5.31) by choosing

$$\theta = \{m \ \ P\} \tag{5.32a}$$

$$c(x) = 1 \tag{5.32b}$$

$$\phi^T(\theta)u(x) = m^T P^{-1} x - \tfrac{1}{2} x^T P^{-1} x \tag{5.32c}$$

$$g(\phi(\theta)) = -\tfrac{1}{2} \ln \det \{2\pi P\} - \tfrac{1}{2} m^T P^{-1} m \,. \tag{5.32d}$$

The vectors $\phi(\theta)$ and $u(x)$ can be found according to Eq. (5.32c) through vector-matrix manipulation and reorganization. It can be observed from Eq. (5.32c) that the natural statistics vector for the Gaussian density contains the first- and second-order monomials in x_i, where $x \triangleq [x_1 \ x_2 \ \cdots \ x_{n_x}]^T$, and is given by

$$u(x) = \begin{bmatrix} x_1 & x_2 & \cdots & x_{n_x} & x_1^2 & x_1 x_2 & \cdots & x_1 x_{n_x} & x_2^2 & x_2 x_3 & \cdots & x_2 x_{n_x} & \cdots & x_{n_x}^2 \end{bmatrix}^T \,.$$

The vector of natural parameters, $\phi(\theta)$, is then defined as the appropriate coefficients corresponding to the entries of $u(x)$ according to Eq. (5.32c). For a given parameter set $\theta = \{m \ \ P\}$, $\phi(\theta)$ is a constant vector; thus, it is sufficient to specify either the parameter set $\theta = \{m \ \ P\}$ or $\phi(\theta)$ in order to define the Gaussian density. Typically, the parameter set $\theta = \{m \ \ P\}$ is specified directly for the Gaussian density since it provides more direct insight into the Gaussian density; however, for some members of the exponential family density, it is more convenient to work with $\phi(\theta)$ directly.

It is well known [58, 59, 60, 61] that the mean and covariance of the Gaussian density that minimize the KL divergence with respect to an arbitrary density are defined by the mean and covariance of the arbitrary density. This result can be derived directly, or, equivalently, a condition can be derived for the exponential family state density and then specialized to the Gaussian density, as it is here and in References [58] and [59].

Theorem 1. *The KL divergence of an exponential family state density with respect to a known state density is minimized when the expected value of the natural statistics vector of the exponential family state density is equivalent for both the exponential family state density and known state density; that is,*

$$\mathrm{E}_{p_e(x;\theta)}\{u(x)\} = \mathrm{E}_{p(x)}\{u(x)\} \,. \tag{5.33}$$

Proof. The KL divergence of $p_e(\boldsymbol{x}; \boldsymbol{\theta})$ with respect to the known state density $p(\boldsymbol{x})$ is given by

$$J = D_{KL}[p\|p_e] = \int p(\boldsymbol{x}) \ln \frac{p(\boldsymbol{x})}{p_e(\boldsymbol{x}; \boldsymbol{\theta})} \, d\boldsymbol{x} \,. \tag{5.34}$$

Necessary and sufficient conditions to minimize J are given by the first and second derivative conditions

$$\left[\frac{\partial J}{\partial \phi(\boldsymbol{\theta})} \right]^T = \boldsymbol{0} \quad \text{and} \quad \frac{\partial^2 J}{\partial \phi(\boldsymbol{\theta})^2} = \frac{\partial}{\partial \phi(\boldsymbol{\theta})} \left[\frac{\partial J}{\partial \phi(\boldsymbol{\theta})} \right]^T > \boldsymbol{0} \,.$$

The differentiation is performed with respect to $\phi(\boldsymbol{\theta})$ instead of the parameter set $\boldsymbol{\theta}$ because it is equivalent to specify either $\phi(\boldsymbol{\theta})$ or $\boldsymbol{\theta}$ in order to define the general exponential density. For this application, it is more convenient to work with $\phi(\boldsymbol{\theta})$ directly.

Differentiating Eq. (5.34) with respect to $\phi(\boldsymbol{\theta})$, transposing the result, simplifying, and enforcing the first derivative condition yields

$$\left[\frac{\partial J}{\partial \phi(\boldsymbol{\theta})} \right]^T = - \int p(\boldsymbol{x}) \boldsymbol{u}(\boldsymbol{x}) \, d\boldsymbol{x} - \frac{\partial g(\phi(\boldsymbol{\theta}))}{\partial \phi(\boldsymbol{\theta})} = \boldsymbol{0} \,. \tag{5.35}$$

Because $p_e(\boldsymbol{x}; \boldsymbol{\theta})$ is a pdf, it must integrate to one according to

$$\int p_e(\boldsymbol{x}; \boldsymbol{\theta}) \, d\boldsymbol{x} = 1 \,. \tag{5.36}$$

Differentiating Eq. (5.36) with respect to $\phi(\boldsymbol{\theta})$ and simplifying yields

$$\frac{\partial}{\partial \phi(\boldsymbol{\theta})} \int p_e(\boldsymbol{x}; \boldsymbol{\theta}) \, d\boldsymbol{x} = \int p_e(\boldsymbol{x}; \boldsymbol{\theta}) \boldsymbol{u}(\boldsymbol{x}) \, d\boldsymbol{x} + \frac{\partial g(\phi(\boldsymbol{\theta}))}{\partial \phi(\boldsymbol{\theta})} = \boldsymbol{0} \,. \tag{5.37}$$

Combining Eqs. (5.35) and (5.37) yields

$$\int p_e(\boldsymbol{x}; \boldsymbol{\theta}) \boldsymbol{u}(\boldsymbol{x}) \, d\boldsymbol{x} = \int p(\boldsymbol{x}) \boldsymbol{u}(\boldsymbol{x}) \, d\boldsymbol{x} \,,$$

which can be expressed with the expected value operator defined in Eq. (3.5) as

$$\mathrm{E}_{p_e(\boldsymbol{x}; \boldsymbol{\theta})} \{ \boldsymbol{u}(\boldsymbol{x}) \} = \mathrm{E}_{p(\boldsymbol{x})} \{ \boldsymbol{u}(\boldsymbol{x}) \} \,. \tag{5.38}$$

Equation (5.38) provides the necessary condition to minimize the KL divergence of an exponential family state density, $p_e(\boldsymbol{x}; \boldsymbol{\theta})$, with respect to the known state density, $p(\boldsymbol{x})$.

In order to ensure that Eq. (5.38) minimizes Eq. (5.34), the second derivative condition must be verified. Equation (5.35) is differentiated with respect to $\phi(\boldsymbol{\theta})$ and simplified to yield an

equivalent condition to the second derivative condition, which is given by

$$\frac{\partial^2 g(\boldsymbol{\phi}(\boldsymbol{\theta}))}{\partial \boldsymbol{\phi}(\boldsymbol{\theta})^2} < \mathbf{0} \,. \tag{5.39}$$

Equations (5.31) and (5.36) can be used to solve for $g(\boldsymbol{\phi}(\boldsymbol{\theta}))$ as

$$g(\boldsymbol{\phi}(\boldsymbol{\theta})) = -\ln \int c(\boldsymbol{x}) \exp \boldsymbol{\phi}^T(\boldsymbol{\theta}) \boldsymbol{u}(\boldsymbol{x}) \, \mathrm{d}\boldsymbol{x} \,. \tag{5.40}$$

Differentiating Eq. (5.40) with respect to $\boldsymbol{\phi}(\boldsymbol{\theta})$ and simplifying yields

$$\frac{\partial g(\boldsymbol{\phi}(\boldsymbol{\theta}))}{\partial \boldsymbol{\phi}(\boldsymbol{\theta})} = -\mathrm{E}_{p_e(\boldsymbol{x};\boldsymbol{\theta})}\{\boldsymbol{u}^T(\boldsymbol{x})\} \triangleq -\hat{\boldsymbol{u}}^T \,. \tag{5.41}$$

Differentiating the transpose of Eq. (5.41) with respect to $\boldsymbol{\phi}(\boldsymbol{\theta})$ and simplifying yields

$$\frac{\partial^2 g(\boldsymbol{\phi}(\boldsymbol{\theta}))}{\partial \boldsymbol{\phi}(\boldsymbol{\theta})^2} = -\mathrm{E}_{p_e(\boldsymbol{x};\boldsymbol{\theta})}\{(\boldsymbol{u}(\boldsymbol{x}) - \hat{\boldsymbol{u}})(\boldsymbol{u}(\boldsymbol{x}) - \hat{\boldsymbol{u}})^T\} < \mathbf{0} \,. \tag{5.42}$$

The inequality in Eq. (5.42) stems from the fact that $\mathrm{E}_{p_e(\boldsymbol{x};\boldsymbol{\theta})}\{(\boldsymbol{u}(\boldsymbol{x}) - \hat{\boldsymbol{u}})(\boldsymbol{u}(\boldsymbol{x}) - \hat{\boldsymbol{u}})^T\}$ is the covariance matrix of $\boldsymbol{u}(\boldsymbol{x})$ with respect to $p_e(\boldsymbol{x};\boldsymbol{\theta})$; thus, it is positive definite, and the second derivative condition is met for all $g(\boldsymbol{\phi}(\boldsymbol{\theta}))$ and Eq. (5.38) minimizes Eq. (5.34). $\qquad\square$

Corollary 1.1. *The Gaussian state density is a member of the exponential family of state densities with its natural statistics vector defined by the first- and second-order monomials in the entries of* $\boldsymbol{x}$*; therefore, the expected value of the natural statistics vector defines the first and second moments of the Gaussian state density. Exploiting Theorem 1, the KL divergence of the Gaussian state density with respect to a known state density is minimized when the first and second moments of the Gaussian state density and the known state density are equivalent. These first and second moments are defined by*

$$\boldsymbol{m} = \mathrm{E}_{p(\boldsymbol{x})}\{\boldsymbol{x}\} \quad \text{and} \quad \boldsymbol{M} = \mathrm{E}_{p(\boldsymbol{x})}\{\boldsymbol{x}\boldsymbol{x}^T\}$$

respectively. The second central moment (covariance) is used along with the first moment to parameterize the Gaussian state density and is defined by the first and second moments of the state density according to

$$\boldsymbol{P} = \boldsymbol{M} - \boldsymbol{m}\boldsymbol{m}^T = \mathrm{E}_{p(\boldsymbol{x})}\{(\boldsymbol{x} - \boldsymbol{m})(\boldsymbol{x} - \boldsymbol{m})^T\} \,.$$

Corollary 1.1 shows that the Gaussian density that best fits a given density in the KL sense is defined by the first and second moments of the given density. This is a useful result because, as long

as the first and second moments of the given density can be found, the best Gaussian approximation of the given density in terms of minimizing the KL divergence is defined by the Gaussian density with these moments.

5.5.2. The Minimum Divergence Filter. The minimum divergence filter (MDF) quantifies the prior and posterior parameter sets of an assumed density, defined as $\boldsymbol{\theta}_k^-$ and $\boldsymbol{\theta}_k^+$, respectively, that minimize the KL divergence of the assumed density from the true state density at each step in the Bayesian recursion. Let the prior and posterior assumed densities at t_k be denoted by $q(\boldsymbol{x}_k; \boldsymbol{\theta}_k^-)$ and $q(\boldsymbol{x}_k; \boldsymbol{\theta}_k^+)$, respectively. Assume that the posterior parameter set is known at an initial time t_0 and is given by $\boldsymbol{\theta}_0^+$. The predictor of the MDF is given by

$$p(\boldsymbol{x}_k|\boldsymbol{z}_{1:k-1}) = \int p(\boldsymbol{x}_k|\boldsymbol{x}_{k-1})q(\boldsymbol{x}_{k-1}; \boldsymbol{\theta}_{k-1}^+)\, \mathrm{d}\boldsymbol{x}_{k-1} \tag{5.43a}$$

$$\boldsymbol{\theta}_k^- = \operatorname*{argmin}_{\boldsymbol{\theta}} \int p(\boldsymbol{x}_k|\boldsymbol{z}_{1:k-1}) \ln \frac{p(\boldsymbol{x}_k|\boldsymbol{z}_{1:k-1})}{q(\boldsymbol{x}_k; \boldsymbol{\theta})}\, \mathrm{d}\boldsymbol{x}_k, \tag{5.43b}$$

where Eq. (5.43a) is a specialization of Eq. (5.1) and quantities the temporal evolution of the posterior assumed density at t_{k-1} to the prior true density at t_k given the transition density from t_{k-1} to t_k. Equation (5.43b) then defines the parameter set, $\boldsymbol{\theta}_k^-$, of the prior assumed density at t_k that minimizes the KL divergence from the prior true density, as defined by the Chapman-Kolmogorov equation.

Similarly, the corrector of the MDF is given by

$$p(\boldsymbol{x}_k|\boldsymbol{z}_{1:k}) = \frac{p(\boldsymbol{z}_k|\boldsymbol{x}_k, \boldsymbol{z}_{1:k-1})q(\boldsymbol{x}_k; \boldsymbol{\theta}_k^-)}{\int p(\boldsymbol{z}_k|\boldsymbol{\xi}, \boldsymbol{z}_{1:k-1})q(\boldsymbol{\xi}; \boldsymbol{\theta}_k^-)\, \mathrm{d}\boldsymbol{\xi}} \tag{5.44a}$$

$$\boldsymbol{\theta}_k^+ = \operatorname*{argmin}_{\boldsymbol{\theta}} \int p(\boldsymbol{x}_k|\boldsymbol{z}_{1:k}) \ln \frac{p(\boldsymbol{x}_k|\boldsymbol{z}_{1:k})}{q(\boldsymbol{x}_k; \boldsymbol{\theta})}\, \mathrm{d}\boldsymbol{x}_k, \tag{5.44b}$$

where Eq. (5.44a) is a specialization of Eq. (5.2) and updates the prior assumed density to the posterior true density upon receiving a measurement at t_k given the measurement likelihood. Equation (5.44b) then finds the parameter set, $\boldsymbol{\theta}_k^+$, of the posterior assumed density at t_k that minimizes the KL divergence from the posterior true density, which is defined by Bayes' rule.

The MDF, as defined by Eqs. (5.43) and (5.44), makes no restriction that the state and measurement vector exist in Euclidean space, as the Kalman filter does. The only requirements to implement the MDF are that the integration and minimization can be performed to find $\boldsymbol{\theta}_k^-$ and $\boldsymbol{\theta}_k^+$. Ideally, this minimization and integration would be performed analytically; however, this is only possible if further restrictions are imposed on the assumed state density, system dynamics, and measurement model. If the minimization and integration to find $\boldsymbol{\theta}_k^-$ and $\boldsymbol{\theta}_k^+$ cannot be performed analytically for the assumed state density, system dynamics, and/or measurement model, numerical methods can potentially be used to perform this integration and/or minimization.

No linear update structure is required for the MDF as is done for the Kalman framework. Because the MDF approximates the true state density by an assumed density, it quantifies the parameters of the assumed density that best fit the assumed density to the true density according to the KL divergence. While some error is incurred in approximating the true density by the assumed density, the assumed density approach provides a tractable solution for the approximate Bayesian filter. The error incurred by the assumed density can accumulate over time and lead to potentially poor performance of the MDF. If the MDF is performing poorly due to this error, state density flattening, which is a type of memory limiting operation that is related to the injection of process noise into the dynamic system, can be implemented in order to improve its performance [62].

5.5.3. The Gaussian Mixture Minimum Divergence Filter. Consider the application of the MDF to the case when an assumed GM density is used to approximate the true state density at each step in the Bayesian recursion. The dynamical system and measurement model under consideration are taken to be nonlinear with additive, Gaussian-distributed noise, as given by Eq. (4.3). In this application, the MDF is not applied directly to the find the parameters of the assumed GM density; it is instead applied on a component-wise basis to find the KL divergence optimal mean and covariance of each component of the assumed GM density from the true evolution of the component. The MDF is applied in this manner for computational tractability. If the MDF were employed directly to find the parameters of the assumed GM density (instead of on a component-wise basis as it is applied), one of two outcomes would occur, depending on if the number of components in the assumed GM density is fixed or is included as a parameter to minimize the KL divergence. If the number of components in the assumed GM density is not fixed, the number of components in the mixture will approach infinity since a larger number of components allows for a better approximation of the true density. If the number of components in the assumed GM density is fixed, it is still necessary to find the weight, mean, and covariance of each component numerically, because the GM density is not an exponential family density and, thus, Theorem 1 cannot be used. Because of this, the computational expense to directly find the parameters of the assumed GM density is intractably high, in general, and thus a component-wise application of the MDF is employed instead. Because the MDF is applied in a component-wise manner, the resulting assumed GM density approximating the true density is not KL divergence optimal in general; however, this application minimizes the KL divergence on a component-wise basis and results in a computationally tractable filter.

Let the initial GM density be defined by

$$\sum_{\ell=1}^{L_0^+} w_0^{(\ell)+} p_g\Big(\boldsymbol{x}_0; \boldsymbol{m}_0^{(\ell)+}, \boldsymbol{P}_0^{(\ell)+}\Big),$$

which has temporal evolution given by Eq. (5.20) for a nonlinear dynamical system with additive, Gaussian-distributed noise. This true predicted density in Eq. (5.20) is now approximated by a GM

density according to

$$\sum_{\ell=1}^{L_k^-} w_k^{(\ell)-} p_g\left(\boldsymbol{x}_k; \boldsymbol{m}_k^{(\ell)-}, \boldsymbol{P}_k^{(\ell)-}\right) \tag{5.45}$$

$$\approx \sum_{\ell=1}^{L_{k-1}^+} w_{k-1}^{(\ell)+} \int p_g(\boldsymbol{x}_k; \boldsymbol{f}(\boldsymbol{x}_{k-1}), \boldsymbol{Q}_{k-1}) p_g\left(\boldsymbol{x}_{k-1}; \boldsymbol{m}_{k-1}^{(\ell)+}, \boldsymbol{P}_{k-1}^{(\ell)+}\right) \mathrm{d}\boldsymbol{x}_{k-1}\,,$$

where it is necessary to find the parameters of the assumed GM density, $w_k^{(\ell)-}$, $\boldsymbol{m}_k^{(\ell)-}$, and $\boldsymbol{P}_k^{(\ell)-}$ for $\ell = 1, 2, \ldots, L_k^-$. These parameters are found on a component-wise basis according to

$$w_k^{(\ell)-} p_g\left(\boldsymbol{x}_k; \boldsymbol{m}_k^{(\ell)-}, \boldsymbol{P}_k^{(\ell)-}\right) \tag{5.46}$$

$$\approx w_{k-1}^{(\ell)+} \int p_g(\boldsymbol{x}_k; \boldsymbol{f}(\boldsymbol{x}_{k-1}), \boldsymbol{Q}_{k-1}) p_g\left(\boldsymbol{x}_{k-1}; \boldsymbol{m}_{k-1}^{(\ell)+}, \boldsymbol{P}_{k-1}^{(\ell)+}\right) \mathrm{d}\boldsymbol{x}_{k-1}\,,$$

for $\ell = 1, 2, \ldots, L_k^-$. This dictates that the number of components in the mixture remains the same in the predictor of the GMMDF; that is $L_k^- = L_{k-1}^+$. In order to obtain the weight update of the predictor, the zeroth moments of both sides of Eq. (5.46) are matched, which yields

$$w_k^{(\ell)-} = w_{k-1}^{(\ell)+}\,, \tag{5.47}$$

for $\ell = 1, 2, \ldots, L_k^-$. Equation (5.47) is substituted into Eq. (5.46) to yield the necessary approximation of each component of the prior GM density according to

$$p_g\left(\boldsymbol{x}_k; \boldsymbol{m}_k^{(\ell)-}, \boldsymbol{P}_k^{(\ell)-}\right) \approx \int p_g(\boldsymbol{x}_k; \boldsymbol{f}(\boldsymbol{x}_{k-1}), \boldsymbol{Q}_{k-1}) p_g\left(\boldsymbol{x}_{k-1}; \boldsymbol{m}_{k-1}^{(\ell)+}, \boldsymbol{P}_{k-1}^{(\ell)+}\right) \mathrm{d}\boldsymbol{x}_{k-1}\,, \tag{5.48}$$

for $\ell = 1, 2, \ldots, L_k^-$. In order to find $\boldsymbol{m}_k^{(\ell)-}$ and $\boldsymbol{P}_k^{(\ell)-}$, the KL divergence of the right-hand side of Eq. (5.48) with respect to its left-hand side is minimized. Because the left-hand side of Eq. (5.48) is a Gaussian density, Corollary 1.1 is used to perform this minimization, which defines $\boldsymbol{m}_k^{(\ell)-}$ and $\boldsymbol{P}_k^{(\ell)-}$ as the mean and covariance of the right-hand side of Eq. (5.48), respectively, which are defined according to

$$\boldsymbol{m}_k^{(\ell)-} = \int \boldsymbol{x}_k \int p_g(\boldsymbol{x}_k; \boldsymbol{f}(\boldsymbol{x}_{k-1}), \boldsymbol{Q}_{k-1}) p_g(\boldsymbol{x}_{k-1}; \boldsymbol{m}_{k-1}^{(\ell)+}, \boldsymbol{P}_{k-1}^{(\ell)+}) \, \mathrm{d}\boldsymbol{x}_{k-1} \, \mathrm{d}\boldsymbol{x}_k$$

$$\boldsymbol{P}_k^{(\ell)-} = \int \boldsymbol{x}_k \boldsymbol{x}_k^T \int p_g(\boldsymbol{x}_k; \boldsymbol{f}(\boldsymbol{x}_{k-1}), \boldsymbol{Q}_{k-1}) p_g(\boldsymbol{x}_{k-1}; \boldsymbol{m}_{k-1}^{(\ell)+}, \boldsymbol{P}_{k-1}^{(\ell)+}) \, \mathrm{d}\boldsymbol{x}_{k-1} \, \mathrm{d}\boldsymbol{x}_k$$

$$- \boldsymbol{m}_k^{(\ell)-} \boldsymbol{m}_k^{(\ell)-T}\,.$$

Reversing the order of integration allows the prior mean and covariance to be expressed as expected values with respect to $p_g(\boldsymbol{x}_{k-1}; \boldsymbol{m}_{k-1}^{(\ell)+}, \boldsymbol{P}_{k-1}^{(\ell)+})$ according to

$$\boldsymbol{m}_k^{(\ell)-} = \mathrm{E}_{p_g(\boldsymbol{x}_{k-1}; \boldsymbol{m}_{k-1}^{(\ell)+}, \boldsymbol{P}_{k-1}^{(\ell)+})} \left\{ \int \boldsymbol{x}_k p_g(\boldsymbol{x}_k; \boldsymbol{f}(\boldsymbol{x}_{k-1}), \boldsymbol{Q}_{k-1}) \, \mathrm{d}\boldsymbol{x}_k \right\} \tag{5.50a}$$

$$\boldsymbol{P}_k^{(\ell)-} = \mathrm{E}_{p_g(\boldsymbol{x}_{k-1}; \boldsymbol{m}_{k-1}^{(\ell)+}, \boldsymbol{P}_{k-1}^{(\ell)+})} \left\{ \int \boldsymbol{x}_k \boldsymbol{x}_k^T p_g(\boldsymbol{x}_k; \boldsymbol{f}(\boldsymbol{x}_{k-1}), \boldsymbol{Q}_{k-1}) \, \mathrm{d}\boldsymbol{x}_k \right\}$$
$$- \boldsymbol{m}_k^{(\ell)-} \boldsymbol{m}_k^{(\ell)-T}. \tag{5.50b}$$

The integrals in the arguments of the expected values define the first and second moments of the Gaussian density $p_g(\boldsymbol{x}_k; \boldsymbol{f}(\boldsymbol{x}_{k-1}), \boldsymbol{Q}_{k-1})$; thus, the solution of the integrals are given by the first and second moments of $p_g(\boldsymbol{x}_k; \boldsymbol{f}(\boldsymbol{x}_{k-1}), \boldsymbol{Q}_{k-1})$ according to

$$\int \boldsymbol{x}_k p_g(\boldsymbol{x}_k; \boldsymbol{f}(\boldsymbol{x}_{k-1}), \boldsymbol{Q}_{k-1}) \, \mathrm{d}\boldsymbol{x}_k = \boldsymbol{f}(\boldsymbol{x}_{k-1}) \tag{5.51a}$$

$$\int \boldsymbol{x}_k \boldsymbol{x}_k^T p_g(\boldsymbol{x}_k; \boldsymbol{f}(\boldsymbol{x}_{k-1}), \boldsymbol{Q}_{k-1}) \, \mathrm{d}\boldsymbol{x}_k = \boldsymbol{f}(\boldsymbol{x}_{k-1}) \boldsymbol{f}(\boldsymbol{x}_{k-1})^T + \boldsymbol{Q}_{k-1}. \tag{5.51b}$$

Substituting Eqs. (5.51) into Eqs. (5.50) and simplifying yields the predictor of the MDF in terms of expected values with respect to ℓ^{th} component of the the posterior GM density as

$$\boldsymbol{m}_k^{(\ell)-} = \mathrm{E}_{p_g(\boldsymbol{x}_{k-1}; \boldsymbol{m}_{k-1}^{(\ell)+}, \boldsymbol{P}_{k-1}^{(\ell)+})} \{ \boldsymbol{f}(\boldsymbol{x}_{k-1}) \} \tag{5.52a}$$

$$\boldsymbol{P}_k^{(\ell)-} = \mathrm{E}_{p_g(\boldsymbol{x}_{k-1}; \boldsymbol{m}_{k-1}^{(\ell)+}, \boldsymbol{P}_{k-1}^{(\ell)+})} \{ (\boldsymbol{f}(\boldsymbol{x}_{k-1}) - \boldsymbol{m}_k^{(\ell)-})(\boldsymbol{f}(\boldsymbol{x}_{k-1}) - \boldsymbol{m}_k^{(\ell)-})^T \} + \boldsymbol{Q}_{k-1}, \tag{5.52b}$$

for $\ell = 1, 2, \ldots, L_k^-$. These expected values are identical to the expected values defining the predictor of the Kalman framework, as defined by Eq. (4.7), under the further condition that the expectation is taken with respect to $p_g(\boldsymbol{x}_{k-1}; \boldsymbol{m}_{k-1}^{(\ell)+}, \boldsymbol{P}_{k-1}^{(\ell)+})$, instead of the unquantified state density like the Kalman framework. Note that Eqs. (4.7) and (5.52) are slightly different because Eq. (4.7) is expressed for the most general dynamical system, as defined by Eq. (4.1a) or Eq. (4.2a), and Eq. (5.52) is expressed for a nonlinear dynamical system with additive process noise, as defined by Eq. (4.3a). If the nonlinear dynamical system with additive process noise is substituted into Eq. (4.7) and it is simplified, it will take the identical form as Eq. (5.52), without the condition that the expected value is calculated with respect to a Gaussian density. Similarly to the Kalman framework, the expected values in Eqs. (5.52) can be approximated using several methods, including linearization like is done in the EKF, or quadrature methods like is done in the UKF and QKF. Note that the EKF, UKF, and QKF are derived under the linear MMSE framework, and the GMMDF is derived under the Bayesian framework; however, the approximation of the expected values present under both frameworks can be performed in the same way.

The true measurement evolution of the prior GM density for a nonlinear measurement model with additive, Gaussian-distributed noise is given by Eq. (5.23). This true corrected density is now approximated by a GM density according to

$$\sum_{\ell=1}^{L_k^+} w_k^{(\ell)+} p_g\left(\boldsymbol{x}_k; \boldsymbol{m}_k^{(\ell)+}, \boldsymbol{P}_k^{(\ell)+}\right) \tag{5.53}$$

$$\approx \frac{\sum_{\ell=1}^{L_k^-} w_k^{(\ell)-} p_g(\boldsymbol{z}_k; \boldsymbol{h}(\boldsymbol{x}_k), \boldsymbol{R}_k) p_g\left(\boldsymbol{x}_k; \boldsymbol{m}_k^{(\ell)-}, \boldsymbol{P}_k^{(\ell)-}\right)}{\sum_{\ell=1}^{L_k^-} w_k^{(\ell)-} \int p_g(\boldsymbol{z}_k; \boldsymbol{h}(\boldsymbol{x}_k), \boldsymbol{R}_k) p_g\left(\boldsymbol{x}_k; \boldsymbol{m}_k^{(\ell)-}, \boldsymbol{P}_k^{(\ell)-}\right) \mathrm{d}\boldsymbol{x}_k} .$$

The denominator of Eq. (5.53) is now manipulated according to

$$\sum_{\ell=1}^{L_k^-} w_k^{(\ell)-} \int p_g(\boldsymbol{z}_k; \boldsymbol{h}(\boldsymbol{x}_k), \boldsymbol{R}_k) p_g\left(\boldsymbol{x}_k; \boldsymbol{m}_k^{(\ell)-}, \boldsymbol{P}_k^{(\ell)-}\right) \mathrm{d}\boldsymbol{x}_k = \sum_{\ell=1}^{L_k^-} w_k^{(\ell)-} k_k^{(\ell)} , \tag{5.54}$$

where $k_k^{(\ell)}$ is a constant which is defined by

$$k_k^{(\ell)} \triangleq \mathrm{E}_{p_g(\boldsymbol{x}_k; \boldsymbol{m}_k^{(\ell)-}, \boldsymbol{P}_k^{(\ell)-})}\left\{p_g(\boldsymbol{z}_k; \boldsymbol{h}(\boldsymbol{x}_k), \boldsymbol{R}_k)\right\} ,$$

which quantifies the likelihood that the measurement $\boldsymbol{z}_k$ originated from the ℓth component of the GM density. Equation (5.54) is now substituted into Eq. (5.53) and the result is manipulated to yield

$$\sum_{\ell=1}^{L_k^+} w_k^{(\ell)+} p_g\left(\boldsymbol{x}_k; \boldsymbol{m}_k^{(\ell)+}, \boldsymbol{P}_k^{(\ell)+}\right) \tag{5.55}$$

$$\approx \sum_{\ell=1}^{L_k^-} \frac{w_k^{(\ell)-}}{\sum_{j=1}^{L_k^-} w_k^{(j)-} k_k^{(j)}} \, p_g(\boldsymbol{z}_k; \boldsymbol{h}(\boldsymbol{x}_k), \boldsymbol{R}_k) p_g\left(\boldsymbol{x}_k; \boldsymbol{m}_k^{(\ell)-}, \boldsymbol{P}_k^{(\ell)-}\right) ,$$

where it is necessary to find the parameters of the assumed GM density, $w_k^{(\ell)+}$, $\boldsymbol{m}_k^{(\ell)+}$, and $\boldsymbol{P}_k^{(\ell)+}$ for $\ell = 1, 2, \ldots, L_k^+$. These parameters are found on a component-wise basis according to

$$w_k^{(\ell)+} p_g\left(\boldsymbol{x}_k; \boldsymbol{m}_k^{(\ell)+}, \boldsymbol{P}_k^{(\ell)+}\right) \approx \frac{w_k^{(\ell)-}}{\sum_{j=1}^{L_k^-} w_k^{(j)-} k_k^{(j)}} \, p_g(\boldsymbol{z}_k; \boldsymbol{h}(\boldsymbol{x}_k), \boldsymbol{R}_k) p_g\left(\boldsymbol{x}_k; \boldsymbol{m}_k^{(\ell)-}, \boldsymbol{P}_k^{(\ell)-}\right) ,$$

$$\tag{5.56}$$

for $\ell = 1, 2, \ldots, L_k^+$. This dictates that the number of components in the mixture remains the same in the corrector of the GMMDF; that is $L_k^+ = L_k^-$. In order to obtain the weight update of the

corrector, the zeroth moments of both sides of Eq. (5.56) are matched, which yields

$$
\begin{aligned}
w_k^{(\ell)+} &= \frac{w_k^{(\ell)-}}{\sum_{j=1}^{L_k^-} w_k^{(j)-} k_k^{(j)}} \int p_g(\boldsymbol{z}_k; \boldsymbol{h}(\boldsymbol{x}_k), \boldsymbol{R}_k) p_g\left(\boldsymbol{x}_k; \boldsymbol{m}_k^{(\ell)-}, \boldsymbol{P}_k^{(\ell)-}\right) \mathrm{d}\boldsymbol{x}_k \\
&= \frac{w_k^{(\ell)-}}{\sum_{j=1}^{L_k^-} w_k^{(j)-} k_k^{(j)}} \mathrm{E}_{p_g(\boldsymbol{x}_k; \boldsymbol{m}_k^{(\ell)-}, \boldsymbol{P}_k^{(\ell)-})}\{p_g(\boldsymbol{z}_k; \boldsymbol{h}(\boldsymbol{x}_k), \boldsymbol{R}_k)\} \\
&= \frac{w_k^{(\ell)-} k_k^{(\ell)}}{\sum_{j=1}^{L_k^-} w_k^{(j)-} k_k^{(j)}} .
\end{aligned}
\tag{5.57}
$$

for $\ell = 1, 2, \ldots, L_k^+$. This weight update is observed to be identical to that of the GMKF, GMEKF, and the quadrature-based GM Kalman filters (with the caveat that $k_k^{(\ell)}$ is approximated differently), which updates the weight of each component according to the relative likelihood that the measurement originated from each component. Equation (5.57) is substituted into Eq. (5.56) to yield the necessary approximation of each component of the posterior GM density according to

$$
p_g\left(\boldsymbol{x}_k; \boldsymbol{m}_k^{(\ell)+}, \boldsymbol{P}_k^{(\ell)+}\right) \approx \frac{1}{k_k^{(\ell)}} p_g(\boldsymbol{z}_k; \boldsymbol{h}(\boldsymbol{x}_k), \boldsymbol{R}_k) p_g\left(\boldsymbol{x}_k; \boldsymbol{m}_k^{(\ell)-}, \boldsymbol{P}_k^{(\ell)-}\right),
\tag{5.58}
$$

In order to find $\boldsymbol{m}_k^{(\ell)+}$ and $\boldsymbol{P}_k^{(\ell)+}$, the KL divergence of the right-hand side of Eq. (5.58) with respect to its left-hand side is minimized. Because the left-hand side of Eq. (5.58) is a Gaussian density, Corollary 1.1 is used to perform this minimization, which defines $\boldsymbol{m}_k^{(\ell)+}$ and $\boldsymbol{P}_k^{(\ell)+}$ as the mean and covariance of the right-hand side of Eq. (5.58), respectively, which are defined according to

$$
\begin{aligned}
\boldsymbol{m}_k^{(\ell)+} &= \frac{1}{k_k^{(\ell)}} \int \boldsymbol{x}_k p_g(\boldsymbol{z}_k; \boldsymbol{h}(\boldsymbol{x}_k), \boldsymbol{R}_k) p_g\left(\boldsymbol{x}_k; \boldsymbol{m}_k^{(\ell)-}, \boldsymbol{P}_k^{(\ell)-}\right) \mathrm{d}\boldsymbol{x}_k \\
\boldsymbol{P}_k^{(\ell)+} &= \frac{1}{k_k^{(\ell)}} \int \boldsymbol{x}_k \boldsymbol{x}_k^T p_g(\boldsymbol{z}_k; \boldsymbol{h}(\boldsymbol{x}_k), \boldsymbol{R}_k) p_g\left(\boldsymbol{x}_k; \boldsymbol{m}_k^{(\ell)-}, \boldsymbol{P}_k^{(\ell)-}\right) \mathrm{d}\boldsymbol{x}_k - \boldsymbol{m}_k^{(\ell)-} \boldsymbol{m}_k^{(\ell)-T},
\end{aligned}
$$

which are expressed as expected values with respect to the ℓth component of the prior GM density according to

$$
\boldsymbol{m}_k^{(\ell)+} = \frac{1}{k_k^{(\ell)}} \mathrm{E}_{p_g(\boldsymbol{x}_k; \boldsymbol{m}_k^{(\ell)-}, \boldsymbol{P}_k^{(\ell)-})}\{\boldsymbol{x}_k p_g(\boldsymbol{z}_k; \boldsymbol{h}(\boldsymbol{x}_k), \boldsymbol{R}_k)\}
\tag{5.60a}
$$

$$
\boldsymbol{P}_k^{(\ell)+} = \frac{1}{k_k^{(\ell)}} \mathrm{E}_{p_g(\boldsymbol{x}_k; \boldsymbol{m}_k^{(\ell)-}, \boldsymbol{P}_k^{(\ell)-})}\{(\boldsymbol{x}_k - \boldsymbol{m}_k^{(\ell)-})(\boldsymbol{x}_k - \boldsymbol{m}_k^{(\ell)-})^T p_g(\boldsymbol{z}_k; \boldsymbol{h}(\boldsymbol{x}_k), \boldsymbol{R}_k)\}, \tag{5.60b}
$$

for $\ell = 1, 2, \ldots, L_k^+$. In order to approximate the expected values in Eq. (5.60), quadrature techniques are employed. When approximating these expected values, special care must be taken if

the measurement noise is small. As the measurement noise becomes small, a higher-order polynomial becomes necessary to approximate $p_g(\boldsymbol{z}_k; \boldsymbol{h}(\boldsymbol{x}_k), \boldsymbol{R}_k)$ without incurring significant error. Since Gauss-Hermite quadrature is exact for polynomials of degree $2q - 1$, where q is the number of points used in the quadrature rule, more quadrature points must be used to approximate these expected values in this case. Progressive Gaussian filtering [60, 63, 64] can be used to reduce the quadrature order required to achieve sufficient accuracy by progressively introducing the measurement information into the posterior density; however, this approach requires the density to be assumed Gaussian at each iteration in introducing the measurement information. Progressive Gaussian filtering exchanges error due to quadrature for error due to the assumed Gaussian density. In some cases, this exchange in error sources is prudent and can provide improved results.

Observation of the GMMDF, with the predictor defined by Eqs. (5.47) and (5.52), and the corrector defined by Eqs. (5.57) and (5.60), shows that the predictor of the GMMDF is identical to the GMEKF, GMUKF, and GMQKF, depending on the type of approximation used to approximate the expected values in Eq. (5.52). The corrector of the GMMDF, however, is different from that of the GMEKF, GMUKF, and GMQKF because it approximates the mean and covariance of each component of the GM density by evaluating the moments of Bayes' rule, which is constructed using the prior component of the GM density, instead of performing the Kalman-like update to each component. The weight update used in the correctors of the GMMDF and the GMEKF, GMUKF, and GMQKF are similar in that they update the weights of the GM density according to the relative likelihood that the measurement originated from each component; however, the relative likelihood is approximated differently between the different filters. Because the corrector of the GMMDF is different from the correctors of the GMEKF, GMUKF, and GMQKF, they are now applied to the *lensing problem* in order to compare and contrast them. In order to simplify the comparison such that meaningful conclusions can be made, a single component GM density, which is simply a Gaussian density, is considered. Because of this, the GMMDF, GMEKF, GMUKF, and GMQKF reduce to the MDF, Bayesian EKF, Bayesian UKF, and Bayesian QKF, respectively.

The lensing problem occurs when the uncertainty in the position of an object has a relatively large uncertainty with respect to the uncertainty of a range measurement taken from a nearby observer. The shape of the resulting true posterior density resembles an optical lens (hence the name *lensing* problem), which may not be well-approximated by a Gaussian density. In this case, the objective is not to capture the lens shape, which is the ultimate objective of the lensing problem, but to accurately capture the first and second moments of the lens. The lensing problem is illustrated in Figure (5.1). In this example, the mean position of the object is $\boldsymbol{m} = \begin{bmatrix} 2 & 0 \end{bmatrix}^T$ meters and the observer is at the origin. A range measurement of 2 meters from the observer to the object is taken and is assumed to be corrupted by additive zero-mean Gaussian noise of standard deviation 0.1 meters. Two Gaussian prior densities for the initial position, one with relatively large uncertainty and

one with relatively small uncertainty, are considered and are shown in Figures. (5.1a) and (5.1b), respectively. The resulting true posterior density for both prior densities, which is defined by Bayes' rule and computed by a grid-based approach, is also shown in Figures. (5.1a) and (5.1b).

When the uncertainty in the prior position density is relatively large with respect to the uncertainty in the range measurement, as it is in Figure (5.1a), the posterior density is highly-skewed and thus is not well-approximated by a Gaussian density. When the uncertainty in the prior position density is relatively small with respect to the uncertainty in the range measurement, as shown in Figure (5.1b), the posterior density is not highly-skewed and can be well-approximated by a Gaussian density.

The corrector of the MDF, as well as the corrector of the Bayesian EKF and Bayesian QKF, are applied to both scenarios to evaluate their performance. Gauss-Hermite quadrature with 1000 points per dimension is used to evaluate the expected values associated with the corrector of the MDF and the Bayesian QKF in order to ensure that the approximation error of the quadrature is negligible and the filters can be compared equally. The posterior assumed Gaussian densities quantified by the corrector of each filter are shown in Figures. (5.1c) and (5.1d).

Before proceeding with analysis of the lensing problem, it is important to consider a property of the Bayesian UKF and Bayesian QKF; these filters are an extension to the Bayesian EKF, in which the evolution of the mean and covariance of the Gaussian density is observed to be identical to that of the EKF (as derived under the linear MMSE framework). Because of this, the UKF and QKF equations (as derived under the linear MMSE framework) are used to quantify the evolution of the mean and covariance as originally quantified by the Bayesian EKF, in which case the Bayesian UKF and Bayesian QKF are born. These filters have *not* been shown to be well-principled; that is, they do not stem directly from the Chapman-Kolmogorov equation and Bayes' rule. Because of this, the Bayesian UKF and Bayesian QKF are restricted to perform a linear measurement update, as is inherent to the *linear* MMSE framework. For the Bayesian EKF, this linear update is shown to stem from Bayes' rule; however, since the Bayesian UKF and Bayesian QKF do not stem directly from Bayes' rule, and rather from the linear MMSE framework, their linear measurement update may not be representative of the true posterior as defined by Bayes' rule. Rather, the Bayesian UKF and Bayesian QKF aim to more accurately capture the evolution of the mean and covariance of the Gaussian density than the Bayesian EKF.

The Bayesian EKF provides a very different posterior density than the MDF and Bayesian QKF when the uncertainty in the prior position density is relatively large with respect to the uncertainty in the range measurement, as it is in Figure (5.1c). In this case, the posterior density of the Bayesian EKF reflects an overconfidence in a poor state estimate due to the linearization error incurred in processing the nonlinear range measurement. The posterior densities of the MDF and the Bayesian QKF are very similar; however, the linear gain measurement update of the Bayesian QKF
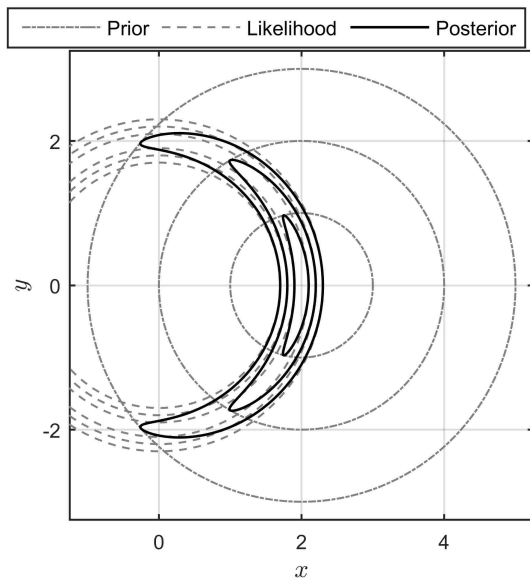
(a) Prior Gaussian density with "large" uncertainty, with the measurement likelihood and true posterior densities.
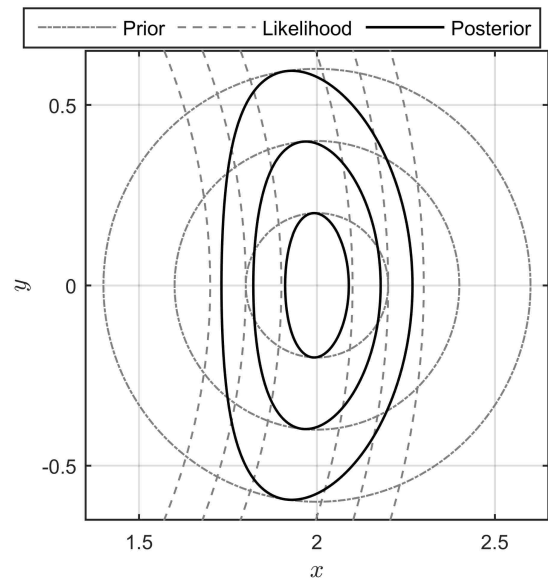
(b) Prior Gaussian density with "small" uncertainty, with the measurement likelihood and true posterior densities.
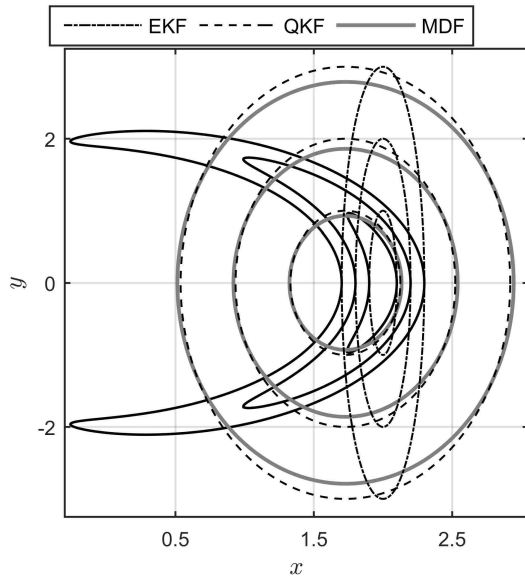
(c) Posterior densities for the prior Gaussian density with "large" uncertainty.
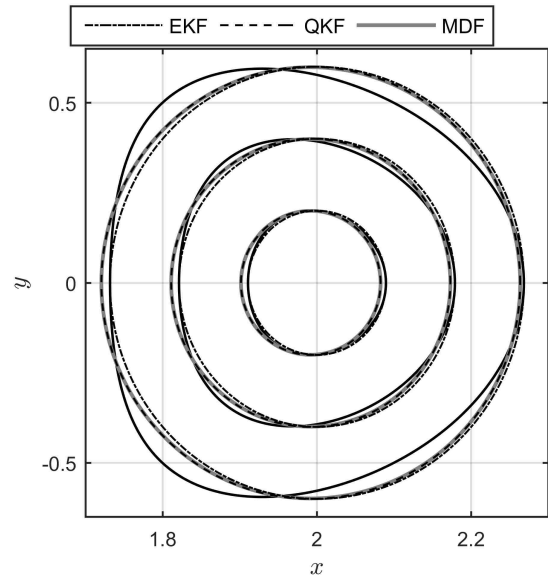
(d) Posterior densities for the prior Gaussian density with "small" uncertainty.

Figure 5.1. Prior, measurement likelihood, and true posterior densities for the lensing problem.

does not allow it to incorporate any of the information gained due to the skewness of the true posterior density. Since the MDF employs a nonlinear update, it is able to incorporate this information. This can be observed by comparing the posterior densities of the MDF and the Bayesian QKF. The two posterior densities are nearly identical in the range (x) direction, but the posterior density of the MDF possesses smaller uncertainty in the y direction since it is the minimum divergence Gaussian density with respect to the skewed true posterior density.

The MDF, Bayesian QKF, and Bayesian EKF all provide very similar posterior densities when the uncertainty in the prior position density is relatively small with respect to the uncertainty in the range measurement, as it is in Figure (5.1d). This is an expected result since the true posterior density can be well-approximated as Gaussian in this case. Furthermore, it is postulated that the correctors of the MDF, EKF, and QKF become identical as the uncertainty in the prior Gaussian density approaches zero. This postulation stems from the fact that the error incurred by the linearization approximation used by the Bayesian EKF, the linear measurement update used by the Bayesian QKF, and the minimum divergence update used by the MDF approaches zero as the uncertainty in the prior Gaussian density goes to zero. This implies that, if a GM density with sufficiently small uncertainty in each component is used instead of a Gaussian density, that the GMMDF, GMEKF, GMUKF, and GMQKF will perform very similarly.

The mean square error of the MDF can be smaller than that of the Bayesian QKF, as can be observed in Figure (5.1c). At first, this may seem counterintuitive because the corrector used under the Kalman filter framework is derived to minimize the mean square error; however, the corrector used under the Kalman filter framework is derived by assuming the posterior mean to be a linear combination of the prior mean and measurement; thus, it minimizes the *linear* mean square error. By employing a nonlinear update, the MDF is able to capture more information from the update and the posterior density possesses a smaller mean square error than does the Bayesian QKF.

6. UNCERTAINTY PROPAGATION WITH THE GAUSS-BINGHAM DENSITY

Consider the Gauss-Bingham-distributed state vector that consists of the attitude quaternion and other Euclidean states, as defined by Eq. (3.49). Ideally, the temporal and measurement evolution of the Gauss-Bingham density would be quantified, either exactly or approximately, under the Bayesian framework. Quantifying this evolution, even approximately, is difficult due to the form of the Gauss-Bingham density, which does not belong to the general exponential family, and, thus, if the MDF is specialized to the Gauss-Bingham density, Theorem 1 cannot be used to perform the associated minimization. Because of this, the MDF specialized to the Gauss-Bingham density is computationally intractable. Theoretically, the MDF specialized to the Gauss-Bingham density can be implemented numerically, which would yield the approximate Bayesian filter; however, this is not performed in lieu of the BGM filter, which does not require numerical optimization, and is presented in Section 7. Instead, an uncertainty propagation strategy is developed for the Gauss-Bingham-distributed state vector [65] that parallels the predictor of the UKF, under the further assumption that the state density is Gaussian-distributed.

In order to propagate the uncertainty of a given Gauss-Bingham-distributed state vector, an unscented transform is used that generates a set of sigma points representing the initial Gauss-Bingham density. These sigma points are then transformed according to the (potentially) nonlinear dynamical system, and the weighted maximum log-likelihood parameters of the Gauss-Bingham density are found. This process of uncertainty propagation is shown to be identical to that of the predictor of the UKF, under the further assumption that the resulting state density is Gaussian-distributed, as is shown in Appendix E.

Assume that discrete-time nonlinear system dynamics are given for the most general nonlinear dynamical system defined by Eq. (4.1a), or equivalently, Eq. (4.2a). Because of the antipodal property of the attitude quaternion, these system dynamics must satisfy

$$
\begin{bmatrix} \bar{q}_k \\ \mathbf{x}_k \end{bmatrix} = \tilde{f}\left(\begin{bmatrix} \bar{q}_{k-1} \\ \mathbf{x}_{k-1} \\ w_{k-1} \end{bmatrix}\right) \quad \text{and} \quad \begin{bmatrix} -\bar{q}_k \\ \mathbf{x}_k \end{bmatrix} = \tilde{f}\left(\begin{bmatrix} -\bar{q}_{k-1} \\ \mathbf{x}_{k-1} \\ w_{k-1} \end{bmatrix}\right), \tag{6.1}
$$

which shows that the quaternion portion of the state vector remains antipodal through the transformation through the dynamical system. Equation (6.1) defines an important property of the system dynamics, $\tilde{f}$. This property states that the system dynamics preserve the antipodal symmetry of the quaternion, which is exploited to reduce the amount of computation necessary to propagate the sigma points representing the Gauss-Bingham density.

In order to simplify the development of the uncertainty propagation scheme, the dynamical system is assumed not to have process noise. When process noise is not present in the state vector, the dynamical system property given in Eq. (6.1) simplifies to

$$\begin{bmatrix} \bar{q}_k \\ \mathbf{x}_k \end{bmatrix} = f\left(\begin{bmatrix} \bar{q}_{k-1} \\ \mathbf{x}_{k-1} \end{bmatrix}\right) \qquad \text{and} \qquad \begin{bmatrix} -\bar{q}_k \\ \mathbf{x}_k \end{bmatrix} = f\left(\begin{bmatrix} -\bar{q}_{k-1} \\ \mathbf{x}_{k-1} \end{bmatrix}\right), \qquad (6.2)$$

which is observed to be the dynamical system defined in Eq. (4.3a) without the inclusion of process noise, as expected. If desired, it is straightforward to extend the presented uncertainty propagation scheme to include Gaussian-distributed process noise by appending it to the Gaussian-distributed portion of the state vector, $\mathbf{x}_{k-1}$.

6.1. UNSCENTED TRANSFORM

In order to select a set of weights and locations for the sigma points of the unscented transform for the canonical Gauss-Bingham density, the zeroth, first, and second moments between the canonical Gauss-Bingham density and the sigma points are matched in $\mathbb{R}^r \times \mathbb{R}^{s+1}$. The moments will be matched in $\mathbb{R}^r \times \mathbb{R}^{s+1}$; however, the sigma points will be parameterized such that they remain on the manifold $\mathbb{R}^r \times \mathbb{S}^s$. After finding sigma points for the canonical Gauss-Bingham density, Eq. (3.54) is then used to convert the locations of the sigma points from the canonical Gauss-Bingham to the given Gauss-Bingham density.

In order to reduce the number of sigma points, only one of each pair of antipodal sigma points is considered and propagated since the system dynamics preserve the antipodal symmetry of the sigma points as shown by Eq. (6.1). To illustrate this concept, consider the following example antipodal sigma points in $\mathbb{R}^1 \times \mathbb{S}^1$ at t_{k-1}, $\mathcal{X}_{k-1}$ and $\mathcal{X}^*_{k-1}$, that are antipodal in $\bar{q}$ and given by

$$\mathcal{X}_{k-1} = \begin{bmatrix} \frac{1}{\sqrt{2}} & \frac{-1}{\sqrt{2}} & 3 \end{bmatrix}^T \qquad \text{and} \qquad \mathcal{X}^*_{k-1} = \begin{bmatrix} \frac{-1}{\sqrt{2}} & \frac{1}{\sqrt{2}} & 3 \end{bmatrix}^T.$$

These sigma points are propagated by some (potentially) nonlinear function, f, that satisfies the property given by Eq. (6.2). Assume that this propagation transforms the sigma points to

$$\mathcal{X}_k = \begin{bmatrix} 0 & 1 & 4 \end{bmatrix}^T \qquad \text{and} \qquad \mathcal{X}^*_k = \begin{bmatrix} 0 & -1 & 4 \end{bmatrix}^T,$$

which are still antipodal in $\bar{q}$; thus, the computational expense can be lowered by considering only $\mathcal{X}_{k-1}$. $\mathcal{X}_{k-1}$ is transformed according to f to obtain $\mathcal{X}_k$, and antipodal symmetry can be used to obtain $\mathcal{X}^*_k$, if desired.

In order to generate the sigma points for the Gauss-Bingham density, motivation is drawn from the $2n + 1$ unscented transform [43]. The $2n + 1$ unscented transform for the canonical Gaussian density places two sigma points at equal but opposite deviations from zero for each of the $n = r$ canonical Gaussian states. A central sigma point is then placed at the origin. When generating sigma points for the canonical Gauss-Bingham density, which considers only one of each pair of antipodal points in the attitude quaternion, a similar approach to that of the $2n + 1$ unscented transform for the canonical Gaussian density is used.

In order to generate the sigma points for the canonical Gauss-Bingham density, first a set of sigma points that quantify deviations from the origin in each state of $\mathbf{z}$ (the portion of the state vector that is canonical Gaussian-distributed) are introduced as $\pm\delta$ while $\bar{p}$ (the portion of the state that is canonical Bingham-distributed) is held constant as the identity quaternion. The locations of these $2r$ sigma points are given by

$$
\boldsymbol{\mathcal{Z}}^{(1),(2)} = \big[\, \overbrace{0 \;\cdots\; 0\; 1}^{\in \mathbb{S}^s} \; \overbrace{\pm\delta\; 0 \;\cdots\; 0}^{\in \mathbb{R}^r} \,\big]^T
$$
$$
\boldsymbol{\mathcal{Z}}^{(3),(4)} = \big[\, 0 \;\cdots\; 0\; 1\; 0 \pm \delta \;\cdots\; 0 \,\big]^T
$$
$$
\vdots
$$
$$
\boldsymbol{\mathcal{Z}}^{(2r-1),(2r)} = \big[\, 0 \;\cdots\; 0\; 1\; 0 \;\cdots\; 0 \pm \delta \,\big]^T,
$$

with corresponding weights given by

$$
w^{(1),(2)} = w^{(3),(4)} = \cdots = w^{(2r-1),(2r)} = \frac{w_g}{4r},
$$

where $\boldsymbol{\mathcal{Z}}^{(i),(j)}$ and $w^{(i),(j)}$ represent the locations and weights of the ith and j^{th} sigma points, respectively, representing the canonical Gauss-Bingham density and w_g is a parameter used to specify the weights of these sigma points. The braces are used to denote the portions of $\boldsymbol{\mathcal{Z}}$ which are the Euclidean and quaternion states.

Next, angular deviations are introduced into the quaternion state as $\pm\alpha_\ell$ for $\ell = 1, 2, \ldots, s$ while $\mathbf{z}$ is held constant at zero in order to guarantee that the perturbed attitude quaternion remains on the unit hypersphere. These $2s$ sigma points are given by

$$
\boldsymbol{\mathcal{Z}}^{(2r+1),(2r+2)} = \big[\, \overbrace{\pm S_{\alpha_1}\; 0 \;\cdots\; 0\; C_{\alpha_1}}^{\in \mathbb{S}^s} \; \overbrace{0 \cdots 0}^{\in \mathbb{R}^r} \,\big]^T
$$
$$
\boldsymbol{\mathcal{Z}}^{(2r+3),(2r+4)} = \big[\, 0 \pm S_{\alpha_2} \;\cdots\; 0\; C_{\alpha_2}\; 0 \cdots 0 \,\big]^T
$$
$$
\vdots
$$
$$
\boldsymbol{\mathcal{Z}}^{(2r+2s-1),(2r+2s)} = \big[\, 0 \;\cdots\; 0 \pm S_{\alpha_s}\; C_{\alpha_s}\; 0 \cdots 0 \,\big]^T,
$$

with corresponding weights given by

$$w^{(2r+1),(2r+2)} = \frac{w_{b_1}}{4}$$

$$w^{(2r+3),(2r+4)} = \frac{w_{b_2}}{4}$$

$$\vdots$$

$$w^{(2r+2s-1),(2r+2s)} = \frac{w_{b_s}}{4} \, ,$$

where w_{b_ℓ}, for $\ell = 1, 2, \ldots, s$, are parameters used to specify the weights of these sigma points and S_α and C_α represent the sine and cosine of α, respectively.

Finally, a central sigma point is placed at $\mathbf{z} = \mathbf{0}$ and in the "zero" direction of $\bar{p}$, which is the identity quaternion. This single sigma point is given by

$$\boldsymbol{\mathcal{Z}}^{(N)} = \left[\overbrace{0 \ \cdots \ 0 \ 1}^{\in \mathbb{S}^s} \ \overbrace{0 \ \cdots \ 0}^{\in \mathbb{R}^r} \right]^T ,$$

with corresponding weight given by

$$w^{(N)} = \frac{w_c}{2} \, ,$$

where w_c is a parameter used to specify the weight of this sigma point and $N = 2r + 2s + 1$ is the total number of sigma points.

In order to find the parameters δ, α_ℓ, w_c, w_g, and w_{b_ℓ}, where $\ell = 1, 2, \ldots, s$, which fully define the weights and locations of the sigma points for the canonical Gauss-Bingham density, the zeroth, first, and second moments between the sigma points and the canonical Gauss-Bingham density are matched in $\mathbb{R}^{s+1} \times \mathbb{R}^r$. The zeroth and first moments of the canonical Gauss-Bingham are 1 and $\mathbf{0}$, respectively. The second moment of the canonical Gauss-Bingham density is given by Eq. (3.22). While only one of each antipodal pair of sigma points is stored and propagated, it is important to note that both of the antipodal sigma points, which are equally weighted, are considered when calculating the moments of the sigma points. After accounting for the antipodal symmetry of each of the sigma points, the first moment of the sigma points is zero for any choice of the parameters. Matching the zeroth and second moments of the sigma points with the canonical Gauss-Bingham density yields

$$\sum_{\ell=1}^{s} w_{b_\ell} + w_c + w_g = 1 \tag{6.3a}$$

$$\frac{\delta^2 w_g}{r} = 1 \tag{6.3b}$$

$$w_{b_\ell} \sin^2 \alpha_\ell = f_\ell \,, \quad \ell = 1, 2, \ldots, s \tag{6.3c}$$

$$\sum_{\ell=1}^{s} w_{b_\ell} \cos^2 \alpha_\ell + w_c + w_g = f_{s+1} \,, \tag{6.3d}$$

where Eq. (6.3a) stems from the zeroth moment and Eqs. (6.3b)–(6.3d) stem from the second moment. Summing Eq. (6.3c) for $\ell = 1$, 2, ... , s and Eq. (6.3d) while noting the properties in Eqs. (3.24) yields Eq. (6.3a); thus, Eq. (6.3d) is redundant and may be neglected. Solving Eqs. (6.3b) and (6.3c) for δ and α_ℓ gives the locations of the sigma points as a function of their weights as

$$\delta = \sqrt{\frac{r}{w_g}} \quad \text{and} \quad \alpha_\ell = \text{asin}\sqrt{\frac{f_\ell}{w_{b_\ell}}} \,, \quad \ell = 1, 2, \ldots, s \,. \tag{6.4}$$

Now, the weights must be selected for the sigma points. In order for Eqs. (6.4) to have real solutions, w_{b_ℓ} must be greater than or equal to f_ℓ for all $\ell = 1$, 2, ... , s. In order to ensure that this condition is met, a somewhat nonintuitive choice for the weights of the sigma points for the canonical Gauss-Bingham density is chosen that parallels the choice of weights of the sigma points for the Bingham density presented in [12]. Noting the properties given in Eqs. (3.24), the weights of the sigma points representing the Gauss-Bingham density which satisfy Eq. (6.3a) are chosen as

$$w_{b_\ell} = f_\ell + (1 - \lambda - \kappa)\frac{f_{s+1}}{s} \,, \quad \ell = 1, 2, \ldots, s \tag{6.5a}$$

$$w_c = \lambda f_{s+1} \tag{6.5b}$$

$$w_g = \kappa f_{s+1} \,, \tag{6.5c}$$

where λ and κ are positive tuning parameters such that $\lambda + \kappa < 1$. While choosing the weights according to Eqs. (6.5) is nonintuitive, this choice of weights satisfies Eq. (6.3a) and provides real locations for the sigma points. λ and κ are chosen such that the weights of all the sigma points approach an equal weight of $1/N$ as the uncertainty in the states corresponding to $\bar{q}$ approaches zero; that is, $Z_1, Z_2, \ldots, Z_s \to -\infty$. This choice of weights ensures that the sigma points possess nearly equal weights, and thus have nearly equal importance, when the uncertainty in the attitude quaternion is small. Using the properties in Eqs. (3.24), the λ and κ that yield equal weights for the sigma points as the uncertainty in the quaternion goes to zero are given by

$$\lambda = \frac{1}{N} \quad \text{and} \quad \kappa = \frac{2r}{N} \,. \tag{6.6}$$

The sigma points for the canonical Gauss-Bingham density, which are defined in terms of the parameters in Eqs. (6.4), (6.5), and (6.6), are transformed from the canonical Gauss-Bingham density to

the Gauss-Bingham density of interest defined by $p_{gb}(\boldsymbol{x}; \boldsymbol{m}, \boldsymbol{P}, \boldsymbol{\phi}_0, \boldsymbol{\beta}, \boldsymbol{Z})$ according to Eqs. (3.54). These transformed sigma points and their associated weights representing the Gauss-Bingham density at t_{k-1} are denoted by $\boldsymbol{\mathcal{X}}_{k-1}^{(i)}$ and $w_{k-1}^{(i)}$, respectively, where $i = 1, 2, \ldots, N$. These sigma points are then transformed according to the nonlinear system dynamics given by Eq. (6.2) to obtain the sigma points and weights representing the Gauss-Bingham density at t_k, denoted by $\boldsymbol{\mathcal{X}}_k$ and $w_k^{(i)}$, respectively, where $i = 1, 2, \ldots, N$ and the weights are unchanged in the transformation; that is, $w_k^{(i)} = w_{k-1}^{(i)}$. If the dynamical system is governed by continuous-time dynamics, the nonlinear discrete-time function in Eq. (6.2), $\boldsymbol{f}$, is given by the integration of $\boldsymbol{\mathcal{X}}_{k-1}$ from t_{k-1} to t_k to obtain $\boldsymbol{\mathcal{X}}_k$.

6.2. MAXIMUM WEIGHTED LOG-LIKELIHOOD GAUSS-BINGHAM PARAMETERS

To obtain the parameters of the best-fit Gauss-Bingham density given the set of sigma points and weights at t_k, the parameters of the Gauss-Bingham density that maximize the weighted log-likelihood of the sigma points are found. To illustrate why the maximum weighted log-likelihood parameters are sought, consider the case when the unscented transform is used for a state that exists in $\mathbb{R}^r$. Given the sigma points and weights from the unscented transform, the mean and covariance are recovered from the weighted sample mean and covariance of the sigma points. It is shown in Appendix E that the weighted sample mean and covariance of the sigma points is the mean and covariance of the Gaussian density that maximizes the weighted log-likelihood of the sigma points.

In this spirit, the parameters of the Gauss-Bingham density are recovered from the sigma points according to

$$\{\boldsymbol{m}_k, \boldsymbol{P}_k, \boldsymbol{\phi}_{0,k}, \boldsymbol{\beta}_k, \boldsymbol{Z}_k\} = \tag{6.7}$$

$$\operatorname*{argmax}_{\boldsymbol{m}, \boldsymbol{P}, \boldsymbol{\phi}_0, \boldsymbol{\beta}, \boldsymbol{Z}} \sum_{i=1}^{N} w_k^{(i)} \ln p_{gb}\left(\boldsymbol{\mathcal{X}}_k^{(i)}; \boldsymbol{m}, \boldsymbol{P}, \boldsymbol{\phi}_0, \boldsymbol{\beta}, \boldsymbol{Z}\right),$$

This maximization can be performed analytically for the mean and covariance of the Gaussian density, $\boldsymbol{m}$ and $\boldsymbol{P}$, as is shown in Appendix F. First, note that the sigma points can be decomposed into their Euclidean and quaternion portions according to $\boldsymbol{\mathcal{X}}_k = [\boldsymbol{\mathcal{X}}_{\mathbf{x},k}^T \ \boldsymbol{\mathcal{X}}_{\bar{\boldsymbol{q}},k}^T]^T$. The mean and covariance of the Gaussian density that maximizes the weighted log-likelihood of the sigma points is given by the sample mean and covariance of the Euclidean portion of the sigma points according to

$$\boldsymbol{m}_k = 2\sum_{i=1}^{N} w_k^{(i)} \boldsymbol{\mathcal{X}}_{\mathbf{x},k}^{(i)} \tag{6.8a}$$

$$\boldsymbol{P}_k = 2 \sum_{i=1}^{N} w_k^{(i)} \left(\boldsymbol{\mathcal{X}}_{\mathbf{x},k}^{(i)} - \boldsymbol{m}_k \right) \left(\boldsymbol{\mathcal{X}}_{\mathbf{x},k}^{(i)} - \boldsymbol{m}_k \right)^T , \tag{6.8b}$$

where the factor of two is included since only one of each antipodal pair of sigma points in the quaternion state is quantified.

After using Eq. (6.8) to determine $\boldsymbol{m}_k$ and $\boldsymbol{P}_k$, Eq. (6.7) becomes

$$\{\boldsymbol{\phi}_{0,k}, \boldsymbol{\beta}_k, \boldsymbol{Z}_k\} = \operatorname*{argmax}_{\boldsymbol{\phi}_0, \boldsymbol{\beta}, \boldsymbol{Z}} J(\boldsymbol{\phi}_0, \boldsymbol{\beta}, \boldsymbol{Z}) , \tag{6.9}$$

where

$$J(\boldsymbol{\phi}_0, \boldsymbol{\beta}, \boldsymbol{Z}) = \sum_{i=1}^{N} w_k^{(i)} \ln p_{gb} \left(\boldsymbol{\mathcal{X}}_k^{(i)}; \boldsymbol{m}_k, \boldsymbol{P}_k, \boldsymbol{\phi}_0, \boldsymbol{\beta}, \boldsymbol{Z} \right) .$$

This maximization is carried out numerically to find $\boldsymbol{\phi}_0$, $\boldsymbol{\beta}$, and $\boldsymbol{Z}$. In order to perform this numerical maximization, it is first transformed into a root-finding problem according to the first derivative conditions of a maximum, i.e.

$$\frac{\partial J(\boldsymbol{\phi}_{0,k}, \boldsymbol{\beta}_k, \boldsymbol{Z}_k)}{\partial \boldsymbol{\phi}_{0,k}} = \mathbf{0} \tag{6.10a}$$

$$\frac{\partial J(\boldsymbol{\phi}_{0,k}, \boldsymbol{\beta}_k, \boldsymbol{Z}_k)}{\partial \boldsymbol{\beta}_k} = \mathbf{0} \tag{6.10b}$$

$$\frac{\partial J(\boldsymbol{\phi}_{0,k}, \boldsymbol{\beta}_k, \boldsymbol{Z}_k)}{\partial \boldsymbol{Z}_k} = \mathbf{0} , \tag{6.10c}$$

where the explicit expressions for the derivatives are included in Appendix F. A root-finding algorithm is used to find the $\boldsymbol{\phi}_{0,k}$, $\boldsymbol{\beta}_k$, and $\boldsymbol{Z}_k$ that satisfy Eqs. (6.10). To initialize the root-finding algorithm, $\boldsymbol{\phi}_{0,k-1}$, $\boldsymbol{\beta}_{k-1}$, and $\boldsymbol{Z}_{k-1}$ are used. By initializing the root-finding algorithm in this way, if the propagation time step is chosen sufficiently small, $\boldsymbol{\phi}_{0,k-1}$, $\boldsymbol{\beta}_{k-1}$, and $\boldsymbol{Z}_{k-1}$ remain close to the local maximum, and a gradient-based root-finding algorithm will converge to $\boldsymbol{\phi}_{0,k}$, $\boldsymbol{\beta}_k$, and $\boldsymbol{Z}_k$ without excessive iteration required or risk of diverging to a different root.

A number of root-finding algorithms can be used to find the $\boldsymbol{\phi}_{0,k}$, $\boldsymbol{\beta}_k$, and $\boldsymbol{Z}_k$ that satisfy Eqs. (6.10). The Levenberg–Marquardt algorithm, a well-known optimizer, is chosen to find these $\boldsymbol{\phi}_{0,k}$, $\boldsymbol{\beta}_k$, and $\boldsymbol{Z}_k$ [66, 67]. This algorithm is used to find the roots of an arbitrary system of equations defined by $\boldsymbol{g}(\boldsymbol{x}) = \mathbf{0}$ by minimizing the cost function $\boldsymbol{g}(\boldsymbol{x})^T \boldsymbol{g}(\boldsymbol{x})$ using $\boldsymbol{x}$ as the minimization variable. The Levenberg–Marquardt algorithm was chosen to find $\boldsymbol{\phi}_{0,k}$, $\boldsymbol{\beta}_k$, and $\boldsymbol{Z}_k$ because the cost function will remain near the minimum if the time step is chosen sufficiently small and $\boldsymbol{\phi}_{0,k-1}$, $\boldsymbol{\beta}_{k-1}$, and $\boldsymbol{Z}_{k-1}$ are used to initialize the algorithm. Applying the Levenberg–Marquardt

algorithm in this manner to find the roots of Eqs. (6.10) was found to be more computationally efficient than applying it to the optimization problem in Eq. (6.9) directly. In summary, the algorithm used to propagate the Gauss-Bingham density is given by Algorithm 6.1.

Algorithm 6.1 Uncertainty Propagation of the Gauss-Bingham density.

- Given:

    - A Gauss-Bingham-distributed state vector at t_0, which is defined by the parameters $\boldsymbol{m}_0$, $\boldsymbol{P}_0$, $\boldsymbol{\phi}_{0,0}$, $\boldsymbol{\beta}_0$, $\boldsymbol{Z}_0$.
    - System dynamics that preserve the antipodal symmetry of the quaternion as defined by the property given by Eq. (6.2).
    - A sequence of times to which to propagate the Gauss-Bingham density, t_1, t_2, ..., t_f.

1. Generate the sigma points and weights according to $p_{gb}(\boldsymbol{x}; \boldsymbol{m}_0, \boldsymbol{P}_0, \boldsymbol{\phi}_{0,0}, \boldsymbol{\beta}_0, \boldsymbol{Z}_0)$.

2. Set the time counter to $k = 1$

3. Propagate the sigma points from t_{k-1} to t_k according to the given system dynamics.

4. Recover $\boldsymbol{m}_k$ and $\boldsymbol{P}_k$ according to Eqs. (6.8).

5. Recover $\boldsymbol{\phi}_{0,k}$, $\boldsymbol{\beta}_k$, and $\boldsymbol{Z}_k$ according to the root-finding problem defined by Eq. (6.10) using $\boldsymbol{\phi}_{0,k-1}$, $\boldsymbol{\beta}_{k-1}$, and $\boldsymbol{Z}_{k-1}$ to initialize the root-finding algorithm.

6. If $t_k = t_f$, stop; if $t_k < t_f$, set $k = k + 1$ and return to step 3.

The sequence of times to which to propagate the Gauss-Bingham density, t_1, t_2, ..., t_f, should be chosen such that the time step is small enough that $\boldsymbol{\phi}_{0,k-1}$, $\boldsymbol{\beta}_{k-1}$, and $\boldsymbol{Z}_{k-1}$ are close to $\boldsymbol{\phi}_{0,k}$, $\boldsymbol{\beta}_k$, and $\boldsymbol{Z}_k$ in order to ensure that the root-finding algorithm converges to the proper solution for $\boldsymbol{\phi}_{0,k}$, $\boldsymbol{\beta}_k$, and $\boldsymbol{Z}_k$. The size of the time step is a compromise between computational cost and ensuring that the root-finding algorithm converges to the correct root. Because the sigma points are not resampled at each time step, no approximation error is introduced by choosing the time step too small. Since the time step chosen is problem dependent, no general guidelines for choosing this time step can be imposed.

6.3. DEMONSTRATIONS

Two demonstrations are performed to illustrate uncertainty propagation using the Gauss-Bingham density. The first demonstration propagates the uncertainty of the planar attitude and angular velocity of a body in $\mathbb{R}^1 \times \mathbb{S}^1$, where the Gauss-Bingham density can be visualized on the

unit cylinder. This demonstration provides an intuitive example of uncertainty propagation using the Gauss-Bingham density. The second demonstration propagates the uncertainty in the dynamic pose (position, velocity, attitude, and angular velocity) of a chase spacecraft with respect to a target spacecraft. This demonstration compares uncertainty propagation using the Gauss-Bingham density to the predictor of the multiplicative extended Kalman filter and a Monte Carlo approach in order to show the efficacy of uncertainty propagation using the Gauss-Bingham density.

6.3.1. Planar Attitude and Angular Velocity. Consider the attitude quaternion and angular velocity representing the one-dimensional attitude motion of a body undergoing rotation about the z-axis. In this case, the state vector of the body is defined by

$$\boldsymbol{x} = \begin{bmatrix} \bar{\boldsymbol{q}} \\ \omega \end{bmatrix} \in \mathbb{S}^1 \times \mathbb{R}^1 \,, \tag{6.11}$$

where $\bar{\boldsymbol{q}}$ represents the one-dimensional attitude quaternion and ω represents the one-dimensional angular velocity of the body. The angular velocity comprises the Gaussian-distributed portion of the state vector, with initial mean and covariance given by

$$\boldsymbol{m}_0 = 0 \quad \text{and} \quad \boldsymbol{P}_0 = (0.01\,°/s)^2 \,, \tag{6.12}$$

respectively. The attitude quaternion comprises the conditional Bingham-distributed portion of the state vector and is initially uncorrelated with the angular velocity (that is, $\boldsymbol{\beta}_0 = 0$). The parameters defining the orientation and concentration of the conditional Bingham-distributed portion of the state vector are given by

$$\boldsymbol{\phi}_0 = 0 \quad \text{and} \quad Z_{1,0} = -100 \,,$$

respectively. The Gauss-Bingham density representing the initial attitude quaternion and angular velocity of the body, as well as the sigma points generated by the unscented transform, are shown in Figure (6.1a). The marginalized density of the initial attitude quaternion is shown in Figure (6.1c).

The body undergoes torque-free motion, that is, $\boldsymbol{\tau}^B = 0$. The temporal evolution of the attitude quaternion and angular velocity are given by Eqs. (2.44) and (2.46), respectively. The uncertainty propagation algorithm summarized in Algorithm 6.1 is used to propagate the uncertainty of the attitude quaternion and angular velocity forward in time. A time step of one minute is used to propagate the uncertainty, which is small enough to ensure that the root-finding algorithm converges to the proper $\phi_{0,k}$, $\boldsymbol{\beta}_k$, and $\boldsymbol{Z}_k$ at each time step. Figure (6.1) shows the evolution of Gauss-Bingham density and sigma points representing the attitude quaternion and angular velocity of the body, as well as the marginalized density of the attitude quaternion over time. Table 6.1 provides the corresponding parameters of the Gauss-Bingham density over time. It is observed that the mean

Table 6.1. Gauss-Bingham parameters over time.

Time [hours]	m [$°/s$]	P [$(°/s)^2$]	ϕ_0	β	Z_1
0	0	$(0.01)^2$	0	0.0000	-100
0.25	0	$(0.01)^2$	0	0.0785	-100
1	0	$(0.01)^2$	0	0.3142	-100
6	0	$(0.01)^2$	0	1.8850	-100

and covariance of the angular velocity, m and P, respectively, remain constant, which is expected because the one-dimensional angular-velocity is constant under torque-free motion.

The concentration matrix of the conditional Bingham density, Z, remains constant (within numerical accuracy of the root finding algorithm). The mean direction of the Gauss-Bingham density, ϕ_0, remains at zero since the mean of the angular velocity is zero for all time; however the linear correlation parameter, β evolves in time in order to quantify the effect of the uncertain angular velocity on the attitude quaternion. It is interesting to note that β evolves linearly in time for this problem. The Gauss-Bingham density eventually wraps around its cylindrical manifold as it is propagated, which causes the attitude quaternion to become equiprobable as time increases, and is apparent in Figure (6.1h). This is an expected result for a body undergoing one-dimensional attitude motion with an uncertain angular velocity; as time increases, the uncertainty in the attitude quaternion of the body grows until the attitude quaternion becomes equiprobable.

Several important properties of the Gauss-Bingham density and its utility in uncertainty propagation can be observed in Figure (6.1). The Gauss-Bingham density is antipodally symmetric in the quaternion state for all time, which is a necessary property to properly quantify the uncertainty in the attitude quaternion. Because this example quantifies the one-dimensional attitude motion in $\mathbb{S}^1 \times \mathbb{R}^1$, $2n + 1 = 5$ sigma points, which are generated similarly to the traditional $2n + 1$ unscented transform and account for implied antipodal symmetry, are required to quantify the temporal evolution of the Gauss-Bingham density. The attitude quaternion becomes equiprobable as the uncertainty is propagated; however, the concentration parameter Z_1 does not approach zero. As the uncertainty is propagated, the attitude quaternion becomes equiprobable due to the wrapping of the Gauss-Bingham density around the cylinder, not because the concentration parameter approaches zero.

6.3.2. Spacecraft Relative Dynamic Pose. Now, consider an example in which a chase spacecraft is orbiting in close proximity to a target spacecraft. The state of the chase spacecraft is defined to be $[\boldsymbol{\omega}^T \ \delta\boldsymbol{r}^T \ \delta\boldsymbol{v}^T \ \bar{\boldsymbol{q}}^T]^T$, where $\bar{\boldsymbol{q}}$ and $\boldsymbol{\omega}$ represent the attitude quaternion and angular velocity of the chase spacecraft, respectively, and $\delta\boldsymbol{r}$ and $\delta\boldsymbol{v}$ represent the relative position and

(a) Initial state density

(b) State density at 15 minutes

(c) Initial quaternion density

(d) Quaternion density at 15 minutes

(e) State density at 1 hour

(f) State density at 6 hours

(g) Quaternion density at 1 hour

(h) Quaternion density at 6 hours
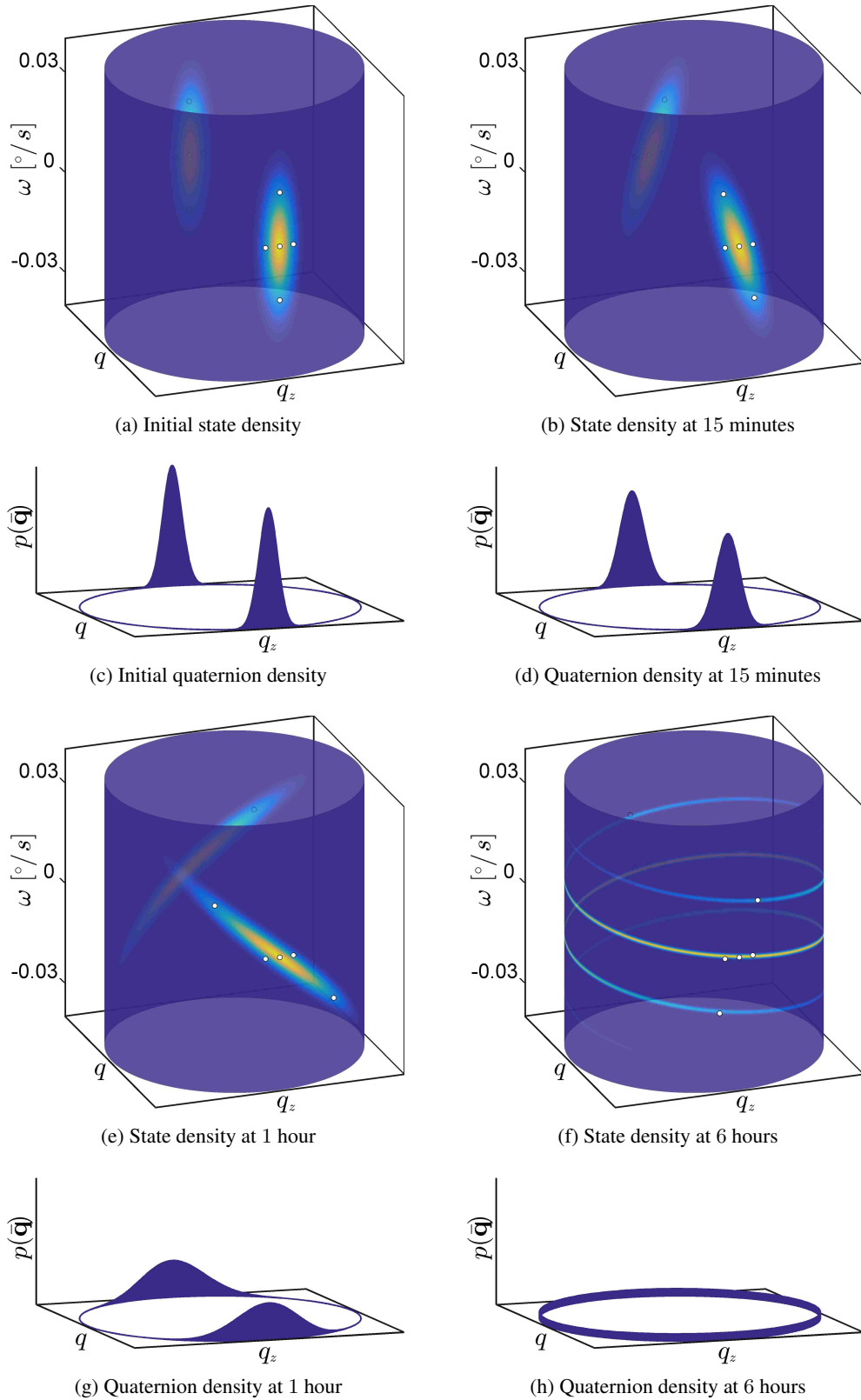
Figure 6.1. Gauss-Bingham uncertainty propagation for one-dimensional attitude motion.

velocity, respectively, of the chase spacecraft with respect to the target spacecraft. The chase space-craft is taken to have an identity inertia tensor and undergoes torque-free motion, with the temporal evolution of the attitude quaternion and angular velocity given by Eqs. (2.44) and (2.46), respectively. Because the body undergoes torque-free motion and has an identity inertia tensor, Eq. (2.46) shows that the angular velocity is constant in time.

In order to quantify the temporal evolution of the relative position and velocity, the Clohessy-Wiltshire equations are used [68, 69, 70]. The Clohessy-Wiltshire equations approximate the relative motion of the chase spacecraft with respect to the target spacecraft under the assumptions that the spacecraft are in close proximity and that the target spacecraft is in a circular orbit. If these assumptions are valid, the Clohessy-Wiltshire equations governing the temporal evolution of the relative position and velocity are

$$
\begin{bmatrix} \delta \dot{\boldsymbol{r}} \\ \delta \dot{\boldsymbol{v}} \end{bmatrix} = \begin{bmatrix} 0 & 0 & 0 & 1 & 0 & 0 \\ 0 & 0 & 0 & 0 & 1 & 0 \\ 0 & 0 & 0 & 0 & 0 & 1 \\ 3n^2 & 0 & 0 & 0 & 2n & 0 \\ 0 & 0 & 0 & -2n & 0 & 0 \\ 0 & 0 & -n^2 & 0 & 0 & 0 \end{bmatrix} \begin{bmatrix} \delta \boldsymbol{r} \\ \delta \boldsymbol{v} \end{bmatrix},
\tag{6.13}
$$

where n is the mean motion of the target spacecraft and $\delta \boldsymbol{r}$ and $\delta \boldsymbol{v}$ are expressed in a rotating coordinate frame with origin at the target spacecraft. The rotating coordinate frame is defined by the position and velocity vectors of the target spacecraft. The target spacecraft is taken to be in a geostationary orbit with an orbital radius of $42,164$ km, which results in a mean motion of the target spacecraft of 7.2920×10^{-5} rad/s.

The Gauss-Bingham density is used to quantify the uncertainty of the state vector of the chase spacecraft. The Gaussian portion of the Gauss-Bingham density quantifies the uncertainty of the angular velocity, relative position, and relative velocity, with initial mean and covariance given

by

$$\boldsymbol{m}_0 = \begin{bmatrix} 0.5\,\text{°/s} \\ 0.8\,\text{°/s} \\ 1.0\,\text{°/s} \\ 0 \\ 10\,\text{km} \\ 0 \\ 0 \\ 0 \\ 0 \end{bmatrix} \quad \text{and} \quad \boldsymbol{P}_0 = \text{diag} \begin{bmatrix} 0.1^2\,(\text{°/s})^2 \\ 0.1^2\,(\text{°/s})^2 \\ 0.1^2\,(\text{°/s})^2 \\ 1\,\text{m}^2 \\ 1\,\text{m}^2 \\ 1\,\text{m}^2 \\ 0.01^2\,(\text{m/s})^2 \\ 0.01^2\,(\text{m/s})^2 \\ 0.01^2\,(\text{m/s})^2 \end{bmatrix}, \tag{6.14}$$

respectively, where the diag $\boldsymbol{v}$ operator constructs a diagonal matrix with entires defined by the arbitrary vector $\boldsymbol{v}$. The attitude quaternion of the chase spacecraft comprises the conditional Bingham-distributed portion of the state vector, which is taken to be initially uncorrelated with the angular velocity, relative position, and relative velocity (that is, $\boldsymbol{\beta}_0 = \boldsymbol{0}$). The parameters defining the initial orientation and concentration of the conditional Bingham-distributed portion of the state vector are given by

$$\boldsymbol{\phi}_0 = \boldsymbol{0} \quad \text{and} \quad Z_{1,0} = Z_{2,0} = Z_{3,0} = -5000\,,$$

respectively.

The uncertainty propagation algorithm given in Algorithm 6.1 is used to propagate the uncertainty of the angular velocity, relative position, relative velocity, and attitude quaternion forward in time. A time step of fifteen seconds is used to propagate the uncertainty, which is small enough to ensure that the root-finding algorithm converges to the proper $\phi_{0,k}$, $\boldsymbol{\beta}_k$, and $\boldsymbol{Z}_k$ at each time step. Uncertainty propagation using the Gauss-Bingham density is compared to two other methods of uncertainty propagation to evaluate its efficacy: a Monte Carlo approach and the predictor step of the multiplicative extended Kalman filter (MEKF) [5, 33, 71]. 100,000 Monte Carlo samples are realized from the initial Gauss-Bingham density using an acceptance sampling method, and are propagated forward in time to quantitatively represent the true evolution of the initial Gauss-Bingham density.

The predictor step of the MEKF quantifies the "mean" using the attitude quaternion and relies on a small angle assumption to project the uncertainty in the attitude quaternion into a three-parameter attitude representation (the rotation vector is used in this analysis). Quotation marks are used around "mean" for the MEKF to indicate that it is not the mean as defined by the first moment of the state vector; rather, it is the "mean" quaternion as defined by one of the antipodal pair used

to quantify the quaternion estimate. In order to find the equivalent "mean" and covariance for the MEKF given the initial Gauss-Bingham density, it is first noted that "mean" attitude quaternion is the identity quaternion since $\phi_0 = \mathbf{0}$ and $\beta_0 = \mathbf{0}$; thus, the mean for the MEKF is given by the concatenation of the mean given in Eq. (6.14) and the identity quaternion. The equivalent covariance of the MEKF state vector, which is expressed using the rotation vector instead of the attitude quaternion, is found by converting the quaternion portion of the initial Monte Carlo samples to their equivalent rotation vector according to Eq. (2.40), and calculating their sample covariance.

Because the angular velocity, relative position, and relative velocity are initially Gaussian-distributed, evolve according to linear dynamics, and their temporal evolution is not a function of the attitude quaternion, they remain Gaussian-distributed for all time. Because of this, both the Gauss-Bingham and MEKF uncertainty propagation methods perfectly capture the evolution of the uncertainty in these states, which is presented in Figures (6.2)–(6.4) and shows the standard deviation of each component of these states quantified by both the MEKF and the Gauss-Bingham density over time. Furthermore, the mean of these quantities is constant for all time since their mean is a stationary solution to Eqs. (2.46) and (6.13) under torque-free motion with an identity inertia tensor. Figure (6.2) shows that the uncertainty of the angular velocity is constant, as expected because the angular velocity is constant. Figure (6.3) shows that the uncertainty in the relative position grows as time increases. Figure (6.4) shows that the uncertainty in the x- and y-components of the relative velocity increase, while the uncertainty in the z-component decreases. This decrease in uncertainty is expected due to the periodicity present in the Clohessy-Wiltshire equations. If the uncertainty is propagated for an entire orbit of the target spacecraft (approximately 24 hours), it would complete one cycle of its period.

Uncertainty propagation using the Gauss-Bingham density does not require that the system dynamics governing the Gaussian-distributed states be linear nor that their temporal evolution be functionally independent of the attitude quaternion. These conditions are used in this example to simplify the presentation and analysis of the results of the uncertainty propagation. If nonlinear system dynamics are used, or if the system dynamics are a function of the attitude quaternion, the best-fit Gaussian density that maximizes the weighted log-likelihood of the sigma points as defined by Eqs. (6.8) is found.

Because the attitude uncertainty quantified by the Gauss-Bingham density and Monte Carlo samples are expressed using the attitude quaternion and the uncertainty quantified by the MEKF predictor is expressed using the rotation vector, the uncertainty quantified by the Gauss-Bingham density and Monte Carlo samples are converted to rotation vector space in order to make a direct comparison. The rotation vector space is chosen for this comparison since it is a three-parameter representation of attitude. In order to convert the uncertainty quantified by the Gauss-Bingham density and Monte Carlo samples from the attitude quaternion representation to the rotation vector
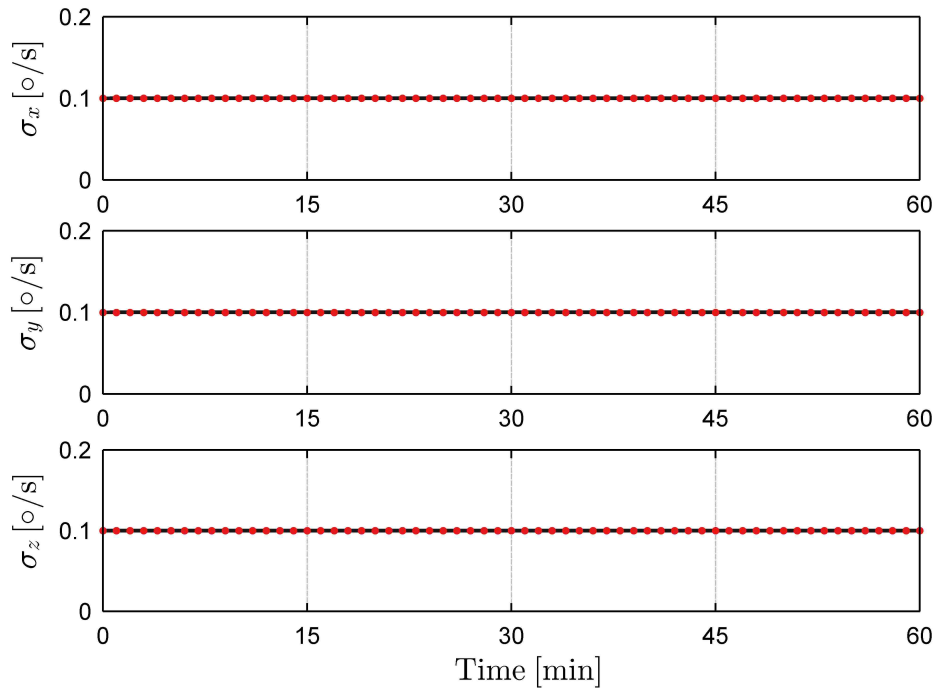
Figure 6.2. Gaussian-distributed angular velocity standard deviation quantified by the Gauss-Bingham density (black) and the predictor of the MEKF (red).
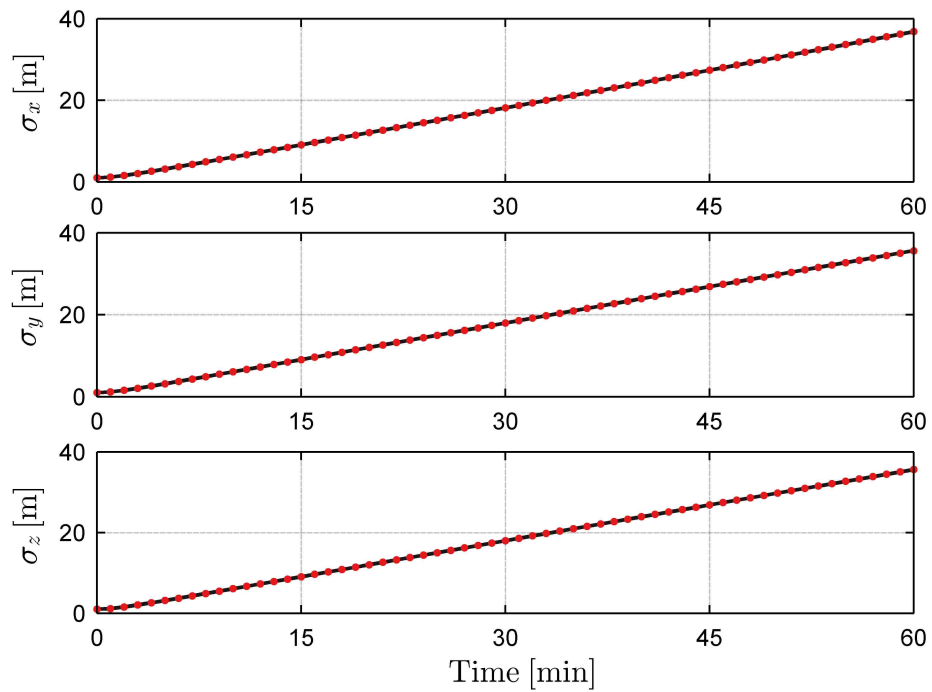
Figure 6.3. Gaussian-distributed relative position standard deviation quantified by the Gauss-Bingham density (black) and the predictor of the MEKF (red).
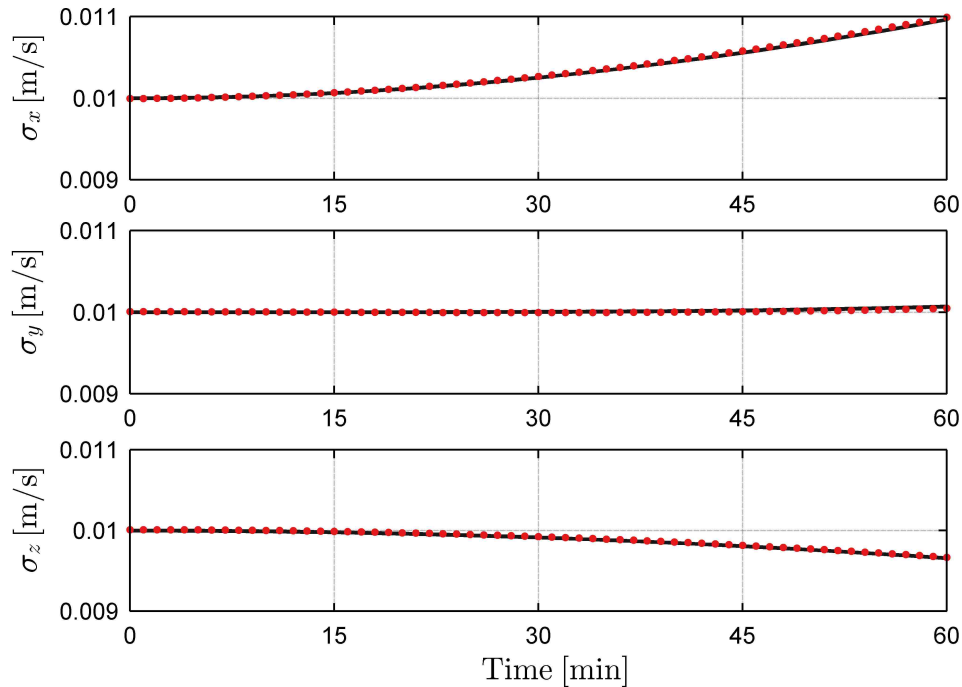
Figure 6.4. Gaussian-distributed relative velocity standard deviation quantified by the Gauss-Bingham density (black) and the predictor of the MEKF (red).

representation, first, 100,000 samples of the Gauss-Bingham density are generated using an acceptance sampling method. The quaternion portion of the Gauss-Bingham samples, as well as the Monte Carlo samples, are then converted to their equivalent rotation vector according to Eq. (2.40). Expectation maximization [72] is then performed for each set of samples to fit a Gaussian mixture density to the x-y, y-z, and x-z projections of the rotation vector portion of the respective samples. This process is used *only* to visualize the uncertainty of the attitude quaternion quantified by the Gauss-Bingham density and the Monte Carlo samples in rotation vector space and is not an element of the uncertainty propagation using the Gauss-Bingham density. Because the MEKF quantifies the mean and covariance of the rotation vector and not its density, the density is assumed to be Gaussian.

The attitude uncertainty quantified by the Gauss-Bingham density, Monte Carlo samples, and MEKF at a time of five minutes are presented in Figure (6.5). Figures (6.5a) and (6.5b) show the x-y projection of the rotation vector for 1,000 of the Monte Carlo and Gauss-Bingham samples, as well as the Gaussian mixture densities fit to these samples to show the agreement between the samples and the densities. These plots are repeated without the samples in Figures. (6.5c) and (6.5d) for clarity along with the uncertainty quantified by the MEKF in red in Figure (6.5d). Figures (6.5e) and (6.5f) and Figures. (6.5g) and (6.5h) show the y-z and x-z projections, respectively, of the

uncertainty quantified by the Gauss-Bingham density, true density (as approximated from the Monte Carlo samples), and MEKF. At the time of five minutes, the Gauss-Bingham density agrees very well with the true density. The MEKF quantifies the mean and covariance of the true density as well, which is attributed to the fact that the attitude uncertainty is still relatively small at this time.

Figure (6.6) shows the uncertainty quantified by the Gauss-Bingham density, true density (as approximated from the Monte Carlo samples), and MEKF at a time of one hour in the same plots as Figure (6.5). After propagating the uncertainty for one hour, the attitude uncertainty quantified by the MEKF does not agree with the true uncertainty, as it has outgrown the $\theta \in [-\pi \ \pi)$ bound on the rotation vector. This uncertainty can potentially be wrapped such that it is expressed in the appropriate bounded region; however, this is not common practice when using the MEKF. The underlying small angle assumption used to derive the predictor of the MEKF becomes invalid when the attitude uncertainties become large; thus, it is not well-suited to propagate large attitude uncertainties.

After propagating the uncertainty for one hour, the Gauss-Bingham density is still in close agreement with the true density as is shown in Figure (6.6). This is due to the fact that the uncertainty propagation using the Gauss-Bingham density does not rely on a small angle assumption. The uncertainty is also quantified on the natural manifold of the attitude quaternion and the other Euclidean states, $\mathbb{R}^9 \times \mathbb{S}^3$, so the uncertainty cannot escape the bounded region on which it is defined. Because of these reasons, uncertainty propagation using the Gauss-Bingham density remains well-suited to quantify attitude uncertainty, even as the attitude uncertainty becomes large.

6.4. GAUSS-BINGHAM CORRECTOR

Ideally, the uncertainty propagation step presented would be used as the predictor step in a filter along with a corrector step to incorporate measurement data into the state density; however, a corrector using the Gauss-Bingham density has been found to be computationally intractable. The corrector of the MDF, as defined by Eqs. (5.44) can be specialized to the Gauss-Bingham density according to

$$p(\boldsymbol{x}_k|\boldsymbol{z}_{1:k}) = \frac{p(\boldsymbol{z}_k|\boldsymbol{x}_k, \boldsymbol{z}_{1:k-1})p_{gb}(\boldsymbol{x}_k; \boldsymbol{m}_k^-, \boldsymbol{P}_k^-, \boldsymbol{\phi}_{0,k}^-, \boldsymbol{\beta}_k^-, \boldsymbol{Z}_k^-)}{\int p(\boldsymbol{z}_k|\boldsymbol{\xi}, \boldsymbol{z}_{1:k-1})p_{gb}(\boldsymbol{\xi}; \boldsymbol{m}_k^-, \boldsymbol{P}_k^-, \boldsymbol{\phi}_{0,k}^-, \boldsymbol{\beta}_k^-, \boldsymbol{Z}_k^-)\, \mathrm{d}\boldsymbol{\xi}}$$

$$\{\boldsymbol{m}_k^+, \boldsymbol{P}_k^+, \boldsymbol{\phi}_{0,k}^+, \boldsymbol{\beta}_k^+, \boldsymbol{Z}_k^+\} = \operatorname*{argmin}_{\boldsymbol{m}, \boldsymbol{P}, \boldsymbol{\phi}_0, \boldsymbol{\beta}, \boldsymbol{Z}} \int p(\boldsymbol{x}_k|\boldsymbol{z}_{1:k}) \ln \frac{p(\boldsymbol{x}_k|\boldsymbol{z}_{1:k})}{p_{gb}(\boldsymbol{x}_k; \boldsymbol{m}, \boldsymbol{P}, \boldsymbol{\phi}_0, \boldsymbol{\beta}, \boldsymbol{Z})}\, \mathrm{d}\boldsymbol{x}_k\,.$$

Numerical methods must be employed in order to perform this integration and minimization, which becomes computationally intractable, even for state vectors with small dimension, because the integration must be performed inside the cost function of the minimization scheme to find $\boldsymbol{m}_k^+, \boldsymbol{P}_k^+,$
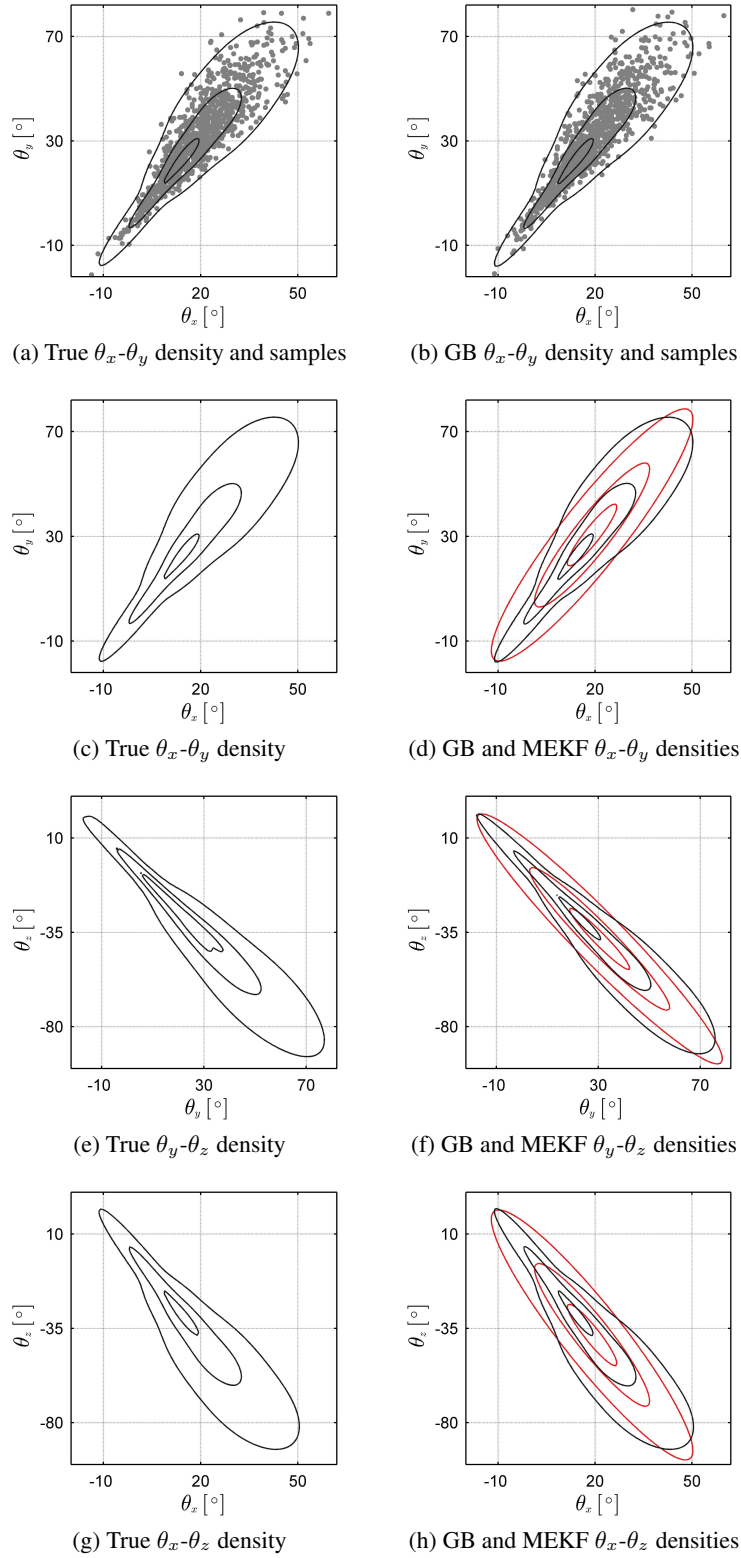
Figure 6.5. True, Gauss-Bingham, and MEKF attitude uncertainties expressed in rotation vector space at a time of five minutes. The MEKF density is shown in red.
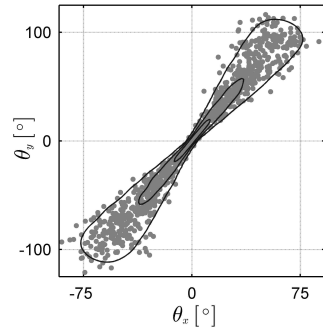
(a) True θ_x-θ_y density and samples
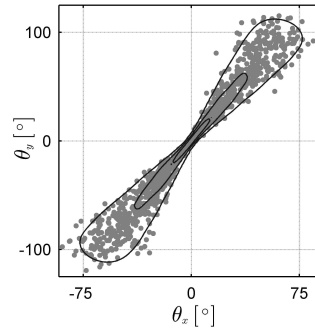
(b) GB θ_x-θ_y density and samples
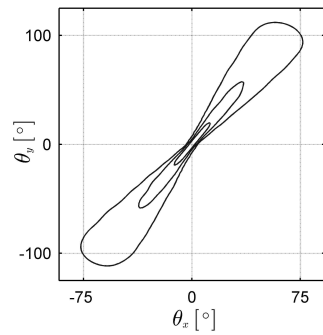
(c) True θ_x-θ_y density
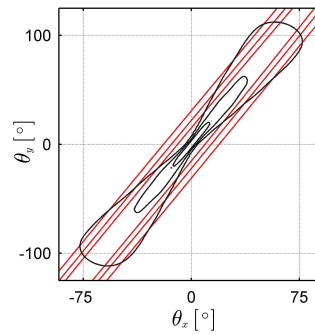
(d) GB and MEKF θ_x-θ_y densities
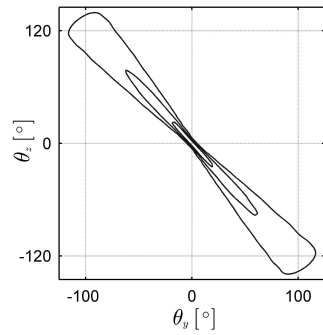
(e) True θ_y-θ_z density
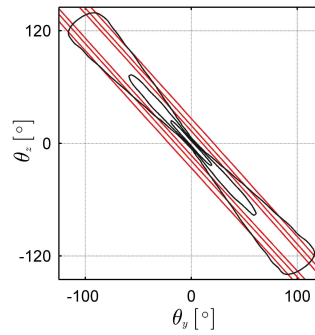
(f) GB and MEKF θ_y-θ_z densities
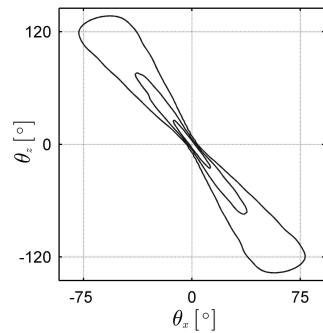
(g) True θ_x-θ_z density
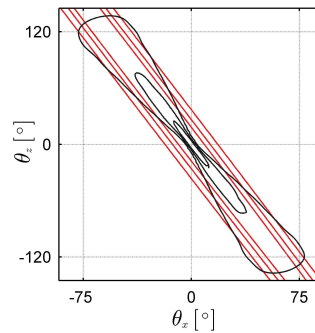
(h) GB and MEKF θ_x-θ_z densities

Figure 6.6. True, Gauss-Bingham, and MEKF attitude uncertainties expressed in rotation vector space at a time of one hour. The MEKF density is shown in red.

$\phi_{0,k}^+$, $\boldsymbol{\beta}_k^+$, and $\boldsymbol{Z}_k^+$. This minimization must be performed numerically because the Gauss-Bingham density is not a member of the general exponential family due to the dependence of the orientation matrix of the Bingham density on the Gaussian-distributed random variable according to $\boldsymbol{M}(\mathbf{x}; \boldsymbol{m}, \boldsymbol{P}, \phi_0, \boldsymbol{\beta})$. This represents a nonlinear transformation of the parameters of the Gauss-Bingham density to specify the orientation matrix of the conditional Bingham density. This nonlinear transformation is the reason that the Gauss-Bingham density does not belong to the general exponential family and makes analytic results using this density difficult to obtain. Because of this, the Bingham-Gauss density, which is a member of the general exponential family and parameterized by its first and second moments, is used to construct an approximate Bayesian filter, as is presented in Chapter 7.

7. THE BINGHAM–GAUSS MIXTURE FILTER

Consider the application of the MDF to the case when an assumed BGM density is used to approximate the true state density at each step in the Bayesian recursion. The dynamical system and measurement model under consideration are taken to be the most general forms, as defined by Eqs. (4.1) or, equivalently, Eqs. (4.2). In this application, the MDF is not applied directly to the find the parameters of the assumed BGM density; it is instead applied on a component-wise basis to find the KL divergence optimal parameters of each component of the assumed BGM density from the true evolution of the component. This is the same manner in which the MDF is applied to develop the GMMDF filter in Section 5.5.3. Because the MDF is applied in a component-wise manner, the resulting assumed BGM density approximating the true density is not KL divergence optimal in general; however, this application minimizes the KL divergence on a component-wise basis and results in a computationally tractable filter.

The BGM filter is an assumed density Bayesian filter in which the temporal and measurement evolution of each component of the BGM density is approximated by its KL optimal Bingham-Gauss density. Because the Bingham-Gauss density is an exponential family density (similar to the Gaussian density), the KL optimal Bingham-Gauss approximation of an arbitrary density is defined by Theorem 1. This result is used to approximate the resulting pdfs from Bayes' rule and the Chapman-Kolmogorov equation in order to make the recursion of the (now approximate) Bayes' filter close. The predictor and corrector of the BGM filter are developed and cast in terms of the integrals defining the parameters of the components of the approximating BGM density, which are then approximated using quadrature-type methods.

Let the initial BGM density, which probabilistically quantifies the initial state vector, $\boldsymbol{x}_0$, be given by

$$p(\boldsymbol{x}_0) = \sum_{\ell=1}^{L_0^+} w_0^{(\ell)+} \, p_{bg}\big(\boldsymbol{x}_0; \boldsymbol{m}_{\mathrm{x},0}^{(\ell)+}, \boldsymbol{P}_{\mathrm{x},0}^{(\ell)+}, \boldsymbol{P}_{q,0}^{(\ell)+}, \boldsymbol{P}_{q\mathrm{x},0}^{(\ell)+}\big).$$

Recall that the state vector augmented with the process noise is defined by $\tilde{\boldsymbol{x}}_{k-1} \triangleq [\boldsymbol{x}_{k-1}^T \ \ \boldsymbol{w}_{k-1}^T]^T$. By augmenting the state vector with the process noise in this way, $\tilde{\boldsymbol{x}}_{k-1}$ is BGM-distributed (provided that the process noise is Gaussian-distributed) according to

$$p(\tilde{\boldsymbol{x}}_{k-1}|\boldsymbol{z}_{1:k-1}) = \sum_{\ell=1}^{L_{k-1}^+} w_{k-1}^{(\ell)+} \, p_{bg}\big(\tilde{\boldsymbol{x}}_{k-1}; \tilde{\boldsymbol{m}}_{\mathrm{x},k-1}^{(\ell)+}, \tilde{\boldsymbol{P}}_{\mathrm{x},k-1}^{(\ell)+}, \boldsymbol{P}_{q,k-1}^{(\ell)+}, \tilde{\boldsymbol{P}}_{q\mathrm{x},k-1}^{(\ell)+}\big) \qquad (7.1)$$

$$\triangleq \sum_{\ell=1}^{L_{k-1}^+} w_{k-1}^{(\ell)+} q^{(\ell)+}(\tilde{\boldsymbol{x}}_{k-1}),\tag{7.2}$$

where

$$\tilde{\boldsymbol{m}}_{\mathrm{x},k-1}^{(\ell)+} = \begin{bmatrix} \boldsymbol{m}_{\mathrm{x},k-1}^{(\ell)+} \\ \boldsymbol{0} \end{bmatrix} \qquad \tilde{\boldsymbol{P}}_{\mathrm{x},k-1}^{(\ell)+} = \begin{bmatrix} \boldsymbol{P}_{\mathrm{x},k-1}^{(\ell)+} & \boldsymbol{0} \\ \boldsymbol{0} & \boldsymbol{Q}_{k-1} \end{bmatrix} \qquad \tilde{\boldsymbol{P}}_{q\mathrm{x},k-1}^{(\ell)+} = \begin{bmatrix} \boldsymbol{P}_{q\mathrm{x},k-1}^{(\ell)+} & \boldsymbol{0} \end{bmatrix},$$

and the $q^{(\ell)+}(\tilde{\boldsymbol{x}}_{k-1})$ notation is introduced for notational convenience. Because the augmented state vector includes all stochastic inputs, the transition density is given by the Dirac density according to

$$p(\boldsymbol{x}_k|\tilde{\boldsymbol{x}}_{k-1}) = \delta(\boldsymbol{x}_k - \tilde{\boldsymbol{f}}(\tilde{\boldsymbol{x}}_{k-1})).\tag{7.3}$$

Equations (7.1) and (7.3) are now substituted into Eq. (5.1) and simplified to yield the true prior density at t_k according to

$$p(\boldsymbol{x}_k|\boldsymbol{z}_{1:k-1}) = \sum_{\ell=1}^{L_{k-1}^+} w_{k-1}^{(\ell)+} \int \delta(\boldsymbol{x}_k - \tilde{\boldsymbol{f}}(\tilde{\boldsymbol{x}}_{k-1})) q^{(\ell)+}(\tilde{\boldsymbol{x}}_{k-1}) \, \mathrm{d}\tilde{\boldsymbol{x}}_{k-1}.\tag{7.4}$$

If the integral in Eq. (7.4) can be calculated exactly, then the true prior density at t_{k-1} is known, and no approximation is necessary. In general, it is not possible nor tractable to calculate this integral, and the true prior density at t_{k-1} is approximated by a BGM density in order to yield a tractable recursion for the Bayesian filter, in which case an approximate Bayesian filter is obtained. This approximation is performed according to

$$\sum_{\ell=1}^{L_k^-} w_k^{(\ell)-} p_{bg}(\boldsymbol{x}_k; \boldsymbol{m}_{\mathrm{x},k}^{(\ell)-}, \boldsymbol{P}_{\mathrm{x},k}^{(\ell)-}, \boldsymbol{P}_{q,k}^{(\ell)-}, \boldsymbol{P}_{q\mathrm{x},k}^{(\ell)-})$$

$$\approx \sum_{\ell=1}^{L_{k-1}^+} w_{k-1}^{(\ell)+} \int \delta(\boldsymbol{x}_k - \tilde{\boldsymbol{f}}(\tilde{\boldsymbol{x}}_{k-1})) q^{(\ell)+}(\tilde{\boldsymbol{x}}_{k-1}) \, \mathrm{d}\tilde{\boldsymbol{x}}_{k-1},$$

where it is necessary to find the parameters defining the BGM mixture approximating the prior density at t_k, which are given by $w_k^{(\ell)-}$, $\boldsymbol{m}_{\mathrm{x},k}^{(\ell)-}$, $\boldsymbol{P}_{\mathrm{x},k}^{(\ell)-}$, $\boldsymbol{P}_{q,k}^{(\ell)-}$, and $\boldsymbol{P}_{q\mathrm{x},k}^{(\ell)-}$ for $\ell = 1, 2, \ldots, L_k^-$. A component-wise approximation of the mixture is performed according to

$$w_k^{(\ell)-} p_{bg}(\boldsymbol{x}_k; \boldsymbol{m}_{\mathrm{x},k}^{(\ell)-}, \boldsymbol{P}_{\mathrm{x},k}^{(\ell)-}, \boldsymbol{P}_{q,k}^{(\ell)-}, \boldsymbol{P}_{q\mathrm{x},k}^{(\ell)-})\tag{7.5}$$

$$\approx w_{k-1}^{(\ell)+} \int \delta(\boldsymbol{x}_k - \tilde{\boldsymbol{f}}(\tilde{\boldsymbol{x}}_{k-1})) q^{(\ell)+}(\tilde{\boldsymbol{x}}_{k-1}) \, \mathrm{d}\tilde{\boldsymbol{x}}_{k-1},$$

for $\ell = 1, 2, \ldots, L_k^-$, which dictates that the number of components remains the same in the predictor; that is, $L_k^- = L_{k-1}^+$. In order to obtain the weight evolution in the predictor, the zeroth moments of both sides of Eq. (7.5) are matched, which yields the weight evolution for the predictor as

$$w_k^{(\ell)-} = w_{k-1}^{(\ell)+}, \tag{7.6}$$

for $\ell = 1, 2, \ldots, L_k^-$. Equation (7.6) is substituted into Eq. (7.5) to yield the necessary approximation of each component of the prior BGM according to

$$p_{bg}\big(\boldsymbol{x}_k; \boldsymbol{m}_{\mathrm{x},k}^{(\ell)-}, \boldsymbol{P}_{\mathrm{x},k}^{(\ell)-}, \boldsymbol{P}_{q,k}^{(\ell)-}, \boldsymbol{P}_{q\mathrm{x},k}^{(\ell)-}\big) \approx \int \delta\big(\boldsymbol{x}_k - \tilde{\boldsymbol{f}}(\tilde{\boldsymbol{x}}_{k-1})\big) q^{(\ell)+}\big(\tilde{\boldsymbol{x}}_{k-1}\big) \, \mathrm{d}\tilde{\boldsymbol{x}}_{k-1}.$$

The parameters of the components of the approximating Bingham-Gauss density are now found such that the KL divergence of the right-hand side of this approximation with respect to its left-hand side is minimized. Because the Bingham-Gauss density is an exponential family density, Theorem 1 states that the parameters of the KL optimal Bingham-Gauss density are given by

$$\boldsymbol{m}_{\mathrm{x},k}^{(\ell)-} = 2 \int_{\mathbb{S}^+} \mathbf{x}_k \int \delta\big(\boldsymbol{x}_k - \tilde{\boldsymbol{f}}(\tilde{\boldsymbol{x}}_{k-1})\big) q^{(\ell)+}\big(\tilde{\boldsymbol{x}}_{k-1}\big) \, \mathrm{d}\tilde{\boldsymbol{x}}_{k-1} \, \mathrm{d}\boldsymbol{x}_k \tag{7.7a}$$

$$\boldsymbol{P}_{\mathrm{x},k}^{(\ell)-} = 2 \int_{\mathbb{S}^+} (\mathbf{x}_k - \boldsymbol{m}_{\mathrm{x},k}^{(\ell)-})(\mathbf{x}_k - \boldsymbol{m}_{\mathrm{x},k}^{(\ell)-})^T \tag{7.7b}$$

$$\times \int \delta\big(\boldsymbol{x}_k - \tilde{\boldsymbol{f}}(\tilde{\boldsymbol{x}}_{k-1})\big) q^{(\ell)+}\big(\tilde{\boldsymbol{x}}_{k-1}\big) \, \mathrm{d}\tilde{\boldsymbol{x}}_{k-1} \, \mathrm{d}\boldsymbol{x}_k$$

$$\boldsymbol{P}_{q,k}^{(\ell)-} = 2 \int_{\mathbb{S}^+} \bar{\boldsymbol{q}}_k \bar{\boldsymbol{q}}_k^T \int \delta\big(\boldsymbol{x}_k - \tilde{\boldsymbol{f}}(\tilde{\boldsymbol{x}}_{k-1})\big) q^{(\ell)+}\big(\tilde{\boldsymbol{x}}_{k-1}\big) \, \mathrm{d}\tilde{\boldsymbol{x}}_{k-1} \, \mathrm{d}\boldsymbol{x}_k \tag{7.7c}$$

$$\pm\boldsymbol{P}_{q\mathrm{x},k}^{(\ell)-} = 2 \int_{\mathbb{S}^+} \bar{\boldsymbol{q}}_k (\mathbf{x}_k - \boldsymbol{m}_{\mathrm{x},k}^{(\ell)-})^T \int \delta\big(\boldsymbol{x}_k - \tilde{\boldsymbol{f}}(\tilde{\boldsymbol{x}}_{k-1})\big) q^{(\ell)+}\big(\tilde{\boldsymbol{x}}_{k-1}\big) \, \mathrm{d}\tilde{\boldsymbol{x}}_{k-1} \, \mathrm{d}\boldsymbol{x}_k, \tag{7.7d}$$

where the $\mathbb{S}^+$ notation on the integral is used to denote that this integration is performed over the entire support of $\mathbf{x}$, but only over the support $\mathbb{S}^+$ for $\bar{\boldsymbol{q}}$. In deriving this result, the antipodal symmetry of the Bingham-Gauss density is exploited to express these integrals defining the parameters of the Bingham-Gauss density over $\mathbb{S}^+$ (instead of over the entire hypersphere, $\mathbb{S}$), which results in the factor of two in front of the integrals. Whether $+\boldsymbol{P}_{q\mathrm{x},k}^{(\ell)-}$ or $-\boldsymbol{P}_{q\mathrm{x},k}^{(\ell)-}$ is obtained, as well as why there is ambiguity in this parameters, is addressed at the end of this subsection for clarity.

In order to manipulate Eqs. (7.7) into a more usable form, first the nonlinear function representing the system dynamics, $\tilde{\boldsymbol{f}}(\tilde{\boldsymbol{x}}_{k-1})$, can be partitioned into two parts representing the quaternion and Euclidean portions of the system dynamics according to

$$\tilde{\boldsymbol{f}}(\tilde{\boldsymbol{x}}_{k-1}) = \begin{bmatrix} \tilde{\boldsymbol{f}}_q(\tilde{\boldsymbol{x}}_{k-1}) \\ \tilde{\boldsymbol{f}}_{\mathrm{x}}(\tilde{\boldsymbol{x}}_{k-1}) \end{bmatrix}.$$

Now, the order of integration in Eqs. (7.7) is reversed and the sifting property of the Dirac delta density is exploited to yield the parameters of the ℓth component of the approximating BGM as

$$m_{\text{x},k}^{(\ell)-} = 2 \int_{\mathbb{S}^+} \tilde{f}_{\text{x}}(\tilde{x}_{k-1}) q^{(\ell)+}(\tilde{x}_{k-1}) \, \mathrm{d}\tilde{x}_{k-1}$$

$$P_{\text{x},k}^{(\ell)-} = 2 \int_{\mathbb{S}^+} \big(\tilde{f}_{\text{x}}(\tilde{x}_{k-1}) - m_{\text{x},k}^{(\ell)-}\big)\big(\tilde{f}_{\text{x}}(\tilde{x}_{k-1}) - m_{\text{x},k}^{(\ell)-}\big)^T q^{(\ell)+}(\tilde{x}_{k-1}) \, \mathrm{d}\tilde{x}_{k-1}$$

$$P_{q,k}^{(\ell)-} = 2 \int_{\mathbb{S}^+} \tilde{f}_q(\tilde{x}_{k-1}) \tilde{f}_q(\tilde{x}_{k-1})^T q^{(\ell)+}(\tilde{x}_{k-1}) \, \mathrm{d}\tilde{x}_{k-1}$$

$$\pm P_{q\text{x},k}^{(\ell)-} = 2 \int_{\mathbb{S}^+} \tilde{f}_q(\tilde{x}_{k-1})\big(\tilde{f}_{\text{x}}(\tilde{x}_{k-1}) - m_{\text{x},k}^{(\ell)-}\big)^T q^{(\ell)+}(\tilde{x}_{k-1}) \, \mathrm{d}\tilde{x}_{k-1} \,.$$

If these integrals can be calculated analytically for a certain $\tilde{f}_{\text{x}}(\tilde{x}_{k-1})$ and/or $\tilde{f}_q(\tilde{x}_{k-1})$, then these parameters are known in closed-form. In general, analytic expressions for these integrals are not possible, so a discrete approximation of the integrals is used to approximate these parameters according to

$$m_{\text{x},k}^{(\ell)-} \approx 2 \sum_{i=1}^{N} w_{k-1}^{(i)} \, \tilde{f}_{\text{x}}(\tilde{\mathcal{X}}_{k-1}^{(i)}) \tag{7.8a}$$

$$P_{\text{x},k}^{(\ell)-} \approx 2 \sum_{i=1}^{N} w_{k-1}^{(i)} \big(\tilde{f}_{\text{x}}(\tilde{\mathcal{X}}_{k-1}^{(i)}) - m_{\text{x},k}^{(\ell)-}\big)\big(\tilde{f}_{\text{x}}(\tilde{\mathcal{X}}_{k-1}^{(i)}) - m_{\text{x},k}^{(\ell)-}\big)^T \tag{7.8b}$$

$$P_{q,k}^{(\ell)-} \approx 2 \sum_{i=1}^{N} w_{k-1}^{(i)} \, \tilde{f}_q(\tilde{\mathcal{X}}_{k-1}^{(i)}) \tilde{f}_q(\tilde{\mathcal{X}}_{k-1}^{(i)})^T \tag{7.8c}$$

$$\pm P_{q\text{x},k}^{(\ell)-} \approx 2 \sum_{i=1}^{N} w_{k-1}^{(i)} \, \tilde{f}_q(\tilde{\mathcal{X}}_{k-1}^{(i)})\big(\tilde{f}_{\text{x}}(\tilde{\mathcal{X}}_{k-1}^{(i)}) - m_{\text{x},k}^{(\ell)-}\big)^T \,, \tag{7.8d}$$

for $\ell = 1, 2, \ldots, L_k^-$, where $w_{k-1}^{(i)}$ and $\tilde{\mathcal{X}}_{k-1}^{(i)}$ for $i = 1, 2, \ldots, N$ are the discrete weights and points that approximate $q^{(\ell)+}(\tilde{x}_{k-1})$ on the "positive" half of the unit hypersphere, $\mathbb{S}^+$. The unscented transform presented in Section 6.1, quadrature, or Monte Carlo integration, among other methods, can be used to obtain these weights and points corresponding to the Bingham-Gauss density. If the unscented transform presented in Section 6.1 is used, it is used to generate the weights and points corresponding to the canonical Bingham-Gauss density (which is identical to the canonical Gauss-Bingham density), and the points are transformed according to Eqs. (3.59) to represent the Bingham-Gauss density of interest. A quadrature scheme and an efficient acceptance sampling method have been developed for the Bingham density in References [73] and [74], respectively. These can be combined with Gauss-Hermite quadrature and a sampling method for the Gaussian

density to obtain a quadrature scheme and a Monte Carlo integration method for the Bingham-Gauss density.

The sign ambiguity in $\pm\boldsymbol{P}_{qx,k}^{(\ell)-}$ is now resolved, which depends on whether or not the weights and quaternion portions of the transformed points, $w_{k-1}^{(i)}$ and $\tilde{\boldsymbol{f}}_q(\tilde{\boldsymbol{\mathcal{X}}}_{k-1}^{(i)})$ for $i = 1, 2, \ldots, N$, define the portion of the Bingham-Gauss density on $\mathbb{S}^+$ or $\mathbb{S}^-$, which is apparent from Eq. (3.58). To determine which half of the Bingham-Gauss density is quantified by these weights and points, first, Eqs. (7.8) are evaluated assuming that $+\boldsymbol{P}_{qx,k}^{(\ell)-}$ is obtained. A consistency check between the weights and points and the Bingham-Gauss densities with $\pm\boldsymbol{P}_{qx,k}^{(\ell)-}$ is then performed. The Bingham-Gauss density that is most consistent with the weights and points determines whether $+\boldsymbol{P}_{qx,k}^{(\ell)-}$ or $-\boldsymbol{P}_{qx,k}^{(\ell)-}$ is actually obtained, and should be used. In this work, the weighted log-likelihood is used as the consistency check, such that if

$$\sum_{i=1}^{N} w_{k-1}^{(i)} \ln p_{bg}\big(\tilde{\boldsymbol{f}}(\tilde{\boldsymbol{\mathcal{X}}}_{k-1}^{(i)}); \boldsymbol{m}_{\mathrm{x},k}^{(\ell)-}, \boldsymbol{P}_{\mathrm{x},k}^{(\ell)-}, \boldsymbol{P}_{q,k}^{(\ell)-}, +\boldsymbol{P}_{qx,k}^{(\ell)-}\big)$$

is greater than

$$\sum_{i=1}^{N} w_{k-1}^{(i)} \ln p_{bg}\big(\tilde{\boldsymbol{f}}(\tilde{\boldsymbol{\mathcal{X}}}_{k-1}^{(i)}); \boldsymbol{m}_{\mathrm{x},k}^{(\ell)-}, \boldsymbol{P}_{\mathrm{x},k}^{(\ell)-}, \boldsymbol{P}_{q,k}^{(\ell)-}, -\boldsymbol{P}_{qx,k}^{(\ell)-}\big),$$

then the weights and transformed points define the portion of the Bingham-Gauss density on $\mathbb{S}^+$ and $+\boldsymbol{P}_{qx,k}^{(\ell)-}$ should be used; if it is not, then the weights and transformed points define the portion of the Bingham-Gauss density on $\mathbb{S}^-$ and $-\boldsymbol{P}_{qx,k}^{(\ell)-}$ should be used.

This consistency check is illustrated in Figure (7.1), which shows the bounds used to define which of the antipodal pair of most likely quaternions defines $\mathbb{S}^{1+}$ as red lines. The one of the antipodal pair of most likely quaternions lying on the right-hand side of the circle defines $\mathbb{S}^{1+}$, as denoted by the green lines. Figure (7.1a) shows the prior Bingham-Gauss density, as well as the $\tilde{\boldsymbol{\mathcal{X}}}_{k-1}^{(i)}$ for $i = 1, 2, \ldots, 5$ which approximate the half of the Bingham-Gauss density on $\mathbb{S}^{1+}$. Figures (7.1b) and (7.1c) show the transformed sigma points, $\tilde{\boldsymbol{f}}(\tilde{\boldsymbol{\mathcal{X}}}_{k-1}^{(i)})$, which are observed to approximate the half of the Bingham-Gauss density on $\mathbb{S}^{1-}$. Because of this, $-\boldsymbol{P}_{qx,k}^{(\ell)-}$ results in the Bingham-Gauss density that is more consistent with the transformed points, as is shown in Figure (7.1b), and, thus, $-\boldsymbol{P}_{qx,k}^{(\ell)-}$ instead of $+\boldsymbol{P}_{qx,k}^{(\ell)-}$ is used to quantify the prior Bingham-Gauss density.

Let the prior BGM density at t_k be given by

$$p(\boldsymbol{x}_k|\boldsymbol{z}_{1:k-1}) = \sum_{\ell=1}^{L_k^-} w_k^{(\ell)-} p_{bg}\big(\boldsymbol{x}_k; \boldsymbol{m}_{\mathrm{x},k}^{(\ell)-}, \boldsymbol{P}_{\mathrm{x},k}^{(\ell)-}, \boldsymbol{P}_{q,k}^{(\ell)-}, \boldsymbol{P}_{qx,k}^{(\ell)-}\big) \triangleq \sum_{\ell=1}^{L_k^-} w_k^{(\ell)-} q^{(\ell)-}(\boldsymbol{x}_k),$$

(a) prior density and points   (b) transformed points with $-\boldsymbol{P}_{qx,k}^{(\ell)-}$ (c) transformed points with $+\boldsymbol{P}_{qx,k}^{(\ell)-}$
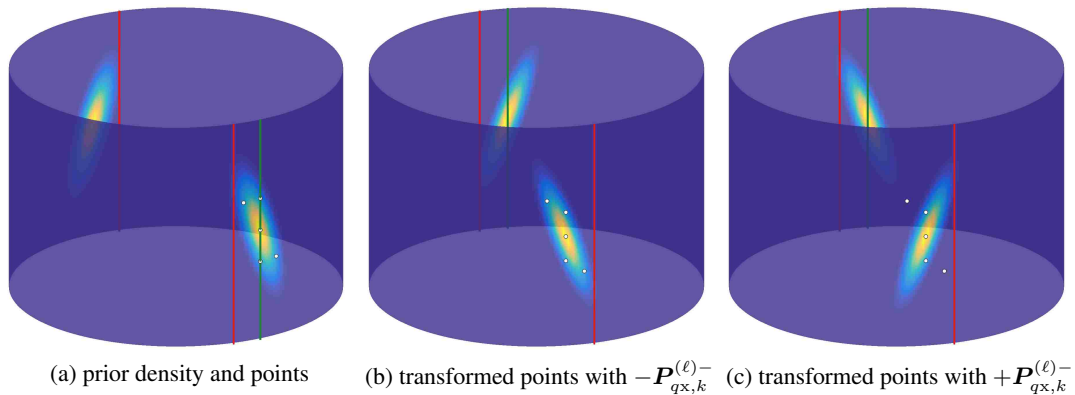
Figure 7.1. Consistency check of the propagated density (with $+\boldsymbol{P}_{qx,k}^{(\ell)-}$ and $-\boldsymbol{P}_{qx,k}^{(\ell)-}$) with the transformed points.

where the $q^{(\ell)-}(\boldsymbol{x}_k)$ notation is introduced for notational convenience. Equation (5.2) is used to define the true posterior density, which is given after simplification according to

$$p(\boldsymbol{x}_k|\boldsymbol{z}_{1:k}) = \frac{\sum_{\ell=1}^{L_k^-} w_k^{(\ell)-} p(\boldsymbol{z}_k|\boldsymbol{x}_k) q^{(\ell)-}(\boldsymbol{x}_k)}{\sum_{j=1}^{L_k^-} w_k^{(j)-} \int p(\boldsymbol{z}_k|\boldsymbol{\xi}) q^{(j)-}(\boldsymbol{\xi}) \, d\boldsymbol{\xi}} \, . \tag{7.9}$$

If this equation can be manipulated into a usable form, then the true posterior density at t_k is known, and no approximation is necessary. In general, it is not possible nor tractable to manipulate this into a usable form, and the true posterior density at t_k is approximated by a BGM density in order to yield a tractable recursion for the Bayesian filter, in a similar manner to the approximation made in the predictor.

Noting the antipodal symmetry of the Bingham-Gauss density, the integral in the denominator of Eq. (7.9) can be expressed as and approximated by

$$k_k^{(\ell)} \triangleq 2 \int_{\mathbb{S}^+} p(\boldsymbol{z}_k|\boldsymbol{\xi}) q^{(\ell)-}(\boldsymbol{\xi}) \, d\boldsymbol{\xi} \approx 2 \sum_{i=1}^{N} w_k^{(i)} p(\boldsymbol{z}_k|\boldsymbol{\mathcal{X}}_k^{(i)}) \, , \tag{7.10}$$

for $\ell = 1, 2, \ldots, L_k^-$, where $w_k^{(i)}$ and $\boldsymbol{\mathcal{X}}_k^{(i)}$ for $i = 1, 2, \ldots, N$ are the discrete weights and points that approximate $q^{(\ell)-}(\boldsymbol{x}_k)$ on the "positive" half of the unit hypersphere, $\mathbb{S}^+$. These weights and points are obtained similarly for the corrector as they are for the predictor. Equation (7.10) is now

substituted into Eq. (7.9) and manipulated to yield

$$p(\boldsymbol{x}_k|\boldsymbol{z}_{1:k}) = \sum_{\ell=1}^{L_k^-} \frac{w_k^{(\ell)-}}{\sum_{j=1}^{L_k^-} w_k^{(j)-} k_k^{(j)}} p(\boldsymbol{z}_k|\boldsymbol{x}_k) q^{(\ell)-}(\boldsymbol{x}_k) \,. \tag{7.11}$$

This true posterior density, as defined by Eq. (7.11), is now approximated by a BGM density according to

$$\sum_{\ell=1}^{L_k^+} w_k^{(\ell)+} p_{bg}\big(\boldsymbol{x}_k; \boldsymbol{m}_{\mathrm{x},k}^{(\ell)+}, \boldsymbol{P}_{\mathrm{x},k}^{(\ell)+}, \boldsymbol{P}_{q,k}^{(\ell)+}, \boldsymbol{P}_{q\mathrm{x},k}^{(\ell)+}\big) \approx \sum_{\ell=1}^{L_k^-} \frac{w_k^{(\ell)-}}{\sum_{j=1}^{L_k^-} w_k^{(j)-} k_k^{(j)}} p(\boldsymbol{z}_k|\boldsymbol{x}_k) q^{(\ell)-}(\boldsymbol{x}_k) \,,$$

where it is necessary to find the parameters defining the BGM mixture approximating the posterior density at t_k, which are given by $w_k^{(\ell)+}$, $\boldsymbol{m}_{\mathrm{x},k}^{(\ell)+}$, $\boldsymbol{P}_{\mathrm{x},k}^{(\ell)+}$, $\boldsymbol{P}_{q,k}^{(\ell)+}$, and $\boldsymbol{P}_{q\mathrm{x},k}^{(\ell)+}$ for $\ell = 1, 2, \ldots, L_k^+$. A component-wise approximation of the mixture is used according to

$$w_k^{(\ell)+} p_{bg}\big(\boldsymbol{x}_k; \boldsymbol{m}_{\mathrm{x},k}^{(\ell)+}, \boldsymbol{P}_{\mathrm{x},k}^{(\ell)+}, \boldsymbol{P}_{q,k}^{(\ell)+}, \boldsymbol{P}_{q\mathrm{x},k}^{(\ell)+}\big) \approx \frac{w_k^{(\ell)-}}{\sum_{j=1}^{L_k^-} w_k^{(j)-} k_k^{(j)}} p(\boldsymbol{z}_k|\boldsymbol{x}_k) q^{(\ell)-}(\boldsymbol{x}_k) \,, \tag{7.12}$$

for $\ell = 1, 2, \ldots, L_k^+$, which dictates that the number of components remains the same in the corrector; that is $L_k^+ = L_k^-$. In order to obtain the weight update in the corrector, the zeroth moments of both sides of Eq. (7.12) are matched, which yields the weight update for the corrector as

$$w_k^{(\ell)+} = \frac{w_k^{(\ell)-}}{\sum_{j=1}^{L_k^-} w_k^{(j)-} k_k^{(j)}} 2 \int_{\mathbb{S}^+} p(\boldsymbol{z}_k|\boldsymbol{\xi}) q^{(\ell)-}(\boldsymbol{\xi}) \, \mathrm{d}\boldsymbol{\xi} \tag{7.13}$$

$$= \frac{w_k^{(\ell)-} k_k^{(\ell)}}{\sum_{j=1}^{L_k^-} w_k^{(j)-} k_k^{(j)}} \,, \tag{7.14}$$

for $\ell = 1, 2, \ldots, L_k^+$, which is observed to be a similar weight update as is used by the corrector of the GMKF, GMEKF, quadrature-based GM Kalman filters, and the GMMDF, which all update the weights according to the relative likelihood that the measurement originated from the ℓth component of the mixture density; however, this relative likelihood is approximated differently between the filters. Equation (7.13) is now substituted into Eq. (7.12) and simplified to yield the necessary approximation of each component according to

$$p_{bg}\big(\boldsymbol{x}_k; \boldsymbol{m}_{\mathrm{x},k}^{(\ell)+}, \boldsymbol{P}_{\mathrm{x},k}^{(\ell)+}, \boldsymbol{P}_{q,k}^{(\ell)+}, \boldsymbol{P}_{q\mathrm{x},k}^{(\ell)+}\big) \approx \frac{p(\boldsymbol{z}_k|\boldsymbol{x}_k) q^{(\ell)-}(\boldsymbol{x}_k)}{k_k^{(\ell)}} \,.$$

The parameters of the components of the approximating Bingham-Gauss mixture density are now found such that the KL divergence of the right-hand side of this approximation with respect to its left-hand side is minimized. Because the Bingham-Gauss density is an exponential family density, Theorem 1 states that the parameters of the KL optimal Bingham-Gauss density are given by

$$
\boldsymbol{m}_{\mathrm{x},k}^{(\ell)+} = \frac{2}{k_k^{(\ell)}} \int_{\mathbb{S}+} \mathbf{x}_k p(\boldsymbol{z}_k|\boldsymbol{x}_k) q^{(\ell)-}(\boldsymbol{x}_k) \,\mathrm{d}\boldsymbol{x}_k
$$

$$
\boldsymbol{P}_{\mathrm{x},k}^{(\ell)+} = \frac{2}{k_k^{(\ell)}} \int_{\mathbb{S}+} (\mathbf{x}_k - \boldsymbol{m}_{\mathrm{x},k}^{(\ell)-})(\mathbf{x}_k - \boldsymbol{m}_{\mathrm{x},k}^{(\ell)-})^T p(\boldsymbol{z}_k|\boldsymbol{x}_k) q^{(\ell)-}(\boldsymbol{x}_k) \,\mathrm{d}\boldsymbol{x}_k
$$

$$
\boldsymbol{P}_{q,k}^{(\ell)+} = \frac{2}{k_k^{(\ell)}} \int_{\mathbb{S}+} \bar{\boldsymbol{q}}_k \bar{\boldsymbol{q}}_k^T p(\boldsymbol{z}_k|\boldsymbol{x}_k) q^{(\ell)-}(\boldsymbol{x}_k) \,\mathrm{d}\boldsymbol{x}_k
$$

$$
\pm\boldsymbol{P}_{q\mathrm{x},k}^{(\ell)+} = \frac{2}{k_k^{(\ell)}} \int_{\mathbb{S}+} \bar{\boldsymbol{q}}_k (\mathbf{x}_k - \boldsymbol{m}_{\mathrm{x},k}^{(\ell)-})^T p(\boldsymbol{z}_k|\boldsymbol{x}_k) q^{(\ell)-}(\boldsymbol{x}_k) \,\mathrm{d}\boldsymbol{x}_k \,,
$$

where the factor of two stems from exploiting the antipodal symmetry of the Bingham-Gauss density. If these integrals can be calculated analytically for a certain $p(\boldsymbol{z}_k|\boldsymbol{x}_k)$, then these parameters are known in closed form. In general, analytic expressions for these integrals are not possible, so quadrature approximation of the integrals is used to approximate these parameters according to

$$
\boldsymbol{m}_{\mathrm{x},k}^{(\ell)+} \approx \frac{2}{k_k^{(\ell)}} \sum_{i=1}^{N} w_k^{(i)} \boldsymbol{\mathcal{X}}_{\mathrm{x},k}^{(i)} p(\boldsymbol{z}_k|\boldsymbol{\mathcal{X}}_k^{(i)})
$$

$$
\boldsymbol{P}_{\mathrm{x},k}^{(\ell)+} \approx \frac{2}{k_k^{(\ell)}} \sum_{i=1}^{N} w_k^{(i)} \left(\boldsymbol{\mathcal{X}}_{\mathrm{x},k}^{(i)} - \boldsymbol{m}_{\mathrm{x},k}^{(\ell)-}\right)\left(\boldsymbol{\mathcal{X}}_{\mathrm{x},k}^{(i)} - \boldsymbol{m}_{\mathrm{x},k}^{(\ell)-}\right)^T p(\boldsymbol{z}_k|\boldsymbol{\mathcal{X}}_k^{(i)})
$$

$$
\boldsymbol{P}_{q,k}^{(\ell)+} \approx \frac{2}{k_k^{(\ell)}} \sum_{i=1}^{N} w_k^{(i)} \boldsymbol{\mathcal{X}}_{q,k}^{(i)} \boldsymbol{\mathcal{X}}_{q,k}^{(i)}{}^T p(\boldsymbol{z}_k|\boldsymbol{\mathcal{X}}_k^{(i)})
$$

$$
\pm\boldsymbol{P}_{q\mathrm{x},k}^{(\ell)+} \approx \frac{2}{k_k^{(\ell)}} \sum_{i=1}^{N} w_k^{(i)} \boldsymbol{\mathcal{X}}_{q,k}^{(i)} \left(\boldsymbol{\mathcal{X}}_{\mathrm{x},k}^{(i)} - \boldsymbol{m}_{\mathrm{x},k}^{(\ell)-}\right)^T p(\boldsymbol{z}_k|\boldsymbol{\mathcal{X}}_k^{(i)}) \,,
$$

for $\ell = 1, 2, \ldots, L_k^+$, where $w_{k-1}^{(i)}$ and $\boldsymbol{\mathcal{X}}_{k-1}^{(i)}$ for $i = 1, 2, \ldots, N$ are the weights and points defined in Eq. (7.10), and $\boldsymbol{\mathcal{X}}_{q,k}^{(i)}$ and $\boldsymbol{\mathcal{X}}_{\mathrm{x},k}^{(i)}$ define the quaternion and Euclidean portions of $\boldsymbol{\mathcal{X}}_k^{(i)}$, respectively. These weights and points can be selected using the unscented transform presented in Section 6.1, a quadrature rule, or Monte Carlo methods, among other methods, similarly to how the weights and points are selected for the predictor.

The sign ambiguity in $\pm\boldsymbol{P}_{q\mathrm{x},k}^{(\ell)+}$ is now resolved in a similar manner to how it is resolved in the predictor. This is performed as a consistency check between the "weights," given by $w_k^{(i)} p(\boldsymbol{z}_k|\boldsymbol{\mathcal{X}}_k^{(i)})$, and points, given by $\boldsymbol{\mathcal{X}}_k^{(i)}$, for $i = 1, 2, \ldots, N$, and the Bingham-Gauss densities with $\pm\boldsymbol{P}_{q\mathrm{x},k}^{(\ell)+}$. The

weighted log-likelihood is used as the consistency check, such that if

$$
\sum_{i=1}^{N} w_k^{(i)} p(\boldsymbol{z}_k | \boldsymbol{\mathcal{X}}_k^{(i)}) \ln p_{bg}\big(\boldsymbol{\mathcal{X}}_k^{(i)}; \boldsymbol{m}_{\text{x},k}^{(\ell)+}, \boldsymbol{P}_{\text{x},k}^{(\ell)+}, \boldsymbol{P}_{q,k}^{(\ell)+}, +\boldsymbol{P}_{\text{qx},k}^{(\ell)+}\big)
$$

is greater than

$$
\sum_{i=1}^{N} w_k^{(i)} p(\boldsymbol{z}_k | \boldsymbol{\mathcal{X}}_k^{(i)}) \ln p_{bg}\big(\boldsymbol{\mathcal{X}}_k^{(i)}; \boldsymbol{m}_{\text{x},k}^{(\ell)+}, \boldsymbol{P}_{\text{x},k}^{(\ell)+}, \boldsymbol{P}_{q,k}^{(\ell)+}, -\boldsymbol{P}_{\text{qx},k}^{(\ell)+}\big) \,,
$$

then $+\boldsymbol{P}_{\text{qx},k}^{(\ell)-}$ should be used to define the posterior Bingham-Gauss density; if it is not, then $-\boldsymbol{P}_{\text{qx},k}^{(\ell)-}$ should be used.

While the number of components in the corrector strictly remains the same, significant computational savings can be obtained by removing components with sufficiently small weights after the corrector is applied. These components are removed, and the weights of the remaining components are renormalized to ensure that they sum to unity. While some approximation error is incurred in removing these components, this error is typically negligible if the weights are forced to be sufficiently small before removing a component, and the computational savings typically outweighs this approximation error.

8. APPLICATIONS

In order to evaluate the efficacy of the Bingham-Gauss mixture filter, it is simulated to estimate the state of three systems: The one-dimensional attitude quaternion and angular velocity of a body, the two-dimensional relative orbit and one-dimensional attitude of an inspector spacecraft approaching a target spacecraft, and the three-dimensional attitude and angular velocity of a spacecraft in low-Earth orbit. The BGM filter is applied to the first system in order to compare it to a multiplicative Kalman filter using a Monte Carlo analysis in order to perform a direct comparison. The BGM filter is applied to the second system to illustrate its efficacy in estimating the planar dynamic pose (two-dimensional relative position and velocity and one-dimensional attitude and angular velocity) of a vehicle given nonlinear measurements of the range between the inspector and target spacecraft and the angle from the inspector to the target spacecraft, taken in the inspector's body frame.

8.1. ONE-DIMENSIONAL ATTITUDE MOTION

In order to compare the BGM filter to the MEKF, both filters are applied to the one-dimensional attitude and angular velocity of a body. The state vector quantifying this motion is defined by

$$\boldsymbol{x} = \begin{bmatrix} \bar{\boldsymbol{q}} \\ \omega \end{bmatrix} \in \mathbb{S}^1 \times \mathbb{R}^1,$$

where $\bar{\boldsymbol{q}} \triangleq \begin{bmatrix} q_z & q \end{bmatrix}^T$ is the attitude quaternion quantifying the one-dimensional attitude of the body and ω is its angular velocity. Assume that no external torques act on the body, such that the equations-of-motion governing the temporal evolution of the state vector are given by

$$\dot{\boldsymbol{x}} = \begin{bmatrix} \dot{q}_z \\ \dot{q} \\ \dot{\omega} \end{bmatrix} = \begin{bmatrix} \frac{1}{2}\omega q \\ -\frac{1}{2}\omega q_z \\ 0 \end{bmatrix},$$

The initial state vector is taken to be Bingham-Gauss distributed with parameters defined by

$$\boldsymbol{m}_{\text{x},0} = 0$$
$$\boldsymbol{P}_{\text{x},0} = 0.1^2 \ (°/\text{s})^2$$

$$\boldsymbol{P}_{q,0} = \text{diag} \begin{bmatrix} 0.5 & 0.5 \end{bmatrix}$$

$$\boldsymbol{P}_{qx,0} = \boldsymbol{0}\,,$$

which represents an equiprobable initial attitude quaternion (that is, no prior attitude knowledge is present) that is uncorrelated with the angular velocity. This initial single-component BGM density is shown in Figure (8.1a), which illustrates that the initial density represents an equiprobable quaternion and a Gaussian-distributed angular velocity, as expected. It is not necessary to implement a multiple-component BGM density in this case to avoid potential discontinuity issues, as illustrated in Figure (3.11), even though the density wraps around the cylinder. This is because the attitude quaternion is equiprobable; thus, the single component BGM density is equal on both sides of the boundary defining the split.

Assume that a sensor on the body measures the inertial x-direction in its body frame every 60 seconds, beginning at $t = 0$, according to

$$z_k = \text{atan2}(y^B, x^B) + v_k\,, \tag{8.1}$$

where x^B and y^B are the inertial x- and y-directions expressed in the body frame, respectively, and v_k is wrapped-normal-distributed [9] noise with a standard deviation parameter of $3°$. The wrapped normal density for a scalar random variable is defined by

$$p_{wn}(\theta; \hat{\theta}, P) = \sum_{k=-\infty}^{\infty} p_g(\theta + 2\pi k; \hat{\theta}, P)\,, \tag{8.2}$$

where $\hat{\theta}$ and P represent the directional "mean" and "covariance" of the random variable θ, and the summation is truncated when $p_g(x + 2\pi k; m, P)$ is effectively zero in practical applications. Equation (8.2) shows that the wrapped normal density represents the Gaussian density wrapped infinitely around the unit circle, which is where the "wrapped normal" nomenclature derives. The vectors x^B and y^B are related to the attitude quaternion according to

$$\begin{bmatrix} x^B \\ y^B \end{bmatrix} = \begin{bmatrix} \cos\theta(\bar{\boldsymbol{q}}) & \sin\theta(\bar{\boldsymbol{q}}) \\ -\sin\theta(\bar{\boldsymbol{q}}) & \cos\theta(\bar{\boldsymbol{q}}) \end{bmatrix} \begin{bmatrix} 1 \\ 0 \end{bmatrix} = \begin{bmatrix} \cos\theta(\bar{\boldsymbol{q}}) \\ -\sin\theta(\bar{\boldsymbol{q}}) \end{bmatrix}\,, \tag{8.3}$$

where $\theta(\bar{\boldsymbol{q}})$ is the heading angle of the spacecraft parameterized by the attitude quaternion. Noting Eqs. (8.1) and (8.3), the measurement likelihood function is given by

$$p(z_k|\boldsymbol{x}_k) = p_{wn}(z_k; \text{atan2}(-\sin\theta(\bar{\boldsymbol{q}}_k), \cos\theta(\bar{\boldsymbol{q}}_k)), (3°)^2)\,,$$

(a) initial single-component Bingham-Gauss density

(b) corrected density at $t = 0$

(c) propagated density at $t = 60$ seconds

(d) corrected density at $t = 60$ seconds
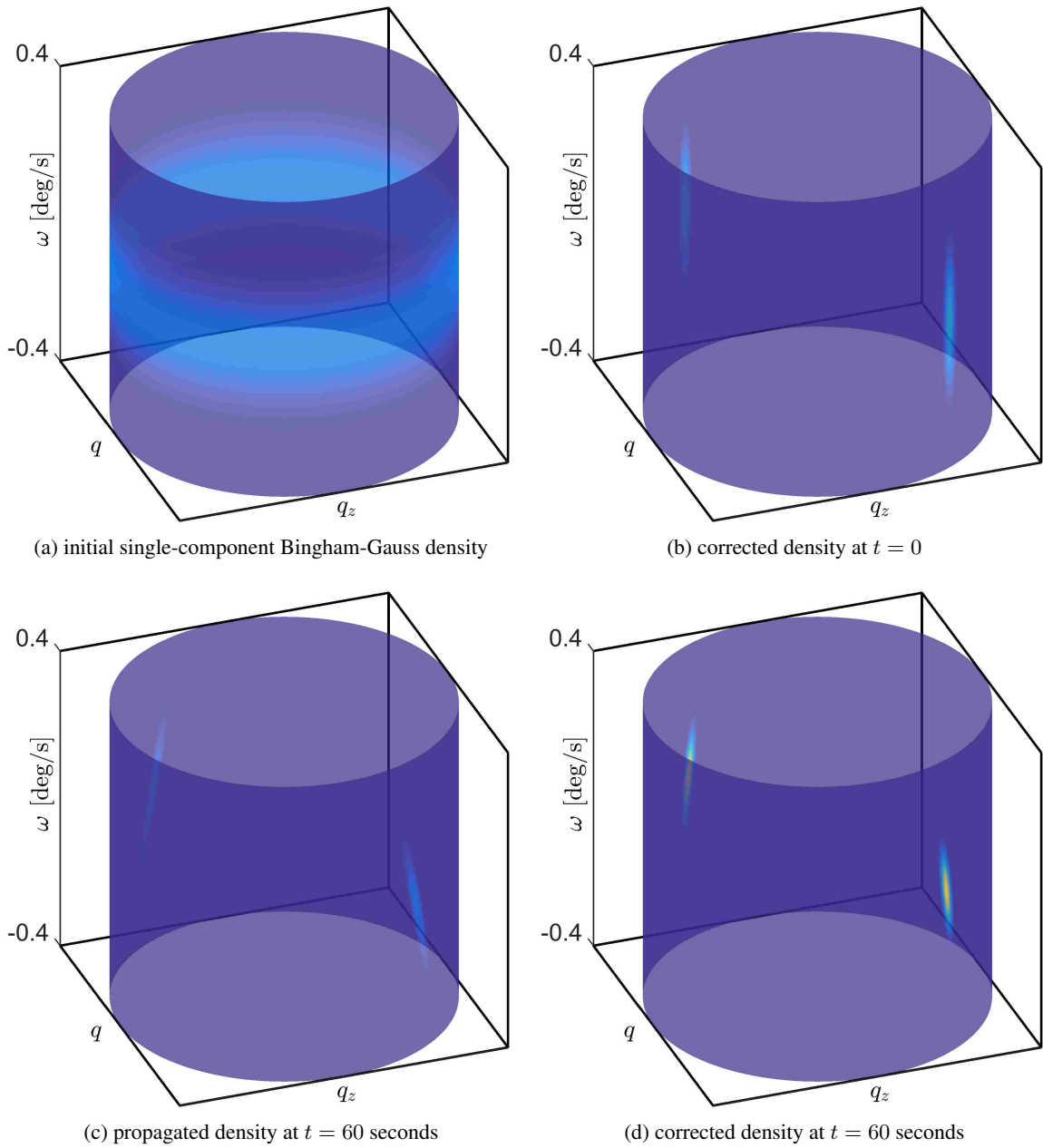
Figure 8.1. Single-component BGM density quantified by the BGM filter.

where special attention is payed to the units used and the summation is performed for $k = -1$ to $k = 1$ to ensure that the periodicity of the $\text{atan2}(-\sin\theta(\bar{\boldsymbol{q}}_k), \cos\theta(\bar{\boldsymbol{q}}_k))$ is effectively covered. If the measurement noise were larger, the summation could be truncated at a larger index; however, because the measurement noise is relatively small, $k = -1$ to $k = 1$ is sufficient because the probability of z_k is effectively zero when a distance of 2π away from the conditional mean, $\text{atan2}(-\sin\theta(\bar{\boldsymbol{q}}_k), \cos\theta(\bar{\boldsymbol{q}}_k))$.

The BGM filter is implemented in order to quantify the temporal and measurement evolution of the single-component BGM density and observe its performance. The quadrature weights and points used in the predictor of the BGM filter are generated using the unscented transform presented in Section 6.1. The unscented transform is first performed for the canonical Bingham-Gauss density (which is identical to the canonical Gauss-Bingham density), and the points are then transformed according to Eqs. (3.59) in order to represent a component of the BGM density. In order to generate the quadrature weights and points for the corrector of the BGM filter, the Monte Carlo sampling technique in Reference [74] is used for the Bingham portion of the BGM component and a standard technique is used to sample the Gaussian portion of the BGM component. $10,000$ Monte Carlo points are used in the corrector, which is found to provide sufficient accuracy.

The corrected density at $t = 0$, as well as the predicted and corrected densities at $t = 60$ seconds, are shown in Figure (8.1), along with the initial density. It is observed that, after the first measurement is processed at $t = 0$, the corrected density, which is shown in Figure (8.1b), is observed to have gained information in the attitude quaternion state, as expected due to the correlation between the bearing measurement and the attitude quaternion; however, no correlation between the attitude quaternion and the angular velocity exists, which is apparent because the density is not "tilted" on the cylinder. Furthermore, it is observed that the corrected density has evolved such that it is effectively zero along the splitting boundary between the two halves of the density. After the density is propagated forward in time for 60 seconds, the attitude quaternion and the angular velocity are correlated, as expected due to the dynamical relationship between these quantities. Another measurement is processed at $t = 60$ seconds to yield the corrected density at this time. It is observed that, after processing this measurement, the uncertainty in the attitude quaternion has decreased, as expected. Because the attitude quaternion and angular velocity are correlated before the corrector is applied, the measurement also decreases the uncertainty in the angular velocity as well. This trend will continue as the predictor/corrector recursion continues, which allows both the attitude quaternion and angular velocity to be estimated given measurements of the bearing of the vehicle.

In order to observe the performance of the BGM filter over a longer time span, the error in the heading angle representation and the angular velocity, as well as their covariance, are calculated over time by sampling the single-component BGM density $10,000$ times, The "average" quaternion

is then found according to Reference [53] and is assumed to be the estimated quaternion. The quaternion representation of the attitude error of each sample is then found and is subsequently converted to its corresponding heading angle. The error covariance of the heading angle and angular velocity are then found in order to calculate the 3σ intervals of error. The error in the heading angle representation and the angular velocity, as well as their covariance, are shown over time in Figure (8.2), alongside the same values as quantified by a multiplicative Kalman filter, which is implemented for comparison.

The multiplicative Kalman filter implemented is a quadrature-based multiplicative Kalman filter. In order to implement the multiplicative Kalman filter in as similar manner to the BGM filter as possible, the predictor of the MUKF, which uses the unscented transform, is implemented along with a Monte Carlo integration-based corrector. This corrector assumes that the error covariance quantified by the multiplicative Kalman filter represents a zero-mean Gaussian density in order to realize the Monte Carlo points in the error space necessary to implement Eq. (4.39). $10,000$ Monte Carlo points are used in this corrector as well to ensure the filters are compared on an equal basis. The initial estimated state and its error covariance are found for the MEKF by sampling the initial BGM density $10,000$ times, finding the average quaternion [53] and angular velocity, calculating the deviation of each sample expressed using the attitude quaternion, converting the deviations to the single-parameter space using the small angle assumption, and collecting the covariance of the deviations. The small angle assumption is used in this process because it is fundamental to the error representation used by a multiplicative Kalman filter.

Observation of Figure (8.2) shows that the estimated heading angle and angular velocity quantified by the BGM filter and multiplicative Kalman filter are very different initially, but converge to very similar solutions over time. The BGM filter is able to converge more quickly on its estimate, which is evident due to the fact that its 3σ interval is smaller than that of the multiplicative Kalman filter, and is most apparent in the zero to ten minute window. In order to check the statistical consistency of both filters, 100 Monte Carlo trials of each filter are run in order to calculate their Monte Carlo error covariance. The results of this Monte Carlo analysis are shown in Figures. (8.3) and (8.4) for the initial and long-term periods, respectively. Figure (8.3) shows that the BGM filter is more statistically consistent than the multiplicative Kalman filter during the initial period, which is when the attitude uncertainties are large. This is most apparent in the zero to one minute range, which is after the first measurement is processed. The single-run and Monte Carlo error covariance of the BGM filter are very close in this range; however, these quantities are not consistent for the multiplicative Kalman filter. It is also observed that the single-run error covariance of the multiplicative Kalman filter is typically smaller than its Monte Carlo error covariance, which is potentially troublesome because it reflects an overconfidence in the estimated state. Because the measurements are nonlinear functions of the state, measurement underweighting [75] can be implemented in order

(a) heading angle

(b) angular velocity
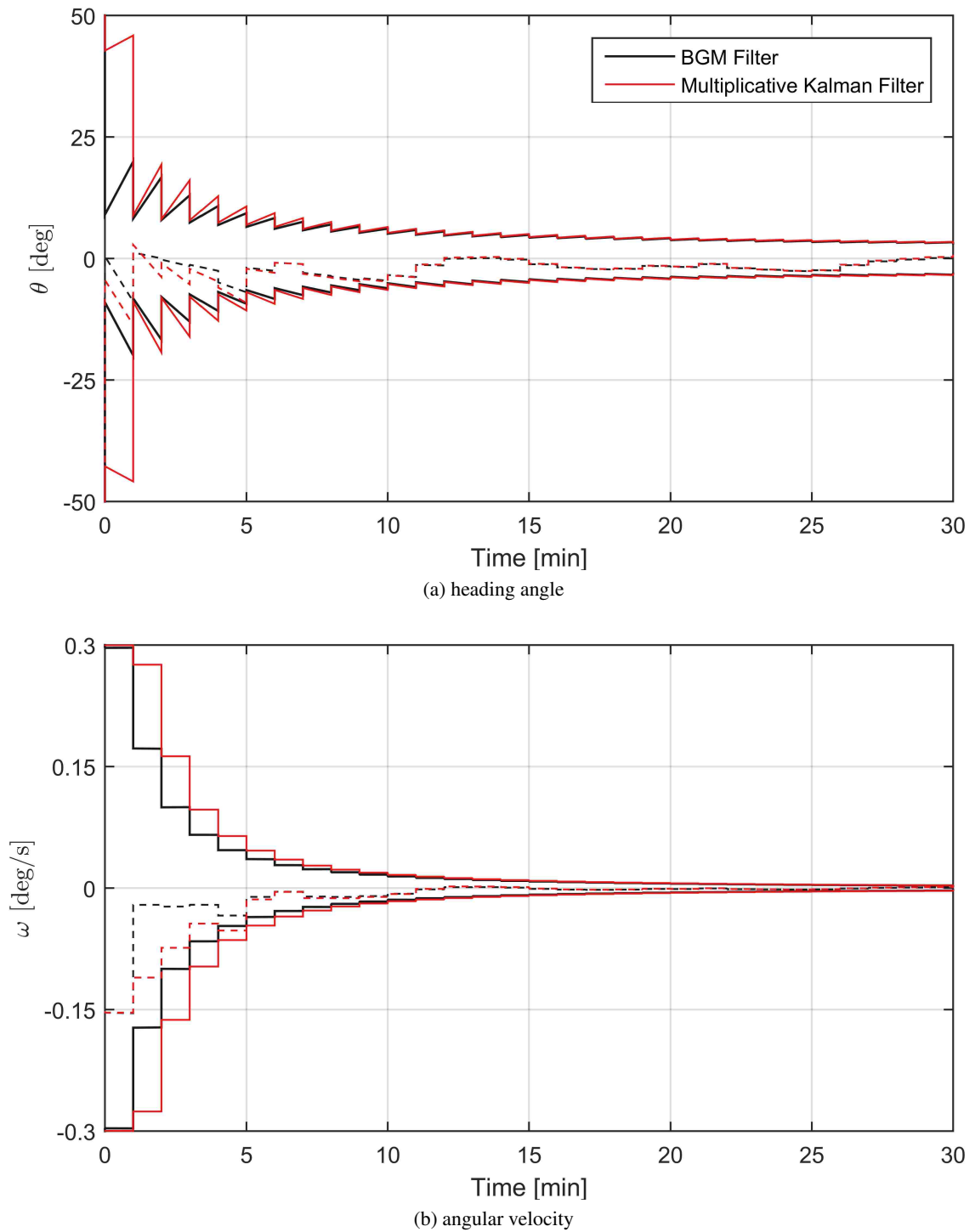
Figure 8.2. Error (dashed lines) and 3σ intervals (solid lines) of the BGM filter and the multiplicative Kalman filter.

to mitigate this over-convergence of the multiplicative Kalman filter when the attitude uncertainty is large with respect to the measurement uncertainty. In this case, the underweighting factor can be chosen in order to make the single-run error covariance of the multiplicative Kalman filter consistent with its Monte Carlo error covariance (which makes the multiplicative Kalman filter statistically consistent). In this case, the state error uncertainty quantified by the multiplicative Kalman filter is representative of the true state error uncertainty; however, this uncertainty is much larger than that of the BGM filter, which shows that the BGM filter more accurately estimates the state than the multiplicative Kalman filter does, even if measurement underweighting is implemented.

The single-run and Monte Carlo angular velocity error covariance are very similar after processing the first measurement at $t = 0$, but not after processing the second measurement at $t = 1$ minute; this is because no correlation is initially present between the attitude and angular velocity in either filter, and thus, no significant updates (only changes due to numeric artifacts) are applied to the angular velocity when processing the first measurement. After processing the first measurement, correlation between the attitude and angular velocity are quantified by both filters, and, therefore, the second measurement updates the angular velocity. The BGM filter quantifies this correlation more accurately, which is apparent because the single-run and Monte Carlo error covariances match very closely for the BGM filter, but not for the multiplicative Kalman filter, after the second measurement is processed. Figure (8.4) shows that the filters converge to the same, and statistically consistent, state estimates as time increases, which is expected because the attitude uncertainty becomes progressively smaller and the small uncertainty assumption of the multiplicative Kalman filter incurs less error.

8.2. PLANAR DYNAMIC POSE

Consider the two-dimensional relative orbit and one-dimensional attitude, which quantifies the planar dynamic pose, of an inspector spacecraft approaching a target spacecraft. In this case, the state vector representing the planar dynamic pose of the inspector spacecraft is given by

$$
\boldsymbol{x} = \begin{bmatrix} \bar{\boldsymbol{q}} \\ \mathbf{x} \end{bmatrix} = \begin{bmatrix} \bar{\boldsymbol{q}} \\ \boldsymbol{r} \\ \boldsymbol{v} \\ \omega \end{bmatrix} \in \mathbb{S}^1 \times \mathbb{R}^5 \,,
$$

where $\bar{\boldsymbol{q}} \triangleq [q_z \ q]^T$ is the attitude quaternion quantifying the one-dimensional attitude of the vehicle with respect to the Hill frame in which the relative motion of the inspector spacecraft is quantified [70], $\boldsymbol{r} \triangleq [r_x \ r_y]^T$ and $\boldsymbol{v} \triangleq [v_x \ v_y]^T$ are the relative position and velocity, respectively, of the

(a) vehicle heading angle

(b) angular velocity
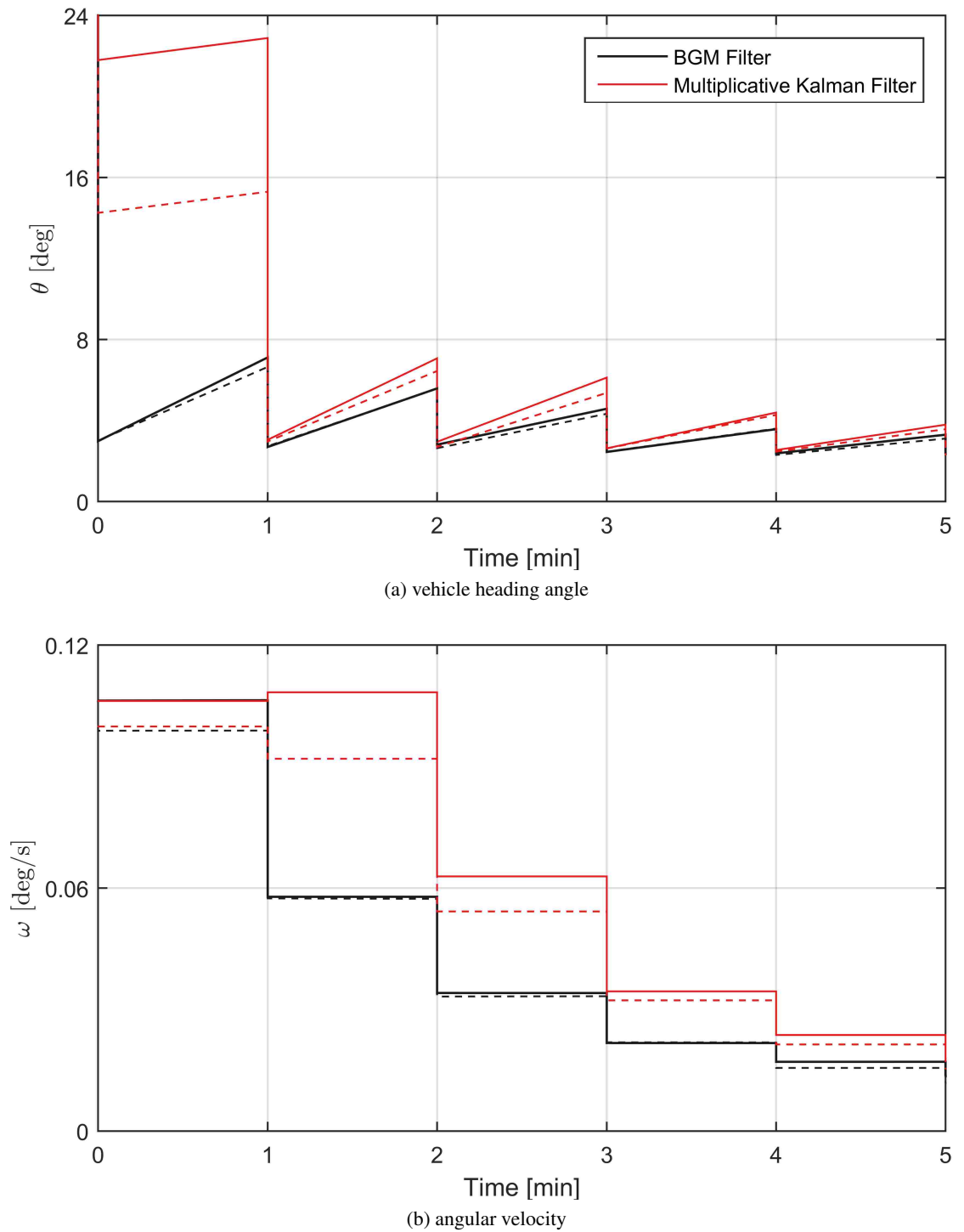
Figure 8.3. BGM filter and multiplicative Kalman filter initial period single-run (dashed lines) and Monte Carlo (solid lines) error standard deviation.

(a) vehicle heading angle
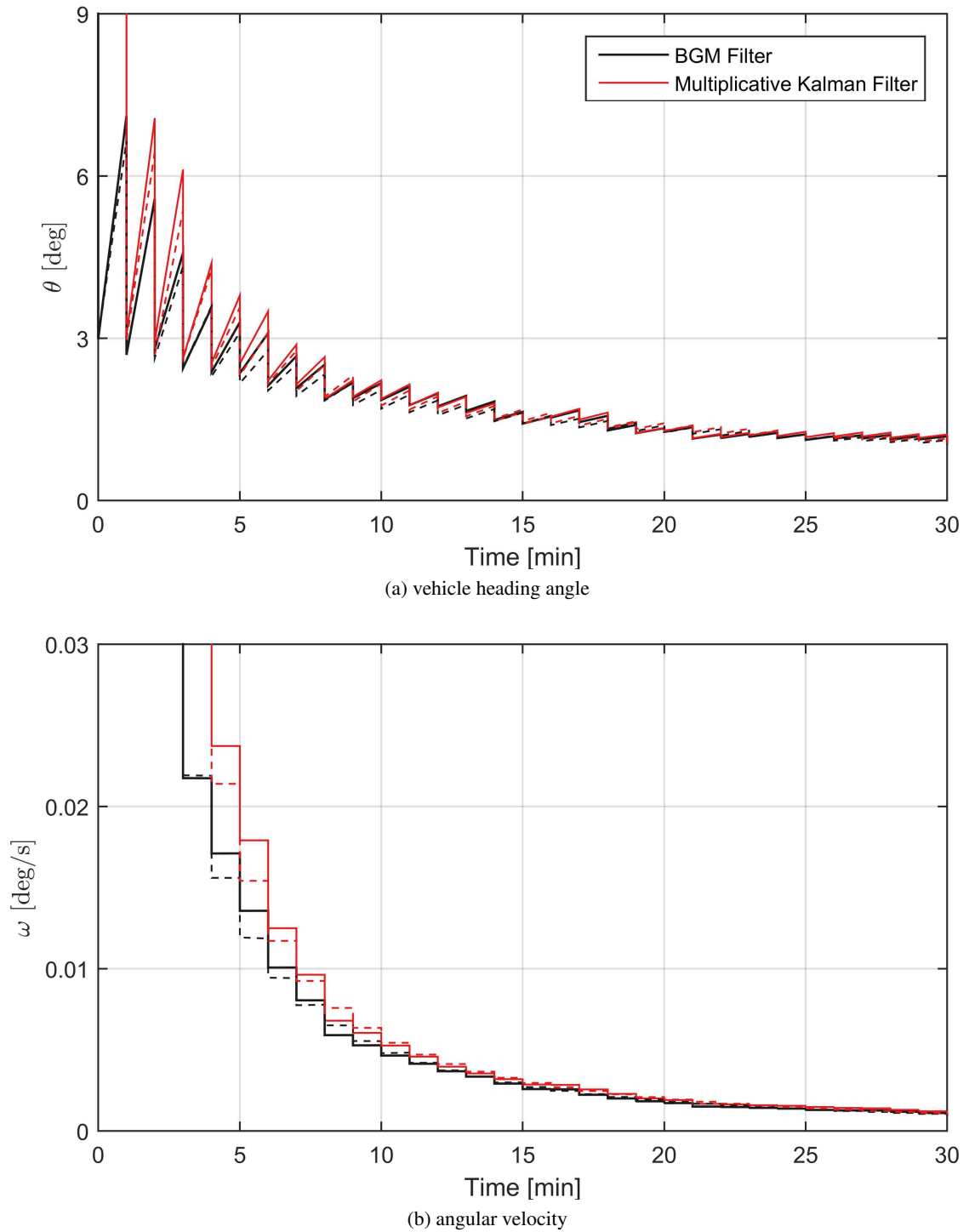
(b) angular velocity

Figure 8.4. BGM filter and multiplicative Kalman filter single-run (dashed lines) and Monte Carlo (solid lines) error standard deviation.

inspector spacecraft with respect to the chief spacecraft, and ω is the angular velocity of the space-craft with respect to the Hill frame. Assuming no external torques act on the inspector spacecraft, the target spacecraft is in a circular orbit Earth orbit of 500 km, and that only two-body gravitational acceleration acts on the spacecraft, the equations of motion governing the temporal evolution of the state vector are given by [5, 70]

$$\dot{\boldsymbol{x}} = \begin{bmatrix} \dot{q}_z \\ \dot{q} \\ \dot{r}_x \\ \dot{r}_y \\ \dot{v}_x \\ \dot{v}_y \\ \dot{\omega} \end{bmatrix} = \begin{bmatrix} \frac{1}{2}\omega q \\ -\frac{1}{2}\omega q_z \\ v_x \\ v_y \\ 2nv_y + 3n^2 r_x \\ -2nv_x \\ 0 \end{bmatrix},$$

where $n = 0.0634$ °/s is the mean motion of the target spacecraft. The initial state vector is taken to be Bingham-Gauss distributed with parameters defined by

$$\boldsymbol{m}_{\mathrm{x},0} = \begin{bmatrix} 0 & 1000 \text{ m} & 0.5534 \text{ m/s} & 0 & 0 \end{bmatrix}^T$$
$$\boldsymbol{P}_{\mathrm{x},0} = \mathrm{diag} \begin{bmatrix} 10^2 \text{ m}^2 & 10^2 \text{ m}^2 & 0.1^2 \text{ (m/s)}^2 & 0.1^2 \text{ (m/s)}^2 & 0.1^2 \text{ (°/s)}^2 \end{bmatrix}^T$$
$$\boldsymbol{P}_{q,0} = \mathrm{diag} \begin{bmatrix} 0.5 & 0.5 \end{bmatrix}$$
$$\boldsymbol{P}_{q\mathrm{x},0} = \boldsymbol{0},$$

which represents an equiprobable initial attitude quaternion (that is, no prior attitude knowledge is available) that is uncorrelated with the Gaussian states. The mean of the position and velocity define a two-by-one ellipse of the inspector spacecraft about the target spacecraft, and their uncertainty represents approximately what would be expected from a GPS solution of these quantities. The initial angular velocity of the inspector spacecraft is assumed zero-mean with a 0.1 °/s standard deviation.

Now, assume that the spacecraft no longer uses GPS to navigate and instead switches to a sensor that measures the range and angle in the spacecraft frame to the target spacecraft, located at the origin of the Hill frame, at a frequency of once per minute. This sensor measures the range and angle in the body frame from the inspector spacecraft to the target spacecraft according to

$$\boldsymbol{z}_k = \begin{bmatrix} \sqrt{r_x^{B2} + r_y^{B2}} + v_{1,k} \\ \mathrm{atan2}(r_y^B, r_x^B) + v_{2,k} \end{bmatrix},$$

where $v_{1,k}$ is zero mean Gaussian-distributed noise with a standard deviation of 3 m, and $v_{2,k}$ is wrapped-normal-distributed noise with a standard deviation parameter of $2°$. r_x^B and r_y^B represent the components of the position vector expressed in the spacecraft frame, which is related to the attitude quaternion and inertial position vector according to

$$\begin{bmatrix} r_x^B \\ r_y^B \end{bmatrix} = \begin{bmatrix} \cos\theta(\bar{q}) & \sin\theta(\bar{q}) \\ -\sin\theta(\bar{q}) & \cos\theta(\bar{q}) \end{bmatrix} \begin{bmatrix} r_x \\ r_y \end{bmatrix},$$

where $\theta(\bar{q})$ is the heading angle of the spacecraft parameterized by the attitude quaternion, which shows that the attitude measurement depends not only on the attitude quaternion but also on the relative position of the inspector spacecraft.

Two BGM filters are implemented in order to observe and compare their performance. The first filter is the BGM filter operating on the initial Bingham-Gauss density, which is a single component BGM density, directly. The second filter is the BGM filter which is initialized with BGM density that approximates the initial Bingham-Gauss density with 11 components in the Bingham portion of the density, 11 components in the position channels of the Gaussian density, and a single component in the velocity and angular velocity channels of the Gaussian density. A ζ value of -22, which defines the size of the Bingham components in the Bingham-Gauss mixture according to Eq. (3.45), is found to provide acceptably small Bingham components without incurring unacceptably large approximation error. The Bingham portion of the density and the position channels of the Gaussian portion of the density are approximated with mixtures because they are the states on which the measurements directly depend; by using mixtures in these states, fewer points can be used in the necessary quadrature approximations since the components of the mixture are smaller than the single component that they approximate.

In order to generate the quadrature weights and points for the predictor of the BGM filter, the unscented transform presented in Section 6.1 is used. In order to generate the quadrature weights and points for the corrector of the BGM filter, the Monte Carlo sampling technique in Reference [74] is used for the Bingham portion of the BGM component, and a standard technique is used to sample the Gaussian portion of the BGM component. Both the unscented transform and the Monte Carlo techniques are used to sample the canonical Bingham-Gauss density (while ensuring that only samples in $\mathbb{S}^{1+}$ are generated), and then the samples are converted to the desired Bingham-Gauss density according to Eqs. (3.59). $100,000$ samples are used in the Monte Carlo integration for the corrector of the single-component BGM filter, and $1,000$ samples per component are used for the multiple-component filter. Components are removed from the mixture if their weights are smaller than 10^{-12}. In order to quantify the uncertainty represented by each filter, each BGM density is sampled at the prior and posterior of each time step $10,000$ times, the error of each sample is calculated, the attitude error portion of the samples is converted to the heading angle representation

of the attitude error, and the 3σ intervals of the heading angle, relative position, relative velocity, and angular velocity are calculated.

The results of both filters are shown for the first 20 minutes of the simulation in Figure (8.5) in order to observe their transient performance. It is observed that the performance of both filters is similar, with the apparent small differences between the filters due to a few reasons. First of all, the error incurred in the approximation of the integrals used in the correctors between the filters is slightly different since the single component filter uses $100,000$ points in the integral approximation, and the mixture filter uses $1,000$ points per component in the integral approximation. While the overall computational effort required by both filters is roughly the same at the beginning of the simulation, fewer points are required for the integral approximation in each component by the mixture filter. As the simulation progresses and components that do not maintain sufficient agreement with the measurement data are trimmed, the mixture filter requires less computation than the single component filter. Second, the BGM filter is capable of quantifying non-Bingham-Gauss densities, which typically occur due to nonlinear system dynamics and/or measurements. The single component filter makes the best Bingham-Gauss approximation (in the KL sense) of these non-Bingham-Gauss densities, which, in general, will incur more approximation error in quantifying the true state density than the mixture filter will. Finally, sampling the densities to discretely calculate the error and 3σ intervals of the single component and mixture densities quantified by the filter introduces some error in these values as well. This sampling to calculate these values is only used for a straightforward visualization of the filter performance; it is *not* integral to the BGM filter. The initial disagreement in the attitude state between the filters is an artifact of this sampling because the initial attitude quaternion is equiprobable. Because of this, the estimated attitude quaternion quantified by this sampling technique is arbitrary and therefore is not meaningful. After measurement data is incorporated into the filters, the attitude error and its 3σ interval are very similar.

Figure (8.6) show the errors and 3σ intervals of the filters for 150 minutes in order to observe their steady state behaviors. Both filters perform very similarly to each other over this time interval as well, with slight differences between the filters due to the aforementioned reasons in the discussion of Figure (8.5). It is interesting to note that, during the beginning of the simulation, when the uncertainty in the relative position of the inspector spacecraft is still high, the attitude uncertainty remains relatively high as well. This is because the angle to the target spacecraft measured by the inspector spacecraft in the body frame depends on the relative position of the inspector spacecraft. Because of this, as the uncertainty in the relative position of the inspector spacecraft decreases, the attitude uncertainty decreases as well. It is also interesting to note that, during the beginning of the simulation, the uncertainty in the relative position is exchanged between the r_x and r_y over time. This is because range measurements between the spacecraft are taken, and measurement information can only be gained into the position density in the direction of this range. As the range

Figure 8.5. Error (dashed lines) and 3σ interval (solid lines) after initialization for the single-component (red) and multiple-component (black) BGM filters.

direction changes, this causes the uncertainty in r_x and r_y to grow and shrink at different times. After sufficient time, the measurement data incorporated into the state density, which is constrained in time by the system dynamics, cause the uncertainty in both r_x and r_y to decrease, as is observed in Figure (8.6).

8.3. INERTIAL MEASUREMENT UNIT-BASED DYNAMIC POSE ESTIMATION

Consider the case when a small spacecraft in low-Earth orbit uses an inertial measurement unit (IMU), magnetometer, and GPS receiver to determine its dynamic pose. The IMU measures the angular velocity and non-gravitational acceleration of the spacecraft, which are used to propagate the state (and its uncertainty) forward in time. The GPS receiver is assumed to provide direct measurements of the spacecraft's position, which is ultimately obtained from processing the pseudorange measurements to the GPS spacecraft in view. The magnetometer measures the Earth's magnetic field over time to resolve the three-dimensional attitude of the spacecraft. The measurements of the Earth's magnetic field provide information about the direction of the magnetic field, but do not provide any information regarding the rotation about the axis defined by this direction. If a magnetometer measurement is taken at a single time, the attitude of the spacecraft is unobservable because the rotation of the spacecraft about the magnetic field direction cannot be resolved; however, taking measurements of the Earth's magnetic field over time can resolve this ambiguity because the attitude of the spacecraft over time is constrained according to its dynamic model. By measuring the angular velocity (and non-gravitational acceleration) of the vehicle and using these measurements to propagate the probabilistic state of the vehicle through time, a three-axis attitude solution of the spacecraft can typically be obtained.

The state vector of the spacecraft is defined to be

$$
\boldsymbol{x} = \begin{bmatrix} \bar{\boldsymbol{q}} \\ \boldsymbol{r} \\ \boldsymbol{v} \end{bmatrix} \in \mathbb{S}^3 \times \mathbb{R}^6 \, ,
$$

where $\bar{\boldsymbol{q}}$ represents the attitude quaternion defining the attitude of the spacecraft, which is defined as the rotation from the Earth-centered inertial (ECI) coordinate-frame to the spacecraft body frame, and $\boldsymbol{r}$ and $\boldsymbol{v}$ are defined to be the position and velocity of the spacecraft, respectively, which are expressed in the ECI frame. The angular velocity is not included in the state vector, even though it is typically part of the state vector quantifying dynamic pose, because it is measured by the IMU. If a model-based approach (as opposed to the IMU-based approach) were used, then it would be necessary to include the angular velocity in the state vector.
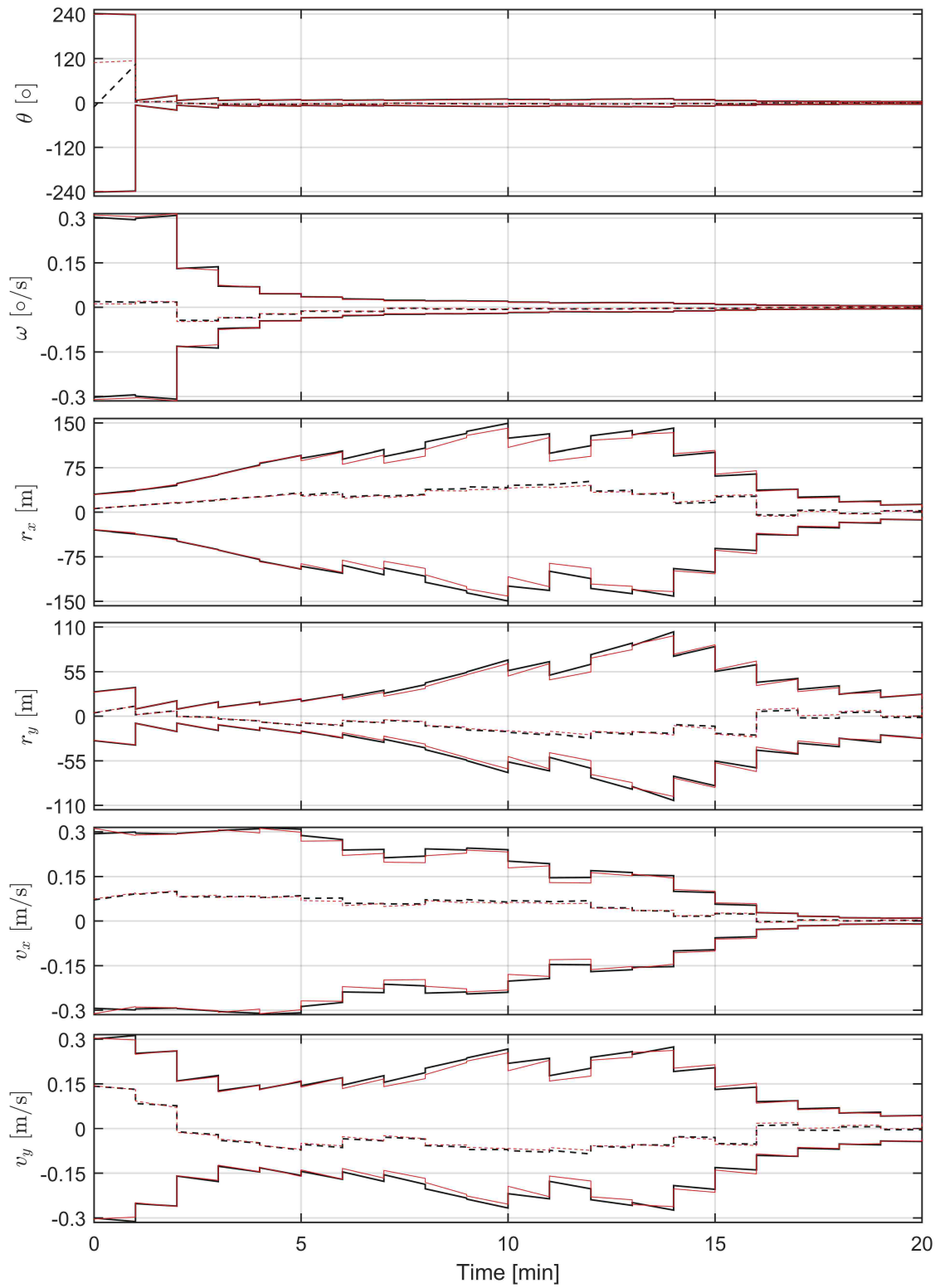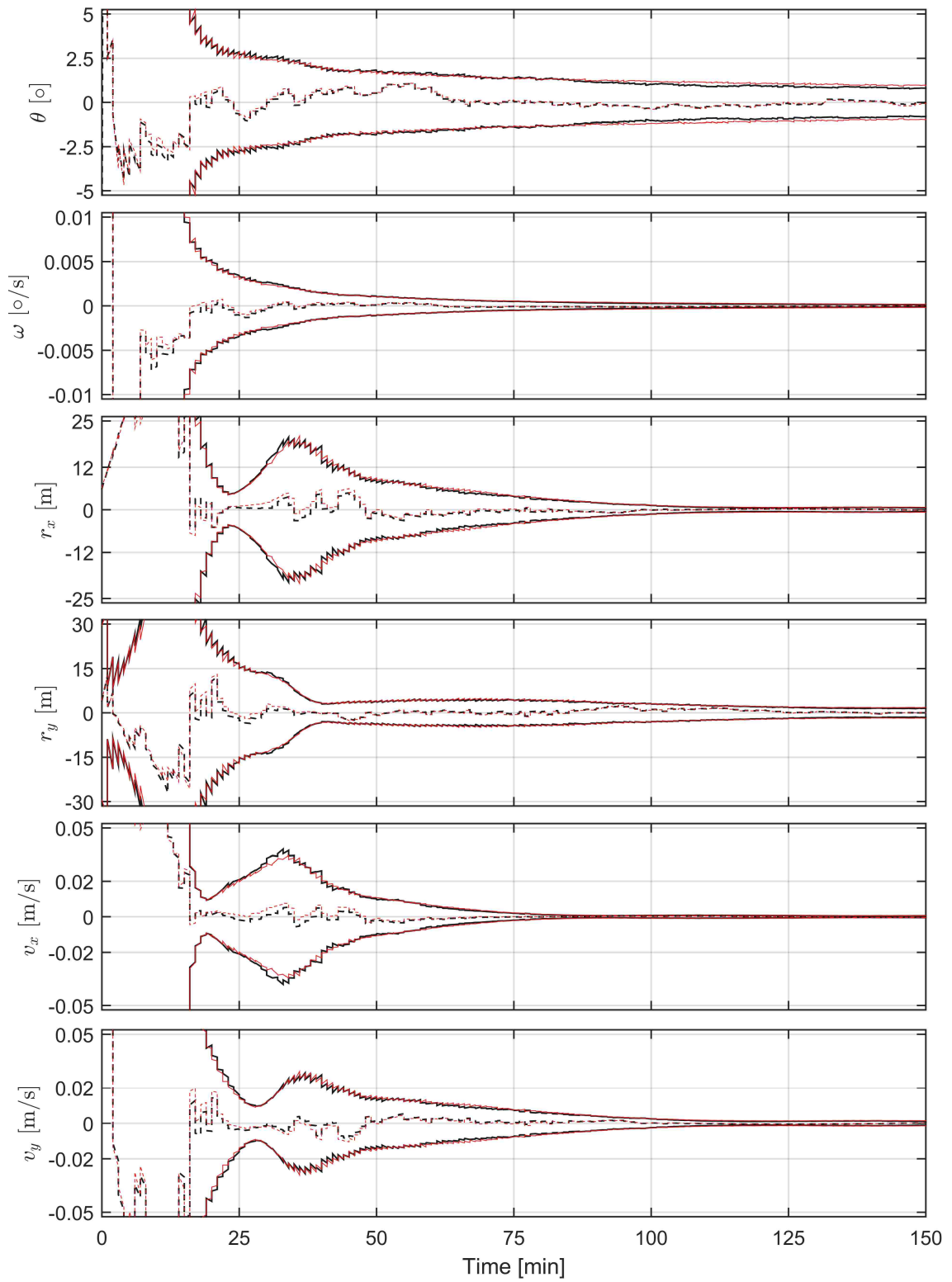
Figure 8.6. Error (dashed lines) and 3σ interval (solid lines) after initialization for the single-component (red) and multiple-component (black) BGM filters.

The measurements of the angular velocity and acceleration of the spacecraft, which are provided by the three-axis gyroscope and accelerometer within the IMU, are assumed to be corrupted only by zero-mean white noise which produces a measurement of the angular velocity and acceleration of the vehicle discretely at time t_k according to

$$\boldsymbol{\omega}_{m,k} = \boldsymbol{\omega}_k + \boldsymbol{w}_{g,k} \tag{8.4}$$

$$\boldsymbol{a}_{m,k} = \boldsymbol{a}_{ng,k} + \boldsymbol{w}_{a,k} \,. \tag{8.5}$$

In the gyroscope model, $\boldsymbol{\omega}_{m,k}$ is the measured angular velocity from the gyroscope, $\boldsymbol{\omega}_k$ is the true angular velocity of the vehicle, and $\boldsymbol{w}_{g,k}$ is a zero-mean, Gaussian-distributed, white-noise sequence of covariance $\boldsymbol{Q}_{g,k}$. In the accelerometer model, $\boldsymbol{a}_{m,k}$ is the measured non-gravitational acceleration from the accelerometer, $\boldsymbol{a}_{ng,k}$ is the true acceleration acting on the spacecraft that is *not* due to gravity, and $\boldsymbol{w}_{a,k}$ is a zero-mean, Gaussian-distributed, white-noise sequence of covariance $\boldsymbol{Q}_{a,k}$. The covariances of the white-noise sequences in the IMU model are chosen to model the Epson M-G364[1] IMU. The relevant specifications from this IMU are summarized in Table 8.1. These IMU specifications are converted into the covariances of the underlying white-noise sequences according to [76]

$$\boldsymbol{Q}_{g,k} = \left[\frac{0.09\frac{\circ}{\sqrt{hr}}}{\sqrt{\Delta t_k}}\right]^2 \boldsymbol{I}_3 \quad = \left[\frac{0.0015\frac{\circ}{\sqrt{s}}}{\sqrt{\Delta t_k}}\right]^2 \boldsymbol{I}_3$$

$$\boldsymbol{Q}_{a,k} = \left[\frac{0.025\frac{m/s}{\sqrt{hr}}}{\sqrt{\Delta t_k}}\right]^2 \boldsymbol{I}_3 \quad = \left[\frac{4.167 \times 10^{-4}\frac{m/s}{\sqrt{s}}}{\sqrt{\Delta t_k}}\right]^2 \boldsymbol{I}_3 \,,$$

where $\Delta t_k = t_k - t_{k-1}$ is the sampling time of the IMU and $\boldsymbol{I}_3$ represents the identity matrix of dimension three. The IMU is assumed to provide measurements of the acceleration and angular velocity at a frequency of 10 Hz, which defines Δt_k as 0.1 s.

Table 8.1. Specifications for the Epson M-G364 IMU.

Angular Random Walk	$0.09\frac{\circ}{\sqrt{hr}}$
Velocity Random Walk	$0.025\frac{m/s}{\sqrt{hr}}$

A three-axis magnetometer is used to measure the Earth's magnetic field vector expressed in the spacecraft's body frame (which is assumed coincident with the magnetometer frame) at a frequency of 0.5 Hz. This magnetic field measurement is assumed to be corrupted by zero mean,

---

[1]http://global.epson.com/products_and_drivers/sensing_system/imu/g364/

Gaussian-distributed noise according to

$$\boldsymbol{z}_{B,k} = \boldsymbol{T}(\bar{\boldsymbol{q}}_k)\boldsymbol{B}_k(\boldsymbol{r}_k) + \boldsymbol{v}_{B,k}\,,$$

where $\boldsymbol{B}_k(\boldsymbol{r}_k)$ represents the Earth's magnetic field vector expressed in the ECI frame, which is functionally dependent on the position of the spacecraft, $\boldsymbol{T}(\bar{\boldsymbol{q}}_k)$ represents the attitude matrix parameterized by the attitude quaternion, and $\boldsymbol{v}_{B,k}$ is zero-mean, Gaussian-distributed noise with covariance matrix defined by

$$\boldsymbol{R}_{B,k} = (1667\text{ nT})^2\boldsymbol{I}_3\,,$$

which is chosen to model the Billingsley TFM100G2 magnetometer[2]. The magnetic field vector, $\boldsymbol{B}_k(\boldsymbol{r}_k)$, is calculated from the 2015 World Magnetic Model[3] [77] for both the filter and the measurement synthesis. A transformation between the ECI and Earth-centered Earth-fixed (ECEF) coordinate frames [78] is used to express the magnetic field vector in the ECI frame. The simulation is assumed to start at 19:00 UTC on October 19th, 2016, which defines the secular effects in the World Magnetic Model and the orientation of the ECEF frame with respect to the ECI frame.

A GPS receiver is assumed to provide measurements of the position of the spacecraft at a frequency of 0.5 Hz, and at the same times as the magnetometer, according to

$$\boldsymbol{z}_{r,k} = \boldsymbol{r}_k + \boldsymbol{v}_{r,k}\,,$$

where $\boldsymbol{v}_{r,k}$ is zero-mean, Gaussian-distributed noise that is independent of $\boldsymbol{v}_{B,k}$ with covariance matrix defined by

$$\boldsymbol{R}_{r,k} = (10\text{ m})^2\boldsymbol{I}_3\,.$$

This position measurement assumes that the measured pseudoranges between the spacecraft and the GPS spacecraft in view of the GPS antenna are preprocessed to provide a "measurement" of the position of the spacecraft. These pseudoranges can be processed into the BGM directly instead of processing the resolved position "measurement," if desired. The resolved position measurement is processed in this application, since the motivation is to show the applicability of the single-component BGM filter to estimate the dynamic pose of a spacecraft and not to analyze different methods of processing GPS data. The position measurements are generated by adding Gaussian-distributed noise to the true position of the spacecraft. Noting the measurement models for the

---

[2]http://magnetometer.com/products/fluxgate-magnetometers/tfm100g2/

[3]MATLAB's implementation of the 2015 World Magnetic Model, "wrldmag," was used in this analysis.

magnetometer and GPS receiver, the measurement likelihood is given by

$$p(\boldsymbol{z}_k|\boldsymbol{x}_k) = p_g(\boldsymbol{z}_{B,k}; \boldsymbol{T}(\bar{\boldsymbol{q}}_k)\boldsymbol{B}_k(\boldsymbol{r}_k), \boldsymbol{R}_{B,k})p_g(\boldsymbol{z}_{r,k}; \boldsymbol{r}_k, \boldsymbol{R}_{r,k}),$$

where $\boldsymbol{z}_k \triangleq [\boldsymbol{z}_{B,k}^T \ \ \boldsymbol{z}_{r,k}^T]^T$.

Assume that an initial single-component BGM density probabilistically represents the attitude quaternion and gyroscope bias according to

$$\boldsymbol{m}_{\mathrm{x},0} = \left[6878.137 \text{ km} \quad 0 \quad 0 \quad 0 \quad 6.59 \text{ km/s} \quad 3.81 \text{ km/s}\right]^T$$

$$\boldsymbol{P}_{\mathrm{x},0} = \mathrm{diag} \left[20^2 \text{ m}^2 \quad 20^2 \text{ m}^2 \quad 20^2 \text{ m}^2 \quad 0.1^2 \text{ (m/s)}^2 \quad 0.1^2 \text{ (m/s)}^2 \quad 0.1^2 \text{ (m/s)}^2\right]^T$$

$$\boldsymbol{P}_{q,0} = \mathrm{diag} \left[0.001 \quad 0.001 \quad 0.001 \quad 0.997\right]$$

$$\boldsymbol{P}_{q\mathrm{x},0} = \boldsymbol{0},$$

where $\boldsymbol{m}_{\mathrm{x},0}$ corresponds to a 500 km altitude circular orbit inclined at $30°$ and $\boldsymbol{P}_{q,0}$ corresponds to a most-likely quaternion of $[0 \ \ 0 \ \ 0 \ \ 1]^T$ and an approximate $10°$ 3σ interval along each of the body axes. The BGM filter is used to quantify the temporal and measurement evolution of this single-component BGM density.

The predictor of the BGM filter uses the unscented transform presented in Section 6.1 to generate the quadrature weights and points. Each predictor step of the BGM filter augments the state vector with the process noise corrupting the angular velocity and acceleration measurements from the IMU, according to Eqs. (8.4), in order to quantify its effect on the temporal evolution of the parameters. Furthermore, the predictor runs at a frequency of 10 Hz, the same frequency that the IMU returns measurements of the angular velocity of the spacecraft. In order to reduce the error present in the single-component BGM filter that accumulates due to the repeated approximations of the true state density at each step in the Bayesian recursion, artificial process noise is added to the accelerometer measurement model used by the filter according to

$$\boldsymbol{a}_{m,k} = \boldsymbol{a}_{ng,k} + \boldsymbol{w}_{a,k} + \boldsymbol{w}_{tune,k}, \tag{8.6}$$

where $\boldsymbol{w}_{tune,k}$ is zero-mean, Gaussian-distributed process noise of covariance

$$\boldsymbol{Q}_{tune,k} = 0.001\frac{(m/s^2)^2}{s}\Delta t_k \boldsymbol{I}.$$

This level of "tuning" process noise is found to provide a stable filter without over convergence over time due to approximation error.

The corrector of the BGM filter uses the Monte Carlo sampling technique in Reference [74] for the Bingham portion of the BGM component, and a standard sampling technique for the Gaussian portion of the BGM component in order to generate the quadrature weights and points. Both the unscented transform and the Monte Carlo techniques are used to sample the canonical Bingham-Gauss density (while ensuring that only samples in $\mathbb{S}^{3+}$ are generated), and then the samples are converted to the desired Bingham-Gauss density according to Eqs. (3.59). $100,000$ samples are used in the Monte Carlo integration for the corrector of the single-component BGM filter.

In order to quantify the uncertainty represented by each filter, each BGM density is sampled at the prior and posterior of each time step $100,000$ times, the error of each sample is calculated, the attitude error portion of the samples is converted to the heading angle representation of the attitude error, and the 3σ intervals of the attitude, position, and velocity error are calculated.

The true initial attitude, position, and velocity are realized from the initial single-component BGM density. The initial angular velocity of the spacecraft is taken to be

$$\boldsymbol{\omega}_0 = \begin{bmatrix} 1^\circ \\ 0 \\ 0 \end{bmatrix},$$

and the spacecraft is assumed to have an identity inertia tensor and undergo torque-free motion. The true orbit of the spacecraft is propagated according to two-body dynamics.

The performance of the single-component BGM filter is shown in Figures (8.7)–(8.9) for the attitude, position, and velocity error, respectively. It is observed that the attitude uncertainty about the body-fixed x-axis decreases more quickly than the attitude uncertainty about the body-fixed y- and z-axes, which occurs because the spacecraft is rotating about the x-axis. Furthermore, it is observed that the uncertainty in the y- and z-axes of the attitude error fluctuates between the axes, as expected since the magnitude of the magnetic field in these directions fluctuates between these axes. Because of this, the amount of information incorporated into each of these axes fluctuates, and, thus, the 3σ intervals of these axes fluctuate. As time increases, the attitude uncertainty decreases even though it still fluctuates about the y- and z-axes, which is expected since more attitude information is incorporated into the filter as time increases.

The position uncertainty decreases quickly to reach a steady-state value along all three axes, as is observed in Figure (8.8). This is expected because linear measurements of the position are processed by the filter. The position error remains inside its 3σ interval (which is a good heuristic to determine whether a filter is performing well), with the exception of a brief time interval just after five minutes along the x-component of velocity. This is likely due to a specific sequence of position measurements that occur, because the error quickly reenters its 3σ interval and remains there throughout the simulation. The velocity uncertainty also decreases to reach a steady-state
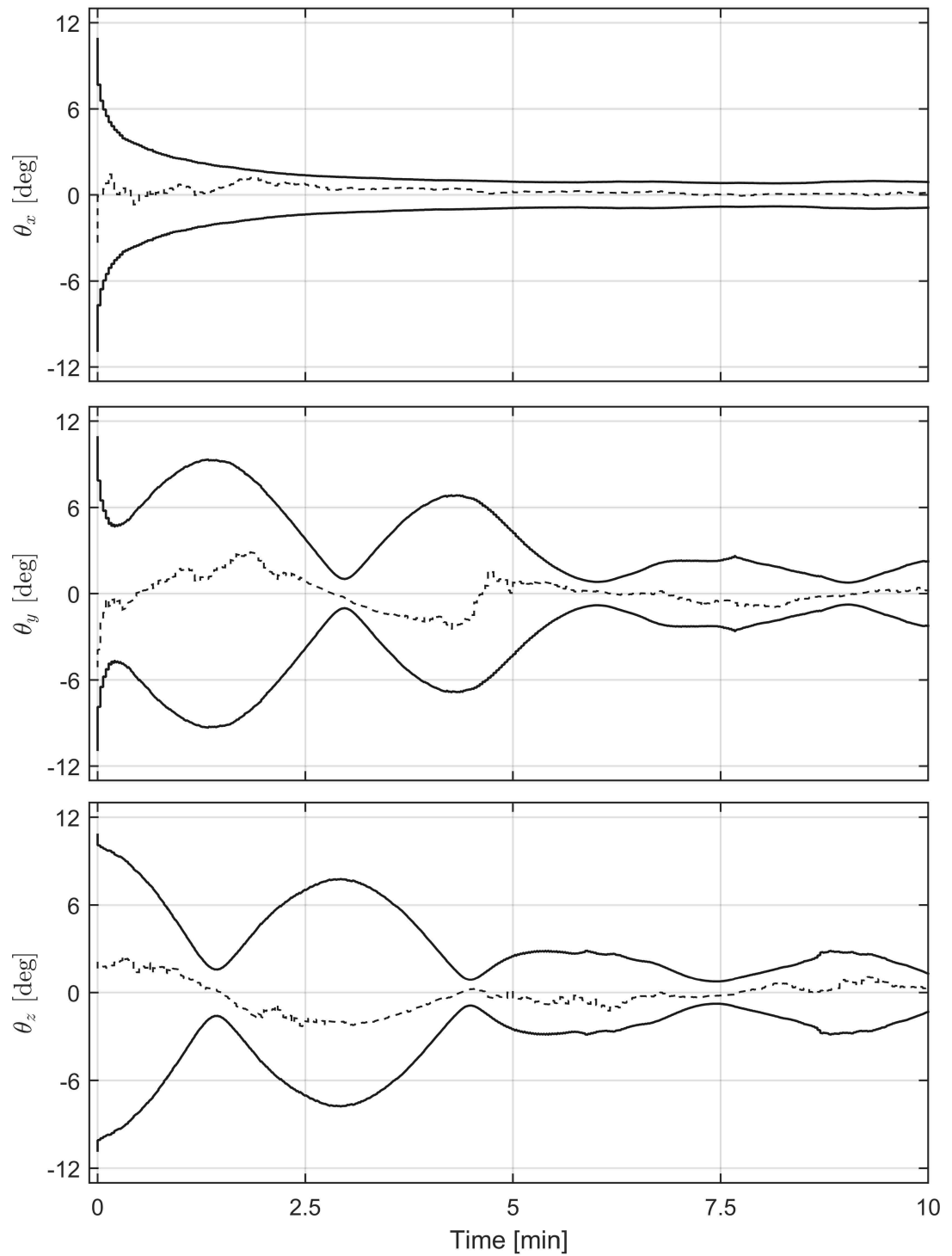
Figure 8.7. Attitude error (dashed lines) and 3σ interval (solid lines) for the single-component BGM filter.

value along all three axes, as is observed in Figure (8.9). This is also expected due to the time-wise correlation between position and velocity and the linear position measurements.

Ideally, a multiple-component BGM filter could be applied to this scenario, in which little or no tuning process noise, as defined by Eq. (8.6), would be necessary to prevent over convergence of the filter due to the accumulation of error due to the repeated approximations of the true state density at each step in the Bayesian recursion. Less error is incurred when using a multiple-component BGM density to quantify the state vector when compared to a single-component BGM density, which is equivalent to the Bingham-Gauss density. This is because the error incurred in the approximation of the true state density at each step in the Bayesian recursion by a Bingham-Gauss mixture density decreases as the uncertainty in each component of the mixture becomes smaller, or equivalently, the number of components in the mixture increases. This becomes computationally infeasible for this application, however, since the approximating mixture would have to be constructed in nine dimensions, which becomes computationally demanding due to the curse of dimensionality. If three, five, and seven components per dimension are used to construct the mixture, $19,683$, $1,953,125$, and $40,353,607$ components exist in the BGM mixture. The inclusion of the tuning process noise added to the single-component BGM filter causes a mismatch between the true dynamical system and the modeled dynamical system for the filter; however, its inclusion results in a computationally feasible filter capable of quantifying the dynamic pose of the spacecraft in this scenario.
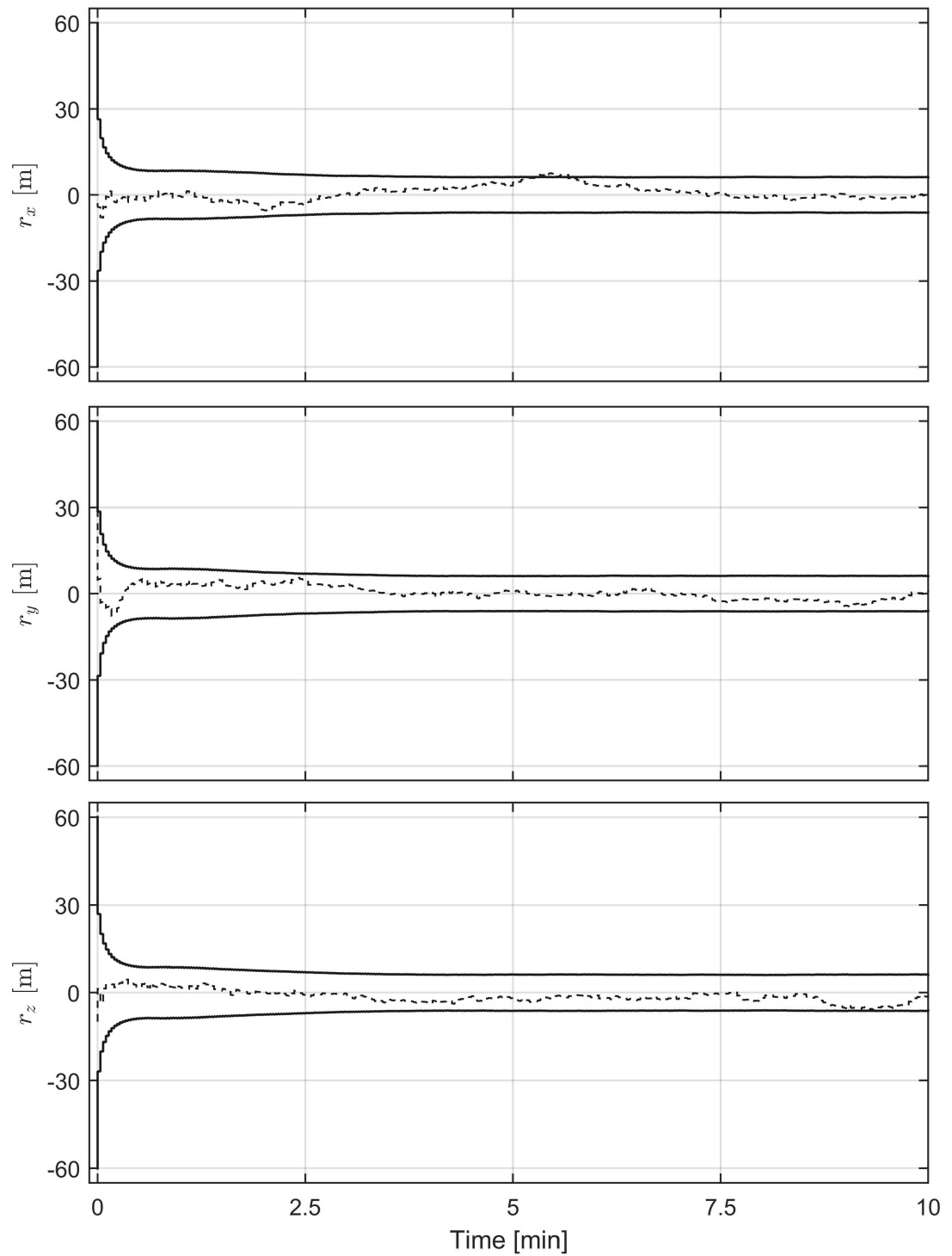
Figure 8.8. Position error (dashed lines) and 3σ interval (solid lines) for the single-component BGM filter.
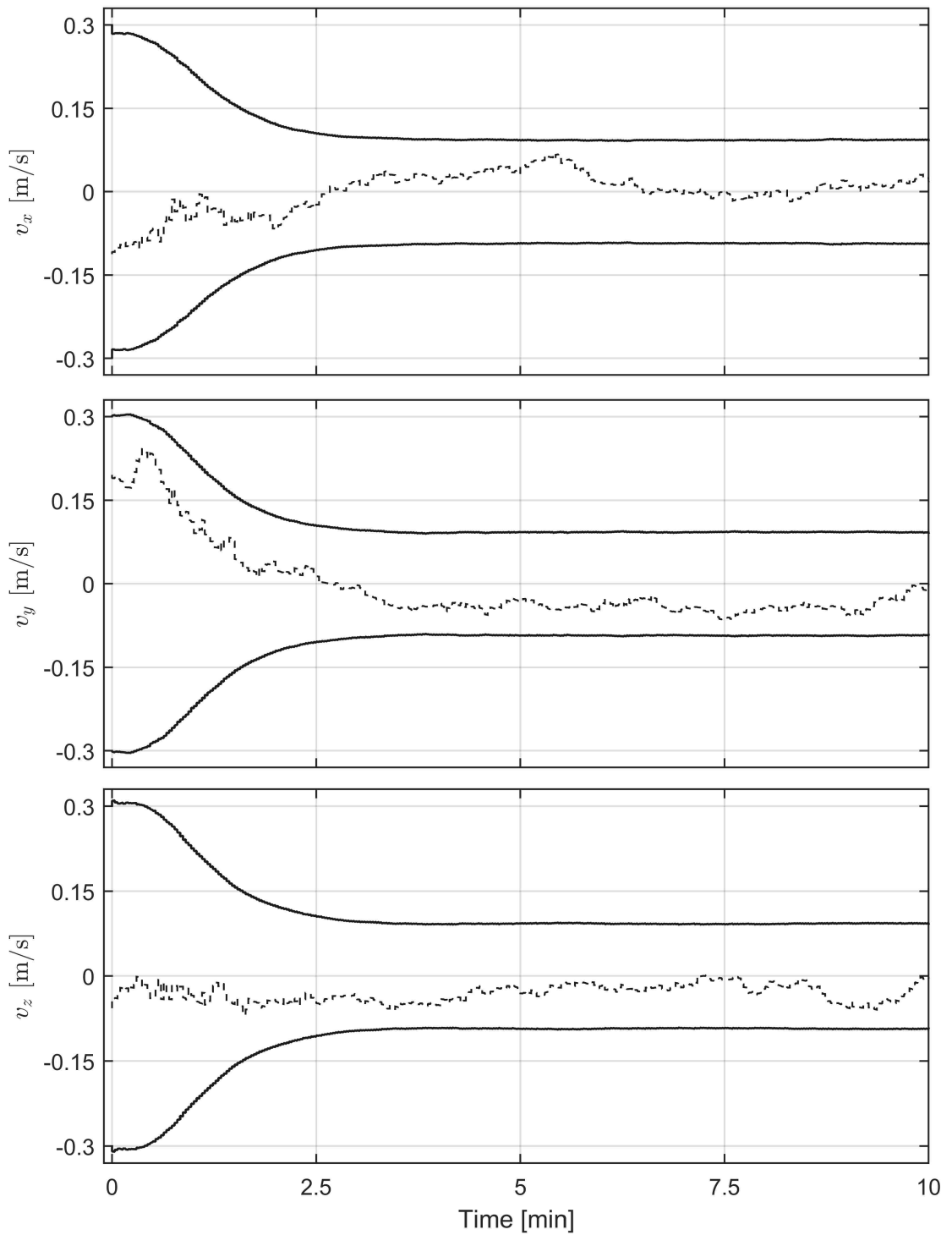
Figure 8.9. Velocity error (dashed lines) and 3σ interval (solid lines) for the single-component BGM filter.

9. CONCLUSIONS

Two new probability density functions (pdfs) were developed, termed the Gauss-Bingham and Bingham-Gauss mixture (BGM) densities, that probabilistically represent a state vector consisting of an attitude quaternion and other Euclidean states. When the state vector consists of the attitude quaternion, position, velocity, and angular velocity of a body, its dynamic pose is probabilistically quantified by these pdfs. The Gauss-Bingham and BGM densities quantify the state vector on its natural manifold, the unit-hypercylinder, and therefore, no small angle assumption is necessary to project the uncertainty in the attitude quaternion portion of the state vector into an approximately additive three-parameter attitude space, as is done by the multiplicative quaternion error representation used by the multiplicative extended Kalman filter (MEKF). An unscented transform-based uncertainty propagation scheme was developed for the Gauss-Bingham density, which quantifies the temporal evolution of the density given a (potentially) nonlinear dynamical system. This uncertainty propagation scheme was shown to quantify the uncertainty in the dynamic pose state vector more accurately than the uncertainty propagation scheme employed by the MEKF, which requires a small attitude uncertainty assumption. Because of this, the increased accuracy of the Gauss-Bingham uncertainty propagation scheme as compared to that of the MEKF is especially apparent when the attitude uncertainty grows large and can be advantageous in situations with sparse or poor attitude information.

A minimum divergence filtering framework was developed, which approximates the true state density at each step in the Bayesian recursion by an assumed density. The parameters of the assumed density are found by minimizing the Kullback-Leibler (KL) divergence of the true density with respect to the assumed density. It was shown that this divergence is minimized for exponential family pdfs when the expected value of the natural statistics vector is identical for both the true and assumed densities. This result is employed to develop the Gaussian mixture minimum divergence filter (GMMDF), which approximates the true temporal and measurement evolution of each component of the Gaussian mixture (GM) pdf with its KL divergence optimal Gaussian density. The predictor of the GMMDF is shown to be identical to other GM filters, with the specific type of GM filter it is identical to defined by the type of calculation or approximation used to evaluate the necessary expected values. The corrector of the GMMDF has a similar weight update to other GM filters, which updates the weight of each component according to the relative likelihood that the measurement originated from that component. The parameters of each component of the GM density are defined by the moments of Bayes' rule, which performs a nonlinear update for each component. This nonlinear update was compared to the update used by the extended Kalman filter (EKF) and quadrature Kalman filter (QKF) for the "lensing" problem, which occurs when an

accurate range measurement is taken to an object with a large position uncertainty, which results in a highly non-Gaussian posterior density. The nonlinear update performed for each component of the GMMDF is capable of incorporating information from the range measurement in the direction perpendicular to the range, which stems from the curvature of the posterior density. The linear update used by the EKF and QKF is not capable of incorporating information in this direction.

The minimum divergence filtering framework was used to develop the BGM filter, which quantifies the temporal and measurement evolution of the parameters of a BGM density according to (potentially) nonlinear dynamical system and measurement models. The BGM filter was cast in terms of its defining integrals, and an unscented transform, which was developed in this work, or Monte Carlo integration was used to approximate these integrals. The BGM filter was applied to three simulations in order to evaluate its efficacy in estimating a state vector that consists of an attitude quaternion and other Euclidean states. The first application compared a single-component BGM filter to an MEKF in estimating the one-dimensional attitude and angular velocity of a body given measurements of a known direction expressed in the body-fixed frame. No initial attitude information was known, and a Monte Carlo analysis of both filters was performed. When the attitude uncertainty was large at the beginning of the simulation, the single-component BGM filter proves to be more statistically consistent than the MEKF, which is expected because the MEKF assumes the attitude uncertainty to be small. When the attitude uncertainty decreases as more measurement information is incorporated, the single-component BGM filter and the MEKF converge to similar state estimates.

The second application of the BGM filter compared the performance of a single-component and a multiple-component BGM filter to estimate the planar relative dynamic pose of a chase spacecraft with respect to a target spacecraft given range and bearing measurements between the spacecraft. Both the single-component and multiple-component filter perform well in estimating the planar relative dynamic pose of a chase spacecraft, which is due to the linear dynamics defining the relative motion between the spacecraft and the amount of attitude information available to the filter, which causes the attitude uncertainty to decrease quickly, and thus, the single-component and multiple-component mixture filters perform nearly identically. The mixture filter requires fewer evaluations of the measurement likelihood, and thus has a lower computational demand, after the first few measurements are processed, however, because the components with significantly low likelihood are trimmed from the mixture over time.

The final application of the BGM filter demonstrates the ability of a single-component BGM filter to estimate the three-dimensional dynamic pose of a spacecraft in low-Earth orbit, given measurements of the Earth's magnetic field and the position of the spacecraft. This application demonstrates the applicability of the BGM filter to a nonlinear dynamical system and measurements. Instead of using a model-based approach, as was used in the first two applications of the

BGM filter, this application uses an inertial measurement unit (IMU)-based approach, in which the non-gravitational acceleration and angular velocity of the spacecraft are measured by the IMU. These measurements are used in the predictor of the single-component BGM filter to propagate the parameters of the BGM filter forward in time. The single-component BGM filter is capable of estimating the dynamic pose of the spacecraft, even though the magnetometer measurements provide relatively little attitude information because they provide a measurement of the direction of a single direction (the direction of the Earth's magnetic field), which changes over time.

Future work includes the development of a pdf that probabilistically represents a state vector comprised of an attitude quaternion and other Euclidean states that exists in the general exponential family and does *not* require splitting across the unit-hypersphere, as the Bingham-Gauss density does. This will facilitate a filter developed under the minimum divergence filtering framework that is similar to the BGM filter that does not require the consistency check of the parameters with the unscented or Monte Carlo points, as the BGM filter does. This will provide a more computationally efficient and robust approximate Bayesian filter that does not require a small angle assumption to quantify the attitude uncertainty.

The integral approximation inherent to the GMMDF and the BGM filter was performed using an unscented transformation or Monte Carlo integration. Future work includes the investigation and implementation of more efficient and/or accurate approximation methods for these integrals, because the current methods of approximating these integrals restricts the applicability of the GMMDF and BGM filter to situations with significant computing resources. If these more accurate and efficient methods of integral approximation can be developed, the GMMDF and BGM filter can potentially be implemented in situations with more limited computing resources, including dynamic pose estimation in near real-time aboard spacecraft and other vehicles.

APPENDIX A

THE L_2 DISTANCE BETWEEN A GAUSSIAN AND A GAUSSIAN MIXTURE DENSITY

The L_2 distance between a Gaussian density, as defined by Eq. (3.4), and a Gaussian mixture (GM) density, as defined by Eq. (3.7), is defined by

$$L_2[p_g||p_{gm}] = \int \left[p_g(\boldsymbol{x}; \boldsymbol{m}, \boldsymbol{P}) - p_{gm}(\boldsymbol{x}) \right]^2 \mathrm{d}\boldsymbol{x} \,. \tag{A.1}$$

This L_2 distance is found in closed-form for an arbitrary Gaussian and GM density, which can then be specialized to the case when the Gaussian density becomes the canonical Gaussian density through the substitution $\boldsymbol{m} = \boldsymbol{0}$ and $\boldsymbol{P} = \boldsymbol{I}$, if desired. In order to simplify the L_2 distance given in Eq. (A.1), the integrand is expanded, the definition of the GM is substituted from Eq. (3.7), and the linearity of the integral and summation is exploited to yield

$$L_2[p_g||p_{gm}] = \int p_g(\boldsymbol{x}; \boldsymbol{m}, \boldsymbol{P})^2 \, \mathrm{d}\boldsymbol{x} - 2 \sum_{\ell=1}^{L} w^{(\ell)} \int p_g(\boldsymbol{x}; \boldsymbol{m}, \boldsymbol{P}) \, p_g\left(\boldsymbol{x}; \boldsymbol{m}^{(\ell)}, \boldsymbol{P}^{(\ell)}\right) \mathrm{d}\boldsymbol{x}$$
$$+ \sum_{\ell=1}^{L} \sum_{j=1}^{L} w^{(\ell)} w^{(j)} \int p_g\left(\boldsymbol{x}; \boldsymbol{m}^{(\ell)}, \boldsymbol{P}^{(\ell)}\right) p_g\left(\boldsymbol{x}; \boldsymbol{m}^{(j)}, \boldsymbol{P}^{(j)}\right) \mathrm{d}\boldsymbol{x} \,. \tag{A.2}$$

Before simplifying Eq. (A.2) further, it is necessary to consider the product of two Gaussian pdfs, which is a scaled Gaussian pdf and is given by [22, 79]

$$p_g(\boldsymbol{x}; \boldsymbol{a}, \boldsymbol{A}) p_g(\boldsymbol{x}; \boldsymbol{b}, \boldsymbol{B}) = \Gamma(\boldsymbol{a}, \boldsymbol{b}, \boldsymbol{A}, \boldsymbol{B}) p_g(\boldsymbol{x}; \boldsymbol{c}, \boldsymbol{C}) \,, \tag{A.3}$$

where

$$\boldsymbol{C} = (\boldsymbol{A}^{-1} + \boldsymbol{B}^{-1})^{-1} \qquad \boldsymbol{c} = \boldsymbol{C}(\boldsymbol{A}^{-1}\boldsymbol{a} + \boldsymbol{B}^{-1}\boldsymbol{b})$$
$$\Gamma(\boldsymbol{a}, \boldsymbol{b}, \boldsymbol{A}, \boldsymbol{B}) = \det \left\{ 2\pi(\boldsymbol{A} + \boldsymbol{B}) \right\}^{-1/2} \exp \left\{ -\frac{1}{2}(\boldsymbol{a} - \boldsymbol{b})^T (\boldsymbol{A} + \boldsymbol{B})^{-1} (\boldsymbol{a} - \boldsymbol{b}) \right\} \,.$$

Equation (A.3) is substituted into Eq. (A.2) and simplified (while noting that $\Gamma(\boldsymbol{a}, \boldsymbol{b}, \boldsymbol{A}, \boldsymbol{B})$ is a constant and the Gaussian pdf integrates to unity over its support) to yield

$$L_2[p||p_{gm}] = \Gamma(\boldsymbol{m}, \boldsymbol{m}, \boldsymbol{P}, \boldsymbol{P}) - 2 \sum_{\ell=1}^{L} w^{(\ell)} \Gamma(\boldsymbol{m}, \boldsymbol{m}^{(\ell)}, \boldsymbol{P}, \boldsymbol{P}^{(\ell)})$$
$$+ \sum_{\ell=1}^{L} \sum_{j=1}^{L} w^{(\ell)} w^{(j)} \Gamma(\boldsymbol{m}^{(\ell)}, \boldsymbol{m}^{(j)}, \boldsymbol{P}^{(\ell)}, \boldsymbol{P}^{(j)}) \,.$$

The function $\Gamma(\boldsymbol{m}, \boldsymbol{m}, \boldsymbol{P}, \boldsymbol{P})$ is further simplified, which yields the final form of the L_2 distance between a Gaussian density and a Gaussian mixture (GM) density as

$$L_2[p||p_{gm}] = \det\{4\pi\boldsymbol{P}\}^{-1/2} - 2\sum_{\ell=1}^{L} w^{(\ell)}\, \Gamma(\boldsymbol{m}, \boldsymbol{m}^{(\ell)}, \boldsymbol{P}, \boldsymbol{P}^{(\ell)})$$
$$+ \sum_{\ell=1}^{L}\sum_{j=1}^{L} w^{(\ell)}w^{(j)}\Gamma(\boldsymbol{m}^{(\ell)}, \boldsymbol{m}^{(j)}, \boldsymbol{P}^{(\ell)}, \boldsymbol{P}^{(j)}).$$

APPENDIX B

TABULATING THE NORMALIZING CONSTANTS OF THE BINGHAM DENSITY

The normalization constant of the Bingham density is given by the hypergeometric function of a matrix argument according to Eq. (3.19), which is given by

$$F(\boldsymbol{Z}) = \int_{\mathbb{S}^s} \exp\left\{\bar{\boldsymbol{q}}^T \boldsymbol{Z} \bar{\boldsymbol{q}}\right\} \mathrm{d}\mathbb{S}^s = |\mathbb{S}^s| \, {}_1F_1\left(\frac{1}{2}; \frac{s+1}{2}; \boldsymbol{Z}\right),$$

(B.1)

where $|\mathbb{S}^s|$ represents the area of the unit-hypersphere of dimension s and $.F.(\cdot; \cdot; \cdot)$ represents the hypergeometric function of a matrix argument. In order to approximate this normalization constant, the integral in Eq. (B.1) is approximated directly instead of approximating the hypergeometric function of a matrix argument. This integral is approximated using Gauss-Legendre quadrature over the spherical coordinates, which is a minimum parameter set defining the unit vector $\bar{\boldsymbol{q}}$ (which is a valid attitude quaternion when $s = 1$ or $s = 3$). Integrating over these spherical coordinates transforms the integral in Eq. (B.1) from integration over the unit-hypersphere to integration over the area of the unit-hypersphere defined by the spherical coordinates according to

$$F(\boldsymbol{Z}) = \int_{A(\boldsymbol{\phi})} \exp\left\{\bar{\boldsymbol{q}}(\boldsymbol{\phi})^T \boldsymbol{Z} \bar{\boldsymbol{q}}(\boldsymbol{\phi})\right\} \mathrm{d}A(\boldsymbol{\phi}),$$

(B.2)

where $\bar{\boldsymbol{q}}(\boldsymbol{\phi})$ represents the attitude quaternion parameterized by spherical coordinates according to Eqs. (3.36) and $\mathrm{d}A(\boldsymbol{\phi})$ represents the differential area of the hypersphere swept out by $\bar{\boldsymbol{q}}(\boldsymbol{\phi})$. Equation (3.37) is substituted into Eq. (B.2) to yield the integral defined directly over the spherical coordinates according to

$$F(\boldsymbol{Z}) = \int_0^{2\pi} \int_0^{\pi} \cdots \int_0^{\pi} \int_0^{\pi} \exp\left\{\bar{\boldsymbol{q}}(\boldsymbol{\phi})^T \boldsymbol{Z} \bar{\boldsymbol{q}}(\boldsymbol{\phi})\right\}$$
$$\times \sin^{s-1}\phi_1 \sin^{s-2}\phi_2 \cdots \sin\phi_{s-1} \, \mathrm{d}\phi_1 \, \mathrm{d}\phi_2 \cdots \mathrm{d}\phi_{s-1} \, \mathrm{d}\phi_s,$$

These integrals can be approximated using quadrature techniques in this form, if desired; however, it is advantageous to exploit the symmetry of the Bingham pdf first to decrease the computational expense of the approximation according to

$$F(\boldsymbol{Z}) = c_s \int_0^{\pi/2} \int_0^{\pi/2} \cdots \int_0^{\pi/2} \int_0^{\pi/2} \exp\left\{\bar{\boldsymbol{q}}(\boldsymbol{\phi})^T \boldsymbol{Z} \bar{\boldsymbol{q}}(\boldsymbol{\phi})\right\}$$
$$\times \sin^{s-1}\phi_1 \sin^{s-2}\phi_2 \cdots \sin\phi_{s-1} \, \mathrm{d}\phi_1 \, \mathrm{d}\phi_2 \cdots \mathrm{d}\phi_{s-1} \, \mathrm{d}\phi_s, \quad \text{(B.3)}$$

where c_s is the factor that is gained due to the symmetry of the Bingham pdf and is given by the recursion

$$c_s = 2c_{s-1},$$

and is initialized with $c_1 = 4$. Noting that the bounds of integration of each spherical coordinate are now identical, Gauss-Legendre quadrature [80] is used to generate N quadrature weights and points for each of the s spherical coordinates over the interval $[0 \ \pi/2]$, which are denoted by $w^{(i)}$ and $\phi_\ell^{(i)}$, respectively, for $\ell = 1, 2, \ldots, s$ and $i = 1, 2, \ldots, N$. The integral in Eq. (B.3) is then approximated according to

$$
F(\boldsymbol{Z}) \approx c_s \sum_{i_1=1}^{N} \sum_{i_2=1}^{N} \cdots \sum_{i_s=1}^{N} w^{(i_1)} w^{(i_2)} \cdots w^{(i_s)}
$$

$$
\times \exp \left\{ \bar{q} \left(\begin{bmatrix} \phi_1^{(i_1)} \\ \phi_2^{(i_2)} \\ \vdots \\ \phi_s^{(i_s)} \end{bmatrix} \right)^T \boldsymbol{Z} \, \bar{q} \left(\begin{bmatrix} \phi_1^{(i_1)} \\ \phi_2^{(i_2)} \\ \vdots \\ \phi_s^{(i_s)} \end{bmatrix} \right) \right\} \sin^{s-1} \phi_1^{(i_1)} \sin^{s-2} \phi_2^{(i_2)} \cdots \sin \phi_{s-1}^{(i_{s-1})}. \quad \text{(B.4)}
$$

If more points are used per dimension, that is, N becomes larger, less error is incurred in the approximation at the expense of computational burden. This computational burden is further exacerbated for higher dimensions due to the curse of dimensionality, which is apparent due to the embedded summations in Eq. (B.4). In this work, $N = 200$ points per dimension is found to provide a sufficient approximation of the normalizing constant.

In order to approximate the f_i for $i = 1, 2, \ldots, s$, which are the unique elements of the diagonal covariance matrix defined by the canonical Bingham pdf and defined by Eq. (3.23), the partial derivatives with respect to each Z_i for $i = 1, 2, \ldots, s$ of Eq. (B.4) are taken and subsequently normalized by $F(\boldsymbol{Z})$. This is equivalent to taking the partial derivatives of the integral definition of $F(\boldsymbol{Z})$ defined in Eq. (B.1), normalizing by $F(\boldsymbol{Z})$, and then using Gauss-Legendre quadrature to approximate the resulting integrals. Noting that $\boldsymbol{Z}$ is a diagonal matrix, the f_i for $i = 1, 2, \ldots, s$ are approximated according to

$$
f_i(\boldsymbol{Z}) \triangleq F^{-1}(\boldsymbol{Z}) \frac{\partial F(\boldsymbol{Z})}{\partial Z_i}
$$

$$
\approx F^{-1}(\boldsymbol{Z}) c_s \sum_{i_1=1}^{N} \sum_{i_2=1}^{N} \cdots \sum_{i_s=1}^{N} w^{(i_1)} w^{(i_2)} \cdots w^{(i_s)} \bar{q}_i \left(\begin{bmatrix} \phi_1^{(i_1)} \\ \phi_2^{(i_2)} \\ \vdots \\ \phi_s^{(i_s)} \end{bmatrix} \right)^2 \quad \text{(B.5)}
$$

$$
\times \exp\left\{ \bar{q}\left(\begin{bmatrix} \phi_1^{(i_1)} \\ \phi_2^{(i_2)} \\ \vdots \\ \phi_s^{(i_s)} \end{bmatrix}\right)^T \mathbf{Z}\, \bar{q}\left(\begin{bmatrix} \phi_1^{(i_1)} \\ \phi_2^{(i_2)} \\ \vdots \\ \phi_s^{(i_s)} \end{bmatrix}\right) \right\} \sin^{s-1}\phi_1^{(i_1)} \sin^{s-2}\phi_2^{(i_2)} \cdots \sin\phi_{s-1}^{(i_{s-1})},
$$

where the explicit functional dependence of f_i is shown for clarity and $\bar{q}_i\,(\phi)$ denotes the ith component of the quaternion defined by the collection of spherical coordinates, ϕ. Similar to the approximation of the normalization constant itself, $N = 200$ points per dimension is found to provide a sufficient approximation of the f_i for $i = 1, 2, \ldots, s$.

For a given $\mathbf{Z}$, Eqs. (B.4) and (B.5) are used to approximate $F(\mathbf{Z})$ and f_i for $i = 1, 2, \ldots, s$. These approximations can potentially be performed online; however, in typical applications, this approximation is too slow to perform online. To circumvent this, these values are approximated and stored over an appropriate range of $\mathbf{Z}$ values and then interpolated online. 100 points over the range $[-100000\ \ 0]$ were used for each Z_i for $i = 1, 2, \ldots, s$ in this work to store these values for later interpolation. These points are chosen to be more densely spaced as they approached zero, which is found to decrease the interpolation error incurred for values of $\mathbf{Z}$ close to zero, where the changes in $F(\mathbf{Z})$ and f_i for $i = 1, 2, \ldots, s$ are larger for a given change in $\mathbf{Z}$.

APPENDIX C

THE L_2 DISTANCE BETWEEN A BINGHAM AND BINGHAM MIXTURE DENSITY

The L_2 distance between a Bingham density, as defined by Eq. (3.18), and a Bingham mixture (BM) density, as defined by Eq. (3.28), is defined by

$$L_2[p_b||p_{bm}] = \int \left[p_b(\bar{q}; \boldsymbol{M}, \boldsymbol{Z}) - p_{bm}(\bar{q}) \right]^2 \mathrm{d}\bar{q} \,. \tag{C.1}$$

This L_2 distance is found in closed-form for an arbitrary Bingham and BM density, which can them be specialized to the case when the Bingham density becomes the canonical Bingham density through the substitution $\boldsymbol{M} = \boldsymbol{I}$, if desired. In order to simplify the L_2 distance given in Eq. (C.1), the integrand is expanded, the definition of the BM is substituted from Eq. (3.28), and the linearity of the integral and summation is exploited to yield

$$L_2[p_b||p_{bm}] = \int p_b(\bar{q}; \boldsymbol{M}, \boldsymbol{Z})^2 \, \mathrm{d}\bar{q} - 2 \sum_{\ell=1}^{L} w^{(\ell)} \int p_b(\bar{q}; \boldsymbol{M}, \boldsymbol{Z}) \, p_b\left(\bar{q}; \boldsymbol{M}^{(\ell)}, \boldsymbol{Z}^{(\ell)} \right) \mathrm{d}\bar{q}$$

$$+ \sum_{\ell=1}^{L} \sum_{j=1}^{L} w^{(\ell)} w^{(j)} \int p_b\left(\bar{q}; \boldsymbol{M}^{(\ell)}, \boldsymbol{Z}^{(\ell)} \right) p_b\left(\bar{q}; \boldsymbol{M}^{(j)}, \boldsymbol{Z}^{(j)} \right) \mathrm{d}\bar{q} \,. \tag{C.2}$$

Before simplifying Eq. (C.2) further, it is necessary to consider the product of two Bingham pdfs, which is given for two arbitrary Bingham pdfs according to

$$p_b(\bar{q}; \boldsymbol{M}_1, \boldsymbol{Z}_1) p_b(\bar{q}; \boldsymbol{M}_2, \boldsymbol{Z}_2) = \frac{1}{F(\boldsymbol{Z}_1)} \exp\left\{ \bar{q}^T \boldsymbol{M}_1 \boldsymbol{Z}_1 \boldsymbol{M}_1^T \bar{q} \right\} \frac{1}{F(\boldsymbol{Z}_2)} \exp\left\{ \bar{q}^T \boldsymbol{M}_2 \boldsymbol{Z}_2 \boldsymbol{M}_2^T \bar{q} \right\}$$

$$= \frac{1}{F(\boldsymbol{Z}_1) F(\boldsymbol{Z}_2)} \exp\left\{ \bar{q}^T (\boldsymbol{M}_1 \boldsymbol{Z}_1 \boldsymbol{M}_1^T + \boldsymbol{M}_2 \boldsymbol{Z}_2 \boldsymbol{M}_2^T) \bar{q} \right\} \,. \tag{C.3}$$

This can be expressed using an eigen-decomposition of $\boldsymbol{M}_1 \boldsymbol{Z}_1 \boldsymbol{M}_1^T + \boldsymbol{M}_2 \boldsymbol{Z}_2 \boldsymbol{M}_2^T$, which is defined according to

$$\boldsymbol{V} \boldsymbol{\Lambda} \boldsymbol{V}^T = \boldsymbol{M}_1 \boldsymbol{Z}_1 \boldsymbol{M}_1^T + \boldsymbol{M}_2 \boldsymbol{Z}_2 \boldsymbol{M}_2^T \,,$$

where $\boldsymbol{V} \in \mathrm{SO}(s+1)$ is a matrix with columns consisting of the eigenvectors and $\boldsymbol{\Lambda}$ is the corresponding diagonal matrix of nondecreasing eigenvalues with maximum eigenvalue denoted by λ. The product of the Bingham densities, given in Eq. (C.3), is now expressed as

$$p_b(\bar{q}; \boldsymbol{M}_1, \boldsymbol{Z}_1) p_b(\bar{q}; \boldsymbol{M}_2, \boldsymbol{Z}_2) = \frac{1}{F(\boldsymbol{Z}_1) F(\boldsymbol{Z}_2)} \exp\left\{ \bar{q}^T \boldsymbol{V} \boldsymbol{\Lambda} \boldsymbol{V}^T \bar{q} \right\} \,.$$

$\lambda \boldsymbol{I}$ is subtracted and added to $\boldsymbol{\Lambda}$ to yield

$$p_b(\bar{q}; \boldsymbol{M}_1, \boldsymbol{Z}_1) p_b(\bar{q}; \boldsymbol{M}_2, \boldsymbol{Z}_2) = \frac{1}{F(\boldsymbol{Z}_1) F(\boldsymbol{Z}_2)} \exp\left\{ \bar{q}^T \boldsymbol{V} \left[\boldsymbol{\Lambda} - \lambda \boldsymbol{I} + \lambda \boldsymbol{I} \right] \boldsymbol{V}^T \bar{q} \right\}$$

$$= \frac{\exp\{\lambda\}}{F(\boldsymbol{Z}_1)F(\boldsymbol{Z}_2)}\exp\{\bar{\boldsymbol{q}}^T\boldsymbol{V}\left[\boldsymbol{\Lambda}-\lambda\boldsymbol{I}\right]\boldsymbol{V}^T\bar{\boldsymbol{q}}\}. \tag{C.4}$$

It is now observed that $\boldsymbol{V}\triangleq\boldsymbol{M}_3$ and $\boldsymbol{\Lambda}-\lambda\boldsymbol{I}\triangleq\boldsymbol{Z}_3$ are a valid orientation matrix and matrix of concentration parameters. Substituting these definitions into Eq. (C.4) yields

$$p_b(\bar{\boldsymbol{q}};\boldsymbol{M}_1,\boldsymbol{Z}_1)p_b(\bar{\boldsymbol{q}};\boldsymbol{M}_2,\boldsymbol{Z}_2) = \frac{\exp\{\lambda\}}{F(\boldsymbol{Z}_1)F(\boldsymbol{Z}_2)}\exp\{\bar{\boldsymbol{q}}^T\boldsymbol{M}_3\boldsymbol{Z}_3\boldsymbol{M}_3^T\bar{\boldsymbol{q}}\}.$$

This is manipulated to show that the product of two Bingham densities is a scaled Bingham density according to

$$p_b(\bar{\boldsymbol{q}};\boldsymbol{M}_1,\boldsymbol{Z}_1)p_b(\bar{\boldsymbol{q}};\boldsymbol{M}_2,\boldsymbol{Z}_2) = \frac{\exp\{\lambda\}F(\boldsymbol{Z}_3)}{F(\boldsymbol{Z}_1)F(\boldsymbol{Z}_2)}\frac{1}{F(\boldsymbol{Z}_3)}\exp\{\bar{\boldsymbol{q}}^T\boldsymbol{M}_3\boldsymbol{Z}_3\boldsymbol{M}_3^T\bar{\boldsymbol{q}}\}$$
$$= \frac{\exp\{\lambda\}F(\boldsymbol{Z}_3)}{F(\boldsymbol{Z}_1)F(\boldsymbol{Z}_2)}p_b(\bar{\boldsymbol{q}};\boldsymbol{M}_3,\boldsymbol{Z}_3). \tag{C.5}$$

This expression can be specialized to the case when a Bingham density is squared, that is $\boldsymbol{M}_1 = \boldsymbol{M}_2\triangleq\boldsymbol{M}$ and $\boldsymbol{Z}_1=\boldsymbol{Z}_2\triangleq\boldsymbol{Z}$. In this case, the the square of the Bingham density is given by

$$p_b(\bar{\boldsymbol{q}};\boldsymbol{M},\boldsymbol{Z})^2 = \frac{\exp\{0\}F(2\boldsymbol{Z})}{F(\boldsymbol{Z})F(\boldsymbol{Z})}p_b(\bar{\boldsymbol{q}};\boldsymbol{M},\boldsymbol{Z}) = \frac{F(2\boldsymbol{Z})}{F(\boldsymbol{Z})^2}p_b(\bar{\boldsymbol{q}};\boldsymbol{M},2\boldsymbol{Z}), \tag{C.6}$$

Now that the product of Bingham densities has been quantified, Eq. (C.2) is simplified using Eqs. (C.5) and (C.6), while noting that the Bingham pdf integrates to unity over its support, according to

$$L_2[p_b||p_{bm}] = \frac{F(2\boldsymbol{Z})}{F(\boldsymbol{Z})^2} - 2\sum_{\ell=1}^{L}w^{(\ell)}\frac{\exp\{\lambda^{(\ell)}\}F(\boldsymbol{Z}_3^{(\ell)})}{F(\boldsymbol{Z})F(\boldsymbol{Z}^{(\ell)})}$$
$$+ \sum_{\ell=1}^{L}\sum_{j=1}^{L}w^{(\ell)}w^{(j)}\frac{\exp\{\lambda^{(\ell j)}\}F(\boldsymbol{Z}_3^{(\ell j)})}{F(\boldsymbol{Z}^{(\ell)})F(\boldsymbol{Z}^{(j)})}, \tag{C.7}$$

where $\lambda^{(\ell)}$ and $\boldsymbol{Z}_3^{(\ell)}$ are the largest eigenvalue and matrix of concentration parameters, respectively, defined by the eigen-decomposition of $\boldsymbol{M}\boldsymbol{Z}\boldsymbol{M}^T + \boldsymbol{M}^{(\ell)}\boldsymbol{Z}^{(\ell)}\boldsymbol{M}^{(\ell)^T}$ and $\lambda^{(\ell j)}$ and $\boldsymbol{Z}_3^{(\ell j)}$ are the largest eigenvalue and matrix of concentration parameters, respectively, defined by the eigen-decomposition of $\boldsymbol{M}^{(\ell)}\boldsymbol{Z}^{(\ell)}\boldsymbol{M}^{(\ell)^T} + \boldsymbol{M}^{(j)}\boldsymbol{Z}^{(j)}\boldsymbol{M}^{(j)^T}$. At the surface, it appears as though Eq. (C.7) does not depend on the orientation matrices of the Bingham density and BM components; however, these orientation matrices are used in the calculation of $\lambda^{(\ell)}$, $\boldsymbol{Z}_3^{(\ell)}$, $\lambda^{(\ell j)}$, and $\boldsymbol{Z}_3^{(\ell j)}$. Because of this, the L_2 distance is affected by the orientation matrices, as intuition suggests.

APPENDIX D

PROOF OF EQUATION 32 IN REFERENCE [54]

Equation (32) in Reference [54] is a crucial relationship used in the derivations of the Bayesian Kalman and Gaussian sum filters. This relationship transforms the product of a Gaussian distribution in $\boldsymbol{x}$ and a Gaussian distribution in $\boldsymbol{z}$ linearly conditioned on $\boldsymbol{x}$ to the product of a Gaussian distribution in $\boldsymbol{z}$ and a Gaussian distribution in $\boldsymbol{x}$ linearly conditioned on $\boldsymbol{z}$. This relationship is given by

$$p_g(\boldsymbol{x}; \boldsymbol{m}, \boldsymbol{P}) p_g(\boldsymbol{z}; \boldsymbol{Hx}, \boldsymbol{R}) = p_g(\boldsymbol{z}; \boldsymbol{Hm}, \boldsymbol{HPH}^T + \boldsymbol{R}) p_g(\boldsymbol{x}; \boldsymbol{\mu}, \boldsymbol{\Pi}), \tag{D.1}$$

where

$$\boldsymbol{\mu} = \boldsymbol{m} + \boldsymbol{K}(\boldsymbol{z} - \boldsymbol{Hm}), \qquad \boldsymbol{\Pi} = \boldsymbol{P} - \boldsymbol{KHP}, \qquad \boldsymbol{K} = \boldsymbol{PH}^T(\boldsymbol{HPH}^T + \boldsymbol{R})^{-1},$$

and the Gaussian pdf is defined by Eq. (3.4). In order to prove Eq. (D.1), its left-hand side is manipulated to yield its right-hand side [81]. The matrix inversion lemma [82] and Sylvester's determinant theorem [83] are used in the process of the proof. This proof is omitted from Ho and Lee's original paper and cannot be found in literature in the form presented here to the best knowledge of the author. Several references, including References [79, 84, 85], use Eq. (D.1) in deriving the Bayesian Kalman or Gaussian sum filter; however, they omit the proof and cite another source for the equation, which can ultimately be tracked back to Ho and Lee's original paper. Reference [86] shows this derivation using a different approach, in which the order of the conditioning is reversed by treating $\boldsymbol{x}$ and $\boldsymbol{z}$ as jointly-Gaussian-distributed random variables and using these properties to obtain a result similar to Eq. (D.1).

Before presenting the proof of Eq. (D.1), another important result is presented, which occurs when Eq. (D.1) is integrated over $\boldsymbol{x}$ according to

$$\int p_g(\boldsymbol{x}; \boldsymbol{m}, \boldsymbol{P}) p_g(\boldsymbol{z}; \boldsymbol{Hx}, \boldsymbol{R}) \, \mathrm{d}\boldsymbol{x} = \int p_g(\boldsymbol{z}; \boldsymbol{Hm}, \boldsymbol{HPH}^T + \boldsymbol{R}) p_g(\boldsymbol{x}; \boldsymbol{\mu}, \boldsymbol{\Pi}) \, \mathrm{d}\boldsymbol{x}. \tag{D.2}$$

Noting that $p_g(\boldsymbol{z}; \boldsymbol{Hm}, \boldsymbol{HPH}^T + \boldsymbol{R})$ does not depend on $\boldsymbol{x}$ and that the Gaussian density integrates to unity over its support, Eq. (D.2) becomes

$$\int p_g(\boldsymbol{x}; \boldsymbol{m}, \boldsymbol{P}) p_g(\boldsymbol{z}; \boldsymbol{Hx}, \boldsymbol{R}) \, \mathrm{d}\boldsymbol{x} = p_g(\boldsymbol{z}; \boldsymbol{Hm}, \boldsymbol{HPH}^T + \boldsymbol{R}), \tag{D.3}$$

which is also used in deriving the Bayesian Kalman or Gaussian sum filter.

Proof. To begin the proof, the definition of the Gaussian distribution given in Eq. (3.4) is substituted into the left-hand side of Eq. (D.1) to give

$$p_g(\boldsymbol{x};\boldsymbol{m},\boldsymbol{P})p_g(\boldsymbol{z};\boldsymbol{H}\boldsymbol{x},\boldsymbol{R}) = \det\left\{2\pi\boldsymbol{P}\right\}^{-1/2}\exp\left\{-\frac{1}{2}(\boldsymbol{x}-\boldsymbol{m})^T\boldsymbol{P}^{-1}(\boldsymbol{x}-\boldsymbol{m})\right\}$$

$$\times \det\left\{2\pi\boldsymbol{R}\right\}^{-1/2}\exp\left\{-\frac{1}{2}(\boldsymbol{z}-\boldsymbol{H}\boldsymbol{x})^T\boldsymbol{R}^{-1}(\boldsymbol{z}-\boldsymbol{H}\boldsymbol{x})\right\}.$$

The exponential terms are now combined according to

$$p_g(\boldsymbol{x};\boldsymbol{m},\boldsymbol{P})p_g(\boldsymbol{z};\boldsymbol{H}\boldsymbol{x},\boldsymbol{R}) = \det\left\{2\pi\boldsymbol{P}\right\}^{-1/2}\det\left\{2\pi\boldsymbol{R}\right\}^{-1/2}$$

$$\exp\left\{-\frac{1}{2}\left[(\boldsymbol{x}-\boldsymbol{m})^T\boldsymbol{P}^{-1}(\boldsymbol{x}-\boldsymbol{m}) + (\boldsymbol{z}-\boldsymbol{H}\boldsymbol{x})^T\boldsymbol{R}^{-1}(\boldsymbol{z}-\boldsymbol{H}\boldsymbol{x})\right]\right\}.$$

The argument of the exponential is now expanded and grouped to make a quadratic equation in $\boldsymbol{x}$ to give

$$p_g(\boldsymbol{x};\boldsymbol{m},\boldsymbol{P})p_g(\boldsymbol{z};\boldsymbol{H}\boldsymbol{x},\boldsymbol{R}) = \det\left\{2\pi\boldsymbol{P}\right\}^{-1/2}\det\left\{2\pi\boldsymbol{R}\right\}^{-1/2}$$

$$\times \exp-\frac{1}{2}\left[\boldsymbol{x}^T\boldsymbol{\Pi}^{-1}\boldsymbol{x} - 2\boldsymbol{x}^T\left(\boldsymbol{H}^T\boldsymbol{R}^{-1}\boldsymbol{z} + \boldsymbol{P}^{-1}\boldsymbol{m}\right) + \boldsymbol{z}^T\boldsymbol{R}^{-1}\boldsymbol{z} + \boldsymbol{m}^T\boldsymbol{P}^{-1}\boldsymbol{m}\right], \quad \text{(D.4)}$$

where

$$\boldsymbol{\Pi}^{-1} \triangleq \boldsymbol{H}^T\boldsymbol{R}^{-1}\boldsymbol{H} + \boldsymbol{P}^{-1}. \tag{D.5}$$

The matrix inversion lemma is used to solve Eq. (D.5) for $\boldsymbol{\Pi}$ as

$$\boldsymbol{\Pi} = \boldsymbol{P} - \boldsymbol{P}\boldsymbol{H}^T(\boldsymbol{H}\boldsymbol{P}\boldsymbol{H}^T + \boldsymbol{R})^{-1}\boldsymbol{H}\boldsymbol{P} = \boldsymbol{P} - \boldsymbol{K}\boldsymbol{H}\boldsymbol{P}, \tag{D.6}$$

where

$$\boldsymbol{K} \triangleq \boldsymbol{P}\boldsymbol{H}^T(\boldsymbol{H}\boldsymbol{P}\boldsymbol{H}^T + \boldsymbol{R})^{-1}. \tag{D.7}$$

Adding a factor of $\boldsymbol{\Pi}^{-1}\boldsymbol{\Pi}$ into the term that is linear in $\boldsymbol{x}$ in Eq. (D.4) yields

$$p_g(\boldsymbol{x};\boldsymbol{m},\boldsymbol{P})p_g(\boldsymbol{z};\boldsymbol{H}\boldsymbol{x},\boldsymbol{R}) = \det\left\{2\pi\boldsymbol{P}\right\}^{-1/2}\det\left\{2\pi\boldsymbol{R}\right\}^{-1/2}$$

$$\times \exp-\frac{1}{2}\left[\boldsymbol{x}^T\boldsymbol{\Pi}^{-1}\boldsymbol{x} - 2\boldsymbol{x}^T\boldsymbol{\Pi}^{-1}\boldsymbol{\mu} + \boldsymbol{z}^T\boldsymbol{R}^{-1}\boldsymbol{z} + \boldsymbol{m}^T\boldsymbol{P}^{-1}\boldsymbol{m}\right], \quad \text{(D.8)}$$

where

$$\boldsymbol{\mu} \triangleq \boldsymbol{\Pi}\left(\boldsymbol{H}^T\boldsymbol{R}^{-1}\boldsymbol{z} + \boldsymbol{P}^{-1}\boldsymbol{m}\right). \tag{D.9}$$

In order to manipulate Eq. (D.9) into a more convenient form, first note that an alternate form for K can be derived by pre- and post-multiplying Eq. (D.5) by Π and P, respectively, to yield

$$P = \Pi H^T R^{-1} H P + \Pi \,. \tag{D.10}$$

Equation (D.10) is now post-multiplied by $H^T R^{-1}$ and manipulated to yield

$$P H^T R^{-1} = \Pi H^T R^{-1} (H P H^T + R) R^{-1} \,. \tag{D.11}$$

Solving Eq. (D.11) for $\Pi H^T R^{-1}$ yields

$$\Pi H^T R^{-1} = P H^T (H P H^T + R)^{-1} \,. \tag{D.12}$$

Combining Eqs. (D.7) and (D.12) yields the alternate expression for K as

$$K = \Pi H^T R^{-1} \,. \tag{D.13}$$

Equations (D.13) and (D.6) is now substitued into Eq. (D.9) to yield

$$\mu = K z + (I - K H) m = m + K(z - H m) \,, \tag{D.14}$$

which is the desired form for μ. Substituting the definition for μ given in Eq. (D.9) into Eq. (D.8) yields

$$p_g(x; m, P) p_g(z; H x, R) = \det\{2\pi P\}^{-1/2} \det\{2\pi R\}^{-1/2}$$
$$\times \exp -\frac{1}{2} \left[x^T \Pi^{-1} x - 2 x^T \Pi^{-1} \mu + z^T R^{-1} z + m^T P^{-1} m \right] \,. \tag{D.15}$$

Completing the square for x in Eq. (D.15) yields

$$p_g(x; m, P) p_g(z; H x, R) = \det\{2\pi P\}^{-1/2} \det\{2\pi R\}^{-1/2}$$
$$\times \exp -\frac{1}{2} \left[(x - \mu)^T \Pi^{-1} (x - \mu) - \mu^T \Pi^{-1} \mu + z^T R^{-1} z + m^T P^{-1} m \right] \,. \tag{D.16}$$

Now, the term $\mu^T \Pi^{-1} \mu$ is manipulated. Substituting Eq. (D.14) into $\mu^T \Pi^{-1} \mu$ and expanding the result yields

$$\mu^T \Pi^{-1} \mu =$$
$$m^T \Pi^{-1} m + 2(z - H m)^T K^T \Pi^{-1} m + (z - H m)^T K^T \Pi^{-1} K (z - H m) \,. \tag{D.17}$$

Equation (D.13) can be manipulated to yield

$$\boldsymbol{K}^T \boldsymbol{\Pi}^{-1} = \boldsymbol{R}^{-1} \boldsymbol{H}\,,$$

which is substituted into Eq. (D.17) and expanded to yield

$$
\begin{aligned}
\boldsymbol{\mu}^T \boldsymbol{\Pi}^{-1} \boldsymbol{\mu} = {}& \boldsymbol{m}^T \boldsymbol{\Pi}^{-1} \boldsymbol{m} + 2\boldsymbol{z}^T \boldsymbol{R}^{-1} \boldsymbol{H}\boldsymbol{m} - 2(\boldsymbol{H}\boldsymbol{m})^T \boldsymbol{R}^{-1} \boldsymbol{H}\boldsymbol{m} \\
& + \boldsymbol{z}^T \boldsymbol{R}^{-1} \boldsymbol{H}\boldsymbol{K}\boldsymbol{z} - 2(\boldsymbol{H}\boldsymbol{m})^T \boldsymbol{R}^{-1} \boldsymbol{H}\boldsymbol{K}\boldsymbol{z} + (\boldsymbol{H}\boldsymbol{m})^T \boldsymbol{R}^{-1} \boldsymbol{H}\boldsymbol{K}\boldsymbol{H}\boldsymbol{m}\,. \quad \text{(D.18)}
\end{aligned}
$$

Substituting Eq. (D.5) into Eq. (D.18) and simplifying yields

$$
\begin{aligned}
\boldsymbol{\mu}^T \boldsymbol{\Pi}^{-1} \boldsymbol{\mu} = {}& \boldsymbol{m}^T \boldsymbol{P}^{-1} \boldsymbol{m} + \boldsymbol{z}^T \boldsymbol{R}^{-1} \boldsymbol{H}\boldsymbol{K}\boldsymbol{z} - (\boldsymbol{H}\boldsymbol{m})^T [\boldsymbol{R}^{-1} - \boldsymbol{R}^{-1} \boldsymbol{H}\boldsymbol{K}](\boldsymbol{H}\boldsymbol{m}) \\
& + 2(\boldsymbol{H}\boldsymbol{m})^T [\boldsymbol{R}^{-1} - \boldsymbol{R}^{-1} \boldsymbol{H}\boldsymbol{K}]\boldsymbol{z}\,. \quad \text{(D.19)}
\end{aligned}
$$

Noting Eq. (D.7), the term $\boldsymbol{R}^{-1} - \boldsymbol{R}^{-1} \boldsymbol{H}\boldsymbol{K}$ can be expressed as

$$
\begin{aligned}
\boldsymbol{R}^{-1} - \boldsymbol{R}^{-1} \boldsymbol{H}\boldsymbol{K} &= \boldsymbol{R}^{-1} - \boldsymbol{R}^{-1} \boldsymbol{H}\boldsymbol{P}\boldsymbol{H}^T (\boldsymbol{H}\boldsymbol{P}\boldsymbol{H}^T + \boldsymbol{R})^{-1} \\
&= \boldsymbol{R}^{-1}[\boldsymbol{I} - \boldsymbol{H}\boldsymbol{P}\boldsymbol{H}^T (\boldsymbol{H}\boldsymbol{P}\boldsymbol{H}^T + \boldsymbol{R})^{-1}] \\
&= \boldsymbol{R}^{-1}[\boldsymbol{H}\boldsymbol{P}\boldsymbol{H}^T + \boldsymbol{R} - \boldsymbol{H}\boldsymbol{P}\boldsymbol{H}^T](\boldsymbol{H}\boldsymbol{P}\boldsymbol{H}^T + \boldsymbol{R})^{-1} \\
&= (\boldsymbol{H}\boldsymbol{P}\boldsymbol{H}^T + \boldsymbol{R})^{-1}\,. \quad \text{(D.20)}
\end{aligned}
$$

Combining Eqs. (D.19) and (D.20) yields

$$
\begin{aligned}
\boldsymbol{\mu}^T \boldsymbol{\Pi}^{-1} \boldsymbol{\mu} = {}& \boldsymbol{m}^T \boldsymbol{P}^{-1} \boldsymbol{m} + \boldsymbol{z}^T \boldsymbol{R}^{-1} \boldsymbol{H}\boldsymbol{K}\boldsymbol{z} - (\boldsymbol{H}\boldsymbol{m})^T (\boldsymbol{H}\boldsymbol{P}\boldsymbol{H}^T + \boldsymbol{R})^{-1}(\boldsymbol{H}\boldsymbol{m}) \\
& + 2(\boldsymbol{H}\boldsymbol{m})^T (\boldsymbol{H}\boldsymbol{P}\boldsymbol{H}^T + \boldsymbol{R})^{-1}\boldsymbol{z}\,. \quad \text{(D.21)}
\end{aligned}
$$

Equation (D.20) can be solved for $\boldsymbol{R}^{-1} \boldsymbol{H}\boldsymbol{K}$ according to

$$\boldsymbol{R}^{-1} \boldsymbol{H}\boldsymbol{K} = \boldsymbol{R}^{-1} - (\boldsymbol{H}\boldsymbol{P}\boldsymbol{H}^T + \boldsymbol{R})^{-1}\,. \quad \text{(D.22)}$$

Equations (D.21) and (D.22) are now combined and the result is simplified to yield

$$\boldsymbol{\mu}^T \boldsymbol{\Pi}^{-1} \boldsymbol{\mu} = \boldsymbol{m}^T \boldsymbol{P}^{-1} \boldsymbol{m} + \boldsymbol{z}^T \boldsymbol{R}^{-1} \boldsymbol{z} - (\boldsymbol{z} - \boldsymbol{H}\boldsymbol{m})^T (\boldsymbol{H}\boldsymbol{P}\boldsymbol{H}^T + \boldsymbol{R})^{-1}(\boldsymbol{z} - \boldsymbol{H}\boldsymbol{m})\,. \quad \text{(D.23)}$$

Equation (D.23) is substituted into Eq. (D.16) to yield

$$p_g(\boldsymbol{x}; \boldsymbol{m}, \boldsymbol{P})p_g(\boldsymbol{z}; \boldsymbol{H}\boldsymbol{x}, \boldsymbol{R}) = \det\{2\pi\boldsymbol{P}\}^{-1/2}\det\{2\pi\boldsymbol{R}\}^{-1/2}$$

$$\times \exp\left\{-\frac{1}{2}\Big[(\boldsymbol{x}-\boldsymbol{\mu})^T\boldsymbol{\Pi}^{-1}(\boldsymbol{x}-\boldsymbol{\mu})+(\boldsymbol{z}-\boldsymbol{H}\boldsymbol{m})^T(\boldsymbol{H}\boldsymbol{P}\boldsymbol{H}^T+\boldsymbol{R})^{-1}(\boldsymbol{z}-\boldsymbol{H}\boldsymbol{m})\Big]\right\}. \quad \text{(D.24)}$$

The exponential term is now broken apart to yield

$$p_g(\boldsymbol{x};\boldsymbol{m},\boldsymbol{P})p_g(\boldsymbol{z};\boldsymbol{H}\boldsymbol{x},\boldsymbol{R}) = \det\{2\pi\boldsymbol{P}\}^{-1/2}\det\{2\pi\boldsymbol{R}\}^{-1/2}\exp\left\{-\frac{1}{2}(\boldsymbol{x}-\boldsymbol{\mu})^T\boldsymbol{\Pi}^{-1}(\boldsymbol{x}-\boldsymbol{\mu})\right\}$$

$$\times \exp\left\{-\frac{1}{2}(\boldsymbol{z}-\boldsymbol{H}\boldsymbol{m})^T(\boldsymbol{H}\boldsymbol{P}\boldsymbol{H}^T+\boldsymbol{R})^{-1}(\boldsymbol{z}-\boldsymbol{H}\boldsymbol{m})\right\}. \quad \text{(D.25)}$$

In order to force these exponential arguments to be Gaussian distributions, Eq. (D.25) is manipulated by multiplying and dividing by the appropriate normalizing constants according to

$$p_g(\boldsymbol{x};\boldsymbol{m},\boldsymbol{P})p_g(\boldsymbol{z};\boldsymbol{H}\boldsymbol{x},\boldsymbol{R}) = \frac{\det\{2\pi\boldsymbol{P}\}^{-1/2}\det\{2\pi\boldsymbol{R}\}^{-1/2}}{\det\{2\pi\boldsymbol{\Pi}\}^{-1/2}\det\{2\pi(\boldsymbol{H}\boldsymbol{P}\boldsymbol{H}^T+\boldsymbol{R})\}^{-1/2}} \quad \text{(D.26)}$$

$$\times \det\{2\pi\boldsymbol{\Pi}\}^{-1/2}\exp\left\{-\frac{1}{2}(\boldsymbol{x}-\boldsymbol{\mu})^T\boldsymbol{\Pi}^{-1}(\boldsymbol{x}-\boldsymbol{\mu})\right\}$$

$$\times \det\{2\pi(\boldsymbol{H}\boldsymbol{P}\boldsymbol{H}^T+\boldsymbol{R})\}^{-1/2}\exp\left\{-\frac{1}{2}(\boldsymbol{z}-\boldsymbol{H}\boldsymbol{m})^T(\boldsymbol{H}\boldsymbol{P}\boldsymbol{H}^T+\boldsymbol{R})^{-1}(\boldsymbol{z}-\boldsymbol{H}\boldsymbol{m})\right\}.$$

Noting the definition of the Gaussian pdf in Eq. (3.4), Eq. (D.26) becomes

$$p_g(\boldsymbol{x};\boldsymbol{m},\boldsymbol{P})p_g(\boldsymbol{z};\boldsymbol{H}\boldsymbol{x},\boldsymbol{R}) = \frac{\det\{2\pi\boldsymbol{P}\}^{-1/2}\det\{2\pi\boldsymbol{R}\}^{-1/2}}{\det\{2\pi\boldsymbol{\Pi}\}^{-1/2}\det\{2\pi(\boldsymbol{H}\boldsymbol{P}\boldsymbol{H}^T+\boldsymbol{R})\}^{-1/2}}$$

$$\times p_g(\boldsymbol{x};\boldsymbol{\mu},\boldsymbol{\Pi})p_g(\boldsymbol{z};\boldsymbol{H}\boldsymbol{m},\boldsymbol{H}\boldsymbol{P}\boldsymbol{H}^T+\boldsymbol{R}). \quad \text{(D.27)}$$

The term

$$\frac{\det\{2\pi\boldsymbol{P}\}^{-1/2}\det\{2\pi\boldsymbol{R}\}^{-1/2}}{\det\{2\pi\boldsymbol{\Pi}\}^{-1/2}\det\{2\pi(\boldsymbol{H}\boldsymbol{P}\boldsymbol{H}^T+\boldsymbol{R})\}^{-1/2}}$$

is now simplified according to

$$\frac{\det\{2\pi\boldsymbol{P}\}^{-1/2}\det\{2\pi\boldsymbol{R}\}^{-1/2}}{\det\{2\pi\boldsymbol{\Pi}\}^{-1/2}\det\{2\pi(\boldsymbol{H}\boldsymbol{P}\boldsymbol{H}^T+\boldsymbol{R})\}^{-1/2}} = \left[\frac{\det\{\boldsymbol{\Pi}\}\det\{(\boldsymbol{H}\boldsymbol{P}\boldsymbol{H}^T+\boldsymbol{R})\}}{\det\{\boldsymbol{P}\}\det\{\boldsymbol{R}\}}\right]^{\frac{1}{2}} \quad \text{(D.28)}$$

$$= \left[\det\{\boldsymbol{\Pi}\boldsymbol{P}^{-1}\}\det\{(\boldsymbol{H}\boldsymbol{P}\boldsymbol{H}^T+\boldsymbol{R})\boldsymbol{R}^{-1}\}\right]^{\frac{1}{2}}$$

$$= \left[\det\{\boldsymbol{\Pi}\boldsymbol{P}^{-1}\}\det\{\boldsymbol{H}\boldsymbol{P}\boldsymbol{H}^T\boldsymbol{R}^{-1}+\boldsymbol{I}\}\right]^{\frac{1}{2}}.$$

Using Sylvester's determinant theorem [83], which is given by

$$\det\{\boldsymbol{I}_n+\boldsymbol{B}\boldsymbol{A}\} = \det\{\boldsymbol{I}_p+\boldsymbol{A}\boldsymbol{B}\},$$

Eq. (D.28) can be expressed as

$$\frac{\det\{2\pi\boldsymbol{P}\}^{-1/2}\det\{2\pi\boldsymbol{R}\}^{-1/2}}{\det\{2\pi\boldsymbol{\Pi}\}^{-1/2}\det\{2\pi(\boldsymbol{H}\boldsymbol{P}\boldsymbol{H}^T+\boldsymbol{R})\}^{-1/2}}$$
$$=\left[\det\{\boldsymbol{\Pi}\boldsymbol{P}^{-1}\}\det\{\boldsymbol{P}\boldsymbol{H}^T\boldsymbol{R}^{-1}\boldsymbol{H}+\boldsymbol{I}\}\right]^{\frac{1}{2}}. \quad\text{(D.29)}$$

Equation (D.5) can be solved for $\boldsymbol{H}^T\boldsymbol{R}^{-1}\boldsymbol{H}$ as

$$\boldsymbol{H}^T\boldsymbol{R}^{-1}\boldsymbol{H}=\boldsymbol{\Pi}^{-1}-\boldsymbol{P}^{-1}. \qquad\qquad\text{(D.30)}$$

Equations (D.29) and (D.30) are now combined to yield

$$\frac{\det\{2\pi\boldsymbol{P}\}^{-1/2}\det\{2\pi\boldsymbol{R}\}^{-1/2}}{\det\{2\pi\boldsymbol{\Pi}\}^{-1/2}\det\{2\pi(\boldsymbol{H}\boldsymbol{P}\boldsymbol{H}^T+\boldsymbol{R})\}^{-1/2}}=\left[\det\{\boldsymbol{\Pi}\boldsymbol{P}^{-1}\}\det\{\boldsymbol{P}(\boldsymbol{\Pi}^{-1}-\boldsymbol{P}^{-1})+\boldsymbol{I}\}\right]^{\frac{1}{2}}$$
$$=\left[\det\{\boldsymbol{\Pi}\boldsymbol{P}^{-1}\}\det\{\boldsymbol{P}\boldsymbol{\Pi}^{-1}\}\right]^{\frac{1}{2}}$$
$$=\left[\det\{\boldsymbol{\Pi}\boldsymbol{P}^{-1}\boldsymbol{P}\boldsymbol{\Pi}^{-1}\}\right]^{\frac{1}{2}}$$
$$=\left[\det\{\boldsymbol{I}\}\right]^{\frac{1}{2}}$$
$$=1. \qquad\qquad\text{(D.31)}$$

Substituting Eq. (D.31) into Eq. (D.27) yields Eq. (D.1) according to

$$p_g(\boldsymbol{x};\boldsymbol{m},\boldsymbol{P})p_g(\boldsymbol{z};\boldsymbol{H}\boldsymbol{x},\boldsymbol{R})=p_g(\boldsymbol{z};(\boldsymbol{H}\boldsymbol{m}),\boldsymbol{H}\boldsymbol{P}\boldsymbol{H}^T+\boldsymbol{R})p_g(\boldsymbol{x};\boldsymbol{\mu},\boldsymbol{\Pi}),$$

which completes the proof. □

APPENDIX E

GAUSSIAN PARAMETERS FROM A SET OF WEIGHTED DISCRETE POINTS

Consider the case when a set of discrete points and weights is used to probabilistically represent a state vector $\boldsymbol{x}$. Let these weights and associated points be denoted by $w^{(i)}$ and $\boldsymbol{\mathcal{X}}^{(i)}$, respectively, where $i = 1, 2, \ldots, N$, respectively. Assume that the points represent a valid probability mass function; that is

$$\sum_{i=1}^{N} w^{(i)} = 1. \tag{E.1}$$

It is desired to find the parameters of the Gaussian distribution, $\boldsymbol{m}$ and $\boldsymbol{P}$, that best fit the weighted points. These best fit parameters are found using the sum of the weighted log-likelihood of the discrete points as the performance index, which is given by

$$J(\boldsymbol{m}, \boldsymbol{P}) = \sum_{i=1}^{N} w^{(i)} \ln p_g(\boldsymbol{\mathcal{X}}^{(i)}; \boldsymbol{m}, \boldsymbol{P}), \tag{E.2}$$

One may be inclined to use the sum of the weighted likelihood or log weighted-likelihood of the sigma points; however, either of these approaches make the performance index independent of the weights, which is undesirable. The definition of the Gaussian density is substituted from Eq. (3.4) into Equation (E.2) to yield the cost function as

$$J(\boldsymbol{m}, \boldsymbol{P}) = -\frac{1}{2}\left[\ln \det\{2\pi\boldsymbol{P}\} + \sum_{i=1}^{N} w^{(i)} \left(\boldsymbol{\mathcal{X}}^{(i)} - \boldsymbol{m}\right)^{T} \boldsymbol{P}^{-1} \left(\boldsymbol{\mathcal{X}}^{(i)} - \boldsymbol{m}\right)\right]. \tag{E.3}$$

Equation (E.3) can be minimized without enforcing the symmetry and positive definiteness of $\boldsymbol{P}$. This method, obviously, does not guarantee the symmetry and positive definiteness of $\boldsymbol{P}$, which may lead to a solution that results in an invalid Gaussian density. Differentiating Eq. (E.3) with respect to $\boldsymbol{m}$ and $\boldsymbol{P}$ and setting the results equal to zero yields the optimality conditions as

$$\frac{\partial J(\boldsymbol{m}, \boldsymbol{P})}{\partial \boldsymbol{m}} = \frac{1}{2}\sum_{i=1}^{N} w^{(i)} \left(\boldsymbol{\mathcal{X}}^{(i)} - \boldsymbol{m}\right)^{T} \left(\boldsymbol{P}^{-T} + \boldsymbol{P}^{-1}\right) = \boldsymbol{0}^{T} \tag{E.4a}$$

$$\frac{\partial J(\boldsymbol{m}, \boldsymbol{P})}{\partial \boldsymbol{P}} = -\frac{1}{2}\left[\boldsymbol{P}^{-T} - \sum_{i=1}^{N} w^{(i)} \boldsymbol{P}^{-T} \left(\boldsymbol{\mathcal{X}}^{(i)} - \boldsymbol{m}\right) \left(\boldsymbol{\mathcal{X}}^{(i)} - \boldsymbol{m}\right)^{T} \boldsymbol{P}^{-T}\right] = \boldsymbol{0}. \tag{E.4b}$$

If $\boldsymbol{P}$ is forced to be symmetric, then Eqs. (E.4) can be simplified to

$$\sum_{i=1}^{N} w^{(i)} \left(\boldsymbol{\mathcal{X}}^{(i)} - \boldsymbol{m}\right)^{T} \boldsymbol{P}^{-1} = \boldsymbol{0}^{T} \tag{E.5a}$$

$$\boldsymbol{P}^{-1} - \sum_{i=1}^{N} w^{(i)} \boldsymbol{P}^{-1} \left(\boldsymbol{\mathcal{X}}^{(i)} - \boldsymbol{m} \right) \left(\boldsymbol{\mathcal{X}}^{(i)} - \boldsymbol{m} \right)^{T} \boldsymbol{P}^{-1} = \boldsymbol{0} \, . \tag{E.5b}$$

If $\boldsymbol{P}$ is forced to be positive definite, then $\boldsymbol{P}$ is full rank (and hence invertible), and Eq. (E.5) can be simplified to

$$\sum_{i=1}^{N} w^{(i)} \left(\boldsymbol{\mathcal{X}}^{(i)} - \boldsymbol{m} \right)^{T} = \boldsymbol{0}^{T} \tag{E.6a}$$

$$\boldsymbol{I} - \sum_{i=1}^{N} w^{(i)} \left(\boldsymbol{\mathcal{X}}^{(i)} - \boldsymbol{m} \right) \left(\boldsymbol{\mathcal{X}}^{(i)} - \boldsymbol{m} \right)^{T} \boldsymbol{P}^{-1} = \boldsymbol{0} \, . \tag{E.6b}$$

Equations (E.6) can then be solved for $\boldsymbol{m}$ and $\boldsymbol{P}$ according to

$$\boldsymbol{m} = \sum_{i=1}^{N} w^{(i)} \boldsymbol{\mathcal{X}}^{(i)} \tag{E.7a}$$

$$\boldsymbol{P} = \sum_{i=1}^{N} w^{(i)} \left(\boldsymbol{\mathcal{X}}^{(i)} - \boldsymbol{m} \right) \left(\boldsymbol{\mathcal{X}}^{(i)} - \boldsymbol{m} \right)^{T} \, . \tag{E.7b}$$

Observation of Eqs. (E.7) shows that the covariance is both positive definite and symmetric, provided that there are at least N linearly independent deviations from the mean, $\boldsymbol{\mathcal{X}}^{(i)} - \boldsymbol{m}$, and this mean and covariance represents a valid Gaussian pdf.

In order to prove that Eqs. (E.7) maximize Eq. (E.3), a second-derivative condition must be shown. Showing this condition for arbitrary dimension becomes quite cumbersome and is omitted for brevity. Instead, the second-derivative condition is shown for the scalar case. In the scalar case, the performance index, as given by Eq. (E.3), simplifies to

$$J(m, \sigma^2) = -\frac{1}{2} \left[\ln\{2\pi\sigma^2\} + \sum_{i=1}^{N} w^{(i)} \frac{\left(\mathcal{X}^{(i)} - m \right)^2}{\sigma^2} \right] \, , \tag{E.8}$$

and the first derivative condition given in Eqs. (E.4) simplifies to

$$\frac{\partial J(m, \sigma^2)}{\partial m} = \sum_{i=1}^{N} w^{(i)} \frac{\mathcal{X}^{(i)} - m}{\sigma^2} \tag{E.9a}$$

$$\frac{\partial J(m, \sigma^2)}{\partial \sigma^2} = -\frac{1}{2} \left[\frac{1}{\sigma^2} - \sum_{i=1}^{N} w^{(i)} \frac{\left(\mathcal{X}^{(i)} - m \right)^2}{\sigma^4} \right] \, . \tag{E.9b}$$

The second derivatives are now found by differentiating each of Eqs. (E.9) with respect to m and σ^2 to yield

$$\frac{\partial^2 J(m,\sigma^2)}{\partial m \partial m} = -\sum_{i=1}^{N} \frac{w^{(i)}}{\sigma^2} = \frac{-1}{\sigma^2} \tag{E.10a}$$

$$\frac{\partial^2 J(m,\sigma^2)}{\partial m \partial \sigma^2} = \frac{\partial^2 J(m,\sigma^2)}{\partial \sigma^2 \partial m} = -\sum_{i=1}^{N} w^{(i)} \frac{\mathcal{X}^{(i)} - m}{\sigma^4} \tag{E.10b}$$

$$\frac{\partial^2 J(m,\sigma^2)}{\partial \sigma^2 \partial \sigma^2} = \frac{1}{2} \left[\frac{1}{\sigma^4} - 2\sum_{i=1}^{N} w^{(i)} \frac{\left(\mathcal{X}^{(i)} - m\right)^2}{\sigma^6} \right] . \tag{E.10c}$$

Equations (E.10) are evaluated at the optimum point defined by Eqs. (E.7) to yield

$$\frac{\partial^2 J(m,\sigma^2)}{\partial m \partial m} = -\sum_{i=1}^{N} \frac{w^{(i)}}{\sigma^2} = \frac{-1}{\sigma^2} \tag{E.11a}$$

$$\frac{\partial^2 J(m,\sigma^2)}{\partial m \partial \sigma^2} = 0 \tag{E.11b}$$

$$\frac{\partial^2 J(m,\sigma^2)}{\partial \sigma^2 \partial \sigma^2} = \frac{-1}{2\sigma^4} , \tag{E.11c}$$

which shows that the optimum point is a maximum because

$$\frac{\partial^2 J(m,\sigma^2)}{\partial m \partial m} \frac{\partial^2 J(m,\sigma^2)}{\partial \sigma^2 \partial \sigma^2} - \left(\frac{\partial^2 J(m,\sigma^2)}{\partial m \partial \sigma^2} \right)^2 = \frac{1}{2\sigma^6} > 0 ,$$

and

$$\frac{\partial^2 J(m,\sigma^2)}{\partial m \partial m} < 0 ,$$

which are sufficient conditions for a local maximum of a performance index of two variables.

APPENDIX F

GAUSS-BINGHAM PARAMETERS FROM A SET OF WEIGHTED DISCRETE POINTS

Consider the case when a set of discrete points with associated weights is used to probabilistically represent the vector $\boldsymbol{x} = [\bar{\boldsymbol{q}}^T \;\; \mathbf{x}^T]^T \in \mathbb{S}^s \times \mathbb{R}^r$. Let these weights and associated points be denoted by $w^{(i)}$ and $\boldsymbol{\mathcal{X}}^{(i)} \triangleq [\boldsymbol{\mathcal{X}}_q^{(i)^T} \;\; \boldsymbol{\mathcal{X}}_{\mathrm{x}}^{(i)^T}]^T$, where $i = 1, 2, \ldots, N$, respectively. Assume that each point, $\boldsymbol{\mathcal{X}}^{(i)}$, has an implied point that is antipodal in the quaternion portion of the state vector, given by $\widetilde{\boldsymbol{X}}^{(i)} \triangleq [-\boldsymbol{\mathcal{X}}_q^{(i)^T} \;\; \boldsymbol{\mathcal{X}}_{\mathrm{x}}^{(i)^T}]^T$. Assume that the points (including the implied antipodal points) represent a valid probability mass function; that is

$$\sum_{i=1}^{N} w^{(i)} = \frac{1}{2} \, . \tag{F.1}$$

It is desired to find the parameters of the Gauss-Bingham distribution, as defined by Eq. (3.53), that best fit the given points in the weighted log-likelihood sense. An equivalent form of the Gauss-Bingham density is used, which is given by

$$p_{gb}(\boldsymbol{x}; \boldsymbol{m}, \boldsymbol{P}, \boldsymbol{\phi}_0, \boldsymbol{\beta}, \boldsymbol{Z}) = p_g(\mathbf{x}; \boldsymbol{m}, \boldsymbol{P}) \, p_b(\bar{\boldsymbol{q}}; \boldsymbol{M}(\mathbf{z}; \boldsymbol{\phi}_0, \boldsymbol{\beta}), \boldsymbol{Z}) \, , \tag{F.2}$$

and uses the canonical Gaussian variable $\mathbf{z}$, as defined by Eq. (3.6), instead of $\mathbf{x}$ for better numerical stability. The best-fit parameters can be found using the sum of the weighted log-likelihood of the discrete points (including the implied antipodal points) as the performance index, which is given by

$$J(\boldsymbol{m}, \boldsymbol{P}, \boldsymbol{\phi}_0, \boldsymbol{\beta}, \boldsymbol{Z}) = \sum_{i=1}^{N} w^{(i)} \ln \left[p_{gb}(\boldsymbol{\mathcal{X}}^{(i)}; \boldsymbol{m}, \boldsymbol{P}, \boldsymbol{\phi}_0, \boldsymbol{\beta}, \boldsymbol{Z}) \right]$$

$$+ \sum_{i=1}^{N} w^{(i)} \ln \left[p_{gb}(\widetilde{\boldsymbol{X}}^{(i)}; \boldsymbol{m}, \boldsymbol{P}, \boldsymbol{\phi}_0, \boldsymbol{\beta}, \boldsymbol{Z}) \right] \, . \tag{F.3}$$

One may be inclined to use the sum of the weighted likelihood or log weighted-likelihood of the sigma points; however, either of these approaches makes the performance index independent of the weights, which is undesirable. Since the Gauss-Bingham distribution is antipodally symmetric in $\bar{\boldsymbol{q}}$, this reduces to

$$J(\boldsymbol{m}, \boldsymbol{P}, \boldsymbol{\phi}_0, \boldsymbol{\beta}, \boldsymbol{Z}) = 2 \sum_{i=1}^{N} w^{(i)} \ln \left[p_{gb}(\boldsymbol{\mathcal{X}}^{(i)}; \boldsymbol{m}, \boldsymbol{P}, \boldsymbol{\phi}_0, \boldsymbol{\beta}, \boldsymbol{Z}) \right] \, . \tag{F.4}$$

Substituting Eqs. (F.2), (3.4), and (3.18) into Eq. (F.4) and exploiting the properties of the natural logarithm yields

$$J(\boldsymbol{m}, \boldsymbol{P}, \boldsymbol{\phi}_0, \boldsymbol{\beta}, \boldsymbol{Z}) = -\frac{1}{2} \left[\ln \det \{ 2\pi \boldsymbol{P} \} + 2 \sum_{i=1}^{N} w^{(i)} \left(\boldsymbol{\mathcal{X}}_{\mathrm{x}}^{(i)} - \boldsymbol{m} \right)^T \boldsymbol{P}^{-1} \left(\boldsymbol{\mathcal{X}}_{\mathrm{x}}^{(i)} - \boldsymbol{m} \right) \right.$$

$$+ 2 \ln F\left(\boldsymbol{Z}\right) - 4 \sum_{i=1}^{N} w^{(i)} \boldsymbol{\mathcal{X}}_{q}^{(i)^{T}} \boldsymbol{M}(\boldsymbol{\mathcal{X}}_{\mathrm{z}}^{(i)}; \boldsymbol{\phi}_0, \boldsymbol{\beta}) \boldsymbol{Z} \boldsymbol{M}(\boldsymbol{\mathcal{X}}_{\mathrm{z}}^{(i)}; \boldsymbol{\phi}_0, \boldsymbol{\beta})^{T} \boldsymbol{\mathcal{X}}_{q}^{(i)} \Bigg], \quad \text{(F.5)}$$

where $\boldsymbol{\mathcal{X}}_{\mathrm{z}}^{(i)}$ represents the transformed $\boldsymbol{\mathcal{X}}_{\mathrm{x}}^{(i)}$ according to

$$\boldsymbol{\mathcal{X}}_{\mathrm{x}}^{(i)} = \boldsymbol{S} \boldsymbol{\mathcal{X}}_{\mathrm{z}}^{(i)} + \boldsymbol{m}, \tag{F.6}$$

where

$$\boldsymbol{S}\boldsymbol{S}^{T} \triangleq \boldsymbol{P}.$$

Equation (F.5) can be maximized analytically for $\boldsymbol{m}$ and $\boldsymbol{P}$ without enforcing the symmetry and positive definiteness of $\boldsymbol{P}$, in a similar manner to how they are found for the Gaussian pdf in Appendix E. Differentiating Eq. (F.5) with respect to $\boldsymbol{m}$ and $\boldsymbol{P}$ and setting the results equal to zero yields the optimality conditions as

$$\frac{\partial J(\boldsymbol{m}, \boldsymbol{P}, \boldsymbol{\phi}_0, \boldsymbol{\beta}, \boldsymbol{Z})}{\partial \boldsymbol{m}} = \sum_{i=1}^{N} w^{(i)} \left(\boldsymbol{\mathcal{X}}_{\mathrm{x}}^{(i)} - \boldsymbol{m} \right)^{T} \left(\boldsymbol{P}^{-T} + \boldsymbol{P}^{-1} \right) = \boldsymbol{0}^{T} \tag{F.7a}$$

$$\frac{\partial J(\boldsymbol{m}, \boldsymbol{P}, \boldsymbol{\phi}_0, \boldsymbol{\beta}, \boldsymbol{Z})}{\partial \boldsymbol{P}} =$$
$$- \frac{1}{2} \left[\boldsymbol{P}^{-T} - 2 \sum_{i=1}^{N} w^{(i)} \boldsymbol{P}^{-T} \left(\boldsymbol{\mathcal{X}}_{\mathrm{x}}^{(i)} - \boldsymbol{m} \right) \left(\boldsymbol{\mathcal{X}}_{\mathrm{x}}^{(i)} - \boldsymbol{m} \right)^{T} \boldsymbol{P}^{-T} \right] = \boldsymbol{0}. \tag{F.7b}$$

If $\boldsymbol{P}$ is forced to be symmetric, then Eqs. (F.7) can be simplified to

$$2 \sum_{i=1}^{N} w^{(i)} \left(\boldsymbol{\mathcal{X}}_{\mathrm{x}}^{(i)} - \boldsymbol{m} \right)^{T} \boldsymbol{P}^{-1} = \boldsymbol{0}^{T} \tag{F.8a}$$

$$\boldsymbol{P}^{-1} - 2 \sum_{i=1}^{N} w^{(i)} \boldsymbol{P}^{-1} \left(\boldsymbol{\mathcal{X}}_{\mathrm{x}}^{(i)} - \boldsymbol{m} \right) \left(\boldsymbol{\mathcal{X}}_{\mathrm{x}}^{(i)} - \boldsymbol{m} \right)^{T} \boldsymbol{P}^{-1} = \boldsymbol{0}. \tag{F.8b}$$

Furthermore, if $\boldsymbol{P}$ is forced to be positive definite, then $\boldsymbol{P}$ is full rank (and hence invertible), and Eq. (F.8) can be simplified to

$$2 \sum_{i=1}^{N} w^{(i)} \left(\boldsymbol{\mathcal{X}}_{\mathrm{x}}^{(i)} - \boldsymbol{m} \right)^{T} = \boldsymbol{0}^{T} \tag{F.9a}$$

$$\boldsymbol{I} - 2 \sum_{i=1}^{N} w^{(i)} \left(\boldsymbol{\mathcal{X}}_{\mathrm{x}}^{(i)} - \boldsymbol{m} \right) \left(\boldsymbol{\mathcal{X}}_{\mathrm{x}}^{(i)} - \boldsymbol{m} \right)^{T} \boldsymbol{P}^{-1} = \boldsymbol{0}. \tag{F.9b}$$

Equation (F.9) can then be solved for $\boldsymbol{m}$ and $\boldsymbol{P}$ according to

$$\boldsymbol{m} = 2 \sum_{i=1}^{N} w^{(i)} \boldsymbol{\mathcal{X}}_{\mathrm{x}}^{(i)} \tag{F.10a}$$

$$\boldsymbol{P} = 2 \sum_{i=1}^{N} w^{(i)} \left(\boldsymbol{\mathcal{X}}_{\mathrm{x}}^{(i)} - \boldsymbol{m} \right) \left(\boldsymbol{\mathcal{X}}_{\mathrm{x}}^{(i)} - \boldsymbol{m} \right)^{T} . \tag{F.10b}$$

Observation of Eqs. (F.10) shows that the covariance is both positive definite and symmetric, provided that there are at least N linearly independent deviations from the mean, $\boldsymbol{\mathcal{X}}_{\mathrm{x}}^{(i)} - \boldsymbol{m}$. Note that the dependence of $\boldsymbol{\mathcal{X}}_{\mathrm{z}}^{(i)}$ on $\boldsymbol{m}$ and $\boldsymbol{P}$ is neglected in finding these parameters analytically. This is not an issue, however, because $\boldsymbol{m}$ and $\boldsymbol{P}$ define a linear transformation of the points for a given $\boldsymbol{m}$ and $\boldsymbol{P}$. Similarly, $\boldsymbol{\phi}_0$ and $\boldsymbol{\beta}$ define a linear function of $\boldsymbol{\mathcal{X}}_{\mathrm{z}}^{(i)}$. Because of this, any deviations in $\boldsymbol{m}$ and $\boldsymbol{P}$ (which would be present if they were not first found analytically) will simply be absorbed by $\boldsymbol{\phi}_0$ and $\boldsymbol{\beta}$. This implies that $\boldsymbol{m}$ and $\boldsymbol{P}$ can be found first and held constant, and then $\boldsymbol{\phi}_0$, $\boldsymbol{\beta}$, and $\boldsymbol{Z}$ can be found that maximize the performance index.

The parameters $\boldsymbol{m}$ and $\boldsymbol{P}$ are now known, so an appropriate cost function is given by a simplification of Eq. (F.5) (noting that $\boldsymbol{m}$ and $\boldsymbol{P}$ are now known and constant) according to

$$J(\boldsymbol{\phi}_0, \boldsymbol{\beta}, \boldsymbol{Z}) = 2 \sum_{i=1}^{N} w^{(i)} \boldsymbol{\mathcal{X}}_{q}^{(i)^{T}} \boldsymbol{M}(\boldsymbol{\mathcal{X}}_{\mathrm{z}}^{(i)}; \boldsymbol{\phi}_0, \boldsymbol{\beta}) \boldsymbol{Z} \boldsymbol{M}(\boldsymbol{\mathcal{X}}_{\mathrm{z}}^{(i)}; \boldsymbol{\phi}_0, \boldsymbol{\beta})^{T} \boldsymbol{\mathcal{X}}_{q}^{(i)} - \ln F(\boldsymbol{Z}) . \tag{F.11}$$

Recall that the conditional orientation matrix of the Gauss-Bingham density is parameterized by a minimum set of parameters that are functionally dependent on $\boldsymbol{\mathcal{X}}_{\mathrm{z}}^{(i)}$, $\boldsymbol{\phi}_0$, and $\boldsymbol{\beta}$ according to $\boldsymbol{M}(\boldsymbol{\mathcal{X}}_{\mathrm{z}}^{(i)}; \boldsymbol{\phi}_0, \boldsymbol{\beta}) = \boldsymbol{M}[\boldsymbol{\phi}(\boldsymbol{\mathcal{X}}_{\mathrm{z}}^{(i)}; \boldsymbol{\phi}_0, \boldsymbol{\beta})]$, such that Eq. (F.11) can be expressed according to

$$J(\boldsymbol{\phi}_0, \boldsymbol{\beta}, \boldsymbol{Z}) = 2 \sum_{i=1}^{N} w^{(i)} \boldsymbol{\mathcal{X}}_{q}^{(i)^{T}} \boldsymbol{M}[\boldsymbol{\phi}(\boldsymbol{\mathcal{X}}_{\mathrm{z}}^{(i)}; \boldsymbol{\phi}_0, \boldsymbol{\beta})] \boldsymbol{Z} \boldsymbol{M}[\boldsymbol{\phi}(\boldsymbol{\mathcal{X}}_{\mathrm{z}}^{(i)}; \boldsymbol{\phi}_0, \boldsymbol{\beta})]^{T} \boldsymbol{\mathcal{X}}_{q}^{(i)}$$

$$- \ln F(\boldsymbol{Z}) , \tag{F.12}$$

where

$$\boldsymbol{\phi}(\boldsymbol{\mathcal{X}}_{\mathrm{z}}^{(i)}; \boldsymbol{\phi}_0, \boldsymbol{\beta}) = \boldsymbol{\phi}_0 + \boldsymbol{\beta} \boldsymbol{\mathcal{X}}_{\mathrm{z}}^{(i)} . \tag{F.13}$$

It is now desired to find the optimality conditions by differentiating Eq. (F.12) with respect to each entry of $\boldsymbol{\phi}_0$, $\boldsymbol{\beta}$, $\boldsymbol{Z}$ and setting the result equal to zero. In order to do this, first, the chain rule for the case of differentiating the function $\boldsymbol{G}(\boldsymbol{F}(\boldsymbol{X}))$ with respect to the entry in the ith row and j^{th}

column of $\boldsymbol{X}$, $X_{i,j}$, is introduced and is given by [87]

$$\frac{\partial \boldsymbol{G}(\boldsymbol{F}(\boldsymbol{X}))}{\partial X_{i,j}} = \sum_{k=1}^{M} \sum_{l=1}^{N} \frac{\partial \boldsymbol{G}(\boldsymbol{F})}{\partial F_{k,\ell}} \frac{\partial F_{k,\ell}}{\partial X_{i,j}} \ . \tag{F.14}$$

If $\boldsymbol{F}$ is a column vector denoted now by $\boldsymbol{f}$, Eq. (F.14) simplifies to

$$\frac{\partial \boldsymbol{G}(\boldsymbol{f}(\boldsymbol{X}))}{\partial X_{i,j}} = \sum_{k=1}^{M} \frac{\partial \boldsymbol{G}(\boldsymbol{f})}{\partial f_k} \frac{\partial f_k}{\partial X_{i,j}} \ . \tag{F.15}$$

If $\boldsymbol{G}$ is a scalar denoted now by g, Eq. (F.14) simplifies to

$$\frac{\partial g(\boldsymbol{F}(\boldsymbol{X}))}{\partial X_{i,j}} = \sum_{k=1}^{M} \sum_{l=1}^{N} \frac{\partial g(\boldsymbol{F})}{\partial F_{k,\ell}} \frac{\partial F_{k,\ell}}{\partial X_{i,j}} \ , \tag{F.16}$$

which can be expressed in matrix form as

$$\frac{\partial g(\boldsymbol{F}(\boldsymbol{X}))}{\partial X_{i,j}} = \mathrm{tr} \left\{ \frac{\partial g(\boldsymbol{F})}{\partial \boldsymbol{F}} \frac{\partial \boldsymbol{F}}{\partial X_{i,j}} \right\} \ . \tag{F.17}$$

These relationships are used in the remainder of this appendix to differentiate the appropriate quantities.

The optimality conditions for the performance index given in Eq. (F.12) are now considered for the $s = 1$ and $s = 3$ cases, separately. These cases are considered because they are the dimensions in which the one- and three-dimensional attitude quaternion exists. For $s = 1$, the cost function simplifies to

$$J(\phi_0, \boldsymbol{\beta}, \boldsymbol{Z}) = 2 \sum_{i=1}^{N} w^{(i)} \boldsymbol{\mathcal{X}}_q^{(i)T} \boldsymbol{M}[\phi(\boldsymbol{\mathcal{X}}_{\mathrm{z}}^{(i)}; \phi_0, \boldsymbol{\beta})] \boldsymbol{Z} \boldsymbol{M}[\phi(\boldsymbol{\mathcal{X}}_{\mathrm{z}}^{(i)}; \phi_0, \boldsymbol{\beta})]^T \boldsymbol{\mathcal{X}}_q^{(i)}$$

$$- \ln F(\boldsymbol{Z}) \ . \tag{F.18}$$

where

$$\boldsymbol{Z} = \begin{bmatrix} Z_1 & 0 \\ 0 & 0 \end{bmatrix} \qquad \text{and} \qquad \boldsymbol{M}(\phi) = \begin{bmatrix} \cos\phi & \sin\phi \\ -\sin\phi & \cos\phi \end{bmatrix} \tag{F.19}$$

For notational simplicity, let the cost function be defined by

$$J(\phi_0, \boldsymbol{\beta}, \boldsymbol{Z}) \triangleq 2 \sum_{i=1}^{N} w^{(i)} K_i(\phi_0, \boldsymbol{\beta}, \boldsymbol{Z}) - \ln F(\boldsymbol{Z}) \ , \tag{F.20}$$

where

$$K_i(\phi_0, \boldsymbol{\beta}, \boldsymbol{Z}) = \boldsymbol{\mathcal{X}}_q^{(i)^T} \boldsymbol{M}[\phi(\boldsymbol{\mathcal{X}}_z^{(i)}; \phi_0, \boldsymbol{\beta})] \boldsymbol{Z} \boldsymbol{M}[\phi(\boldsymbol{\mathcal{X}}_z^{(i)}; \phi_0, \boldsymbol{\beta})]^T \boldsymbol{\mathcal{X}}_q^{(i)}$$

The partial derivative of the cost function with respect to and arbitrary parameter that is denoted by the symbol "$\star$" can then be expressed as

$$\frac{\partial J(\phi_0, \boldsymbol{\beta}, \boldsymbol{Z})}{\partial \star} = 2 \sum_{i=1}^{N} w^{(i)} \frac{\partial K_i(\phi_0, \boldsymbol{\beta}, \boldsymbol{Z})}{\partial \star} - \frac{\partial \ln F(\boldsymbol{Z})}{\partial \star} .$$

It is now necessary to find these partial derivatives with respect to Z_1, ϕ_0, and $\boldsymbol{\beta}$. The term $\ln F(\boldsymbol{Z})$ is solely a function of Z_1; therefore, its only nonzero partial derivative is with respect to Z_1 according to

$$\frac{\partial \ln F(\boldsymbol{Z})}{\partial Z_1} = \text{tr} \left\{ \frac{\partial \ln F(\boldsymbol{Z})}{\partial F(\boldsymbol{Z})} \frac{\partial F(\boldsymbol{Z})}{\partial Z_1} \right\} = F^{-1}(\boldsymbol{Z}) \frac{\partial F(\boldsymbol{Z})}{\partial Z_1} = f_1 .$$

Now the partial derivatives of $K_i(\phi_0, \boldsymbol{\beta}, \boldsymbol{Z})$ with respect to Z_1, ϕ_0, and $\boldsymbol{\beta}$ must be found. Its partial derivative with respect to Z_1 is given by

$$\frac{\partial K_i(\phi_0, \boldsymbol{\beta}, \boldsymbol{Z})}{\partial Z_1} = \text{tr} \left\{ \frac{\partial \boldsymbol{\mathcal{X}}_q^{(i)^T} \boldsymbol{M}[\phi(\boldsymbol{\mathcal{X}}_z^{(i)}; \phi_0, \boldsymbol{\beta})] \boldsymbol{Z} \boldsymbol{M}[\phi(\boldsymbol{\mathcal{X}}_z^{(i)}; \phi_0, \boldsymbol{\beta})]^T \boldsymbol{\mathcal{X}}_q^{(i)}}{\partial \boldsymbol{Z}} \frac{\partial \boldsymbol{Z}}{\partial Z_1} \right\} . \quad \text{(F.21)}$$

Calculating the derivatives in Eq. (F.21) yields

$$\frac{\partial K_i(\phi_0, \boldsymbol{\beta}, \boldsymbol{Z})}{\partial Z_1} = \text{tr} \left\{ \boldsymbol{M}[\phi(\boldsymbol{\mathcal{X}}_z^{(i)}; \phi_0, \boldsymbol{\beta})]^T \boldsymbol{\mathcal{X}}_q^{(i)} \boldsymbol{\mathcal{X}}_q^{(i)^T} \boldsymbol{M}[\phi(\boldsymbol{\mathcal{X}}_z^{(i)}; \phi_0, \boldsymbol{\beta})] \boldsymbol{1}_{1,1}^{2,2} \right\} . \quad \text{(F.22)}$$

where the $\boldsymbol{1}_{i,j}^{k,\ell}$ matrix represents a k by ℓ matrix of all zeros, except the i, j entry which is one. Using the cyclic property of the trace, Eq. (F.22) can be expressed as

$$\frac{\partial K_i(\phi_0, \boldsymbol{\beta}, \boldsymbol{Z})}{\partial Z_1} = \boldsymbol{\mathcal{X}}_q^{(i)^T} \boldsymbol{M}[\phi(\boldsymbol{\mathcal{X}}_z^{(i)}; \phi_0, \boldsymbol{\beta})] \boldsymbol{1}_{1,1}^{2,2} \boldsymbol{M}[\phi(\boldsymbol{\mathcal{X}}_z^{(i)}; \phi_0, \boldsymbol{\beta})]^T \boldsymbol{\mathcal{X}}_q^{(i)} .$$

The partial derivative of $K_i(\phi_0, \boldsymbol{\beta}, \boldsymbol{Z})$ with respect to ϕ_0 is given by

$$\frac{\partial K_i(\phi_0, \boldsymbol{\beta}, \boldsymbol{Z})}{\partial \phi_0} = \text{tr} \left\{ \frac{\partial \boldsymbol{\mathcal{X}}_q^{(i)^T} \boldsymbol{M}[\phi(\boldsymbol{\mathcal{X}}_z^{(i)}; \phi_0, \boldsymbol{\beta})] \boldsymbol{Z} \boldsymbol{M}[\phi(\boldsymbol{\mathcal{X}}_z^{(i)}; \phi_0, \boldsymbol{\beta})]^T \boldsymbol{\mathcal{X}}_q^{(i)}}{\partial \boldsymbol{M}[\phi(\boldsymbol{\mathcal{X}}_z^{(i)}; \phi_0, \boldsymbol{\beta})]} \right. \quad \text{(F.23)}$$
$$\left. \times \frac{\partial \boldsymbol{M}[\phi(\boldsymbol{\mathcal{X}}_z^{(i)}; \phi_0, \boldsymbol{\beta})]}{\partial \phi_0} \right\} .$$

The former derivative of the chain rule in Eq. (F.23) is calculated as

$$\frac{\partial \boldsymbol{\mathcal{X}}_q^{(i)T} \boldsymbol{M}[\phi(\boldsymbol{\mathcal{X}}_z^{(i)}; \phi_0, \boldsymbol{\beta})] \boldsymbol{Z} \boldsymbol{M}[\phi(\boldsymbol{\mathcal{X}}_z^{(i)}; \phi_0, \boldsymbol{\beta})]^T \boldsymbol{\mathcal{X}}_q^{(i)}}{\partial \boldsymbol{M}[\phi(\boldsymbol{\mathcal{X}}_z^{(i)}; \phi_0, \boldsymbol{\beta})]} = \tag{F.24}$$

$$2\boldsymbol{\mathcal{X}}_q^{(i)} \boldsymbol{\mathcal{X}}_q^{(i)T} \boldsymbol{M}[\phi(\boldsymbol{\mathcal{X}}_z^{(i)}; \phi_0, \boldsymbol{\beta})] \boldsymbol{Z} \,.$$

The latter derivative of the chain rule in Eq. (F.23) is calculated (using the chain rule again) as

$$\frac{\partial \boldsymbol{M}[\phi(\boldsymbol{\mathcal{X}}_z^{(i)}; \phi_0, \boldsymbol{\beta})]}{\partial \phi_0} = \frac{\partial \boldsymbol{M}[\phi(\boldsymbol{\mathcal{X}}_z^{(i)}; \phi_0, \boldsymbol{\beta})]}{\partial \phi(\boldsymbol{\mathcal{X}}_z^{(i)}; \phi_0, \boldsymbol{\beta})} \frac{\partial \phi(\boldsymbol{\mathcal{X}}_z^{(i)}; \phi_0, \boldsymbol{\beta})}{\partial \phi_0} \,. \tag{F.25}$$

The derivatives in the right hand side of Eq. (F.25) can now be calculated from Eqs. (F.13) and (F.19) as

$$\frac{\partial \boldsymbol{M}(\phi)}{\partial \phi} \triangleq \boldsymbol{M}'(\phi) = \begin{bmatrix} -\sin\phi & \cos\phi \\ -\cos\phi & -\sin\phi \end{bmatrix} \quad \text{and} \quad \frac{\partial \phi(\boldsymbol{\mathcal{X}}_z^{(i)}; \phi_0, \boldsymbol{\beta})}{\partial \phi_0} = 1 \,, \tag{F.26}$$

such that Eq. (F.25) becomes

$$\frac{\partial \boldsymbol{M}[\phi(\boldsymbol{\mathcal{X}}_z^{(i)}; \phi_0, \boldsymbol{\beta})]}{\partial \phi_0} = \boldsymbol{M}'[\phi(\boldsymbol{\mathcal{X}}_z^{(i)}; \phi_0, \boldsymbol{\beta})] \tag{F.27}$$

Substituting Eqs. (F.24) and (F.27) into Eq. (F.23) becomes

$$\frac{\partial K_i(\phi_0, \boldsymbol{\beta}, \boldsymbol{Z})}{\partial \phi_0} = \text{tr} \left\{ 2\boldsymbol{\mathcal{X}}_q^{(i)} \boldsymbol{\mathcal{X}}_q^{(i)T} \boldsymbol{M}[\phi(\boldsymbol{\mathcal{X}}_z^{(i)}; \phi_0, \boldsymbol{\beta})] \boldsymbol{Z} \boldsymbol{M}' \left[\phi(\boldsymbol{\mathcal{X}}_z^{(i)}; \phi_0, \boldsymbol{\beta}) \right] \right\} \,. \tag{F.28}$$

Using the cyclic property of the trace, Eq. (F.28) can be expressed as

$$\frac{\partial K_i(\phi_0, \boldsymbol{\beta}, \boldsymbol{Z})}{\partial \phi_0} = 2\boldsymbol{\mathcal{X}}_q^{(i)T} \boldsymbol{M}[\phi(\boldsymbol{\mathcal{X}}_z^{(i)}; \phi_0, \boldsymbol{\beta})] \boldsymbol{Z} \boldsymbol{M}' \left[\phi(\boldsymbol{\mathcal{X}}_z^{(i)}; \phi_0, \boldsymbol{\beta}) \right] \boldsymbol{\mathcal{X}}_q^{(i)} \,. \tag{F.29}$$

The partial derivative of $K_i(\phi_0, \boldsymbol{\beta}, \boldsymbol{Z})$ with respect to $\beta_{1,k}$, where $k = 1, 2, \ldots, r$ is given by

$$\frac{\partial K_i(\phi_0, \boldsymbol{\beta}, \boldsymbol{Z})}{\partial \beta_{1,k}}$$

$$= \text{tr} \left\{ \frac{\partial \boldsymbol{\mathcal{X}}_q^{(i)T} \boldsymbol{M}[\phi(\boldsymbol{\mathcal{X}}_z^{(i)}; \phi_0, \boldsymbol{\beta})] \boldsymbol{Z} \boldsymbol{M}[\phi(\boldsymbol{\mathcal{X}}_z^{(i)}; \phi_0, \boldsymbol{\beta})]^T \boldsymbol{\mathcal{X}}_q^{(i)}}{\partial \boldsymbol{M}[\phi(\boldsymbol{\mathcal{X}}_z^{(i)}; \phi_0, \boldsymbol{\beta})]} \frac{\partial \boldsymbol{M}[\phi(\boldsymbol{\mathcal{X}}_z^{(i)}; \phi_0, \boldsymbol{\beta})]}{\partial \beta_{1,k}} \right\} \,. \tag{F.30}$$

The former derivative of the chain rule in Eq. (F.30) is given by Eq. (F.24). The latter derivative of the chain rule in Eq. (F.30) is calculated (using the chain rule again) as

$$\frac{\partial \boldsymbol{M}[\phi(\boldsymbol{\mathcal{X}}_{\mathrm{z}}^{(i)};\phi_0,\boldsymbol{\beta})]}{\partial \beta_{1,k}} = \frac{\partial \boldsymbol{M}[\phi(\boldsymbol{\mathcal{X}}_{\mathrm{z}}^{(i)};\phi_0,\boldsymbol{\beta})]}{\partial \phi(\boldsymbol{\mathcal{X}}_{\mathrm{z}}^{(i)};\phi_0,\boldsymbol{\beta})} \frac{\partial \phi(\boldsymbol{\mathcal{X}}_{\mathrm{z}}^{(i)};\phi_0,\boldsymbol{\beta})}{\partial \beta_{1,k}} \ . \tag{F.31}$$

The former derivative of the right hand side of Eq. (F.31) is given by Eq. (F.26). The latter derivative is given by (using the chain rule again)

$$\frac{\partial \phi(\boldsymbol{\mathcal{X}}_{\mathrm{z}}^{(i)};\phi_0,\boldsymbol{\beta})}{\partial \beta_{1,k}} = \frac{\partial \phi(\boldsymbol{\mathcal{X}}_{\mathrm{z}}^{(i)};\phi_0,\boldsymbol{\beta})}{\partial \boldsymbol{\beta}} \frac{\partial \boldsymbol{\beta}}{\partial \beta_{1,k}} \tag{F.32}$$

The former derivative in the right hand side of Eq. (F.32) can now be calculated from Eq. (F.19) as

$$\frac{\partial \phi(\boldsymbol{\mathcal{X}}_{\mathrm{z}}^{(i)};\phi_0,\boldsymbol{\beta})}{\partial \boldsymbol{\beta}} = \boldsymbol{\mathcal{X}}_{\mathrm{z}}^{(i)^T} \tag{F.33}$$

Substituting Eq. (F.33) into Eq. (F.32) yields

$$\frac{\partial \phi(\boldsymbol{\mathcal{X}}_{\mathrm{z}}^{(i)};\phi_0,\boldsymbol{\beta})}{\partial \beta_{1,k}} = \mathcal{X}_{\mathrm{z},k}^{(i)}, \tag{F.34}$$

where $\mathcal{X}_{\mathrm{z},k}^{(i)}$ represents the kth entry of $\boldsymbol{\mathcal{X}}_{\mathrm{z}}^{(i)}$. Substituting Eqs. (F.26) and (F.34) into Eq. (F.31) yields

$$\frac{\partial \boldsymbol{M}[\phi(\boldsymbol{\mathcal{X}}_{\mathrm{z}}^{(i)};\phi_0,\boldsymbol{\beta})]}{\partial \beta_{1,k}} = \boldsymbol{M}'\left[\phi(\boldsymbol{\mathcal{X}}_{\mathrm{z}}^{(i)};\phi_0,\boldsymbol{\beta})\right]\mathcal{X}_{\mathrm{z},k}^{(i)}. \tag{F.35}$$

Substituting Eqs. (F.24) and (F.35) into Eq. (F.30) yields

$$\frac{\partial K_i(\phi_0,\boldsymbol{\beta},\boldsymbol{Z})}{\partial \beta_{1,k}} = \mathrm{tr}\left\{2\boldsymbol{\mathcal{X}}_q^{(i)}\boldsymbol{\mathcal{X}}_q^{(i)^T}\boldsymbol{M}[\phi(\boldsymbol{\mathcal{X}}_{\mathrm{z}}^{(i)};\phi_0,\boldsymbol{\beta})]\boldsymbol{Z}\boldsymbol{M}'\left[\phi(\boldsymbol{\mathcal{X}}_{\mathrm{z}}^{(i)};\phi_0,\boldsymbol{\beta})\right]\mathcal{X}_{\mathrm{z},k}^{(i)}\right\}. \tag{F.36}$$

Using the cyclic property of the trace, Eq. (F.36) can be expressed as

$$\frac{\partial K_i(\phi_0,\boldsymbol{\beta},\boldsymbol{Z})}{\partial \beta_{1,k}} = 2\boldsymbol{\mathcal{X}}_q^{(i)^T}\boldsymbol{M}[\phi(\boldsymbol{\mathcal{X}}_{\mathrm{z}}^{(i)};\phi_0,\boldsymbol{\beta})]\boldsymbol{Z}\boldsymbol{M}'\left[\phi(\boldsymbol{\mathcal{X}}_{\mathrm{z}}^{(i)};\phi_0,\boldsymbol{\beta})\right]\boldsymbol{\mathcal{X}}_q^{(i)}\mathcal{X}_{\mathrm{z},k}^{(i)}. \tag{F.37}$$

In summary the optimality conditions are given for $s = 1$ (with some minor algebraic simplification) by

$$\frac{\partial J(\phi_0,\boldsymbol{\beta},\boldsymbol{Z})}{\partial \phi_0} = 4\sum_{i=1}^{N} w^{(i)}\left[\boldsymbol{\mathcal{X}}_q^{(i)^T}\boldsymbol{M}[\phi(\boldsymbol{\mathcal{X}}_{\mathrm{z}}^{(i)};\phi_0,\boldsymbol{\beta})]\boldsymbol{Z}\boldsymbol{M}'\left[\phi(\boldsymbol{\mathcal{X}}_{\mathrm{z}}^{(i)};\phi_0,\boldsymbol{\beta})\right]\boldsymbol{\mathcal{X}}_q^{(i)}\right] = 0$$

$$\frac{\partial J(\boldsymbol{\phi}_0, \boldsymbol{\beta}, \boldsymbol{Z})}{\partial Z_1} = 2 \sum_{i=1}^{N} w^{(i)} \left[\boldsymbol{\mathcal{X}}_q^{(i)T} \boldsymbol{M}[\phi(\boldsymbol{\mathcal{X}}_z^{(i)}; \boldsymbol{\phi}_0, \boldsymbol{\beta})] \mathbf{1}_{1,1}^{2,2} \boldsymbol{M}[\phi(\boldsymbol{\mathcal{X}}_z^{(i)}; \boldsymbol{\phi}_0, \boldsymbol{\beta})]^T \boldsymbol{\mathcal{X}}_q^{(i)} \right] - f_1 = 0$$

$$\frac{\partial J(\boldsymbol{\phi}_0, \boldsymbol{\beta}, \boldsymbol{Z})}{\partial \beta_{1,k}} = 4 \sum_{i=1}^{N} w^{(i)} \left[\boldsymbol{\mathcal{X}}_q^{(i)T} \boldsymbol{M}[\phi(\boldsymbol{\mathcal{X}}_z^{(i)}; \boldsymbol{\phi}_0, \boldsymbol{\beta})] \boldsymbol{Z} \boldsymbol{M}' \left[\phi(\boldsymbol{\mathcal{X}}_z^{(i)}; \boldsymbol{\phi}_0, \boldsymbol{\beta}) \right] \boldsymbol{\mathcal{X}}_q^{(i)} \boldsymbol{\mathcal{X}}_{z,k}^{(i)} \right] = 0$$

For $s = 3$, the cost function is given by

$$J(\boldsymbol{\phi}_0, \boldsymbol{\beta}, \boldsymbol{Z}) = 2 \sum_{i=1}^{N} w^{(i)} \boldsymbol{\mathcal{X}}_q^{(i)T} \boldsymbol{M}[\phi(\boldsymbol{\mathcal{X}}_z^{(i)}; \boldsymbol{\phi}_0, \boldsymbol{\beta})] \boldsymbol{Z} \boldsymbol{M}[\phi(\boldsymbol{\mathcal{X}}_z^{(i)}; \boldsymbol{\phi}_0, \boldsymbol{\beta})]^T \boldsymbol{\mathcal{X}}_q^{(i)}$$

$$- \ln F\left(\boldsymbol{Z}\right). \quad \text{(F.38)}$$

where

$$\boldsymbol{Z} = \begin{bmatrix} Z_1 & 0 & 0 & 0 \\ 0 & Z_2 & 0 & 0 \\ 0 & 0 & Z_3 & 0 \\ 0 & 0 & 0 & 0 \end{bmatrix} \quad \text{and} \quad \boldsymbol{M}\left(\begin{bmatrix} \boldsymbol{\theta}_L \\ \boldsymbol{\theta}_R \end{bmatrix}\right) = \boldsymbol{R}_L(\bar{\boldsymbol{q}}(\boldsymbol{\theta}_L)) \boldsymbol{R}_R(\bar{\boldsymbol{q}}(\boldsymbol{\theta}_R)), \quad \text{(F.39)}$$

and

$$\boldsymbol{R}_L(\bar{\boldsymbol{q}}) = \begin{bmatrix} q_4 & -q_3 & q_2 & -q_1 \\ q_3 & q_4 & -q_1 & -q_2 \\ -q_2 & q_1 & q_4 & -q_3 \\ q_1 & q_2 & q_3 & q_4 \end{bmatrix} \quad \text{and} \quad \boldsymbol{R}_R(\bar{\boldsymbol{q}}) = \begin{bmatrix} q_4 & -q_3 & q_2 & q_1 \\ q_3 & q_4 & -q_1 & q_2 \\ -q_2 & q_1 & q_4 & q_3 \\ -q_1 & -q_2 & -q_3 & q_4 \end{bmatrix}, \quad \text{(F.40)}$$

and

$$\bar{\boldsymbol{q}}(\boldsymbol{\theta}) = \begin{bmatrix} \frac{\boldsymbol{\theta}}{\theta} \sin \frac{\theta}{2} \\ \cos \frac{\theta}{2} \end{bmatrix}. \quad \text{(F.41)}$$

For convenience, $\boldsymbol{\phi}_0$ and $\boldsymbol{\beta}$ are now decomposed into their top and bottom halves representing the left and right isoclinic rotations, respectively, according to

$$\boldsymbol{\phi}_0 = \begin{bmatrix} \boldsymbol{\theta}_{0,L} \\ \boldsymbol{\theta}_{0,R} \end{bmatrix} \quad \text{and} \quad \boldsymbol{\beta} = \begin{bmatrix} \boldsymbol{\beta}_L \\ \boldsymbol{\beta}_R \end{bmatrix},$$

such that Eq. (F.42) can be equivalently parameterized by the according to

$$J(\boldsymbol{\theta}_{0,L}, \boldsymbol{\theta}_{0,R}, \boldsymbol{\beta}_L, \boldsymbol{\beta}_R, \boldsymbol{Z}) = 2 \sum_{i=1}^{N} w^{(i)} \left[\boldsymbol{\mathcal{X}}_q^{(i)T} \boldsymbol{R}_L \left\{ \bar{\boldsymbol{q}} \left[\boldsymbol{\theta} \left(\boldsymbol{\mathcal{X}}_z^{(i)}; \boldsymbol{\theta}_{0,L}, \boldsymbol{\beta}_L \right) \right] \right\}$$

$$\times \, \boldsymbol{R}_R \left\{ \bar{q} \left[\boldsymbol{\theta} \left(\boldsymbol{\mathcal{Z}}^{(i)}; \boldsymbol{\theta}_{0,R}, \boldsymbol{\beta}_R \right) \right] \right\} \boldsymbol{Z} \boldsymbol{R}_R^T \left\{ \bar{q} \left[\boldsymbol{\theta} \left(\boldsymbol{\mathcal{X}}_{\mathrm{z}}^{(i)}; \boldsymbol{\theta}_{0,R}, \boldsymbol{\beta}_R \right) \right] \right\}$$

$$\times \, \boldsymbol{R}_L^T \left\{ \bar{q} \left[\boldsymbol{\theta} \left(\boldsymbol{\mathcal{X}}_{\mathrm{z}}^{(i)}; \boldsymbol{\theta}_{0,L}, \boldsymbol{\beta}_L \right) \right] \right\} \boldsymbol{\mathcal{X}}_q^{(i)} \Big] - \ln F \left(\boldsymbol{Z} \right) , \tag{F.42}$$

where $\boldsymbol{\theta} \left(\boldsymbol{\mathcal{X}}_{\mathrm{z}}^{(i)}; \boldsymbol{\theta}_{0,L}, \boldsymbol{\beta}_L \right) = \boldsymbol{\theta}_{0,L} + \boldsymbol{\beta}_L \boldsymbol{\mathcal{X}}_{\mathrm{z}}^{(i)}$. The cost function is now defined by

$$J(\boldsymbol{\theta}_{0,L}, \boldsymbol{\theta}_{0,R}, \boldsymbol{\beta}_L, \boldsymbol{\beta}_R, \boldsymbol{Z}) = 2 \sum_{i=1}^N w^{(i)} K_i(\boldsymbol{\theta}_{0,L}, \boldsymbol{\theta}_{0,R}, \boldsymbol{\beta}_L, \boldsymbol{\beta}_R, \boldsymbol{Z}) - \ln F \left(\boldsymbol{Z} \right) . \tag{F.43}$$

where

$$K_i(\boldsymbol{\theta}_{0,L}, \boldsymbol{\theta}_{0,R}, \boldsymbol{\beta}_L, \boldsymbol{\beta}_R, \boldsymbol{Z}) = \boldsymbol{\mathcal{X}}_q^{(i)T} \boldsymbol{R}_L \left\{ \bar{q} \left[\boldsymbol{\theta} \left(\boldsymbol{\mathcal{X}}_{\mathrm{z}}^{(i)}; \boldsymbol{\theta}_{0,L}, \boldsymbol{\beta}_L \right) \right] \right\} \boldsymbol{R}_R \left\{ \bar{q} \left[\boldsymbol{\theta} \left(\boldsymbol{\mathcal{X}}_{\mathrm{z}}^{(i)}; \boldsymbol{\theta}_{0,R}, \boldsymbol{\beta}_R \right) \right] \right\}$$

$$\times \, \boldsymbol{Z} \boldsymbol{R}_R^T \left\{ \bar{q} \left[\boldsymbol{\theta} \left(\boldsymbol{\mathcal{X}}_{\mathrm{z}}^{(i)}; \boldsymbol{\theta}_{0,R}, \boldsymbol{\beta}_R \right) \right] \right\} \boldsymbol{R}_L^T \left\{ \bar{q} \left[\boldsymbol{\theta} \left(\boldsymbol{\mathcal{X}}_{\mathrm{z}}^{(i)}; \boldsymbol{\theta}_{0,L}, \boldsymbol{\beta}_L \right) \right] \right\} \boldsymbol{\mathcal{X}}_q^{(i)}$$

The partial derivative of the cost function with respect to an arbitrary parameter denoted by the symbol $\star$ can then be expressed as

$$\frac{\partial J(\boldsymbol{\theta}_{0,L}, \boldsymbol{\theta}_{0,R}, \boldsymbol{\beta}_L, \boldsymbol{\beta}_R, \boldsymbol{Z})}{\partial \star} = 2 \sum_{i=1}^N w^{(i)} \frac{\partial K_i(\boldsymbol{\theta}_{0,L}, \boldsymbol{\theta}_{0,R}, \boldsymbol{\beta}_L, \boldsymbol{\beta}_R, \boldsymbol{Z})}{\partial \star} - \frac{\partial \ln F \left(\boldsymbol{Z} \right)}{\partial \star} .$$

It is now necessary to find these partial derivatives with respect to Z_1, Z_2, and Z_3, as well as each entry of $\boldsymbol{\theta}_{0,L}$, $\boldsymbol{\theta}_{0,R}$, $\boldsymbol{\beta}_L$, and $\boldsymbol{\beta}_R$. The term $\ln F \left(\boldsymbol{Z} \right)$ is solely a function of Z_k, where $k = 1, 2, 3$; therefore, its only nonzero partial derivative is with respect to these Z_k according to

$$\frac{\partial \ln F \left(\boldsymbol{Z} \right)}{\partial Z_k} = \mathrm{tr} \left\{ \frac{\partial \ln F \left(\boldsymbol{Z} \right)}{\partial F \left(\boldsymbol{Z} \right)} \frac{\partial F \left(\boldsymbol{Z} \right)}{\partial Z_k} \right\} = F^{-1} \left(\boldsymbol{Z} \right) \frac{\partial F \left(\boldsymbol{Z} \right)}{\partial Z_k} = f_k .$$

Now the partial derivatives of $K_i(\boldsymbol{\theta}_{0,L}, \boldsymbol{\theta}_{0,R}, \boldsymbol{\beta}_L, \boldsymbol{\beta}_R, \boldsymbol{Z})$ with respect to Z_1, Z_2, and Z_3, as well as each entry of $\boldsymbol{\theta}_{0,L}$, $\boldsymbol{\theta}_{0,R}$, $\boldsymbol{\beta}_L$, and $\boldsymbol{\beta}_R$ must be found. Its partial derivative with respect to the Z_k is given by

$$\frac{\partial K_i(\boldsymbol{\theta}_{0,L}, \boldsymbol{\theta}_{0,R}, \boldsymbol{\beta}_L, \boldsymbol{\beta}_R, \boldsymbol{Z})}{\partial Z_k} = \tag{F.44}$$

$$\mathrm{tr} \left\{ \frac{\partial \boldsymbol{\mathcal{X}}_q^{(i)T} \left[\boldsymbol{R}_L \left\{ \bar{q} \left[\boldsymbol{\theta} \left(\boldsymbol{\mathcal{X}}_{\mathrm{z}}^{(i)}; \boldsymbol{\theta}_{0,L}, \boldsymbol{\beta}_L \right) \right] \right\} \boldsymbol{R}_R \left\{ \bar{q} \left[\boldsymbol{\theta} \left(\boldsymbol{\mathcal{X}}_{\mathrm{z}}^{(i)}; \boldsymbol{\theta}_{0,R}, \boldsymbol{\beta}_R \right) \right] \right\} \right] \boldsymbol{Z} \left[\ldots \right]^T \boldsymbol{\mathcal{X}}_q^{(i)}}{\partial \boldsymbol{Z}} \frac{\partial \boldsymbol{Z}}{\partial Z_k} \right\} ,$$

where the $[\cdots]$ represents the same term as what is in the previous $[\ ]$. Calculating the derivatives in Eq. (F.44) yields

$$\frac{\partial K_i(\boldsymbol{\theta}_{0,L}, \boldsymbol{\theta}_{0,R}, \boldsymbol{\beta}_L, \boldsymbol{\beta}_R, \boldsymbol{Z})}{\partial Z_k} = \tag{F.45}$$

$$\text{tr} \left\{ \left[\boldsymbol{R}_L \left\{ \bar{q} \left[\boldsymbol{\theta} \left(\boldsymbol{\mathcal{X}}_z^{(i)}; \boldsymbol{\theta}_{0,L}, \boldsymbol{\beta}_L \right) \right] \right\} \boldsymbol{R}_R \left\{ \bar{q} \left[\boldsymbol{\theta} \left(\boldsymbol{\mathcal{X}}_z^{(i)}; \boldsymbol{\theta}_{0,R}, \boldsymbol{\beta}_R \right) \right] \right\} \right]^T \boldsymbol{\mathcal{X}}_q^{(i)} \boldsymbol{\mathcal{X}}_q^{(i)T} \left[\ldots \right] \boldsymbol{1}_{k,k}^{4,4} \right\} .$$

Using the cyclic property of the trace, Eq. (F.45) can be expressed as

$$\frac{\partial K_i(\boldsymbol{\theta}_{0,L}, \boldsymbol{\theta}_{0,R}, \boldsymbol{\beta}_L, \boldsymbol{\beta}_R, \boldsymbol{Z})}{\partial Z_k} =$$

$$\boldsymbol{\mathcal{X}}_q^{(i)T} \left[\boldsymbol{R}_L \left\{ \bar{q} \left[\boldsymbol{\theta} \left(\boldsymbol{\mathcal{X}}_z^{(i)}; \boldsymbol{\theta}_{0,L}, \boldsymbol{\beta}_L \right) \right] \right\} \boldsymbol{R}_R \left\{ \bar{q} \left[\boldsymbol{\theta} \left(\boldsymbol{\mathcal{X}}_z^{(i)}; \boldsymbol{\theta}_{0,R}, \boldsymbol{\beta}_R \right) \right] \right\} \right] \boldsymbol{1}_{k,k}^{4,4} \left[\ldots \right]^T \boldsymbol{\mathcal{X}}_q^{(i)} .$$

The partial derivative of $K_i(\boldsymbol{\theta}_{0,L}, \boldsymbol{\theta}_{0,R}, \boldsymbol{\beta}_L, \boldsymbol{\beta}_R, \boldsymbol{Z})$ with respect to the kth entry of $\boldsymbol{\theta}_{0,L}$, $\theta_{0,L,k}$ for $k = 1, 2, 3$, is given by

$$\frac{\partial K_i(\boldsymbol{\theta}_{0,L}, \boldsymbol{\theta}_{0,R}, \boldsymbol{\beta}_L, \boldsymbol{\beta}_R, \boldsymbol{Z})}{\partial \theta_{0,L,k}} = \tag{F.46}$$

$$\text{tr} \left\{ \frac{\partial \boldsymbol{\mathcal{X}}_q^{(i)T} \left[\boldsymbol{R}_L \left\{ \bar{q} \left[\boldsymbol{\theta} \left(\boldsymbol{\mathcal{X}}_z^{(i)}; \boldsymbol{\theta}_{0,L}, \boldsymbol{\beta}_L \right) \right] \right\} \boldsymbol{R}_R \left\{ \bar{q} \left[\boldsymbol{\theta} \left(\boldsymbol{\mathcal{X}}_z^{(i)}; \boldsymbol{\theta}_{0,R}, \boldsymbol{\beta}_R \right) \right] \right\} \right] \boldsymbol{Z} \left[\ldots \right]^T \boldsymbol{\mathcal{X}}_q^{(i)}}{\partial \boldsymbol{R}_L \left\{ \bar{q} \left[\boldsymbol{\theta} \left(\boldsymbol{\mathcal{X}}_z^{(i)}; \boldsymbol{\theta}_{0,L}, \boldsymbol{\beta}_L \right) \right] \right\}} \right.$$

$$\left. \times \frac{\partial \boldsymbol{R}_L \left\{ \bar{q} \left[\boldsymbol{\theta} \left(\boldsymbol{\mathcal{X}}_z^{(i)}; \boldsymbol{\theta}_{0,L}, \boldsymbol{\beta}_L \right) \right] \right\}}{\partial \theta_{0,L,k}} \right\} .$$

The former derivative of the chain rule in Eq. (F.46) is calculated as

$$\frac{\partial \boldsymbol{\mathcal{X}}_q^{(i)T} \left[\boldsymbol{R}_L \left\{ \bar{q} \left[\boldsymbol{\theta} \left(\boldsymbol{\mathcal{X}}_z^{(i)}; \boldsymbol{\theta}_{0,L}, \boldsymbol{\beta}_L \right) \right] \right\} \boldsymbol{R}_R \left\{ \bar{q} \left[\boldsymbol{\theta} \left(\boldsymbol{\mathcal{X}}_z^{(i)}; \boldsymbol{\theta}_{0,R}, \boldsymbol{\beta}_R \right) \right] \right\} \right] \boldsymbol{Z} \left[\ldots \right]^T \boldsymbol{\mathcal{X}}_q^{(i)}}{\partial \boldsymbol{R}_L \left\{ \bar{q} \left[\boldsymbol{\theta} \left(\boldsymbol{\mathcal{X}}_z^{(i)}; \boldsymbol{\theta}_{0,L}, \boldsymbol{\beta}_L \right) \right] \right\}} \tag{F.47}$$

$$= 2 \boldsymbol{R}_R \left\{ \bar{q} \left[\boldsymbol{\theta} \left(\boldsymbol{\mathcal{X}}_z^{(i)}; \boldsymbol{\theta}_{0,R}, \boldsymbol{\beta}_R \right) \right] \right\} \boldsymbol{Z} \boldsymbol{R}_R^T \left\{ \bar{q} \left[\boldsymbol{\theta} \left(\boldsymbol{\mathcal{X}}_z^{(i)}; \boldsymbol{\theta}_{0,R}, \boldsymbol{\beta}_R \right) \right] \right\}$$

$$\times \boldsymbol{R}_L^T \left\{ \bar{q} \left[\boldsymbol{\theta} \left(\boldsymbol{\mathcal{X}}_z^{(i)}; \boldsymbol{\theta}_{0,L}, \boldsymbol{\beta}_L \right) \right] \right\} \boldsymbol{\mathcal{X}}_q^{(i)} \boldsymbol{\mathcal{X}}_q^{(i)T} .$$

The latter derivative of the chain rule in Eq. (F.46) is calculated as

$$\frac{\partial \boldsymbol{R}_L \left\{ \bar{q} \left[\boldsymbol{\theta} \left(\boldsymbol{\mathcal{X}}_{\mathrm{z}}^{(i)}; \boldsymbol{\theta}_{0,L}, \boldsymbol{\beta}_L \right) \right] \right\}}{\partial \theta_{0,L,k}} = \sum_{a=1}^{4} \frac{\partial \boldsymbol{R}_L \left\{ \bar{q} \left[\boldsymbol{\theta} \left(\boldsymbol{\mathcal{X}}_{\mathrm{z}}^{(i)}; \boldsymbol{\theta}_{0,L}, \boldsymbol{\beta}_L \right) \right] \right\}}{\partial q_a \left[\boldsymbol{\theta} \left(\boldsymbol{\mathcal{X}}_{\mathrm{z}}^{(i)}; \boldsymbol{\theta}_{0,L}, \boldsymbol{\beta}_L \right) \right]} \tag{F.48}$$
$$\times \frac{\partial q_a \left[\boldsymbol{\theta} \left(\boldsymbol{\mathcal{X}}_{\mathrm{z}}^{(i)}; \boldsymbol{\theta}_{0,L}, \boldsymbol{\beta}_L \right) \right]}{\partial \theta_{0,L,k}} .$$

The former derivative of the right hand side of Eq. (F.48) is calculated from Eq. (F.40) according to

$$\frac{\partial \boldsymbol{R}_L \left\{ \bar{q} \left[\boldsymbol{\theta} \left(\boldsymbol{\mathcal{X}}_{\mathrm{z}}^{(i)}; \boldsymbol{\theta}_{0,L}, \boldsymbol{\beta}_L \right) \right] \right\}}{\partial q_1 \left[\boldsymbol{\theta} \left(\boldsymbol{\mathcal{X}}_{\mathrm{z}}^{(i)}; \boldsymbol{\theta}_{0,L}, \boldsymbol{\beta}_L \right) \right]} = \begin{bmatrix} 0 & 0 & 0 & -1 \\ 0 & 0 & -1 & 0 \\ 0 & 1 & 0 & 0 \\ 1 & 0 & 0 & 0 \end{bmatrix} \tag{F.49a}$$

$$\frac{\partial \boldsymbol{R}_L \left\{ \bar{q} \left[\boldsymbol{\theta} \left(\boldsymbol{\mathcal{X}}_{\mathrm{z}}^{(i)}; \boldsymbol{\theta}_{0,L}, \boldsymbol{\beta}_L \right) \right] \right\}}{\partial q_2 \left[\boldsymbol{\theta} \left(\boldsymbol{\mathcal{X}}_{\mathrm{z}}^{(i)}; \boldsymbol{\theta}_{0,L}, \boldsymbol{\beta}_L \right) \right]} = \begin{bmatrix} 0 & 0 & 1 & 0 \\ 0 & 0 & 0 & -1 \\ -1 & 0 & 0 & 0 \\ 0 & 1 & 0 & 0 \end{bmatrix} \tag{F.49b}$$

$$\frac{\partial \boldsymbol{R}_L \left\{ \bar{q} \left[\boldsymbol{\theta} \left(\boldsymbol{\mathcal{X}}_{\mathrm{z}}^{(i)}; \boldsymbol{\theta}_{0,L}, \boldsymbol{\beta}_L \right) \right] \right\}}{\partial q_3 \left[\boldsymbol{\theta} \left(\boldsymbol{\mathcal{X}}_{\mathrm{z}}^{(i)}; \boldsymbol{\theta}_{0,L}, \boldsymbol{\beta}_L \right) \right]} = \begin{bmatrix} 0 & -1 & 0 & 0 \\ 1 & 0 & 0 & 0 \\ 0 & 0 & 0 & -1 \\ 0 & 0 & 1 & 0 \end{bmatrix} \tag{F.49c}$$

$$\frac{\partial \boldsymbol{R}_L \left\{ \bar{q} \left[\boldsymbol{\theta} \left(\boldsymbol{\mathcal{X}}_{\mathrm{z}}^{(i)}; \boldsymbol{\theta}_{0,L}, \boldsymbol{\beta}_L \right) \right] \right\}}{\partial q_4 \left[\boldsymbol{\theta} \left(\boldsymbol{\mathcal{X}}_{\mathrm{z}}^{(i)}; \boldsymbol{\theta}_{0,L}, \boldsymbol{\beta}_L \right) \right]} = \begin{bmatrix} 1 & 0 & 0 & 0 \\ 0 & 1 & 0 & 0 \\ 0 & 0 & 1 & 0 \\ 0 & 0 & 0 & 1 \end{bmatrix} \tag{F.49d}$$

The latter derivative of the right hand side of Eq. (F.48) is calculated according to

$$\frac{\partial q_a \left[\boldsymbol{\theta} \left(\boldsymbol{\mathcal{X}}_{\mathrm{z}}^{(i)}; \boldsymbol{\theta}_{0,L}, \boldsymbol{\beta}_L \right) \right]}{\partial \theta_{0,L,k}} = \frac{\partial q_a \left[\boldsymbol{\theta} \left(\boldsymbol{\mathcal{X}}_{\mathrm{z}}^{(i)}; \boldsymbol{\theta}_{0,L}, \boldsymbol{\beta}_L \right) \right]}{\partial \boldsymbol{\theta} \left(\boldsymbol{\mathcal{X}}_{\mathrm{z}}^{(i)}; \boldsymbol{\theta}_{0,L}, \boldsymbol{\beta}_L \right)} \frac{\partial \boldsymbol{\theta} \left(\boldsymbol{\mathcal{X}}_{\mathrm{z}}^{(i)}; \boldsymbol{\theta}_{0,L}, \boldsymbol{\beta}_L \right)}{\partial \theta_{0,L,k}} . \tag{F.50}$$

The former derivative of the right hand side of Eq. (F.50) is calculated from Eq. (F.41) and is given by

$$\frac{\partial \bar{q} (\boldsymbol{\theta})}{\partial \boldsymbol{\theta}} = \begin{bmatrix} \left(\frac{1}{2\theta^2} \cos \frac{\theta}{2} - \frac{1}{\theta^3} \sin \frac{\theta}{2} \right) \boldsymbol{\theta} \boldsymbol{\theta}^T + \frac{1}{\theta} \sin \frac{\theta}{2} \boldsymbol{I} \\ -\frac{1}{2\theta} \sin \frac{\theta}{2} \boldsymbol{\theta}^T \end{bmatrix} . \tag{F.51}$$

The latter derivative of the right hand side of Eq. (F.50) is calculated from Eq. (F.13) is given by

$$\frac{\partial \boldsymbol{\theta}\left(\boldsymbol{\mathcal{X}}_{\mathrm{z}}^{(i)}; \boldsymbol{\theta}_{0,L}, \boldsymbol{\beta}_L\right)}{\partial \theta_{0,L,k}} = \sum_{b=1}^{3} \frac{\partial \boldsymbol{\theta}\left(\boldsymbol{\mathcal{X}}_{\mathrm{z}}^{(i)}; \boldsymbol{\theta}_{0,L}, \boldsymbol{\beta}_L\right)}{\partial \theta_{0,L,b}} \frac{\partial \theta_{0,L,b}}{\partial \theta_{0,L,k}}$$
$$= \mathbf{1}_{k,1}^{3,1}. \tag{F.52}$$

Substituting Eq. (F.52) into Eq. (F.50) yields

$$\frac{\partial q_a\left[\boldsymbol{\theta}\left(\boldsymbol{\mathcal{X}}_{\mathrm{z}}^{(i)}; \boldsymbol{\theta}_{0,L}, \boldsymbol{\beta}_L\right)\right]}{\partial \theta_{0,L,k}} = \frac{\partial q_a\left[\boldsymbol{\theta}\left(\boldsymbol{\mathcal{X}}_{\mathrm{z}}^{(i)}; \boldsymbol{\theta}_{0,L}, \boldsymbol{\beta}_L\right)\right]}{\partial \boldsymbol{\theta}\left(\boldsymbol{\mathcal{X}}_{\mathrm{z}}^{(i)}; \boldsymbol{\theta}_{0,L}, \boldsymbol{\beta}_L\right)} \mathbf{1}_{k,1}^{3,1}. \tag{F.53}$$

It is now noted that Eq. (F.53) can be expressed as

$$\frac{\partial q_a\left[\boldsymbol{\theta}\left(\boldsymbol{\mathcal{X}}_{\mathrm{z}}^{(i)}; \boldsymbol{\theta}_{0,L}, \boldsymbol{\beta}_L\right)\right]}{\partial \theta_{0,L,k}} = \left[\frac{\partial \bar{q}\left[\boldsymbol{\theta}\left(\boldsymbol{\mathcal{X}}_{\mathrm{z}}^{(i)}; \boldsymbol{\theta}_{0,L}, \boldsymbol{\beta}_L\right)\right]}{\partial \boldsymbol{\theta}\left(\boldsymbol{\mathcal{X}}_{\mathrm{z}}^{(i)}; \boldsymbol{\theta}_{0,L}, \boldsymbol{\beta}_L\right)}\right]_{a,k} \triangleq \alpha_{L,a,k}, \tag{F.54}$$

where $\boldsymbol{M}_{a,k}$ represents the entry in the ath-row and k^{th}-column of the arbitrary matrix $\boldsymbol{M}$. Substituting Eq. (F.54) into Eq. (F.48) yields

$$\frac{\partial \boldsymbol{R}_L\left\{\bar{q}\left[\boldsymbol{\theta}\left(\boldsymbol{\mathcal{X}}_{\mathrm{z}}^{(i)}; \boldsymbol{\theta}_{0,L}, \boldsymbol{\beta}_L\right)\right]\right\}}{\partial \theta_{0,L,k}} = \sum_{a=1}^{4} \frac{\partial \boldsymbol{R}_L\left\{\bar{q}\left[\boldsymbol{\theta}\left(\boldsymbol{\mathcal{X}}_{\mathrm{z}}^{(i)}; \boldsymbol{\theta}_{0,L}, \boldsymbol{\beta}_L\right)\right]\right\}}{\partial q_a\left[\boldsymbol{\theta}\left(\boldsymbol{\mathcal{X}}_{\mathrm{z}}^{(i)}; \boldsymbol{\theta}_{0,L}, \boldsymbol{\beta}_L\right)\right]} \alpha_{L,a,k}. \tag{F.55}$$

which can be simplified noting Eqs. (F.49) to yield

$$\frac{\partial \boldsymbol{R}_L\left\{\bar{q}\left[\boldsymbol{\theta}\left(\boldsymbol{\mathcal{X}}_{\mathrm{z}}^{(i)}; \boldsymbol{\theta}_{0,L}, \boldsymbol{\beta}_L\right)\right]\right\}}{\partial \theta_{0,L,k}} = \begin{bmatrix} \alpha_{L,4,k} & -\alpha_{L,3,k} & \alpha_{L,2,k} & -\alpha_{L,1,k} \\ \alpha_{L,3,k} & \alpha_{L,4,k} & -\alpha_{L,1,k} & -\alpha_{L,2,k} \\ -\alpha_{L,2,k} & \alpha_{L,1,k} & \alpha_{L,4,k} & -\alpha_{L,3,k} \\ \alpha_{L,1,k} & \alpha_{L,2,k} & \alpha_{L,3,k} & \alpha_{L,4,k} \end{bmatrix} \triangleq \boldsymbol{A}_{L,k}. \tag{F.56}$$

Substituting Eqs. (F.47) and (F.56) into Eq. (F.46) yields

$$\frac{\partial K_i(\boldsymbol{\theta}_{0,L}, \boldsymbol{\theta}_{0,R}, \boldsymbol{\beta}_L, \boldsymbol{\beta}_R, \boldsymbol{Z})}{\partial \theta_{0,L,k}} = \mathrm{tr}\left\{2\boldsymbol{R}_R\left\{\bar{q}\left[\boldsymbol{\theta}\left(\boldsymbol{\mathcal{X}}_{\mathrm{z}}^{(i)}; \boldsymbol{\theta}_{0,R}, \boldsymbol{\beta}_R\right)\right]\right\}\boldsymbol{Z}\right. \tag{F.57}$$
$$\left. \times \boldsymbol{R}_R^T\left\{\bar{q}\left[\boldsymbol{\theta}\left(\boldsymbol{\mathcal{X}}_{\mathrm{z}}^{(i)}; \boldsymbol{\theta}_{0,R}, \boldsymbol{\beta}_R\right)\right]\right\} \boldsymbol{R}_L^T\left\{\bar{q}\left[\boldsymbol{\theta}\left(\boldsymbol{\mathcal{X}}_{\mathrm{z}}^{(i)}; \boldsymbol{\theta}_{0,L}, \boldsymbol{\beta}_L\right)\right]\right\} \boldsymbol{\mathcal{X}}_q^{(i)} \boldsymbol{\mathcal{X}}_q^{(i)T} \boldsymbol{A}_{L,k}\right\}.$$

Exploiting the cyclic property of the trace, Eq. (F.57) can be expressed as

$$\frac{\partial K_i(\boldsymbol{\theta}_{0,L}, \boldsymbol{\theta}_{0,R}, \boldsymbol{\beta}_L, \boldsymbol{\beta}_R, \boldsymbol{Z})}{\partial \theta_{0,L,k}} = 2\boldsymbol{\mathcal{X}}_q^{(i)T} \boldsymbol{A}_{L,k} \boldsymbol{R}_R \left\{ \bar{\boldsymbol{q}} \left[\boldsymbol{\theta} \left(\boldsymbol{\mathcal{X}}_z^{(i)}; \boldsymbol{\theta}_{0,R}, \boldsymbol{\beta}_R \right) \right] \right\} \boldsymbol{Z} \qquad \text{(F.58)}$$

$$\boldsymbol{R}_R^T \left\{ \bar{\boldsymbol{q}} \left[\boldsymbol{\theta} \left(\boldsymbol{\mathcal{X}}_z^{(i)}; \boldsymbol{\theta}_{0,R}, \boldsymbol{\beta}_R \right) \right] \right\} \boldsymbol{R}_L^T \left\{ \bar{\boldsymbol{q}} \left[\boldsymbol{\theta} \left(\boldsymbol{\mathcal{X}}_z^{(i)}; \boldsymbol{\theta}_{0,L}, \boldsymbol{\beta}_L \right) \right] \right\} \boldsymbol{\mathcal{X}}_q^{(i)} .$$

The partial derivative of $K_i(\boldsymbol{\theta}_{0,L}, \boldsymbol{\theta}_{0,R}, \boldsymbol{\beta}_L, \boldsymbol{\beta}_R, \boldsymbol{Z})$ with respect to the kth row and ℓ^{th} entry of $\boldsymbol{\beta}_L$, $\beta_{L,k,\ell}$ for $k = 1, 2, 3$ and $\ell = 1, 2, \ldots, r$, is given by

$$\frac{\partial K_i(\boldsymbol{\theta}_{0,L}, \boldsymbol{\theta}_{0,R}, \boldsymbol{\beta}_L, \boldsymbol{\beta}_R, \boldsymbol{Z})}{\partial \beta_{L,k,\ell}} = \qquad \text{(F.59)}$$

$$\text{tr} \left\{ \frac{\partial \boldsymbol{\mathcal{X}}_q^{(i)T} \left[\boldsymbol{R}_L \left\{ \bar{\boldsymbol{q}} \left[\boldsymbol{\theta} \left(\boldsymbol{\mathcal{X}}_z^{(i)}; \boldsymbol{\theta}_{0,L}, \boldsymbol{\beta}_L \right) \right] \right\} \boldsymbol{R}_R \left\{ \bar{\boldsymbol{q}} \left[\boldsymbol{\theta} \left(\boldsymbol{\mathcal{X}}_z^{(i)}; \boldsymbol{\theta}_{0,R}, \boldsymbol{\beta}_R \right) \right] \right\} \right] \boldsymbol{Z} \left[\ldots \right]^T \boldsymbol{\mathcal{X}}_q^{(i)}}{\partial \boldsymbol{R}_L \left\{ \bar{\boldsymbol{q}} \left[\boldsymbol{\theta} \left(\boldsymbol{\mathcal{X}}_z^{(i)}; \boldsymbol{\theta}_{0,L}, \boldsymbol{\beta}_L \right) \right] \right\}} \right.$$

$$\left. \times \frac{\partial \boldsymbol{R}_L \left\{ \bar{\boldsymbol{q}} \left[\boldsymbol{\theta} \left(\boldsymbol{\mathcal{X}}_z^{(i)}; \boldsymbol{\theta}_{0,L}, \boldsymbol{\beta}_L \right) \right] \right\}}{\partial \beta_{L,k,\ell}} \right\} .$$

The former derivative of the chain rule in Eq. (F.59) is given by Eq. (F.47). The latter derivative of the chain rule in Eq. (F.59) is calculated as

$$\frac{\partial \boldsymbol{R}_L \left\{ \bar{\boldsymbol{q}} \left[\boldsymbol{\theta} \left(\boldsymbol{\mathcal{X}}_z^{(i)}; \boldsymbol{\theta}_{0,L}, \boldsymbol{\beta}_L \right) \right] \right\}}{\partial \beta_{L,k,\ell}} = \sum_{a=1}^{4} \frac{\partial \boldsymbol{R}_L \left\{ \bar{\boldsymbol{q}} \left[\boldsymbol{\theta} \left(\boldsymbol{\mathcal{X}}_z^{(i)}; \boldsymbol{\theta}_{0,L}, \boldsymbol{\beta}_L \right) \right] \right\}}{\partial q_a \left[\boldsymbol{\theta} \left(\boldsymbol{\mathcal{X}}_z^{(i)}; \boldsymbol{\theta}_{0,L}, \boldsymbol{\beta}_L \right) \right]} \qquad \text{(F.60)}$$

$$\times \frac{\partial q_a \left[\boldsymbol{\theta} \left(\boldsymbol{\mathcal{X}}_z^{(i)}; \boldsymbol{\theta}_{0,L}, \boldsymbol{\beta}_L \right) \right]}{\partial \beta_{L,k,\ell}} .$$

The former derivative of the right hand side of Eq. (F.60) is given by Eq. (F.49). The latter derivative of the right hand side of Eq. (F.60) is calculated according to

$$\frac{\partial q_a \left[\boldsymbol{\theta} \left(\boldsymbol{\mathcal{X}}_z^{(i)}; \boldsymbol{\theta}_{0,L}, \boldsymbol{\beta}_L \right) \right]}{\partial \beta_{L,k,\ell}} = \frac{\partial q_a \left[\boldsymbol{\theta} \left(\boldsymbol{\mathcal{X}}_z^{(i)}; \boldsymbol{\theta}_{0,L}, \boldsymbol{\beta}_L \right) \right]}{\partial \boldsymbol{\theta} \left(\boldsymbol{\mathcal{X}}_z^{(i)}; \boldsymbol{\theta}_{0,L}, \boldsymbol{\beta}_L \right)} \frac{\partial \boldsymbol{\theta} \left(\boldsymbol{\mathcal{X}}_z^{(i)}; \boldsymbol{\theta}_{0,L}, \boldsymbol{\beta}_L \right)}{\partial \beta_{L,k,\ell}} . \qquad \text{(F.61)}$$

The former derivative of the right hand side of Eq. (F.61) is given by Eq. (F.51). The latter derivative of the right hand side of Eq. (F.61) is calculated from Eq. (F.13) and is given by

$$\frac{\partial \boldsymbol{\theta} \left(\boldsymbol{\mathcal{X}}_z^{(i)}; \boldsymbol{\theta}_{0,L}, \boldsymbol{\beta}_L \right)}{\partial \beta_{L,k,\ell}} = \sum_{b=1}^{3} \sum_{c=1}^{r} \frac{\partial \boldsymbol{\theta} \left(\boldsymbol{\mathcal{X}}_z^{(i)}; \boldsymbol{\theta}_{0,L}, \boldsymbol{\beta}_L \right)}{\partial \beta_{L,b,c}} \frac{\partial \beta_{L,b,c}}{\partial \beta_{L,k,\ell}}$$

$$= \mathcal{X}_{\mathrm{z},\ell}^{(i)} \mathbf{1}_{k,1}^{3,1} . \tag{F.62}$$

Substituting Eq. (F.62) into Eq. (F.61) yields

$$\frac{\partial q_a \left[\boldsymbol{\theta} \left(\mathcal{X}_{\mathrm{z}}^{(i)}; \boldsymbol{\theta}_{0,L}, \boldsymbol{\beta}_L \right) \right]}{\partial \beta_{L,k,\ell}} = \frac{\partial q_a \left[\boldsymbol{\theta} \left(\mathcal{X}_{\mathrm{z}}^{(i)}; \boldsymbol{\theta}_{0,L}, \boldsymbol{\beta}_L \right) \right]}{\partial \boldsymbol{\theta} \left(\mathcal{X}_{\mathrm{z}}^{(i)}; \boldsymbol{\theta}_{0,L}, \boldsymbol{\beta}_L \right)} \mathcal{X}_{\mathrm{z},\ell}^{(i)} \mathbf{1}_{k,1}^{3,1} . \tag{F.63}$$

It is now noted that Eq. (F.63) can be expressed as

$$\frac{\partial q_a \left[\boldsymbol{\theta} \left(\mathcal{X}_{\mathrm{z}}^{(i)}; \boldsymbol{\theta}_{0,L}, \boldsymbol{\beta}_L \right) \right]}{\partial \beta_{L,k,\ell}} = \left[\frac{\partial \bar{q} \left[\boldsymbol{\theta} \left(\mathcal{X}_{\mathrm{z}}^{(i)}; \boldsymbol{\theta}_{0,L}, \boldsymbol{\beta}_L \right) \right]}{\partial \boldsymbol{\theta} \left(\mathcal{X}_{\mathrm{z}}^{(i)}; \boldsymbol{\theta}_{0,L}, \boldsymbol{\beta}_L \right)} \right]_{a,k} \mathcal{X}_{\mathrm{z},\ell}^{(i)} \triangleq \alpha_{L,a,k} \mathcal{X}_{\mathrm{z},\ell}^{(i)} . \tag{F.64}$$

Substituting Eq. (F.64) into Eq. (F.60) yields

$$\frac{\partial \boldsymbol{R}_L \left\{ \bar{q} \left[\boldsymbol{\theta} \left(\mathcal{X}_{\mathrm{z}}^{(i)}; \boldsymbol{\theta}_{0,L}, \boldsymbol{\beta}_L \right) \right] \right\}}{\partial \beta_{L,k,\ell}} = \sum_{a=1}^{4} \frac{\partial \boldsymbol{R}_L \left\{ \bar{q} \left[\boldsymbol{\theta} \left(\mathcal{X}_{\mathrm{z}}^{(i)}; \boldsymbol{\theta}_{0,L}, \boldsymbol{\beta}_L \right) \right] \right\}}{\partial q_a \left[\boldsymbol{\theta} \left(\mathcal{X}_{\mathrm{z}}^{(i)}; \boldsymbol{\theta}_{0,L}, \boldsymbol{\beta}_L \right) \right]} \alpha_{L,a,k} \mathcal{X}_{\mathrm{z},\ell}^{(i)} . \tag{F.65}$$

which can be simplified to yield

$$\frac{\partial \boldsymbol{R}_L \left\{ \bar{q} \left[\boldsymbol{\theta} \left(\mathcal{X}_{\mathrm{z}}^{(i)}; \boldsymbol{\theta}_{0,L}, \boldsymbol{\beta}_L \right) \right] \right\}}{\partial \beta_{L,k,\ell}} = \boldsymbol{A}_{L,k} \mathcal{X}_{\mathrm{z},\ell}^{(i)} . \tag{F.66}$$

Substituting Eqs. (F.47) and (F.66) into Eq. (F.59) yields

$$\frac{\partial K_i(\boldsymbol{\theta}_{0,L}, \boldsymbol{\theta}_{0,R}, \boldsymbol{\beta}_L, \boldsymbol{\beta}_R, \boldsymbol{Z})}{\partial \beta_{L,k,\ell}} = \mathrm{tr} \left\{ 2 \boldsymbol{R}_R \left\{ \bar{q} \left[\boldsymbol{\theta} \left(\mathcal{X}_{\mathrm{z}}^{(i)}; \boldsymbol{\theta}_{0,R}, \boldsymbol{\beta}_R \right) \right] \right\} \boldsymbol{Z} \right. \tag{F.67}$$
$$\times \boldsymbol{R}_R^T \left\{ \bar{q} \left[\boldsymbol{\theta} \left(\mathcal{X}_{\mathrm{z}}^{(i)}; \boldsymbol{\theta}_{0,R}, \boldsymbol{\beta}_R \right) \right] \right\} \boldsymbol{R}_L^T \left\{ \bar{q} \left[\boldsymbol{\theta} \left(\mathcal{X}_{\mathrm{z}}^{(i)}; \boldsymbol{\theta}_{0,L}, \boldsymbol{\beta}_L \right) \right] \right\} \mathcal{X}_q^{(i)} \mathcal{X}_q^{(i)T} \boldsymbol{A}_{L,k} \mathcal{X}_{\mathrm{z},\ell}^{(i)} \right\} .$$

Exploiting the cyclic property of the trace, Eq. (F.67) can be expressed as

$$\frac{\partial K_i(\boldsymbol{\theta}_{0,L}, \boldsymbol{\theta}_{0,R}, \boldsymbol{\beta}_L, \boldsymbol{\beta}_R, \boldsymbol{Z})}{\partial \beta_{L,k,\ell}} = 2 \mathcal{X}_{\mathrm{z},\ell}^{(i)} \mathcal{X}_q^{(i)T} \boldsymbol{A}_{L,k} \boldsymbol{R}_R \left\{ \bar{q} \left[\boldsymbol{\theta} \left(\mathcal{X}_{\mathrm{z}}^{(i)}; \boldsymbol{\theta}_{0,R}, \boldsymbol{\beta}_R \right) \right] \right\} \boldsymbol{Z} \tag{F.68}$$
$$\boldsymbol{R}_R^T \left\{ \bar{q} \left[\boldsymbol{\theta} \left(\mathcal{X}_{\mathrm{z}}^{(i)}; \boldsymbol{\theta}_{0,R}, \boldsymbol{\beta}_R \right) \right] \right\} \boldsymbol{R}_L^T \left\{ \bar{q} \left[\boldsymbol{\theta} \left(\mathcal{X}_{\mathrm{z}}^{(i)}; \boldsymbol{\theta}_{0,L}, \boldsymbol{\beta}_L \right) \right] \right\} \mathcal{X}_q^{(i)} .$$

The partial derivative of $K_i(\boldsymbol{\theta}_{0,L}, \boldsymbol{\theta}_{0,R}, \boldsymbol{\beta}_L, \boldsymbol{\beta}_R, \boldsymbol{Z})$ with respect to the kth entry of $\boldsymbol{\theta}_{0,R}$, $\theta_{0,R,k}$ for $k = 1, 2, 3$, is given by

$$\frac{\partial K_i(\boldsymbol{\theta}_{0,L}, \boldsymbol{\theta}_{0,R}, \boldsymbol{\beta}_L, \boldsymbol{\beta}_R, \boldsymbol{Z})}{\partial \theta_{0,R,k}} = \tag{F.69}$$

$$\mathrm{tr}\left\{\frac{\partial \boldsymbol{\mathcal{X}}_q^{(i)^T}\left[\boldsymbol{R}_L\left\{\bar{\boldsymbol{q}}\left[\boldsymbol{\theta}\left(\boldsymbol{\mathcal{X}}_z^{(i)};\boldsymbol{\theta}_{0,L},\boldsymbol{\beta}_L\right)\right]\right\}\boldsymbol{R}_R\left\{\bar{\boldsymbol{q}}\left[\boldsymbol{\theta}\left(\boldsymbol{\mathcal{X}}_z^{(i)};\boldsymbol{\theta}_{0,R},\boldsymbol{\beta}_R\right)\right]\right\}\right]\boldsymbol{Z}\left[\ldots\right]^T\boldsymbol{\mathcal{X}}_q^{(i)}}{\partial\boldsymbol{R}_R\left\{\bar{\boldsymbol{q}}\left[\boldsymbol{\theta}\left(\boldsymbol{\mathcal{X}}_z^{(i)};\boldsymbol{\theta}_{0,R},\boldsymbol{\beta}_R\right)\right]\right\}}\right.$$

$$\left.\times\frac{\partial\boldsymbol{R}_R\left\{\bar{\boldsymbol{q}}\left[\boldsymbol{\theta}\left(\boldsymbol{\mathcal{X}}_z^{(i)};\boldsymbol{\theta}_{0,R},\boldsymbol{\beta}_R\right)\right]\right\}}{\partial\theta_{0,R,k}}\right\}\;.$$

The former derivative of the chain rule in Eq. (F.69) is calculated as

$$\frac{\partial \boldsymbol{\mathcal{X}}_q^{(i)^T}\left[\boldsymbol{R}_L\left\{\bar{\boldsymbol{q}}\left[\boldsymbol{\theta}\left(\boldsymbol{\mathcal{X}}_z^{(i)};\boldsymbol{\theta}_{0,L},\boldsymbol{\beta}_L\right)\right]\right\}\boldsymbol{R}_R\left\{\bar{\boldsymbol{q}}\left[\boldsymbol{\theta}\left(\boldsymbol{\mathcal{X}}_z^{(i)};\boldsymbol{\theta}_{0,R},\boldsymbol{\beta}_R\right)\right]\right\}\right]\boldsymbol{Z}\left[\ldots\right]^T\boldsymbol{\mathcal{X}}_q^{(i)}}{\partial\boldsymbol{R}_L\left\{\bar{\boldsymbol{q}}\left[\boldsymbol{\theta}\left(\boldsymbol{\mathcal{X}}_z^{(i)};\boldsymbol{\theta}_{0,L},\boldsymbol{\beta}_L\right)\right]\right\}}=$$

$$2\boldsymbol{Z}\boldsymbol{R}_R^T\left\{\bar{\boldsymbol{q}}\left[\boldsymbol{\theta}\left(\boldsymbol{\mathcal{X}}_z^{(i)};\boldsymbol{\theta}_{0,R},\boldsymbol{\beta}_R\right)\right]\right\}\boldsymbol{R}_L^T\left\{\bar{\boldsymbol{q}}\left[\boldsymbol{\theta}\left(\boldsymbol{\mathcal{X}}_z^{(i)};\boldsymbol{\theta}_{0,L},\boldsymbol{\beta}_L\right)\right]\right\} \tag{F.70}$$

$$\times\,\boldsymbol{\mathcal{X}}_q^{(i)}\boldsymbol{\mathcal{X}}_q^{(i)^T}\boldsymbol{R}_L\left\{\bar{\boldsymbol{q}}\left[\boldsymbol{\theta}\left(\boldsymbol{\mathcal{X}}_z^{(i)};\boldsymbol{\theta}_{0,L},\boldsymbol{\beta}_L\right)\right]\right\}\;.$$

The latter derivative of the chain rule in Eq. (F.69) is calculated as

$$\frac{\partial\boldsymbol{R}_R\left\{\bar{\boldsymbol{q}}\left[\boldsymbol{\theta}\left(\boldsymbol{\mathcal{X}}_z^{(i)};\boldsymbol{\theta}_{0,R},\boldsymbol{\beta}_R\right)\right]\right\}}{\partial\theta_{0,R,k}}=\sum_{a=1}^{4}\frac{\partial\boldsymbol{R}_R\left\{\bar{\boldsymbol{q}}\left[\boldsymbol{\theta}\left(\boldsymbol{\mathcal{X}}_z^{(i)};\boldsymbol{\theta}_{0,R},\boldsymbol{\beta}_R\right)\right]\right\}}{\partial q_a\left[\boldsymbol{\theta}\left(\boldsymbol{\mathcal{X}}_z^{(i)};\boldsymbol{\theta}_{0,R},\boldsymbol{\beta}_R\right)\right]} \tag{F.71}$$

$$\times\frac{\partial q_a\left[\boldsymbol{\theta}\left(\boldsymbol{\mathcal{X}}_z^{(i)};\boldsymbol{\theta}_{0,R},\boldsymbol{\beta}_R\right)\right]}{\partial\theta_{0,R,k}}\;.$$

The former derivative of the right hand side of Eq. (F.71) is calculated from Eq. (F.40) according to

$$\frac{\partial\boldsymbol{R}_R\left\{\bar{\boldsymbol{q}}\left[\boldsymbol{\theta}\left(\boldsymbol{\mathcal{X}}_z^{(i)};\boldsymbol{\theta}_{0,R},\boldsymbol{\beta}_R\right)\right]\right\}}{\partial q_1\left[\boldsymbol{\theta}\left(\boldsymbol{\mathcal{X}}_z^{(i)};\boldsymbol{\theta}_{0,R},\boldsymbol{\beta}_R\right)\right]}=\begin{bmatrix}0&0&0&1\\0&0&-1&0\\0&1&0&0\\-1&0&0&0\end{bmatrix} \tag{F.72a}$$

$$\frac{\partial\boldsymbol{R}_R\left\{\bar{\boldsymbol{q}}\left[\boldsymbol{\theta}\left(\boldsymbol{\mathcal{X}}_z^{(i)};\boldsymbol{\theta}_{0,R},\boldsymbol{\beta}_R\right)\right]\right\}}{\partial q_2\left[\boldsymbol{\theta}\left(\boldsymbol{\mathcal{X}}_z^{(i)};\boldsymbol{\theta}_{0,R},\boldsymbol{\beta}_R\right)\right]}=\begin{bmatrix}0&0&1&0\\0&0&0&1\\-1&0&0&0\\0&-1&0&0\end{bmatrix} \tag{F.72b}$$

$$\frac{\partial \boldsymbol{R}_R \left\{ \bar{\boldsymbol{q}} \left[\boldsymbol{\theta} \left(\boldsymbol{\mathcal{X}}_{\mathrm{z}}^{(i)}; \boldsymbol{\theta}_{0,R}, \boldsymbol{\beta}_R \right) \right] \right\}}{\partial q_3 \left[\boldsymbol{\theta} \left(\boldsymbol{\mathcal{X}}_{\mathrm{z}}^{(i)}; \boldsymbol{\theta}_{0,R}, \boldsymbol{\beta}_R \right) \right]} = \begin{bmatrix} 0 & -1 & 0 & 0 \\ 1 & 0 & 0 & 0 \\ 0 & 0 & 0 & 1 \\ 0 & 0 & -1 & 0 \end{bmatrix} \tag{F.72c}$$

$$\frac{\partial \boldsymbol{R}_R \left\{ \bar{\boldsymbol{q}} \left[\boldsymbol{\theta} \left(\boldsymbol{\mathcal{X}}_{\mathrm{z}}^{(i)}; \boldsymbol{\theta}_{0,R}, \boldsymbol{\beta}_R \right) \right] \right\}}{\partial q_4 \left[\boldsymbol{\theta} \left(\boldsymbol{\mathcal{X}}_{\mathrm{z}}^{(i)}; \boldsymbol{\theta}_{0,R}, \boldsymbol{\beta}_R \right) \right]} = \begin{bmatrix} 1 & 0 & 0 & 0 \\ 0 & 1 & 0 & 0 \\ 0 & 0 & 1 & 0 \\ 0 & 0 & 0 & 1 \end{bmatrix} . \tag{F.72d}$$

The latter derivative of the right hand side of Eq. (F.71) is calculated according to

$$\frac{\partial q_a \left[\boldsymbol{\theta} \left(\boldsymbol{\mathcal{X}}_{\mathrm{z}}^{(i)}; \boldsymbol{\theta}_{0,R}, \boldsymbol{\beta}_R \right) \right]}{\partial \theta_{0,R,k}} = \frac{\partial q_a \left[\boldsymbol{\theta} \left(\boldsymbol{\mathcal{X}}_{\mathrm{z}}^{(i)}; \boldsymbol{\theta}_{0,R}, \boldsymbol{\beta}_R \right) \right]}{\partial \boldsymbol{\theta} \left(\boldsymbol{\mathcal{X}}_{\mathrm{z}}^{(i)}; \boldsymbol{\theta}_{0,R}, \boldsymbol{\beta}_R \right)} \frac{\partial \boldsymbol{\theta} \left(\boldsymbol{\mathcal{X}}_{\mathrm{z}}^{(i)}; \boldsymbol{\theta}_{0,R}, \boldsymbol{\beta}_R \right)}{\partial \theta_{0,R,k}} . \tag{F.73}$$

Substituting Eqs. (F.51) and (F.52) into Eq. (F.73) yields

$$\frac{\partial q_a \left[\boldsymbol{\theta} \left(\boldsymbol{\mathcal{X}}_{\mathrm{z}}^{(i)}; \boldsymbol{\theta}_{0,R}, \boldsymbol{\beta}_R \right) \right]}{\partial \theta_{0,R,k}} = \frac{\partial q_a \left[\boldsymbol{\theta} \left(\boldsymbol{\mathcal{X}}_{\mathrm{z}}^{(i)}; \boldsymbol{\theta}_{0,R}, \boldsymbol{\beta}_R \right) \right]}{\partial \boldsymbol{\theta} \left(\boldsymbol{\mathcal{X}}_{\mathrm{z}}^{(i)}; \boldsymbol{\theta}_{0,R}, \boldsymbol{\beta}_R \right)} \mathbf{1}_{k,1}^{3,1} . \tag{F.74}$$

It is now noted that Eq. (F.74) can be expressed as

$$\frac{\partial q_a \left[\boldsymbol{\theta} \left(\boldsymbol{\mathcal{X}}_{\mathrm{z}}^{(i)}; \boldsymbol{\theta}_{0,R}, \boldsymbol{\beta}_R \right) \right]}{\partial \theta_{0,R,k}} = \left[\frac{\partial \bar{\boldsymbol{q}} \left[\boldsymbol{\theta} \left(\boldsymbol{\mathcal{X}}_{\mathrm{z}}^{(i)}; \boldsymbol{\theta}_{0,R}, \boldsymbol{\beta}_R \right) \right]}{\partial \boldsymbol{\theta} \left(\boldsymbol{\mathcal{X}}_{\mathrm{z}}^{(i)}; \boldsymbol{\theta}_{0,R}, \boldsymbol{\beta}_R \right)} \right]_{a,k} \triangleq \alpha_{R,a,k} . \tag{F.75}$$

Substituting Eq. (F.75) into Eq. (F.71) yields

$$\frac{\partial \boldsymbol{R}_R \left\{ \bar{\boldsymbol{q}} \left[\boldsymbol{\theta} \left(\boldsymbol{\mathcal{X}}_{\mathrm{z}}^{(i)}; \boldsymbol{\theta}_{0,R}, \boldsymbol{\beta}_R \right) \right] \right\}}{\partial \theta_{0,R,k}} = \sum_{a=1}^{4} \frac{\partial \boldsymbol{R}_R \left\{ \bar{\boldsymbol{q}} \left[\boldsymbol{\theta} \left(\boldsymbol{\mathcal{X}}_{\mathrm{z}}^{(i)}; \boldsymbol{\theta}_{0,R}, \boldsymbol{\beta}_R \right) \right] \right\}}{\partial q_a \left[\boldsymbol{\theta} \left(\boldsymbol{\mathcal{X}}_{\mathrm{z}}^{(i)}; \boldsymbol{\theta}_{0,R}, \boldsymbol{\beta}_R \right) \right]} \alpha_{R,a,k} . \tag{F.76}$$

which can be simplified to yield

$$\frac{\partial \boldsymbol{R}_R \left\{ \bar{\boldsymbol{q}} \left[\boldsymbol{\theta} \left(\boldsymbol{\mathcal{X}}_{\mathrm{z}}^{(i)}; \boldsymbol{\theta}_{0,R}, \boldsymbol{\beta}_R \right) \right] \right\}}{\partial \theta_{0,R,k}} = \begin{bmatrix} \alpha_{R,4,k} & -\alpha_{R,3,k} & \alpha_{R,2,k} & \alpha_{R,1,k} \\ \alpha_{R,3,k} & \alpha_{R,4,k} & -\alpha_{R,1,k} & \alpha_{R,2,k} \\ -\alpha_{R,2,k} & \alpha_{R,1,k} & \alpha_{R,4,k} & \alpha_{R,3,k} \\ -\alpha_{R,1,k} & -\alpha_{R,2,k} & -\alpha_{R,3,k} & \alpha_{R,4,k} \end{bmatrix} \triangleq \boldsymbol{A}_{R,k} . \tag{F.77}$$

Substituting Eqs. (F.70) and (F.77) into Eq. (F.69) yields

$$\frac{\partial K_i(\boldsymbol{\theta}_{0,L}, \boldsymbol{\theta}_{0,R}, \boldsymbol{\beta}_L, \boldsymbol{\beta}_R, \boldsymbol{Z})}{\partial \theta_{0,R,k}} = \tag{F.78}$$

$$\text{tr}\left\{2\boldsymbol{Z}\boldsymbol{R}_R^T\left\{\bar{q}\left[\boldsymbol{\theta}\left(\boldsymbol{\mathcal{X}}_z^{(i)}; \boldsymbol{\theta}_{0,R}, \boldsymbol{\beta}_R\right)\right]\right\}\boldsymbol{R}_L^T\left\{\bar{q}\left[\boldsymbol{\theta}\left(\boldsymbol{\mathcal{X}}_z^{(i)}; \boldsymbol{\theta}_{0,L}, \boldsymbol{\beta}_L\right)\right]\right\}\boldsymbol{\mathcal{X}}_q^{(i)}\boldsymbol{\mathcal{X}}_q^{(i)T}\right.$$
$$\left.\times \boldsymbol{R}_L\left\{\bar{q}\left[\boldsymbol{\theta}\left(\boldsymbol{\mathcal{X}}_z^{(i)}; \boldsymbol{\theta}_{0,L}, \boldsymbol{\beta}_L\right)\right]\right\}\boldsymbol{A}_{R,k}\right\}.$$

Exploiting the cyclic property of the trace, Eq. (F.78) can be expressed as

$$\frac{\partial K_i(\boldsymbol{\theta}_{0,L}, \boldsymbol{\theta}_{0,R}, \boldsymbol{\beta}_L, \boldsymbol{\beta}_R, \boldsymbol{Z})}{\partial \theta_{0,L,k}} = 2\boldsymbol{\mathcal{X}}_q^{(i)T}\boldsymbol{R}_L\left\{\bar{q}\left[\boldsymbol{\theta}\left(\boldsymbol{\mathcal{X}}_z^{(i)}; \boldsymbol{\theta}_{0,L}, \boldsymbol{\beta}_L\right)\right]\right\}\boldsymbol{A}_{R,k}\boldsymbol{Z} \tag{F.79}$$
$$\times \boldsymbol{R}_R^T\left\{\bar{q}\left[\boldsymbol{\theta}\left(\boldsymbol{\mathcal{X}}_z^{(i)}; \boldsymbol{\theta}_{0,R}, \boldsymbol{\beta}_R\right)\right]\right\}\boldsymbol{R}_L^T\left\{\bar{q}\left[\boldsymbol{\theta}\left(\boldsymbol{\mathcal{X}}_z^{(i)}; \boldsymbol{\theta}_{0,L}, \boldsymbol{\beta}_L\right)\right]\right\}\boldsymbol{\mathcal{X}}_q^{(i)}.$$

The partial derivative of $K_i(\boldsymbol{\theta}_{0,L}, \boldsymbol{\theta}_{0,R}, \boldsymbol{\beta}_L, \boldsymbol{\beta}_R, \boldsymbol{Z})$ with respect to the kth row and ℓ^{th} entry of $\boldsymbol{\beta}_R$, $\beta_{R,k,\ell}$ for $k = 1, 2, 3$ and $\ell = 1, 2, \ldots, r$, is given by

$$\frac{\partial K_i(\boldsymbol{\theta}_{0,L}, \boldsymbol{\theta}_{0,R}, \boldsymbol{\beta}_L, \boldsymbol{\beta}_R, \boldsymbol{Z})}{\partial \beta_{R,k,\ell}} = \tag{F.80}$$

$$\text{tr}\left\{\frac{\partial \boldsymbol{\mathcal{X}}_q^{(i)T}\left[\boldsymbol{R}_L\left\{\bar{q}\left[\boldsymbol{\theta}\left(\boldsymbol{\mathcal{X}}_z^{(i)}; \boldsymbol{\theta}_{0,L}, \boldsymbol{\beta}_L\right)\right]\right\}\boldsymbol{R}_R\left\{\bar{q}\left[\boldsymbol{\theta}\left(\boldsymbol{\mathcal{X}}_z^{(i)}; \boldsymbol{\theta}_{0,R}, \boldsymbol{\beta}_R\right)\right]\right\}\right]\boldsymbol{Z}\left[\ldots\right]^T\boldsymbol{\mathcal{X}}_q^{(i)}}{\partial \boldsymbol{R}_R\left\{\bar{q}\left[\boldsymbol{\theta}\left(\boldsymbol{\mathcal{X}}_z^{(i)}; \boldsymbol{\theta}_{0,R}, \boldsymbol{\beta}_R\right)\right]\right\}}\right.$$

$$\left.\times\frac{\partial \boldsymbol{R}_R\left\{\bar{q}\left[\boldsymbol{\theta}\left(\boldsymbol{\mathcal{X}}_z^{(i)}; \boldsymbol{\theta}_{0,R}, \boldsymbol{\beta}_R\right)\right]\right\}}{\partial \beta_{R,k,\ell}}\right\}.$$

The former derivative of the chain rule in Eq. (F.80) is given by Eq. (F.70). The latter derivative of the chain rule in Eq. (F.80) is calculated as

$$\frac{\partial \boldsymbol{R}_R\left\{\bar{q}\left[\boldsymbol{\theta}\left(\boldsymbol{\mathcal{X}}_z^{(i)}; \boldsymbol{\theta}_{0,R}, \boldsymbol{\beta}_R\right)\right]\right\}}{\partial \beta_{R,k,\ell}} = \sum_{a=1}^{4}\frac{\partial \boldsymbol{R}_R\left\{\bar{q}\left[\boldsymbol{\theta}\left(\boldsymbol{\mathcal{X}}_z^{(i)}; \boldsymbol{\theta}_{0,R}, \boldsymbol{\beta}_R\right)\right]\right\}}{\partial q_a\left[\boldsymbol{\theta}\left(\boldsymbol{\mathcal{X}}_z^{(i)}; \boldsymbol{\theta}_{0,R}, \boldsymbol{\beta}_R\right)\right]} \tag{F.81}$$

$$\times\frac{\partial q_a\left[\boldsymbol{\theta}\left(\boldsymbol{\mathcal{X}}_z^{(i)}; \boldsymbol{\theta}_{0,R}, \boldsymbol{\beta}_R\right)\right]}{\partial \beta_{R,k,\ell}}.$$

The former derivative of the right hand side of Eq. (F.81) is given by Eq. (F.72). The latter derivative of the right hand side of Eq. (F.81) is calculated according to

$$\frac{\partial q_a \left[\boldsymbol{\theta} \left(\boldsymbol{\mathcal{X}}_z^{(i)}; \boldsymbol{\theta}_{0,R}, \boldsymbol{\beta}_R \right) \right]}{\partial \beta_{R,k,\ell}} = \frac{\partial q_a \left[\boldsymbol{\theta} \left(\boldsymbol{\mathcal{X}}_z^{(i)}; \boldsymbol{\theta}_{0,R}, \boldsymbol{\beta}_R \right) \right]}{\partial \boldsymbol{\theta} \left(\boldsymbol{\mathcal{X}}_z^{(i)}; \boldsymbol{\theta}_{0,R}, \boldsymbol{\beta}_R \right)} \frac{\partial \boldsymbol{\theta} \left(\boldsymbol{\mathcal{X}}_z^{(i)}; \boldsymbol{\theta}_{0,R}, \boldsymbol{\beta}_R \right)}{\partial \beta_{R,k,\ell}} \ . \tag{F.82}$$

The former derivative of the right hand side of Eq. (F.82) is given by Eq. (F.51). The latter derivative of the right hand side of Eq. (F.82) is calculated from Eq. (F.13) and is given by

$$\frac{\partial \boldsymbol{\theta} \left(\boldsymbol{\mathcal{X}}_z^{(i)}; \boldsymbol{\theta}_{0,R}, \boldsymbol{\beta}_R \right)}{\partial \beta_{R,k,\ell}} = \sum_{b=1}^{3} \sum_{c=1}^{r} \frac{\partial \boldsymbol{\theta} \left(\boldsymbol{\mathcal{X}}_z^{(i)}; \boldsymbol{\theta}_{0,R}, \boldsymbol{\beta}_R \right)}{\partial \beta_{R,b,c}} \frac{\partial \beta_{R,b,c}}{\partial \beta_{R,k,\ell}}$$
$$= \mathcal{X}_{z,\ell}^{(i)} \mathbf{1}_{k,1}^{3,1} \ . \tag{F.83}$$

Substituting Eq. (F.83) into Eq. (F.82) yields

$$\frac{\partial q_a \left[\boldsymbol{\theta} \left(\boldsymbol{\mathcal{X}}_z^{(i)}; \boldsymbol{\theta}_{0,R}, \boldsymbol{\beta}_R \right) \right]}{\partial \beta_{R,k,\ell}} = \frac{\partial q_a \left[\boldsymbol{\theta} \left(\boldsymbol{\mathcal{X}}_z^{(i)}; \boldsymbol{\theta}_{0,R}, \boldsymbol{\beta}_R \right) \right]}{\partial \boldsymbol{\theta} \left(\boldsymbol{\mathcal{X}}_z^{(i)}; \boldsymbol{\theta}_{0,R}, \boldsymbol{\beta}_R \right)} \mathcal{X}_{z,\ell}^{(i)} \mathbf{1}_{k,1}^{3,1} \ . \tag{F.84}$$

It is now noted that Eq. (F.84) can be expressed as

$$\frac{\partial q_a \left[\boldsymbol{\theta} \left(\boldsymbol{\mathcal{X}}_z^{(i)}; \boldsymbol{\theta}_{0,R}, \boldsymbol{\beta}_R \right) \right]}{\partial \beta_{R,k,\ell}} = \left[\frac{\partial \bar{\boldsymbol{q}} \left[\boldsymbol{\theta} \left(\boldsymbol{\mathcal{X}}_z^{(i)}; \boldsymbol{\theta}_{0,R}, \boldsymbol{\beta}_R \right) \right]}{\partial \boldsymbol{\theta} \left(\boldsymbol{\mathcal{X}}_z^{(i)}; \boldsymbol{\theta}_{0,R}, \boldsymbol{\beta}_R \right)} \right]_{a,k} \mathcal{X}_{z,\ell}^{(i)} \triangleq \alpha_{R,a,k} \mathcal{X}_{z,\ell}^{(i)} \ . \tag{F.85}$$

Substituting Eq. (F.85) into Eq. (F.81) yields

$$\frac{\partial \boldsymbol{R}_R \left\{ \bar{\boldsymbol{q}} \left[\boldsymbol{\theta} \left(\boldsymbol{\mathcal{X}}_z^{(i)}; \boldsymbol{\theta}_{0,R}, \boldsymbol{\beta}_R \right) \right] \right\}}{\partial \beta_{R,k,\ell}} = \sum_{a=1}^{4} \frac{\partial \boldsymbol{R}_R \left\{ \bar{\boldsymbol{q}} \left[\boldsymbol{\theta} \left(\boldsymbol{\mathcal{X}}_z^{(i)}; \boldsymbol{\theta}_{0,R}, \boldsymbol{\beta}_R \right) \right] \right\}}{\partial q_a \left[\boldsymbol{\theta} \left(\boldsymbol{\mathcal{X}}_z^{(i)}; \boldsymbol{\theta}_{0,R}, \boldsymbol{\beta}_R \right) \right]} \alpha_{R,a,k} \mathcal{X}_{z,\ell}^{(i)} \ . \tag{F.86}$$

which can be simplified to yield

$$\frac{\partial \boldsymbol{R}_R \left\{ \bar{\boldsymbol{q}} \left[\boldsymbol{\theta} \left(\boldsymbol{\mathcal{X}}_z^{(i)}; \boldsymbol{\theta}_{0,R}, \boldsymbol{\beta}_R \right) \right] \right\}}{\partial \beta_{R,k,\ell}} = \boldsymbol{A}_{R,k} \mathcal{X}_{z,\ell}^{(i)} \ . \tag{F.87}$$

Substituting Eqs. (F.70) and (F.87) into Eq. (F.80) yields

$$\frac{\partial K_i(\boldsymbol{\theta}_{0,L}, \boldsymbol{\theta}_{0,R}, \boldsymbol{\beta}_L, \boldsymbol{\beta}_R, \boldsymbol{Z})}{\partial \beta_{R,k,\ell}} = \text{tr} \left\{ 2 \boldsymbol{Z} \boldsymbol{R}_R^T \left\{ \bar{\boldsymbol{q}} \left[\boldsymbol{\theta} \left(\boldsymbol{\mathcal{X}}_z^{(i)}; \boldsymbol{\theta}_{0,R}, \boldsymbol{\beta}_R \right) \right] \right\} \right\} \tag{F.88}$$

$$\times \boldsymbol{R}_L^T \left\{ \bar{q} \left[\boldsymbol{\theta} \left(\boldsymbol{\mathcal{X}}_{\mathrm{z}}^{(i)}; \boldsymbol{\theta}_{0,L}, \boldsymbol{\beta}_L \right) \right] \right\} \boldsymbol{\mathcal{X}}_q^{(i)} \boldsymbol{\mathcal{X}}_q^{(i)T} \boldsymbol{R}_L \left\{ \bar{q} \left[\boldsymbol{\theta} \left(\boldsymbol{\mathcal{X}}_{\mathrm{z}}^{(i)}; \boldsymbol{\theta}_{0,L}, \boldsymbol{\beta}_L \right) \right] \right\} \boldsymbol{A}_{R,k} \boldsymbol{\mathcal{X}}_{\mathrm{z},\ell}^{(i)} \right\} .$$

Exploiting the cyclic property of the trace, Eq. (F.88) can be expressed as

$$\frac{\partial K_i(\boldsymbol{\theta}_{0,L}, \boldsymbol{\theta}_{0,R}, \boldsymbol{\beta}_L, \boldsymbol{\beta}_R, \boldsymbol{Z})}{\partial \beta_{R,k,\ell}} = 2 \boldsymbol{\mathcal{X}}_{\mathrm{z},\ell}^{(i)} \boldsymbol{\mathcal{X}}_q^{(i)T} \boldsymbol{R}_L \left\{ \bar{q} \left[\boldsymbol{\theta} \left(\boldsymbol{\mathcal{X}}_{\mathrm{z}}^{(i)}; \boldsymbol{\theta}_{0,L}, \boldsymbol{\beta}_L \right) \right] \right\} \boldsymbol{A}_{R,k} \boldsymbol{Z} \qquad \text{(F.89)}$$
$$\times \boldsymbol{R}_R^T \left\{ \bar{q} \left[\boldsymbol{\theta} \left(\boldsymbol{\mathcal{X}}_{\mathrm{z}}^{(i)}; \boldsymbol{\theta}_{0,R}, \boldsymbol{\beta}_R \right) \right] \right\} \boldsymbol{R}_L^T \left\{ \bar{q} \left[\boldsymbol{\theta} \left(\boldsymbol{\mathcal{X}}_{\mathrm{z}}^{(i)}; \boldsymbol{\theta}_{0,L}, \boldsymbol{\beta}_L \right) \right] \right\} \boldsymbol{\mathcal{X}}_q^{(i)} .$$

In summary the optimality conditions for $s = 3$ are given (with some minor algebraic simplification) by

$$\frac{\partial J(\boldsymbol{\theta}_{0,L}, \boldsymbol{\theta}_{0,R}, \boldsymbol{\beta}_L, \boldsymbol{\beta}_R, \boldsymbol{Z})}{\partial Z_k} = 2 \sum_{i=1}^{N} w^{(i)} \boldsymbol{\mathcal{X}}_q^{(i)T} \boldsymbol{R}_L^{(i)} \boldsymbol{R}_R^{(i)} \mathbf{1}_{k,k}^{4,4} \boldsymbol{R}_R^{(i)T} \boldsymbol{R}_L^{(i)T} \boldsymbol{\mathcal{X}}_q^{(i)} - f_k = 0$$

$$\frac{\partial J(\boldsymbol{\theta}_{0,L}, \boldsymbol{\theta}_{0,R}, \boldsymbol{\beta}_L, \boldsymbol{\beta}_R, \boldsymbol{Z})}{\partial \theta_{0,L,k}} = 4 \sum_{i=1}^{N} w^{(i)} \boldsymbol{\mathcal{X}}_q^{(i)T} \boldsymbol{A}_{L,k} \boldsymbol{R}_R^{(i)} \boldsymbol{Z} \boldsymbol{R}_R^{(i)T} \boldsymbol{R}_L^{(i)T} \boldsymbol{\mathcal{X}}_q^{(i)} = 0$$

$$\frac{\partial J(\boldsymbol{\theta}_{0,L}, \boldsymbol{\theta}_{0,R}, \boldsymbol{\beta}_L, \boldsymbol{\beta}_R, \boldsymbol{Z})}{\partial \beta_{L,k,\ell}} = 4 \sum_{i=1}^{N} w^{(i)} \boldsymbol{\mathcal{X}}_{\mathrm{z},\ell}^{(i)} \boldsymbol{\mathcal{X}}_q^{(i)T} \boldsymbol{A}_{L,k} \boldsymbol{R}_R^{(i)} \boldsymbol{Z} \boldsymbol{R}_R^{(i)T} \boldsymbol{R}_L^{(i)T} \boldsymbol{\mathcal{X}}_q^{(i)} = 0$$

$$\frac{\partial J(\boldsymbol{\theta}_{0,L}, \boldsymbol{\theta}_{0,R}, \boldsymbol{\beta}_L, \boldsymbol{\beta}_R, \boldsymbol{Z})}{\partial \theta_{0,R,k}} = 4 \sum_{i=1}^{N} w^{(i)} \boldsymbol{\mathcal{X}}_q^{(i)T} \boldsymbol{R}_L^{(i)} \boldsymbol{A}_{R,k} \boldsymbol{Z} \boldsymbol{R}_R^{(i)T} \boldsymbol{R}_L^{(i)T} \boldsymbol{\mathcal{X}}_q^{(i)} = 0$$

$$\frac{\partial J(\boldsymbol{\theta}_{0,L}, \boldsymbol{\theta}_{0,R}, \boldsymbol{\beta}_L, \boldsymbol{\beta}_R, \boldsymbol{Z})}{\partial \beta_{R,k,\ell}} = 4 \sum_{i=1}^{N} w^{(i)} \boldsymbol{\mathcal{X}}_{\mathrm{z},\ell}^{(i)} \boldsymbol{\mathcal{X}}_q^{(i)T} \boldsymbol{R}_L^{(i)} \boldsymbol{A}_{R,k} \boldsymbol{Z} \boldsymbol{R}_R^{(i)T} \boldsymbol{R}_L^{(i)T} \boldsymbol{\mathcal{X}}_q^{(i)} = 0 \,,$$

where

$$\boldsymbol{R}_L^{(i)} = \boldsymbol{R}_L \left\{ \bar{q} \left[\boldsymbol{\theta} \left(\boldsymbol{\mathcal{X}}_{\mathrm{z}}^{(i)}; \boldsymbol{\theta}_{0,L}, \boldsymbol{\beta}_L \right) \right] \right\}$$
$$\boldsymbol{R}_R^{(i)} = \boldsymbol{R}_R \left\{ \bar{q} \left[\boldsymbol{\theta} \left(\boldsymbol{\mathcal{X}}_{\mathrm{z}}^{(i)}; \boldsymbol{\theta}_{0,R}, \boldsymbol{\beta}_R \right) \right] \right\} .$$

BIBLIOGRAPHY

[1] G. Stienne, S. Reboul, M. Azmani, J. B. Choquel, and M. Benjelloun. A multi-temporal multi-sensor circular fusion filter. *Information Fusion*, 18:86–100, 2014.

[2] Gerhard Kurz, Igor Gilitschenski, and Uwe D. Hanebeck. Recursive Bayesian filtering in circular state spaces. *Computing Research Repository*, arXiv:1501.05151, 2015.

[3] K. V. Mardia and T. W. Sutton. A model for cylindrical variables with applications. *Journal of the Royal Statistical Society. Series B (Methodological)*, 40(2):229–233, 1978.

[4] Joshua T. Horwood and Aubrey B. Poore. Gauss von Mises distribution for improved uncertainty realism in space situational awareness. *SIAM/ASA Journal of Uncertainty Quantification*, 2(1):276–304, 2014.

[5] F. Landis Markley and John L. Crassidis. *Fundamentals of Spacecraft Attitude Determination and Control*. Springer, 2014.

[6] Malcolm D. Shuster. A survey of attitude representations. *The Journal of the Astronautical Sciences*, 41(4):439–517, 1993.

[7] Peter C. Hughes. *Spacecraft Attitude Dynamics*. John Wiley & Sons, 1986.

[8] Christopher Bingham. An antipodally symmetric distribution on the sphere. *The Annals of Statistics*, 2(6):1201–1225, 1974.

[9] Kanti V. Mardia and Peter E. Jupp. *Directional Statistics*. John Wiley & Sons, 2000.

[10] Gerhard Kurz, Igor Gilitschenski, Simon Julier, and Uwe D. Hanebeck. Recursive Bingham filter for directional estimation involving 180 degree symmetry. *Journal of Advances in Information Fusion*, 9(2):90–105, 2014.

[11] Jared Glover and Leslie Pack Kaelbling. Tracking the spin on a ping pong ball with the quaternion Bingham filter. In *IEEE International Conference on Robotics and Automation*, 2014.

[12] Igor Gilitschenski, Gerhard Kurz, Simon J. Julier, and Uwe D. Hanebeck. Unscented orientation estimation based on the Bingham distribution. *IEEE Transactions on Automatic Control*, 61(1):172–177, 2016.

[13] Igor Gilitschenski, Gerhard Kurz, Simon J. Julier, and Uwe D. Hanebeck. A new probability distribution for simultaneous representation of uncertain position and orientation. In *17th Annual International Conference on Information Fusion*, 2014.

[14] Gerhard Kurz, Igor Gilitschenski, and Uwe D. Hanebeck. The partially wrapped normal distribution for SE(2) estimation. In *IEEE International Conference on Multisensor Fusion and Information Integration*, 2014.

[15] Daniele Mortari. On the rigid rotation concept in n-dimensional spaces. *The Journal of the Astronautical Sciences*, 49(3):401–420, 2001.

[16] Andrew J. Sinclair and John E. Hurtado. Minimum parameter representations of N-dimensional principal rotations. *Journal of the Astronautical Sciences*, 53(3):317–326, 2005.

[17] Hanspeter Schaub and John L. Junkins. *Analytical Mechanics of Space Systems*. AIAA, 2003.

[18] F. Landis Markley. Unit quaternion from rotation matrix. *Journal of Guidance, Control, and Dynamics*, 31(2):1458–1465, 2008.

[19] Federico Thomas and Alba Pérez-Gracia. On Cayley's factorization of 4D rotations and applications. *Advances in Applied Clifford Algebras*, 2016 (to appear).

[20] C. Y. Hsiung and G. Y. Mao. *Linear Algebra*. World Scientific, 1998.

[21] H. W. Sorenson and D. L. Alspach. Recursive Bayesian estimation using Gaussian sums. *Automatica*, 7(4):465–479, 1971.

[22] Kyle J. DeMars and Moriba Jah. Probabilistic initial orbit determination using Gaussian mixture models. *Journal of Guidance, Control, and Dynamics*, 36(5):1324–1335, 2013.

[23] Vivek Vittaldev and Ryan P. Russell. Collision probability for space objects using Gaussian mixture models. In *AAS/AIAA Space Flight Mechanics Meeting*, number AAS 13-351, 2013.

[24] Plamen Koev and Alan Edelman. The efficient evaluation of the hypergeometric function of a matrix argument. *Mathematics of Computation*, 75(254):833–846, 2006.

[25] A. Kume and Andrew T. A. Wood. Saddlepoint approximations for the Bingham and Fisher-Bingham normalising constants. *Biometrika*, 92(2):465–476, 2005.

[26] Igor Gilitschenski, Gerhard Kurz, Simon J. Julier, and Uwe D. Hanebeck. Efficient Bingham filtering based on saddlepoint approximations. In *IEEE International Conference on Multisensor Fusion and Information Integration for Intelligent Systems*, 2014.

[27] Tomonari Sei and Alfred Kume. Calculating the normalising constant of the Bingham distribution on the sphere using the holonomic gradient method. *Statistics and Computing*, 25(2): 321–332, 2015.

[28] Jared Glover. Bingham statistics library, 2009.

[29] Sadri Hassani. *Mathematical Physics*. Springer, 2013.

[30] Andrew H. Jazwinski. *Stochastic Processes and Filtering Theory*. Elsevier, 1970.

[31] Rudolf E. Kalman. A new approach to linear filtering and prediction problems. *Journal of Basic Engineering*, 82(1):35–45, 1960.

[32] Rudolf E. Kalman and Richard S. Bucy. New results in linear filtering and prediction theory. *Journal of Basic Engineering*, 83(1):95–108, 1961.

[33] John L. Crassidis and John L. Junkins. *Optimal Estimation of Dynamic Systems*. CRC press, 2012.

[34] Renato Zanetti, Manoranjan Majji, Robert H. Bishop, and Daniele Mortari. Norm-constrained Kalman filtering. *Journal of Guidance, Control, and Dynamics*, 32(5):1458–1465, 2009.

[35] Thomas Ainscough, Renato Zanetti, John Christian, and Pol. D. Spanos. Q-method extended Kalman filter. *Journal of Guidance, Control, and Dynamics*, 38(4):752–760, 2015.

[36] Arthur Gelb. *Applied Optimal Estimation*. The M.I.T. Press, 1974.

[37] Leonard A. McGee and Stanley F. Schmidt. Discovery of the Kalman filter as a practical tool for aerospace and industry. Technical Report 86847, National Aeronautics and Space Administration, 1985.

[38] Kazufumi Ito and Kaiqi Xiong. Gaussian filters for nonlinear filtering problems. *IEEE Transactions on Automatic Control*, 45(5):910–927, 2000.

[39] Ienkaran Arasaratnam, Simon Haykin, and Robert J. Elliott. Discrete-time nonlinear filtering algorithms using Gauss-Hermite quadrature. *Proceedings of the IEEE*, 95(5):953–977, 2007.

[40] Ienkaran Arasaratnam and Simon Haykin. Square-root quadrature Kalman filtering. *IEEE Transactions on Signal Processing*, 56(6):2589–2593, 2008.

[41] Ienkaran Arasaratnam and Simon Haykin. Cubature Kalman filters. *IEEE Transactions on Automatic Control*, 54(6):1254–1269, 2009.

[42] Simon J. Julier. The scaled unscented transformation. In *AACC American Control Conference*, 2002.

[43] Henrique M. T. Menegaz, João Y. Ishihara, Geovany A. Borges, and Alessandro N. Vargas. A systematization of the unscented Kalman filter theory. *IEEE Transactions on Automatic Control*, 60(10):2583–2598, 2015.

[44] Simon J. Julier and Jeffrey K. Uhlmann. Unscented filtering and nonlinear estimation. *Proceedings of the IEEE*, 92(3):401–422, 2004.

[45] Eric A Wan and Rudolf van der Merwe. The unscented Kalman filter for nonlinear estimation. In *IEEE Adaptive Systems for Signal Processing, Communications, and Control Symposium*, pages 153–158, 2000.

[46] Bin Jia, Ming Xin, and Yang Cheng. Sparse Gauss-Hermite quadrature filter with application to spacecraft attitude estimation. *Journal of Guidance, Control, and Dynamics*, 34(2): 367–379, 2011.

[47] Nagavenkat Adurthi, Puneet Singla, and Tarunraj Singh. Conjugate unscented transform and its application to filtering and stochastic integral calculation. In *AIAA Guidance, Navigation, and Control Conference*, number AIAA 2012-4934, 2012.

[48] Nagavenkat Adurthi, Puneet Singla, and Tarunraj Singh. The conjugate unscented transform - an approach to evaluate multi-dimensional expectation integrals. In *AACC American Control Conference*, 2012.

[49] F. Landis Markley. Attitude error representations for kalman filtering. *Journal of Guidance, Control, and Dynamics*, 26(2):311–317, 2003.

[50] Renato Zanetti. *Advanced Navigation Algorithms for Precision Landing*. PhD thesis, The University of Texas at Austin, 2007.

[51] Kyle J. DeMars. Precision navigation for lunar descent and landing. Master's thesis, The University of Texas at Austin, May 2007.

[52] Jacob E. Darling, James S. McCabe, Henry J. Pernicka, and Kyle J. DeMars. Linear and unscented covariance analysis for spacecraft close proximity relative navigation. In *AAS/AIAA Space Flight Mechanics Meeting*, number AAS 14-257, 2014.

[53] F. Landis Markley, Yang Cheng, John L. Crassidis, and Yaakov Oshman. Averaging quaternions. *Journal of Guidance, Control, and Dynamics*, 30(4):1193–1197, 2007.

[54] Y. C. Ho and R. C. K. Lee. A Bayesian approach to problems in stochastic estimation and control. *IEEE Transactions on Automatic Control*, 9(4):333–339, 1964.

[55] Daniel L. Alspach and Harold W. Sorenson. Nonlinear Bayesian estimation using Gaussian sum approximations. *IEEE Transactions on Automatic Control*, 17(4):439–448, 1972.

[56] Kyle J. DeMars, Robert H. Bishop, and Moriba K. Jah. Entropy-based approach for uncertainty propagation of nonlinear dynamical systems. *Journal of Guidance, Control, and Dynamics*, 36(4):1047–1057, 2013.

[57] S. Kullback and R. A. Leibler. On information and sufficiency. *The Annals of Mathematical Statistics*, 22(1):79–86, 1951.

[58] Ananth Ranganathan. Assumed density filtering. Technical report, Honda Research Institute, 2004.

[59] Ralf Herbrich. Minimising the Kullback-Leibler divergence. Technical report, Microsoft Research, 2005.

[60] Uwe D. Hanebeck. PGF 42: Progressive Gaussian filtering with a twist. In *16th Annual International Conference on Information Fusion*, 2013.

[61] Gerhard Kurz and Uwe D. Hanebeck. Trigonometric moment matching and minimization of the Kullback-Leibler divergence. *IEEE Transactions on Aerospace and Electronic Systems*, 51(4):3480–3484, 2015.

[62] Miroslav Kárnỳ. Approximate Bayesian recursive estimation. *Information Sciences*, 285: 100–111, 2014.

[63] Jannik Steinbring and Uwe D. Hanebeck. Progressive Gaussian filtering using explicit likelihoods. In *17th Annual International Conference on Information Fusion*, 2014.

[64] Uwe D. Hanebeck and Jannik Steinbring. Progressive Gaussian filtering. *Computing Research Repository*, arXiv:1204.0133, 2012.

[65] Jacob E. Darling and Kyle J. DeMars. Uncertainty propagation of correlated quaternion and Euclidean states using the Gauss–Bingham density. *Journal of Advances in Information Fusion*, 11(2), December 2016 (to appear).

[66] Kenneth Levenberg. A method for the solution of certain non-linear problems in least squares. *Quarterly of Applied Mathematics*, 2(2):164–168, 1944.

[67] Donald W. Marquardt. An algorithm for least-squares estimation of nonlinear parameters. *Journal of the Society for Industrial and Applied Mathematics*, 11(2):431–441, 1963.

[68] W. H. Clohessy and R. S. Wiltshire. Terminal guidance system for satellite rendezvous. *Journal of the Aerospace Sciences*, 27(9):653–658, 1960.

[69] Kyle T. Alfriend, Srinivas R. Vadali, Pini Gurfil, Jonathan P. How, and Louis S. Berger. *Spacecraft Formation Flying*. Elsevier, 2010.

[70] David A. Vallado. *Fundamentals of Astrodynamics and Applications*. Microcosm, 2001.

[71] John L. Crassidis, F. Landis Markley, and Yang Cheng. Survey of nonlinear attitude estimation methods. *Journal of Guidance, Control, and Dynamics*, 30(1):12–28, 2007.

[72] Geoffrey McLachlan and Thriyambakam Krishnan. *The EM Algorithm and Extensions*. John Wiley & Sons, 2008.

[73] Igor Gilitschenski, Gerhard Kurz, Uwe D. Hanebeck, and Roland Siegwart. Optimal quantization of circular distributions. In *19th Annual International Conference on Information Fusion*, 2016.

[74] John T. Kent, Asaad M. Ganeiber, and Kanti V. Mardia. A new method to simulate the Bingham and related distributions in directional data analysis with applications. *Computing Research Repository*, arXiv:1310.8110, 2013.

[75] Renato Zanetti, Kyle J. DeMars, and Robert H. Bishop. Underweighting nonlinear measurements. *Journal of Guidance, Control, and Dynamics*, 33(5):1670–1675, 2010.

[76] Oliver J. Woodman. An introduction to inertial navigation. Master's thesis, University of Cambridge, 2007.

[77] Arnaud Chulliat, Susan Macmillan, Patrick Alken, Ciaran Beggan, Manoj Nair, Brian Hamilton, Adam Woods, Victoria Ridley, Stefan Maus, and Alan Thomson. The US/UK world magnetic model for 2015-2020. Technical report, British Geological Survey and National Oceanic and Atmospheric Association, 2015.

[78] Byron D. Tapley, Bob E. Schutz, and George H. Born. *Statistical Orbit Determination*. Academic Press, 2004.

[79] Ba-Ngu Vo. *Random Finite Sets in Multi-Object Filtering*. PhD thesis, The University of Western Australia, 2008.

[80] Gene H. Golub and John H. Welsch. Calculation of Gauss quadrature rules. *Mathematics of Computation*, 23(106):221–230, 1969.

[81] Kyle J. DeMars and Jacob E. Darling. Proof of Equation 32 in *A Bayesian Approach to Problems in Stochastic Estimation and Control* by Yu-Chi Ho and R. C. K. Lee. Technical Report AREUS 1501, Missouri University of Science and Technology AREUS Laboratory, 2015.

[82] Max A. Woodbury. Inverting modified matrices. Technical Report no. 42, Statistical Research Group, Princeton University, 1950.

[83] James Joseph Sylvester. On the relation between the minor determinants of linearly equivalent quadratic functions. *Philosophical Magazine*, 1:295–305, 1851.

[84] Branko Ristic, Sanjeev Arulampalam, and Neil Gordon. *Beyond the Kalman Filter*. Artech House, 2004.

[85] Brian D.O. Anderson and John B. Moore. *Optimal filtering*. Dover Publications, 1979.

[86] Peter S. Maybeck. *Stochastic Models, Estimation, and Control*, volume 1. Academic Press, 1979.

[87] Kaare Brandt Petersen and Michael Syskind Pedersen. The matrix cookbook. *Technical University of Denmark*, 7:15, 2008.

VITA

Jacob Edward Darling was born and raised in Potosi, MO. He graduated from Potosi High School in 2007, and began the pursuit of a B.S. degree in Aerospace Engineering at Missouri University of Science and Technology the same year. He graduated summa cum laude with his B.S. degree in May 2011, and began the pursuit of a Ph.D. in Aerospace Engineering in August 2011. He received the Science, Mathematics, and Research for Transformation (SMART) fellowship in August 2013. In December 2016, he received his Ph.D. in Aerospace Engineering from Missouri University of Science and Technology. During his tenure as a doctoral student, he completed multiple internships with the Air Force Research Laboratory's guidance, navigation, and control group (AFRL-RVSVC).